Experimental and numerical study of the combustion and emissions of natural gas/diesel dual-fuel engine under different engine load-speed conditions

By

Amin Yousefi

A Thesis submitted to the Faculty of Graduate Studies of

The University of Manitoba

in partial fulfillment of the requirements of the degree of

Doctor of Philosophy

Department of Mechanical Engineering

University of Manitoba

Winnipeg

Abstract

Universal concerns about degradation in air quality, stringent emissions regulations, energy scarcity, and global warming have prompted research and development of compressed ignition engines using alternative combustion concepts. Natural gas/diesel dual-fuel combustion is an advanced combustion concept for compression ignition diesel engines, which has attracted global attention in recent years. This combustion concept is accomplished by creating reactivity stratification in the cylinder via the use of two fuels characterized by distinctly different reactivities. The low reactivity and main fuel (i.e., natural gas) is firstly premixed with air and then charged into the cylinder through the intake manifold, and the high reactivity fuel (i.e., diesel) is then injected into the charged mixture through a direct injector. This combustion concept offers prominent benefits in terms of a significant reduction of particulate matter (PM) and sometimes nitrogen oxides (NOx) emissions while maintaining comparable fuel efficiency compared to diesel engine. However, low thermal efficiency and high greenhouse gas (GHG) emissions under low load conditions are major challenges which prevented the implementation of dual-fuel concept in commercial automative engines.

The present study investigates different combustion approaches with the aim to enhance combustion performance and reduce emissions of unburned methane, CO, NOx, soot, and GHG of natural gas/diesel dual-fuel engines under different engine load-speed conditions. In particular, the main focus of this thesis is on low load conditions where GHG emissions of conventional natural gas/diesel dual-fuel engine is much higher than that of conventional diesel engine. Alongside the experimental study, a computational fluid dynamic (CFD) model is developed to help understand the behaviour of natural gas/diesel dual-fuel combustion process under different engine load-speed conditions.

The studied approaches showed that the fuel efficiency and GHG emissions of natural gas/diesel dual-fuel engine can be significantly improved under low engine load conditions compared to diesel engine.

Acknowledgements

First, I have to thank my research supervisors Dr. Madjid Birouk and Dr. Hongsheng Guo who offered continuous advice and encouragement throughout the course of this thesis. Without their assistance and dedicated involvement in every step throughout the process, this thesis would have never been accomplished. I really would like to appreciate them for their support and understanding over these past four years.

I also would like to thank my committee members, Dr. (**External Examiner**), Dr. Robert Derksen, and Dr. Marolo Alfaro for their efforts put into reviewing the thesis, and their invaluable comments and suggestions. The help of Mr. Brian Liko from NRC in preparing and running the engine test and sharing his technical expertise for this project is greatly appreciated.

I would like to acknowledge the financial support received from the University of Manitoba Graduate Scholarship (UMGF). Funding for the experimental work was provided by Natural Resources Canada through the PERD Energy End Use (project 3B03.003) and National Research Council Canada through the internal Bioenergy Program. CONVERGENT Science Inc. and Compute Canada are gratefully acknowledged for providing CONVERGE CFD software and advanced computing systems, respectively.

Finally, and most importantly, none of this was possible without the encouragement and supports that I received from my family who have sacrificed their lives for me and provided unconditional love and care. I would like to dedicate this thesis to my beloved parents, sister, and brother. They have always given me the determination to overcome many trying moments to pursue my dreams.

Table of Contents

List of Figures:

List of Tables:

Declaration of the academic achievement

The outline of this thesis follows “sandwich format” whose guidelines are appointed by the Faculty of Graduate Studies, University of Manitoba. It merges five individual papers prepared for publication in peer-reviewed journals. Chapter 1 contains an introduction about the problem statement and the thesis contributions; Chapter 2 to Chapter 6 are manuscripts containing an abstract, introduction, methods, results and discussion; Chapter 7 provides the conclusions of the work and recommendations for future research directions. The comparison between two adopted CFD software is shown in Appendix.

Chapter 2 to Chapter 4 and Chapter 6 are papers which have already been published, and Chapter 5 has just been submitted for publication in a peer-reviewed journal. The contribution of **A. Yousefi** consisted mainly of developing the CFD models, performing the engine tests, comparison and validation between numerical predictions and experimental measurements, data analysis, and preparing the first drafts of manuscripts. My supervisors (Dr. Birouk and Dr. Guo) supervised the research, including constant feedback during the development of the model, analysis of data and manuscripts preparations. My Co-author (Mr. Liko) contribution in Chapter 5 consisted of preparing and running the engine setup during the experiments.

Copyright notice

1. With permission from Elsevier:

A. Yousefi, M. Birouk, H. Guo. An experimental and numerical study of the effect of diesel injection timing on natural gas/diesel dual-fuel combustion at low engine load. Fuel, 203 (2017) 642-657.

2. With permission from Elsevier:

A. Yousefi, H. Guo, M. Birouk. Experimental and numerical study on diesel injection split of a natural gas/diesel dual-fuel engine at a low engine load. Fuel 212 (2018) 332-346.

3. With permission from Elsevier:

A. Yousefi, H. Guo, M. Birouk. Effect of diesel injection timing on the combustion of natural gas/diesel dual-fuel engine at low-high load and low-high speed conditions, Fuel 235 (2019), 838-846.

4. With permission from Elsevier:

A. Yousefi, H. Guo, M. Birouk. Effect of swirl ratio on natural gas/diesel dual-fuel engine under different engine load-speed conditions, Applied Energy 229 (2018) 375-388.

5. With permission from Elsevier

A. Yousefi, H. Guo, M. Birouk, B. Liko. On greenhouse gas emissions and thermal efficiency of natural gas/diesel dual-fuel engine at low load conditions: Coupled effect of injector rail pressure and split injection, Applied Energy (2018) Submitted.

Chapter 1: Introduction

1.1.Background and scope

Compression ignition (CI) diesel engines are the most common internal combustion (IC) engines in the transportation and power generation industries owing to their excellent efficiency and overall performance. A primary drawback of CI diesel engines is the high level of particulate matter (PM) and nitrogen oxides (NO_x) emissions, which have always been the main concern to engine manufacturers because of their adverse effects on environment and human health [1]. The increasing energy demand coupled with the ever-increasing fossil fuels' price, their limited availability, and environmental impacts have forced researchers and engine manufactures to review conventional CI diesel engines and consequently develop new combustion strategies that can use alternative fuels. In the last two decades, many research studies focused on combustion strategies and alternative fuels, aiming at improving fuel efficiency and/or reducing emissions. Due to superior thermal efficiency and ultra-low NO_x and soot emissions, advanced combustion strategies such as low temperature combustion (LTC) attracted much more attention [2–4]. In order to reduce NOx emissions, combustion temperature is reduced via the dilution of the in-cylinder combustible mixture by using either excess charge gas to create fuel-lean mixtures or using moderate to high levels of exhaust gas recirculation (EGR),. Moreover, LTC strategies aim at reducing or eliminating soot-forming by increasing pre-combustion mixing and avoiding fuel-rich regions during the combustion process. Fully premixed LTC strategy, also known as homogeneous charge compression ignition (HCCI), typically employs long in-cylinder mixing time prior to combustion or external mixing strategies (e.g., intake port injection) to produce uniform fuel-lean mixtures throughout the combustion chamber. The mixture is compressed and auto-ignited as a result of temperature increase near the end

of the compression stoke and ignition of the whole cylinder charge takes place without any diffusion flame or flame front propagation [5]. In HCCI, auto-ignition is fully controlled by chemical kinetics and therefore decoupled from the timing of fuel injection event [5,6]. HCCI combustion has some benefits relative to conventional combustion modes, such as high thermal efficiency, fuel flexibility, and ultra-low NO_x and soot emissions [7,8]. However, this combustion mode suffers from the inability to control combustion phasing, the lack of reliable auto-ignition, high level of unburned hydrocarbon (UHC) and carbon monoxide (CO) emissions, as well as knock and misfiring under certain operating conditions, all of which made it difficult to implement HCCI combustion in commercial engines [9]. In contrast, heterogeneous LTC strategies (e.g., dual-fuel combustion) have been developed in which two fuels with different reactivity are used to improve the controllability and load range, while at the same time retaining the advantage of high efficiency and low NOx and soot emissions of HCCI combustion [10]. In these combustion strategies, a low reactivity fuel is premixed with the intake air and a high reactivity fuel is directly injected to ignite the gaseous mixture and consequently start the combustion. The ignition timing is more closely coupled to the timing of direct fuel injection event, though chemical kinetics still play a pivotal role [11]. Although dual-fuel combustion is not fully premixed, it uses essentially the same principles as HCCI to achieve low emissions. The distinction between dual-fuel and HCCI combustion is that the charge distribution of dual-fuel combustion is more heterogeneous than HCCI, as it consists of lean and rich regions at the time of ignition.

In common dual-fuel combustion, a homogeneous lean premixed low reactivity fuel and air mixture is compressed rapidly below its auto-ignition temperature, and then ignited by injecting a small amount of a pilot liquid fuel with high reactivity near the top dead center (TDC) [12]. The low cost with the possibility to convert conventional diesel engines into dual-fuel operation with minor modifications is one of the major benefits of this combustion concept. Maintaining the same compression ratio and original diesel injection system while achieving diesel-like efficiency with

much lower PM emissions is another benefit of this combustion concept [13]. Moreover, dual-fuel mode has the flexibility to be switched back to full diesel combustion in the case premixed fuel is unavailable [12].

1.1.1. **Natural gas as alternative fuels for diesel engine**

Natural gas used in vehicles possesses the same composition as the natural gas used for domestic cooking and heat. However, the natural gas used for vehicles is compressed and stored usually in rigid pressurized metallic cylinders at a pressure of 200-248 bar. Natural gas is a hydrocarbon gaseous fuel consisting primarily of methane, with a small amount of other hydrocarbons (i.e. ethane, propane, n-butane and isobutene, and pentanes), carbon dioxide (CO_2), nitrogen, and hydrogen sulfide. The composition and content of natural gas varies slightly depending on the source and the production process. A comparison of the physiochemical properties of natural gas with those of diesel fuel is shown in Table 1-1. With natural gas found in several areas worldwide, either together with other fossil fuels or on its own, it has larger proven reserves compared to crude oil; the current known reserves to production ratio for the natural gas is almost 53% [14].

Table 1-1. Physiochemical properties of natural gas and diesel [14–16]

Fuel properties	Unite	Natural gas	Diesel
Lower heating value (LHV)	(MJ/kg)	38-50	42.5 -43.6
Octane/Cetane number	-	120-130	45-55
Molar mass	(kg/kmol)	16-19	170-204
Stoichiometric air-fuel ratio (AFR)	-	16.4-17.2	14.3-14.6
Stoichiometric mixture density	(kg/m^3)	1.25	830
Auto-ignition temperature	(°C)	540-650	180-316
Adiabatic flame temperature	(°C)	1890	2054
Boiling temperature	(°C)	-162	180-380
Flammability limit in air	(vol. % in air)	4.3-15.2	1-6

Natural gas has lower reactivity compared to diesel in terms of auto-ignition performance. It also has higher hydrogen to carbon ratio (~4.0) compared to gasoline and diesel, and thus burns more cleanly in terms of CO_2 emissions. As a result, natural gas is widely recognized as an alternative fuel

for reducing greenhouse gas (GHG) emissions [17]. Furthermore, natural gas, having methane as the main constituent which is the lowest member in the paraffin family, possesses very small tendency to produce particulate matter (PM) emissions [18].

The utilization of natural gas as the main fuel for heavy-duty diesel engines may have more significant impact on transportation because most transportation fleets are diesel operated [19]. CI diesel engines have inherently higher compression ratio than SI engines, which results in higher thermal efficiency. However, the high auto-ignition temperature and low cetane number of natural gas restrict their direct application in typical CI engines. Therefore, simply compressing natural gas and air mixtures will not ignite the air/fuel mixture, and hence a small amount of liquid fuel must be supplied to initiate the combustion process. The liquid fuel is called pilot fuel which acts as a source of ignition for the gaseous fuel. Therefore, natural gas is often used to power CI engines via dual-fuel mode at which a high cetane number fuel is injected along with the gaseous fuel in order to provide a source of ignition for premixed gaseous fuel/air mixture [15]. In most applications, natural gas is inducted or injected into the intake manifold to mix uniformly with air, and the natural gas-air mixtures is then introduced into the cylinder to be compressed (Figure 1-1a). However, in some applications, natural gas is directly injected into the cylinder via a high pressure direct injection (HPDI) technology shortly after the injection of pilot diesel in the late compression stroke (Figure 1-1b) [20]. At some point during the time interval between the two injections or early of the natural gas injection, the diesel fuel auto-ignites and consequently initiates the combustion of the compressed natural gas air mixture. Natural gas burns in a predominantly non-premixed combustion mode. This stratified combustion provides better fuel economy and more efficient combustion, while it maintains a power output and thermal efficiency comparable to those of conventional diesel engine, especially at low loads. However, the structure of the injector is more complicated and costly. Therefore, the port injection of natural gas (PFI) seems to be more practical since it is easier to

implement in existing diesel engine without serious engine modifications. In this thesis, the PFI natural gas/diesel dual-fuel engine is investigated.

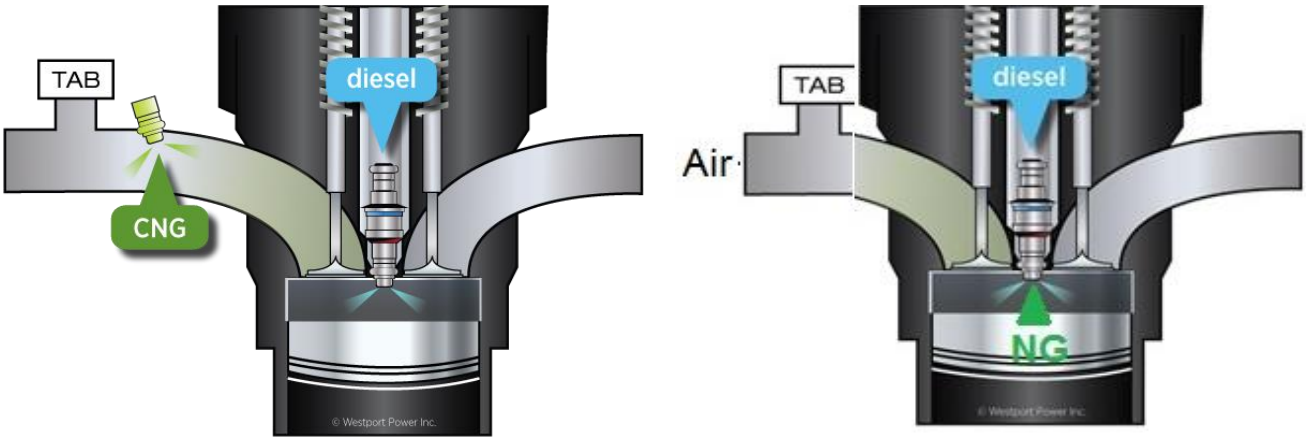

a) Port fuel injection (PFI) dual-fuel engine b) High pressure direct injection (HPDI) dual-fuel engine

Figure 1-1. Schematic of PFI and HPDI dual-fuel engines, Westport engine

1.2. Problem definition and motivation

The combustion process of conventional natural gas/diesel dual-fuel engine takes place in three stages at medium to high engine load conditions, as shown in Figure 1-2a. The first stage consists of premixed combustion of the pilot diesel and a small portion of entrained natural gas/air mixture. The second stage involves diffusion combustion of pilot diesel along with the initiation and flame propagation of natural gas/air mixture. During this stage, the combustion of pilot diesel fuel is mixing-controlled and the premixed natural gas flame propagates from the ignition kernels. The third stage involves diffusion combustion of the residual pilot diesel and subsequent turbulent flame propagation (and sometimes auto-ignition) of natural gas [21,22] (Figure 1-2a).

However, at low to medium engine loads, the equivalence ratio of the natural gas/air mixture is lower than the flammability limit, and therefore there is almost no flame propagation of natural gas/air mixture. At these conditions, the bulk of energy release comes from the ignition and subsequent rapid combustion of pilot diesel and a small part of entrained natural gas-air mixture ((Figure 1-2b, stages I and II) where higher temperatures and relatively richer mixture regions are present. Only relatively

little contribution to the energy release may come from the bulk of the gaseous fuel-air charge farther away from the diesel spray plume (stage III) [22].

Sections 1.2.1 and 1.2.2 carefully outline the main issues of natural gas/diesel dual-fuel engine under low-medium load and medium-high load conditions, respectively.

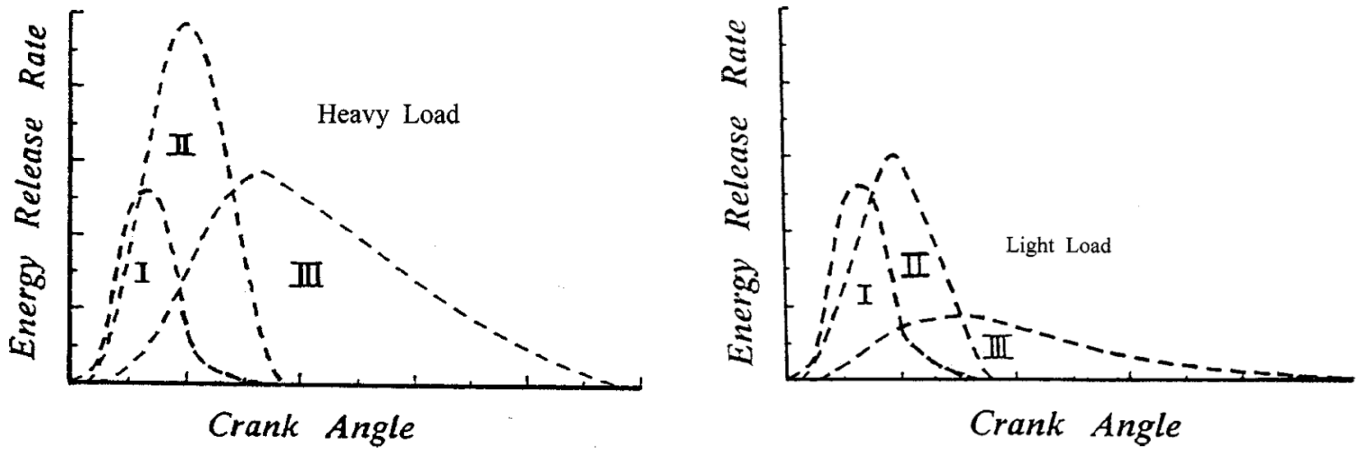

a) Medium to high load b) Low to medium load

Figure 1-2: Schematic representation of the different components of the heat release rate of a conventional dual-fuel engine [22].

1.2.1. Natural gas/diesel dual-fuel engine at low to medium load conditions

Several studies reported that a natural gas/diesel dual-fuel combustion engine is plagued by the problem of unstable combustion performance, low thermal efficiency, and high emissions of unburned methane, CO, and GHG at low to medium engine loads when compared to a diesel engine [15,23,24]. At these engine load conditions, the premixed natural gas-air mixture does not promote the propagation of the flames initiated by the pilot diesel fuel. Thus, the portions of the charge situated far away from the pilot ignition nuclei escape the combustion process. As a consequence, after an initial fast oxidation of the pilot diesel injection, the subsequent combustion process is slow and incomplete, which results in misfiring or partial burning and hence leads to high level of unburned methane and CO emissions at the engine exhaust [25]. These drawbacks offset the benefit of the lower CO_2 emissions in terms of overall GHG emissions, since methane has a global warming impact which is about 20-34 times greater than that of CO_2 over a 100 year period [26]. Therefore, low

thermal efficiency and high unburned methane and CO emissions under low to medium load conditions is a major concern of natural gas/diesel dual-fuel engine.

1.2.2. Natural gas/diesel dual-fuel engine at medium to high load conditions

Natural gas/diesel dual-fuel engines perform better under medium-to-high loads and can often reach or exceed the fuel conversion efficiency of a diesel engine while still generate significantly lower GHG emissions [27–29]. The torque and power of natural gas/diesel duel-fuel operation are also comparable to those of diesel operation under medium to high load conditions [30]. Under these engine load conditions, the premixed natural gas-air mixture is rich enough to guarantee a stable propagation of the flame fronts throughout the in-cylinder charge. Therefore, improved fuel conversion efficiency can be achieved. The amount and the fuel concentration of the induced mixture via the intake port are also increased, resulting in an intensified flow movement and a faster flame propagation, which consequently promotes the burning fuel in later combustion stages. The improvement in fuel utilization causes a dramatic reduction in unburned methane, CO, and GHG emissions [31]. However, stringent emission regulations on NO_x and soot emissions, and the recent targets for GHG emissions reduction have always been the main concern of heavy-duty diesel engine manufacturer. For instance, the U.S. Environmental Protection Agency (EPA) introduced the soot emissions limits of 0.013 g/kW.hr in 2015 for heavy-duty diesel engines. Moreover, EPA has initiated regulations on GHG emissions and fuel efficiency standards for light-duty vehicles by 2018 and heavy-duty vehicles by 2025 [32]. Therefore, further improvement of natural gas/diesel dual-fuel engine under medium to high load conditions is necessary to meet the emission regulations and fuel efficiency of future.

1.3. Research objectives

The purpose of this thesis is to examine different methods/approaches with the aim to enhance combustion performance and reduce emissions of unburned methane, CO, NOx, soot, and GHG in

natural gas/diesel dual-fuel engines under different engine load-speed conditions. In particular, the main focus of this thesis is put on low load conditions where GHG emissions of conventional natural gas/diesel dual-fuel engine is much higher than that of conventional diesel engine. In addition to the experimental study, a computational fluid dynamic (CFD) model based on AVL FIRE or CONVERGE 2.4 are developed to provide further details in order to optimize and help understand the behaviour of natural gas/diesel dual-fuel combustion process under different engine load-speed conditions. The specific objectives of the present thesis are:

- Understand the underlying phenomenon of the effect of diesel injection timing on natural gas/diesel dual-fuel engine at low load-low speed conditions.
- Examine the effect of diesel injection split on natural gas/diesel dual-fuel engine at low load-low speed conditions.
- Examine the effect of diesel injection timing on the combustion of natural gas/diesel dual-fuel engine at low-high load and low-high speed conditions.
- Investigate the effect of diesel injection rail pressure and diesel split injection on greenhouse gas emissions and thermal efficiency of natural gas/diesel dual-fuel engine at low load conditions.
- Optimize the initial swirl ratio on the combustion performance of natural gas/diesel dual-fuel engine under low-high load conditions.

1.4. Outline of the thesis

As mentioned above, the main objective of this thesis is to examine different strategies aiming to improve the thermal efficiency and emissions of unburned methane, CO, GHG, and NOx of natural gas/diesel dual-fuel engine. A roadmap of the research undertaken in this thesis is schematically presented in Figure 1-3. The thesis is organized as follows:

Chapter 2 presents the experimental results of the effect of diesel injection timing (-10 to -50 °ATDC) on the combustion performance and emissions of natural gas/diesel dual-fuel engine at engine load of BMEP=4.05 bar and engine speed of 910 RPM. In addition, a CFD model based on AVL-FIRE –CHEMKIN software is developed to provide an insight into the optimization mechanism of diesel injection timing.

The effect of diesel injection split on the combustion performance and emissions of natural gas/diesel dual-fuel engine under the same engine load speed condition is studied in Chapter 3 based on the developed CFD model in Chapter 2. The predicted results are compared with the measured data and the fundamental mechanism of split injection is investigated.

Chapter 4 presents the effect of diesel injection timing on natural gas/diesel dual-fuel engine under low to high load and low to high speed conditions. A new CFD model based on CONVERGE 2.4 software is developed to investigate the underlying phenomenon. The new model has the capability to predict flame propagation which cannot be predicted using the AVL-FIRE software under medium-high load conditions. This is the main reason that CONVRGE software is introduced as a more reliable CFD tool for the rest of this thesis. More details can be found in Appendix.

Chapter 5 experimentally and numerically investigates the coupled effects of rail pressure increase and diesel fuel split injection on thermal efficiency and GHG emissions of natural gas/diesel dual-fuel engine at engine load of 4.05 bar and speed of 910 RPM. In this chapter, the results of dual-fuel engine when simultaneously changing diesel fuel split injection and increase rail pressure are compared with those of dual-fuel and diesel engines with the combination of increased rail pressure and single injection.

Chapter 6 numerically investigates the influence of swirl ratio on the combustion performance and emissions of a natural gas/diesel dual-fuel engine under low to high load conditions. An extensive study is performed under different engine load-speed conditions in order to optimize swirl ratio. A computational optimization based on CONVERGE 2.4 software is conducted by considering the

combustion and emissions under three engine load-speed conditions, a low load-low speed (BMEP=4.05 bar and rpm=910), a high load-low speed (BMEP=17.6 bar and rpm=1120), and a medium load-high speed (BMEP=11.24 bar and rpm=1750) in order to identify an optimal swirl ratio.

Finally, Chapter 7 summarizes the key findings of this thesis and outlines some recommendations for future work.

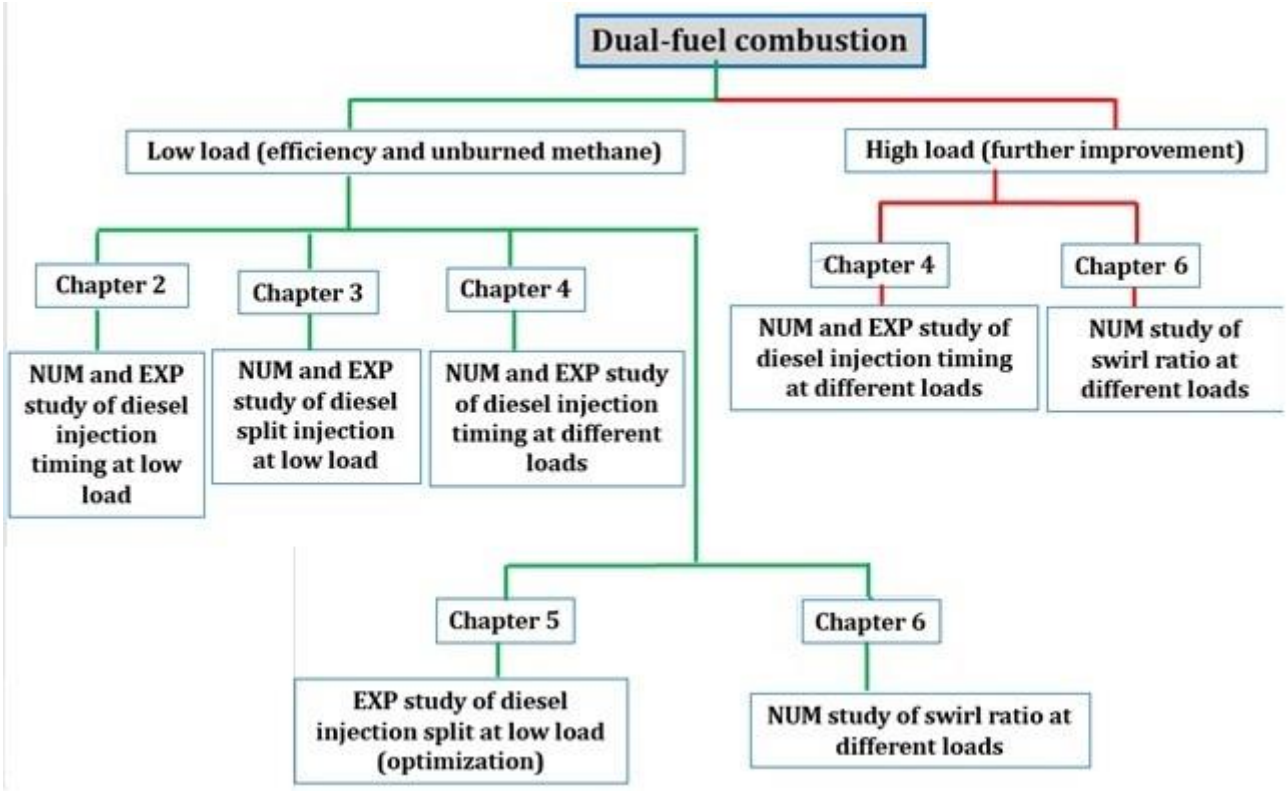

Figure 1-3. Schematic roadmap of the research performed in this thesis.

1.5. References

[1] Imran A, Varman M, Masjuki HH, Kalam MA. Review on alcohol fumigation on diesel engine: A viable alternative dual fuel technology for satisfactory engine performance and reduction of environment concerning emission. Renew Sustain Energy Rev 2013;26:739–51. doi:10.1016/j.rser.2013.05.070.

[2] Zhou DZ, Yang WM, An H, Li J, Shu C. A numerical study on RCCI engine fueled by biodiesel/methanol. Energy Convers Manag 2015;89:798–807.

doi:10.1016/j.enconman.2014.10.054.

[3] Jung D, Iida N. Closed-loop control of HCCI combustion for DME using external EGR and rebreathed EGR to reduce pressure-rise rate with combustion-phasing retard. Appl Energy 2015;138:315–30. doi:10.1016/j.apenergy.2014.10.085.

[4] Asad U, Kumar R, Zheng M, Tjong J. Ethanol-fueled low temperature combustion: A pathway to clean and efficient diesel engine cycles. Appl Energy 2014;157:838–50. doi:10.1016/j.apenergy.2015.01.057.

[5] Hairuddin AA, Yusaf T, Wandel AP. A review of hydrogen and natural gas addition in diesel HCCI engines. Renew Sustain Energy Rev 2014;32:739–61. doi:10.1016/j.rser.2014.01.018.

[6] Komninos NP, Rakopoulos CD. Modeling HCCI combustion of biofuels: A review. Renew Sustain Energy Rev 2012;16:1588–610. doi:10.1016/j.rser.2011.11.026.

[7] Canakci M. Combustion characteristics of a DI-HCCI gasoline engine running at different boost pressures. Fuel 2012;96:546–55. doi:10.1016/j.fuel.2012.01.042.

[8] Bendu H, Murugan S. Homogeneous charge compression ignition (HCCI) combustion: Mixture preparation and control strategies in diesel engines. Renew Sustain Energy Rev 2014;38:732–46. doi:10.1016/j.rser.2014.07.019.

[9] He BQ, Liu M Bin, Zhao H. Comparison of combustion characteristics of n-butanol/ethanol-gasoline blends in a HCCI engine. Energy Convers Manag 2015;95:101–9. doi:10.1016/j.enconman.2015.02.019.

[10] Reitz RD, Duraisamy G. Review of high efficiency and clean reactivity controlled compression ignition (RCCI) combustion in internal combustion engines. Prog Energy Combust Sci 2015;46:12–71. doi:10.1016/j.pecs.2014.05.003.

[11] Musculus MPB, Miles PC, Pickett LM. Conceptual models for partially premixed low-

temperature diesel combustion. vol. 39. Elsevier Ltd; 2013. doi:10.1016/j.pecs.2012.09.001.

[12] Karim G a. A Review of Combustion Processes in the Dual Fuel Engine - The Gas Diesel Engine. Prog Energy Combust Sci 1980;6:277–85. doi:10.1016/0360-1285(80)90019-2.

[13] Carlucci AP, Laforgia D, Saracino R, Toto G. Combustion and emissions control in diesel-methane dual fuel engines: The effects of methane supply method combined with variable in-cylinder charge bulk motion. Energy Convers Manag 2011;52:3004–17. doi:10.1016/j.enconman.2011.04.012.

[14] Hegab A, La Rocca A, Shayler P. Towards keeping diesel fuel supply and demand in balance: Dual-fuelling of diesel engines with natural gas. Renew Sustain Energy Rev 2017;70:666–97. doi:10.1016/j.rser.2016.11.249.

[15] Li W, Liu Z, Wang Z. Experimental and theoretical analysis of the combustion process at low loads of a diesel natural gas dual-fuel engine 2016. doi:10.1016/j.energy.2015.11.052.

[16] Hao H, Liu Z, Zhao F, Li W. Natural gas as vehicle fuel in China: A review. Renew Sustain Energy Rev 2016;62:521–33. doi:10.1016/j.rser.2016.05.015.

[17] Li M, Zhang Q, Li G, Shao S. Experimental investigation on performance and heat release analysis of a pilot ignited direct injection natural gas engine. Energy 2015;90:1251–60. doi:10.1016/j.energy.2015.06.089.

[18] Papagiannakis RG, Rakopoulos CD, Hountalas DT, Rakopoulos DC. Emission characteristics of high speed, dual fuel, compression ignition engine operating in a wide range of natural gas/diesel fuel proportions. Fuel 2010. doi:10.1016/j.fuel.2009.11.001.

[19] Wei L, Geng P. A review on natural gas/diesel dual fuel combustion, emissions and performance. Fuel Process Technol 2016. doi:10.1016/j.fuproc.2015.09.018.

[20] McTaggart-Cowan GP, Jones HL, Rogak SN, Bushe WK, Hill PG, Munshi SR. The Effects

of High-Pressure Injection on a Compression–Ignition, Direct Injection of Natural Gas Engine. J Eng Gas Turbines Power 2007;129:579. doi:10.1115/1.2432894.

[21] Sahoo BB, Sahoo N, Saha UK. Effect of engine parameters and type of gaseous fuel on the performance of dual-fuel gas diesel engines-A critical review. Renew Sustain Energy Rev 2009. doi:10.1016/j.rser.2008.08.003.

[22] Karim GA. Combustion in Gas Fueled Compression: Ignition Engines of the Dual Fuel Type. J Eng Gas Turbines Power 2003;125:827. doi:10.1115/1.1581894.

[23] Mousavi SM, Saray RK, Poorghasemi K, Maghbouli A. A numerical investigation on combustion and emission characteristics of a dual fuel engine at part load condition. Fuel 2016;166:309–19. doi:10.1016/j.fuel.2015.10.052.

[24] Lounici MS, Loubar K, Tarabet L, Balistrou M, Niculescu DC, Tazerout M. Towards improvement of natural gas-diesel dual fuel mode: An experimental investigation on performance and exhaust emissions. Energy 2014. doi:10.1016/j.energy.2013.10.091.

[25] Abdelaal MM, Hegab AH. Combustion and emission characteristics of a natural gas-fueled diesel engine with EGR. Energy Convers. Manag., 2012. doi:10.1016/j.enconman.2012.05.021.

[26] Hongsheng Guo, Brian Liko AY. Effect of Diesel Injection Split on Combustion and Emissions Performance of a Natural Gas–Diesel Dual Fuel Engine at a Low Load Condition. Proc Combust Inst – Can Sect 2018;1. doi:10.1115/ICEF2017-3584.

[27] Hosmath RS, Banapurmath NR, Khandal S V., Gaitonde VN, Basavarajappa YH, Yaliwal VS. Effect of compression ratio, CNG flow rate and injection timing on the performance of dual fuel engine operated on honge oil methyl ester (HOME) and compressed natural gas (CNG). Renew Energy 2016;93:579–90. doi:10.1016/j.renene.2016.03.010.

[28] Krishnan SR, Srinivasan KK, Singh S, Bell SR, Midkiff KC, Gong W, et al. Strategies for Reduced NO[sub x] Emissions in Pilot-Ignited Natural Gas Engines. J Eng Gas Turbines Power 2004;126:665. doi:10.1115/1.1760530.

[29] Nithyanandan K, Zhang J, Li Y, Meng X, Donahue R, Lee C-F, et al. Diesel-Like Efficiency Using Compressed Natural Gas/Diesel Dual-Fuel Combustion. J Energy Resour Technol 2016;138:052201. doi:10.1115/1.4032621.

[30] Abdelaal MM, Hegab AH. Combustion and emission characteristics of a natural gas-fueled diesel engine with EGR. Energy Convers Manag 2012;64:301–12. doi:10.1016/j.enconman.2012.05.021.

[31] Lounici MS, Loubar K, Tarabet L, Balistrou M, Niculescu DC, Tazerout M. Towards improvement of natural gas-diesel dual fuel mode: An experimental investigation on performance and exhaust emissions. Energy 2014;64:200–11. doi:10.1016/j.energy.2013.10.091.

[32] Hockett A, Hampson G, Marchese AJ. Development and Validation of a Reduced Chemical Kinetic Mechanism for Computational Fluid Dynamics Simulations of Natural Gas/Diesel Dual-Fuel Engines. Energy & Fuels 2016;30:2414–27. doi:10.1021/acs.energyfuels.5b02655.

Chapter 2: An experimental and numerical study of the effect of diesel injection timing on natural gas/diesel dual-fuel combustion at low load

2.1. Abstract

Natural gas/diesel dual-fuel combustion compression ignition engine has the potential to reduce NO_x and soot emissions. However, this combustion mode still suffers from low thermal efficiency and high level of unburned methane and CO emissions at low load conditions. The present paper reports the results of an experimental and numerical study on the effect of diesel injection timings (ranging from 10 to 50 °BTDC) on the combustion performance and emissions of a heavy duty natural gas/diesel dual-fuel engine at 25% engine load. Both experimental and numerical results revealed that advancing the injection timing up to 30 °BTDC increases the maximum in-cylinder pressure. However, with further advancing the injection timing up to 50 °BTDC, the maximum in-cylinder pressure decreases which is mainly due to the lower in-cylinder temperature before SOC. Moreover, the analysis of OH spatial distribution shows that, at very advanced diesel injection timings, the non-reactive zones are much narrower than later injection timings during the last stages of combustion, indicating a more predominant premixed combustion mode. At retarded diesel injection timings, the consumption of premixed fuel in the outer part of the charge is likely to be a significant challenge for dual-fuel combustion engine at low engine load conditions. However, with advancing the diesel injection timing, the OH radical becomes more uniform throughout the combustion chamber, which confirms that high temperature combustion reactions can occur in the central part of the charge. Diesel injection timing of 30 °BTDC appears to be the conversion point of all conventional dual-fuel combustion modes. Further advancing diesel injection timing beyond this point (30 °BTDC) results in noticeable reduction in NO_x and unburned methane emissions, while CO emissions exhibit only

slight drop. However, at very advanced diesel injection timings of 46 and 50 °BTDC, NO_x and unburned methane emissions continue to drop, whereas CO emissions tend to increase. The results showed also that the highest indicated thermal efficiency is achieved at these very advanced diesel injection timings of 46 and 50 °BTDC. Finally, the results revealed that, by advancing diesel injection timing from 10 °BTDC to 50 °BTDC, NO_x, unburned methane, and CO emissions are reduced, respectively, by 65.8%, 83%, and 60% while thermal efficiency is increased by 7.5%.

Abbreviations

ADIT	After Diesel Injection Timing	$ISNO_x$	Indicated Specific NO_x
AHR	Accumulated Heat Release	ITE	Indicated Thermal Efficiency
ASOC	After Start of Combustion	IVC	Inlet Valve Closing
BDC	Bottom Dead Center	IVO	Inlet Valve Opening
BMEP	Break Mean Effective Pressure	KH	Kelvin-Helmholtz
BTDC	Before Top Dead Center	LHV	Lower Heating Value
CA_{50}	Crank Angle of 50% Accumulated Heat Release	LTC	Low Temperature Combustion
CFD	Computational Fluid Dynamic	NO_x	Nitrogen Oxides
CI	Compression Ignition	PFI	Port Fuel Injection
CO	Carbon Oxide	PISO	Pressure Implicit with Splitting of Operators
COV	Coefficient of Variation	PM	Particulate Matter
DI	Direct Injection	PRR	Pressure Rise Rate
DIT	Diesel Injection Timing	RANS	Reynolds Averaged Navier-Stokes
EGR	Exhaust Gas Recirculation	RCCI	Reactivity Controlled Compression Ignition
EVC	Exhaust Valve Closing	RNG	Renormalization Group
EVO	Exhaust Valve Opening	RT	Rayleigh-Taylor
HCCI	Homogeneous Charge Compression Ignition	SOC	Start of Combustion
HRR	Heat Release Rate	TDC	Top Dead Center
IMEP	Indicated Mean Effective Pressure	UHC	Unburned Hydrocarbon
$ISCH_4$	Indicated Specific CH_4	ULSD	Ultra-Low-Sulfur Diesel
ISCO	Indicated Specific CO	VCR	Variable Compression Ratio

2.2. Introduction

Diesel engine has been widely used in transportation, due to mainly its higher reliability and superior fuel conversion efficiency. However, due to locally rich air-fuel mixture and non-uniform temperature distribution in the combustion chamber, it is very difficult to reduce simultaneously NO_x and soot emissions for diesel engine [1,2]. Recent stringent regulations on environmental pollutants and the ever-increasing fossil fuel price, as well as the urgent need to reduce fossil fuel dependency, prompted further research efforts to review and improve the performance of conventional diesel engine [3]. Several studies proposed a variety of advanced combustion strategies originated from low

temperature combustion (LTC) concepts. These alternative combustion strategies are generally centred on completely or partially homogeneous and lean premixed charge, lower local equivalence ratios, improved fuel atomization and mixture preparation, reduced in-cylinder peak temperature, and alternative fuels [4–8]. One of the most promising alternative combustion strategies is dual-fuel combustion which consists of the preparation of a premixed fuel (main fuel) and intake air, whose ignition is triggered by the injection of a small amount of a more ignitable fuel, usually diesel fuel. A typical dual-fuel combustion combines port fuel injection (PFI) of a low reactivity fuel to create a well-mixed charge of the main premixed fuel and air, and the direct injection of high reactivity fuel (i.e., diesel) as an ignition source. Because of its higher ignition temperature, natural gas is a suitable candidate for the low reactivity fuel of dual-fuel combustion. The normal combustion process in a natural gas/diesel dual-fuel engine takes place in three stages. The first stage consists of premixed combustion of the pilot diesel and a small portion of entrained natural gas fuel. Due to the high activation energy and the resulting high auto-ignition temperature of natural gas, the combustion of premixed diesel formed during pilot fuel ignition delay is the main contributor in this stage, during which a rapid pressure rise occurs resulting from the initiation of diesel combustion. The second stage involves diffusion combustion of pilot diesel along with the initiation and flame propagation of natural gas combustion. During this stage, the combustion of pilot diesel fuel is mixing-controlled and the premixed natural gas flame propagates from the ignition kernels. The third stage involves diffusion combustion of the residual pilot diesel and late combustion phase of natural gas [9–12].

Using natural gas in dual-fuel compression ignition (CI) engines has attracted much attention due to its high efficiency [13–15]. In fact, this technology is currently in use in public transportation buses, stationary power generation, and large-scale ships [7]. Natural gas/diesel dual-fuel combustion tends to retain most of the positive features of conventional diesel engine and even surpasses occasionally those of conventional diesel engine, producing comparable power output and efficiency at different engine loads. In addition, significantly reduced NO_x and soot emissions can also be

achieved [16–18]. Moreover, this combustion concept relies on natural gas fuel as the major energy resource, which consequently alleviates diesel fossil fuel dependency. Furthermore, the low cost associated with the conversion of a conventional diesel engine to a PFI natural gas fuelled diesel engine with minor alterations is another benefit of this combustion concept. Additionally, dual-fuel combustion mode allows switching back to fully diesel combustion in case premixed fuel is unavailable [19].

However, some technical issues are still unresolved when CI engine operates under natural gas/diesel dual-fuel mode at low load conditions [20–25]. Compared to diesel fuel engine, natural gas/diesel dual-fuel engine is known to experience unstable combustion performance, low thermal efficiency, and high levels of unburned methane and CO emissions at low load conditions. This is because that, at low loads and with small quantities of pilot diesel, flame propagation front does not reach portions of the charge situated far away from the pilot ignition nuclei. As a consequence, after an initial fast oxidation of the injected pilot fuel, the rate of combustion slows down leading to incomplete combustion, which in turn results in misfiring or partial burning and hence high level of unburned methane and CO emissions at the engine exhaust [18,25,26]. Reducing unburned methane emissions in dual-fuel combustion mode is important because of the strong greenhouse effect of methane, which is 25 times greater than that of carbon dioxide over a 100 year period [27]. Many studies have addressed these issues by examining the effect of combustion boundaries, such as pilot diesel injection timing and pressure [23,28–31], natural gas energy fraction [32–36], variable compression ratio (VCR) [37–39], liquid biofuels as pilot fuel [40,41], natural gas injection timing [31,42], and the use of exhaust gas recirculation (EGR) [25,43]. Amongst these strategies, diesel (or pilot liquid fuel) injection timing is of great interest and is usually regarded as a critical factor which has influence on the combustion phasing and emissions characteristics of natural gas/diesel dual-fuel engines at low load conditions.

For dual-fuel combustion engine, diesel injection timing affects the ignition delay because the in-cylinder charge temperature and pressure change significantly close to the top dead center (TDC). Advancing diesel injection timing usually increases the ignition delay because the in-cylinder mean charge temperature and pressure are lower. However, retarding or advancing diesel injection timing beyond certain limits may result in poor combustion efficiency. Variation of diesel injection timing has also strong effect on NO_x formation [44]. Retarding diesel injection timing may help to control NO_x emissions with substantial penalty in fuel consumption, and also an increase in CO, UHC, and PM emissions at low load. Therefore, finding an optimum injection timing for the best performance and emissions are of great importance to natural gas/diesel dual-fuel combustion at low engine loads.

The present study reports a detailed experimental and numerical investigation of the effect of diesel injection timing on the combustion performance and emissions of natural gas/diesel dual-fuel combustion at low load. A single-cylinder diesel engine is modified to operate in natural gas/diesel dual-fuel mode with natural gas as the primary fuel (75% natural gas energy fraction) and diesel as the pilot fuel. In both experiment and simulation, the operating/test conditions are kept constant and only the pilot diesel injection timing is varied (10-50° BTDC with 4° increment) to examine the combustion performance and emissions of dual-fuel engine under 25% engine load (BMEP= 4.05 bar). Moreover, a computational fluid dynamic (CFD) model based on AVL FIRE-CHEMKIN software is developed to provide further details in order to help understand the behaviour of natural gas/diesel dual-fuel combustion process at a low engine load. The in-cylinder pressure, heat release rate (HRR), combustion phasing (CA_{50}), thermal efficiency, and engine out emissions are carefully evaluated under dual-fuel operation at low load conditions. The ultimate aim of the comprehensive numerical analysis of the combustion performance and emissions is to provide an insight into the optimization of pilot injection timing under dual-fuel mode.

2.3. Experimental setup and procedure

2.3.1. Test engine

The engine used in this investigation is a modified single-cylinder version of Caterpillar's 3400-series heavy-duty engine. More details about the experimental setup and engine configuration can be found elsewhere [45]. Table 2-1 shows the specifics of the engine.

Natural gas was injected into the intake port by a fuel injection manifold. Diesel fuel was directly injected into the cylinder using a prototype common-rail fuel injector system. The start of injection and injection pulse width for both diesel and natural gas were controlled by a driven system provided by National Instruments and LabVIEW-based software. The flow rates of diesel, natural gas, and air were measured by a TRICOR mass flowmeter, a Bronkhorst mass flowmeter, and a turbine mass flowmeter, respectively.

Table 2-1. Engine specifications

Engine type	Single cylinder-caterpillar 3400 heavy duty engine
Bore×Stroke	137.2 mm ×165.1 mm
Conn. rod length	261.62 mm
Displacement vol.	2.44 L
Compression ratio	16.25
Diesel fuel injector	Common rail injector
Injector tip length	1.51 mm
Number of nozzle hole×diameter	6×0.23 mm
Natural gas injection timing	-355 °ATDC
Inlet valve opening (IVO)	-358.3 °ATDC
Inlet valve closing (IVC)	-169.7 °ATDC
Exhaust valve opening (EVO)	145.3 °ATDC
Exhaust valve closing (EVC)	2.3 °ATDC

2.3.2. Fuels and their supply systems

Diesel fuel used in this study was a Canadian ultra-low-sulfur diesel (ULSD) derived from oil sands sources, and the natural gas used in this research was supplied by Enbridge Inc. Table 2-2 displays the properties of both diesel and natural gas used in this study.

Table 2-2. Fuel properties

Fuel type	**Natural gas**	**Diesel**
Density (kg/m^3)		814.8
Cetane number	-	44
LHV (MJ/kg)	48.4	44.643
Viscosity (cSt 40 °C)		1.483
H/C ratio	-	1.897
Component (% Vol.)	Methane: 95.691 Ethane: 2.404 Propane: 0.414 Butane: 0.058 Nitrogen: 0.833 Carbon dioxide: 0.6	

2.3.3. Test procedure and conditions

The experiments were conducted at an engine speed of 910 rpm and a brake mean effective pressure (BMEP) of 4.05 bar, which corresponded to 25% engine load. The intake temperature was kept constant at 40 $^{\circ}$C during the experiments. The intake and exhaust manifold pressures were kept at 1.05 and 1.20 bar, respectively. The diesel injector rail pressure was 525 bar. EGR was not used in this study. During the tests, a sweep of the start of diesel injection timing was conducted. Table 2-3 shows details of the diesel injection timings tested in the experiments.

Table 2-3. Experimental test cases - diesel injection timing sweep under 75% natural gas energy fraction and 25% engine load.

Case no.	**P_{intake} (bar)**	**T_{intake} (K)**	**$P_{exhaust}$ (bar)**	**Speed (rpm)**	**SOI (°BTDC)**	**EOI (°BTDC)**	**Air flow (kg/h)**	**Diesel flow (kg/h)**	**NG flow (kg/h)**
1					10	3.57	66.93	0.5238	1.470
2					14	7.71	67.21	0.4948	1.389
3					18	11.81	67.57	0.4710	1.306
4					22	15.89	67.45	0.4503	1.259
5					26	19.95	67.08	0.4370	1.237
6	1.05	313	1.2	910	30	23.86	66.70	0.4552	1.234
7					34	27.99	67.24	0.4337	1.215
8					38	32.01	67.62	0.4314	1.199
9					42	36.04	67.73	0.4167	1.190
10					46	40.12	67.65	0.4122	1.179
11					50	44.15	67.85	0.4134	1.164

2.4. Numerical model

2.4.1. Flow and combustion modelling

In order to better understand the combustion process and pollutant formation mechanisms of the natural gas/diesel dual-fuel engine, numerical simulations were performed using AVL FIRE v2014 software coupled with CHEMKIN solver for flow and chemistry calculations. Both flow and combustion were modelled by solving the complete set of Navier-Stokes equations. CHEMKIN package was used to acquire reactions rates and thermal and transport properties of species. A reactions mechanism, consisting of 42 species and 168 reactions, developed at Chalmers University [46] and validated at engine relevant conditions by Aggarwal [47]was used in the calculation. In this chemical mechanism, n-heptane was used to represent diesel, and methane was used to represent natural gas. Renormalization group (RNG) k-ε turbulence model, Reynolds Averaged Navier-Stokes (RANS), and pressure implicit with splitting of operators (PISO) algorithm were used to simulate the transient turbulent flow in the combustion chamber [48]. At each time step, conservation equations of momentum, mass, energy, and pressure were solved. After correcting mass fluxes and velocities for the new pressure field, the boundary conditions were updated. The ‘’Kong-Reitz’’ combustion model was used in the simulation. It assumes that the reaction rate of each species is determined by the kinetic process and the relative magnitude of mixing and reaction, which can be characterized by a local Damköhler number defined as the ratio of flow mixing to kinetic time scale [49]. In the present study, the flow behaviour near the cylinder wall and the heat transfer between the working fluid and the cylinder wall were modeled using the Hybrid Wall Treatment and Standard Wall Function models [50]. The Heywood original NO_x mechanism was used in this study to account for thermal and prompt NO_x formation [50].

2.4.2. Spray modelling

The Euler-Lagrangian approach was employed in this study. The Lagrangian formulation was used to track droplets motion through the flow field, and the Eulerian formulation was used to solve the gas phase. In the Eulerian approach, the conservation equations of mass, momentum, and enthalpy were solved. The liquid and gas phase coupling was achieved by introducing adequate source terms for the equations of mass, momentum, and enthalpy. The break-up process of diesel spray was simulated using WAVE model based on the physical properties (for the spray and mixing process) of diesel fuel [51]. In this model, the growth of an initial perturbation on the liquid surface is linked to its wavelength and other physical and dynamic parameters of the injected fuel and the in-cylinder gas. There exist two break-up regimes, one for high velocity Kevin-Helmholtz (KH) type and the other for low velocity Rayleigh-Taylor (RT) type break-up [52]. For the first case, the size of droplets is set equal to the wavelength of the fastest growing or most probable unstable surface wave. Rayleigh type break-up produces droplets that are larger than the original parent drops. This regime is not important for high pressure injection systems. The use of WAVE model in the present study, which was developed for KH instabilities, is an appropriate approach for high pressure injection system [51]. Primary parcels (blobs) are injected with a diameter similar to the nozzle orifice and a velocity which is a function of the injected mass flow rate. Particles passing through the flow interact with turbulent eddies. Such interaction results in deflecting particles by the instantaneous velocity of turbulent eddies and particles inertia. This additional turbulence effect on the spray particles could not be resolved by the flow field and consequently the O'Rourke turbulent dispersion model was used in the present study [51].

Dukowicz model [53] was used for the heat-up and evaporation of droplets. It assumes that droplets evaporate in a non-condensable gas environment. Therefore, it uses a two-component system in the gas-phase which consists of vapor and non-condensable gas where each component may be composed of a mixture of different species.

Wall interaction of liquid droplets can play a major role for direct injection (DI) engines. Especially for small bore diesel engines, since the distance between the injector and the bowl can be very small, large parts of the fuel hit the wall before they atomize or evaporate. This influences the combustion process and consequently pollutant formation, as incomplete combustion in the vicinity of the wall leads to high UHC and soot emissions. The behavior of the interaction between a droplet and a wall depends on several parameters, such as droplet velocity, diameter, properties, and wall surface roughness and temperature. In the present study, the Wall jet model, which is based on the spray/wall impingement model of Naber and Reitz [54], was used to simulate the droplet interaction with the cylinder wall. This model assumes that a droplet which hits the wall either rebounds or reflects depending on Weber number.

2.4.3. Computational domain and initial conditions

The computational mesh was created by FIRE ESE-Diesel platform. Since the diesel injector has six equally spaced nozzle's orifices, a sector mesh of 60° was used to model one spray plume to take advantage of the axial symmetry. To ensure mesh independency, an optimized average cell size of 1.5 mm consisting of 22,049 control volumes at the top dead center (TDC) and 56,593 control volumes at the bottom dead center (BDC) was used. Further refinement on the mesh resolution up to 1 mm did not produce any significant improvement in the accuracy of the predictions, while the required computational runtime was 30% longer. The simulation time step was varied in the range from 0.2 to 0.5 crank angle (°CA) based on temporal gradients of the computed parameters. Computation was performed in series on 8 cores and lasted approximately 6 hours CPU time. The computational domain at the TDC is shown in Figure 2-1. The boundary conditions at the engine head and piston surfaces were defined as impermeable wall boundary conditions. The cylinder geometry was assumed to be symmetric around the cylinder axis, and cyclic boundary conditions were applied to the cutting surfaces as shown in Figure 2-1.

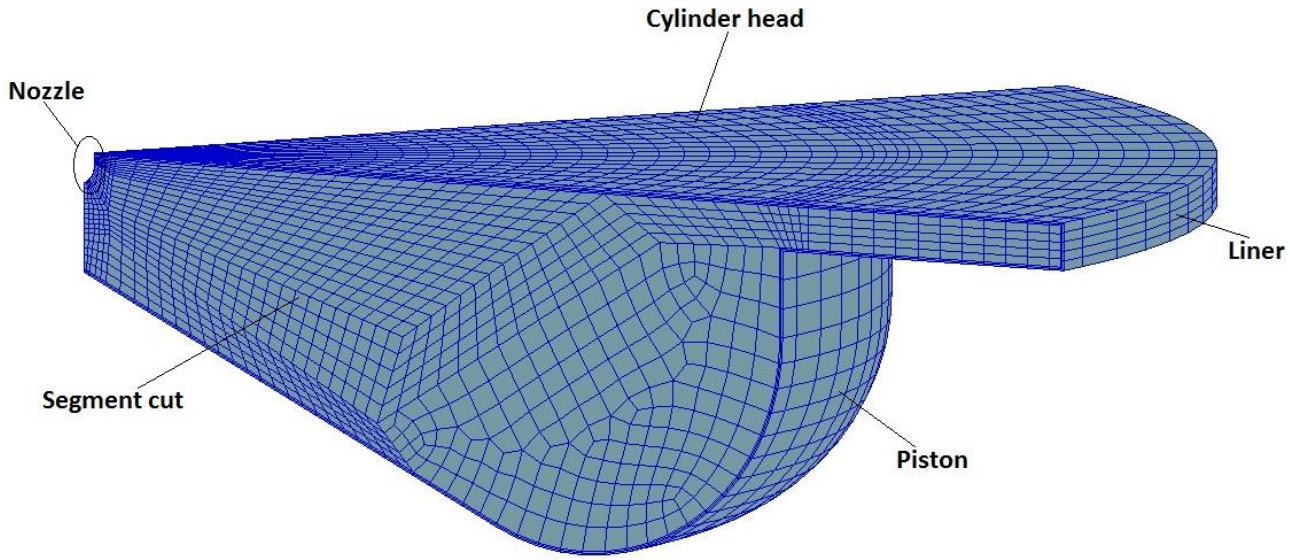

Figure 2-1. Computational domain of the combustion chamber at the TDC.

Simulation was initialized at IVC and terminated prior to EVO. The port fuel injected natural gas was considered to be homogeneously mixed with air at IVC. Table 2-4 provides the boundary and initial conditions for the numerically simulated cases. During the simulation, the initial conditions, cylinder wall temperature, and spray model constants were adjusted and held unchanged for all additional simulations. For instance, the in-cylinder wall temperature and model constants were adjusted based on experimental in-cylinder pressure and HRR of diesel injection timing of 30 °BTDC (case 6). After this adjustment, the simulated in-cylinder pressure and HRR matched experimental data and all initial conditions, model constants, and wall temperature were held unchanged for other diesel injection timings. This is because during the experiment, the intake conditions, wall temperature, and fuel injector properties were kept constant, while diesel injection timing on natural gas/diesel dual-fuel combustion was varied.

Table 2-4. Initial and boundary conditions

Boundary conditions	**Boundary type/specific condition**
Cylinder head	Wall-temperature 400 K
Piston	Mesh movement-temperature 400 K
Segment cut	Periodic inlet/outlet
Liner	Wall-temperature 400 K
Initial conditions	

Pressure at IVC	1.02 bar
Temperature at IVC	360 K
Turb. kin. energy	10 m^2/s^2
Turb. length scale	0.003 m
Turb. diss. Rate	1732 m^2/s^3

2.4.4. Test conditions

According to the experimental test cases (Table 2-3), all test conditions, including engine load (25% load and BMEP=4.05 bar), speed (910 rpm), natural gas energy fraction (75%), diesel injector rail pressure (525 bar), and intake temperature and pressure (P_{intake} = 1.05 bar, T_{intake} = 313 K, and EGR=0%) were kept constant and only the diesel injection timing was swept in the range between 10 and 50 °BTDC with an increment of 4 °CA. It should be noted that, during the experiments, diesel injection timing is indicated by the time at which an electronic trigger is sent to the injector. The occurrence of this in the cycle is selected as the indicated diesel injection timing. Due to the mechanical response of the injector, there is a lag between the indicated and actual diesel injection timing when the diesel fuel exits the injector nozzle into the combustion chamber. However, this lag is not considered in the CFD simulation. The total equivalence ratio for each simulation (i.e., diesel injection timing) case was adjusted to reproduce the experimental conditions, as shown in *Figure 2-2*.

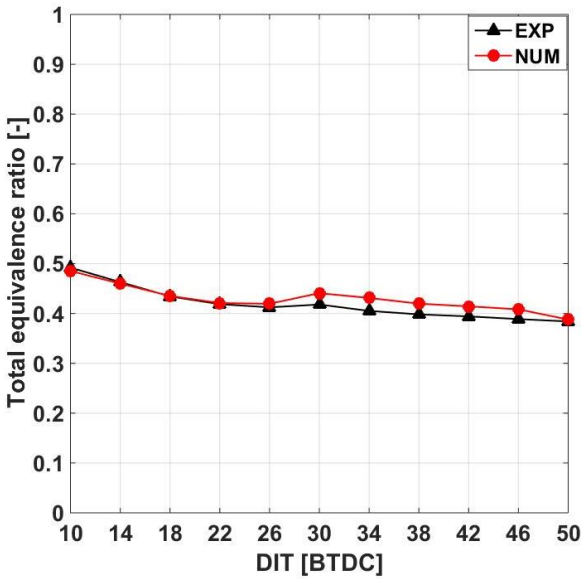

Figure 2-2. Total equivalence ratio versus different diesel injection timings

2.5. Results and discussion

This section reports experimental and numerical results of the effect of diesel injection timing (10-50 °BTDC with step of 4 °CA) on the combustion performance and emissions of natural gas/diesel dual-fuel mode at 25% engine load (BMEP= 4.05 bar). Numerical simulation results (e.g., in-cylinder pressure, HRR, thermal efficiency, and NO_x, CO, unburned methane emissions, and spatial and temporal contours of the mean charge temperature and equivalence ratio) are provided to further help understand the behaviour of natural gas/diesel dual-fuel combustion process at a low engine load.

2.5.1. Effect of diesel injection timing on combustion performance

Figure 2-3 shows the effect of pilot diesel injection timings on the in-cylinder pressure and HRR of natural gas/diesel dual-fuel mode under 25% engine load. It can be seen that there is a perfect match between the measured and calculated in-cylinder pressure and HRR profiles, confirming the ability of the CFD model. Moreover, the numerical simulation successfully captured the measured ignition delay and combustion phasing (CA_{50}), as shown in Figure 2-4. The ignition delay is defined as the crank angle difference between the start of diesel fuel injection and the start of combustion (SOC). The SOC and CA_{50} are, respectively, defined as the crank angle positions of the maximum HRR and 50% accumulated heat release (AHR). The measured heat release rate for each case was calculated from the average in-cylinder pressure based on the first law of thermodynamics and the ideal gas law.

It can be observed from Figure 2-3 that both experimental and numerical results show a significant variation in the behaviour of the in-cylinder pressure when advancing diesel injection timing. Advancing the injection timing up to 30 °BTDC (cases 1-6) increases the maximum in-cylinder pressure and shifts the in-cylinder peak pressure close to the TDC. This is mainly attributed to the variations in the in-cylinder temperature during the diesel injection and before SOC and also to the local equivalence ratio inside the ignition pockets. Figure 2-5 displays the in-cylinder temperature

contours at 5 °CA after diesel injection timing (ADIT) for all cases. As can be seen in this figure, advancing the diesel injection timing up to 30 °BTDC leads to a reduction in the average in-cylinder temperature when diesel fuel is injected into the cylinder. For instance, the average in-cylinder temperature is around 950 K and 750 K for DIT=10 °BTDC and DIT=30 °BTDC, respectively. This consequently leads to a prolonged ignition delay as shown in Figure 2-4a. As a result, more premixed mixture (diesel and premixed natural gas-air) is formed during the ignition delay period. This can be confirmed by calculating the spatial and temporal contours of total equivalence ratio before the SOC for each case (Figure 2-6). This figure shows that advancing diesel fuel injection timing reduces the fuel concentration gradient in the cylinder and avoids the local fuel rich combustion zones. This figure shows also that the premixed natural gas-air and diesel fuel mixture is more homogeneous for DIT=30 °BTDC than that of DIT=10 °BTDC at SOC. Therefore, combined with appropriate average in-cylinder temperature (more than 800 K before SOC timing), a larger number and a wider space distribution of ignition kernel are produced. Consequently, the proportion of premixed combustion is increased.

With further advancing the injection timing (cases 7-11), the crank angle of the peak pressure is retarded and the maximum in-cylinder pressure is decreased. For these cases, the ignition delay also increases when advancing the diesel injection timing (Figure 2-4), and the diesel fuel experiences very long atomization and evaporation processes. As a result, the combustion chamber volume becomes more and more uniform without remarkable fuel stratification during the ignition delay (Figure 2-6). However, the in-cylinder temperature is not high enough (lower than 750K) which leads to a retarded combustion phasing (Figure 2-4b) and a reduced maximum in-cylinder pressure. For very advanced diesel injection timing, the pilot diesel ignition mode is similar to that encountered in a homogeneous charge compression ignition (HCCI) engine, where late combustion phasing happens in the expansion stroke (Figure 2-4b).

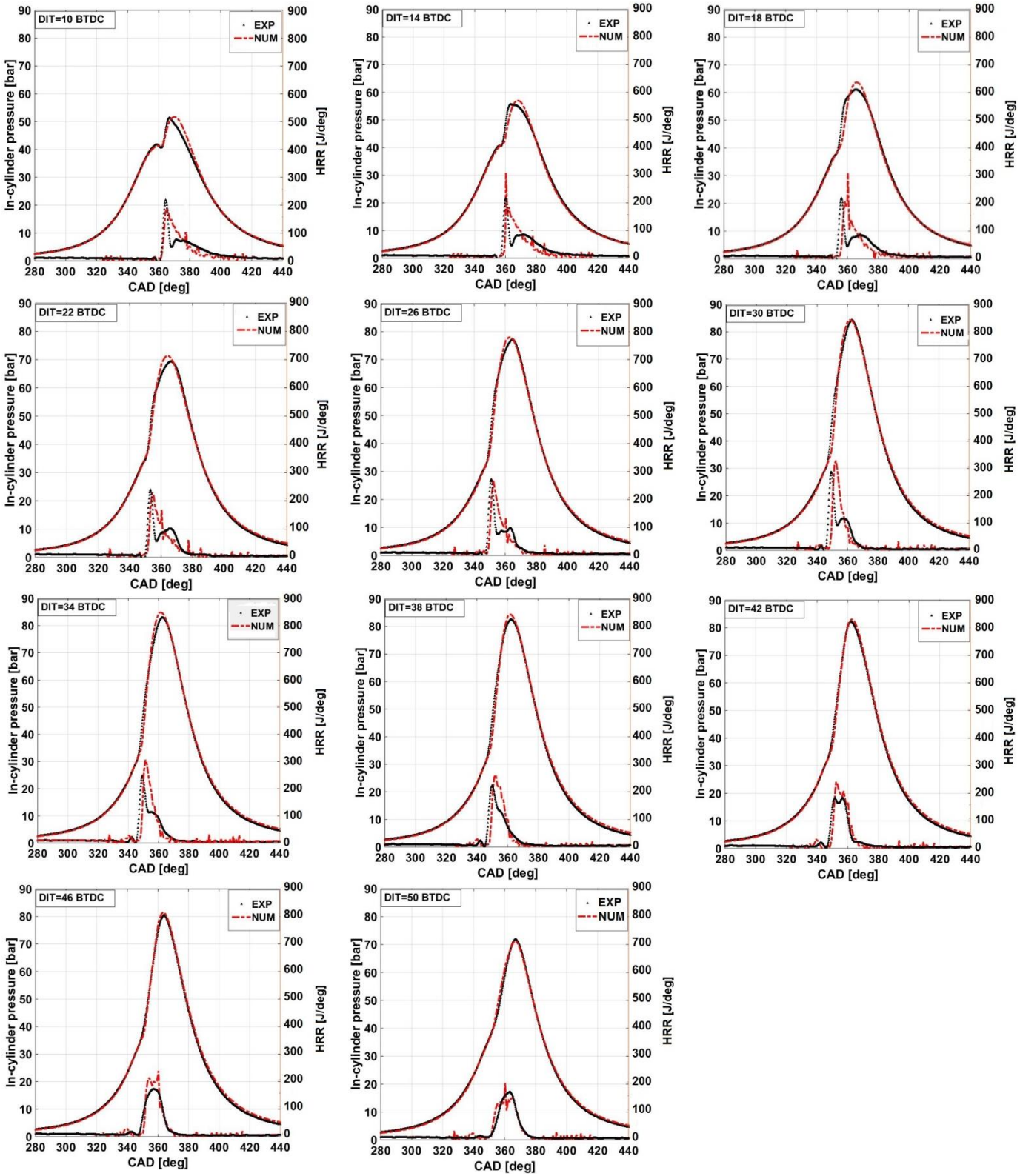

Figure 2-3. Experimental and numerical in-cylinder pressure and HRR of natural gas/diesel dual-fuel mode at different injection timings (cases 1-11) under 25% engine load

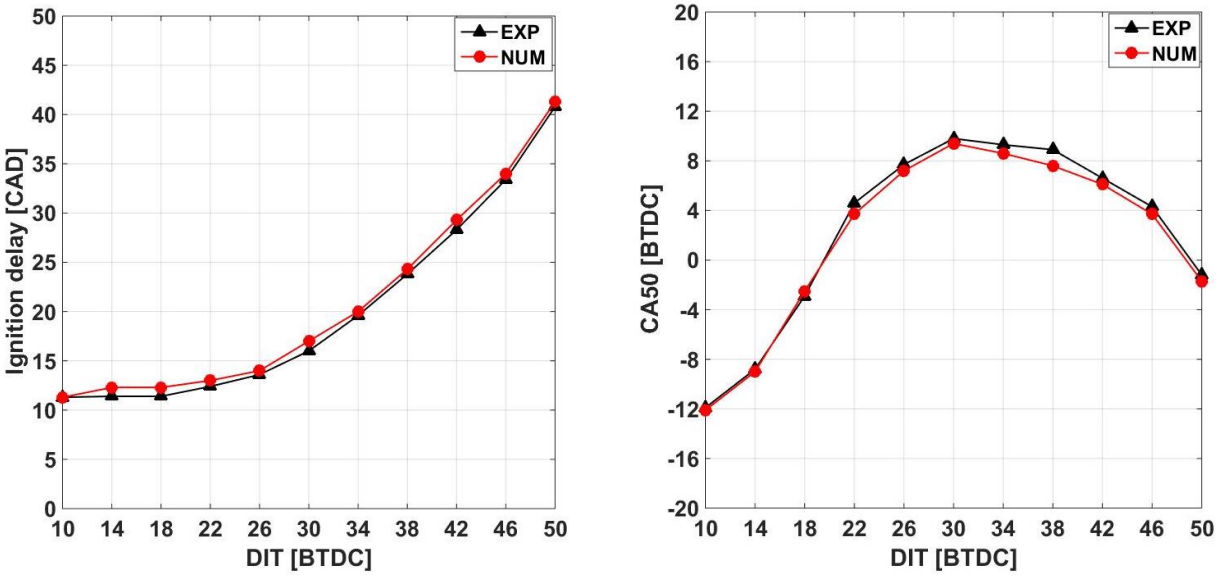

a) Ignition delay b) combustion phasing (CA_{50})

Figure 2-4. Ignition delay and combustion phasing of natural gas/diesel dual-fuel mode with different diesel injection timings under 25% engine load.

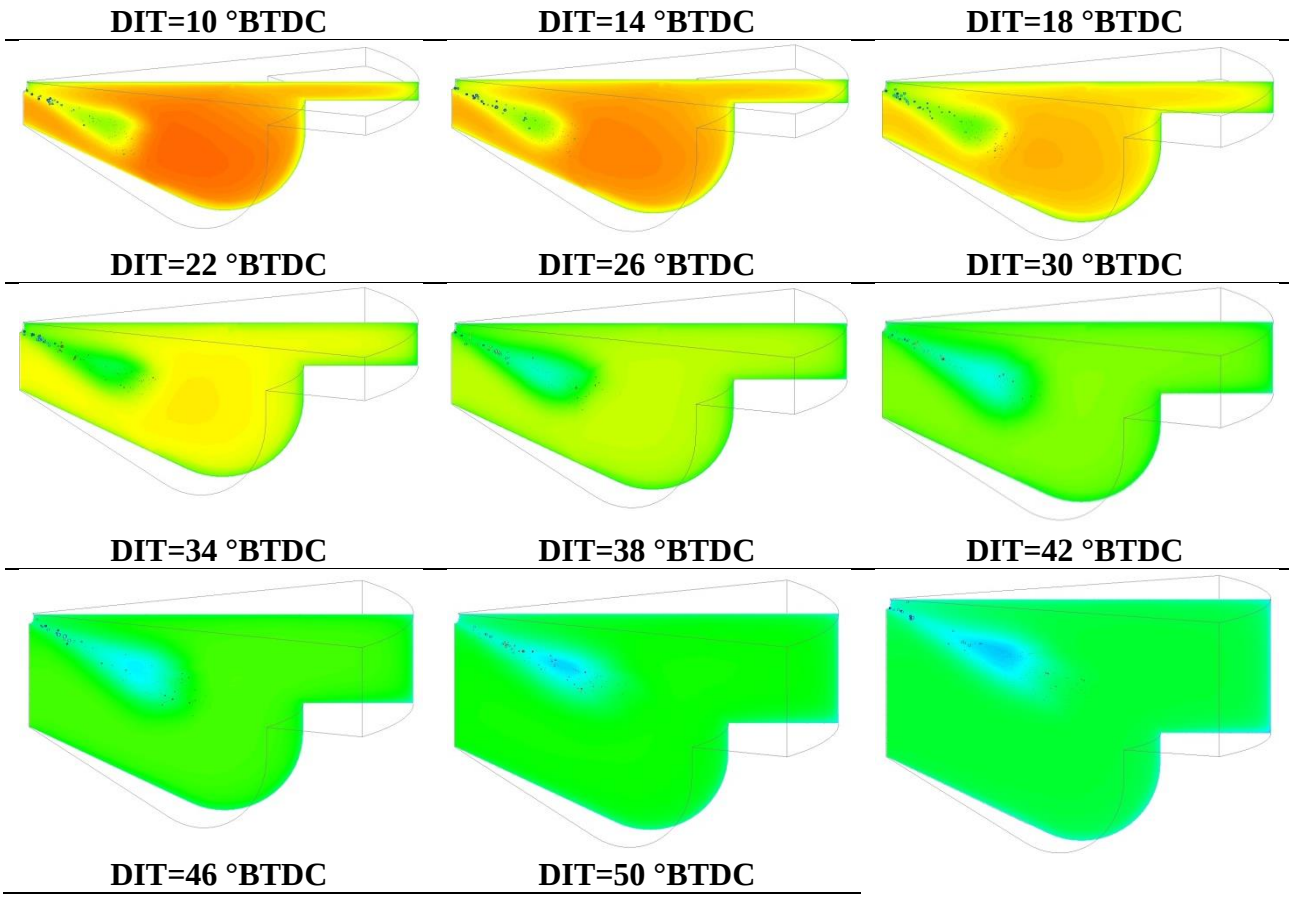

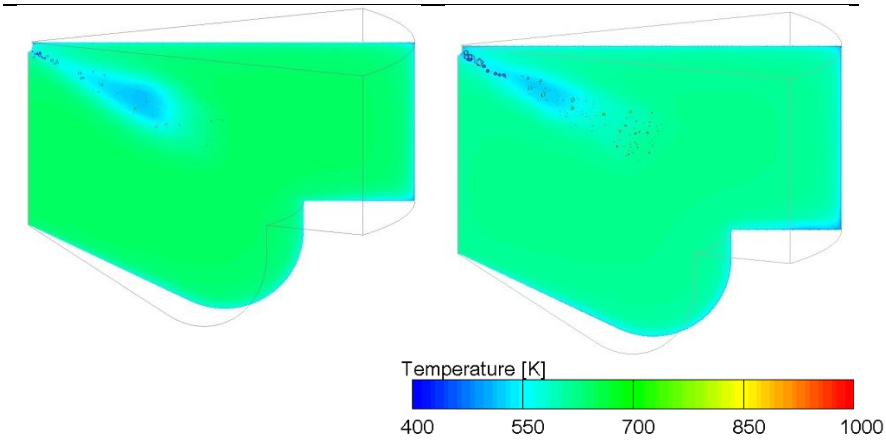

Figure 2-5. In-cylinder temperature contours (at 5 °CA ADIT) for various diesel injection timings of natural gas/diesel dual-fuel mode under 25% engine load

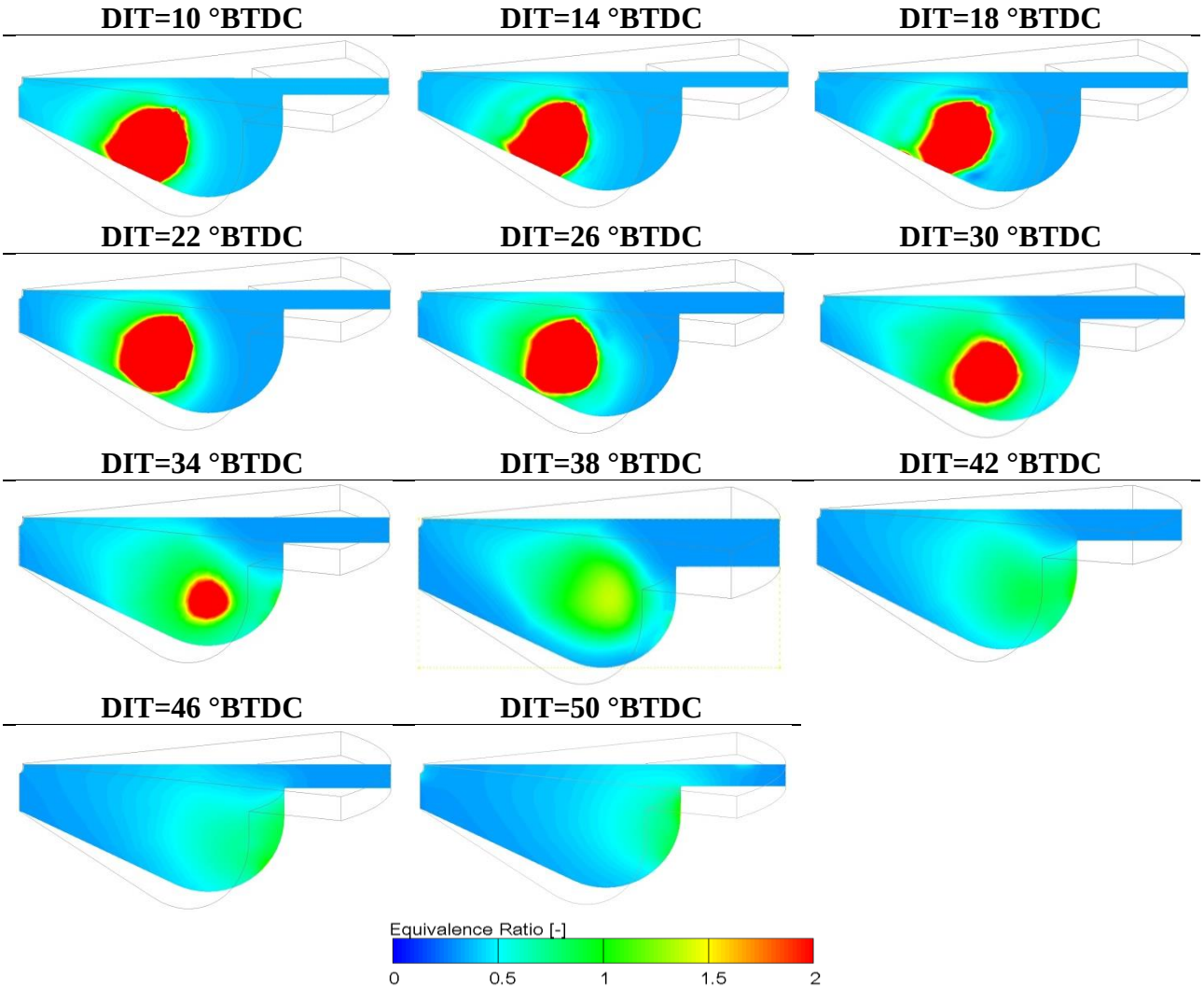

Figure 2-6**.** Spatial contours of total equivalence ratio (at SOC timing) of various diesel injection timings for natural gas/diesel dual-fuel mode under 25% engine load

Figure 2-7 presents the spatial distribution of OH radical mass fraction for different diesel injection timings at four selected frames of 4, 8, 12, and 16 ° after the start of combustion (ASOC). The contours plane is located at a vertical distance of 11 mm from the nozzle tip. OH radical, which is released during the oxidation process, is crucial for intermediate reactions. It is obvious that OH radical distribution is wider for injection timings of 30 °BTDC than for other injection timings at frame contour of 4 °ASOC (early stage of combustion). However, at diesel injection timings of 38 and 46 °BTDC, the blue non-reactive zones are much narrower than other injection timings during the last stages of combustion (12 and 16 °ASOC), indicating that a more premixed combustion takes place in these cases. It is notable that the blue non-reactive zone for each case shows that very limited high temperature oxidation reactions occur in this zone. Moreover, as the diesel injection timing advances, the highest OH concentration is detected exclusively near the wall region of the piston bowl which corresponds to the fuel rich zones (Figure 2-6). For example, at diesel injection timings of 46 °BTDC, the highest OH concentration is located near the piston wall. On the contrary, at diesel injection timing of 14 °BTDC, the highest OH concentration is closer to the cylinder axis and nozzle tip. These contours reveal that, for late diesel injection timings (such as DIT= 14 °BTDC), the consumption of premixed fuel in the outer part of the charge (far away from diesel spray nuclei) is likely to be a significant challenge for dual-fuel combustion engine at low engine load. This observation is important, since it could explain why natural gas/diesel dual-fuel combustion mode under low engine load often suffers from high unburned methane emissions. However, with advanced diesel injection timing, the OH radical distribution is more uniform throughout the combustion chamber, which makes the combustion look similar to that in a HCCI engine and, therefore, helps reduce unburned methane emissions.

	4 °ASOC	**8 °ASOC**	**12 °ASOC**	**16 °ASOC**

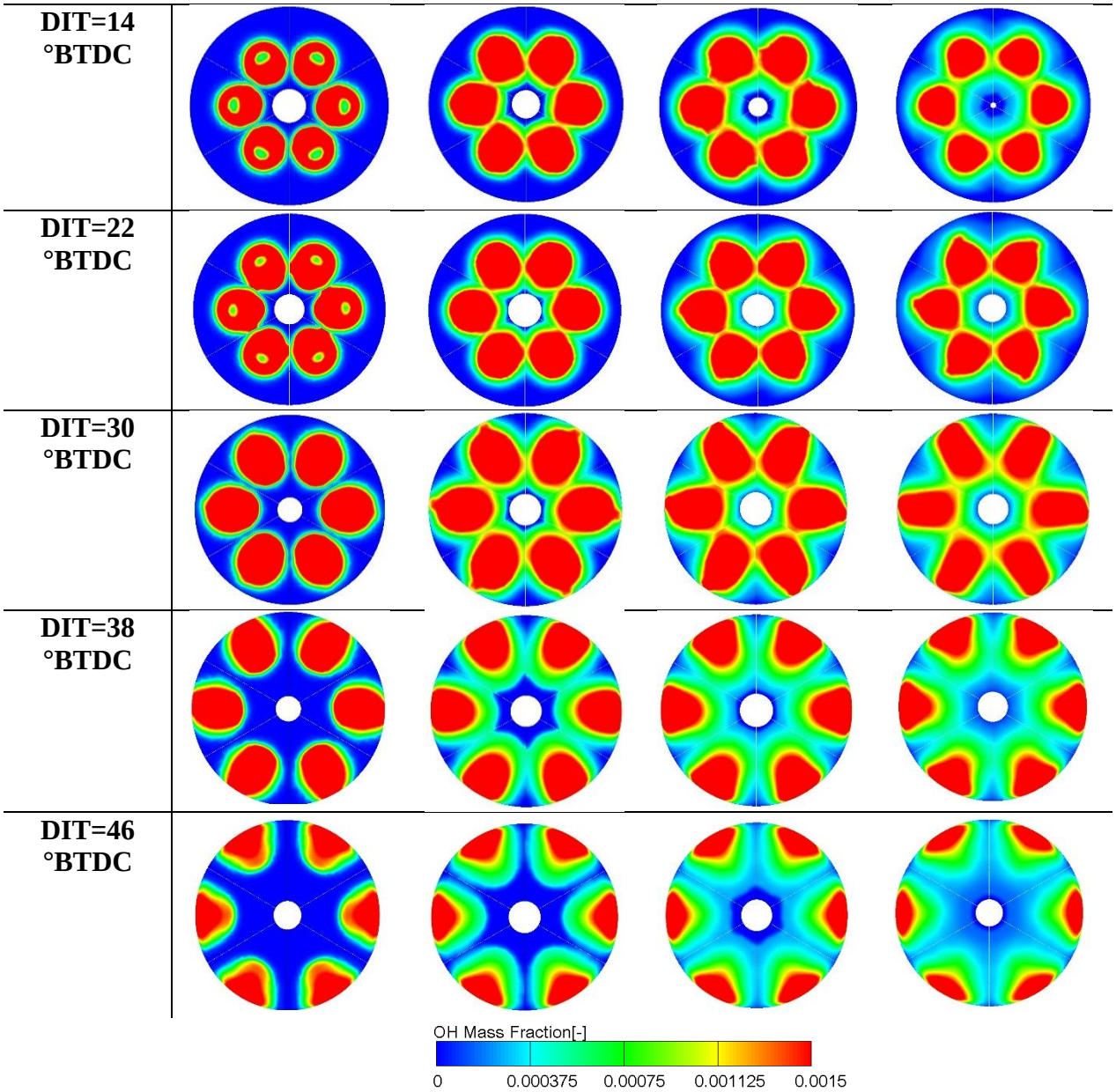

Figure 2-7. Spatial contours of OH radical for various diesel injection timings of natural gas/diesel dual-fuel mode under 25% engine load

Figure 2-8a shows the variation of the indicated thermal efficiency (ITE) as a function of diesel injection timings under 25% engine load. In order to support in more detail the results regarding the effect of diesel injection timing on ITE of the dual-fuel engine at low load, it is needed to investigate the heat release rate and CA_{50} corresponding to each examined case (Figure 2-3 and Figure 2-4b). For very retarded diesel injection timings (i.e., 10 and 14 °BTDC), the peak of the in-cylinder pressure is low and CA_{50} is located far away from TDC. The combustion rate of natural gas is very slow and

the fuel utilization is significantly poor. This is because the combustion of natural gas-air mixture is significantly delayed compared to that of diesel-air mixture. The HRR profile exhibits a single obvious peak which is relatively high as the second peak is almost indistinguishable, and thus the HRR profile is not symmetric. For these cases, the combustion rate of the main combustion stage is too slow, and the combustion efficiency of natural gas is extremely low (second peak of HRR). However, advancing the diesel injection timing from 10 to 30 °BTDC advances combustion phasing, increases the second peak of HRR, and its crank angle becomes closer to the first peak (diesel premixed combustion). This is due to the fact that advancing the diesel injection timing prolongs the ignition delay and thus more premixed natural gas-air and diesel mixture is formed before SOC. In addition, the prolonged ignition allows the formation of larger number and wider space distribution of ignition kernel. As a result, the combustion efficiency of natural gas and the ITE are improved, as shown in Figure 2-8a.

As shown in Figure 2-3, dual-fuel combustion with diesel injection timings between 34 to 42 °BTDC (cases 7-9) has a faster combustion rate of natural gas-air mixture compared to previous cases (cases 1-6). For these diesel injection timings (cases 7-9), diesel fuel experiences very long atomization and evaporation processes. The CA_{50} is retarded and the combustion phasing continues into the expansion stroke. The multipoint premixed combustion dominated by natural gas occurs quickly after the premixed combustion of pilot diesel fuel. For these cases, the premixed combustion of natural gas significantly improves and more heat is released at the premixed combustion stage. This late released heat positively affects the expansion pressure which leads to an increase in ITE, as shown in Figure 2-8a.

In dual-fuel combustion mode with very advanced diesel injection timing (cases 10 and 11), low temperature chemical kinetics reactions are often observed before the main combustion stage. The premixed ignition of diesel-air-natural gas mixture provides a significant wide ignition source for natural gas, resulting in a very fast combustion rate of natural gas-air mixture (Figure 2-8b). Before

the start of the main combustion, a lower peak, which is caused by low temperature chemical kinetics reactions, appears in the HRR profile (Figure 2-3, cases 10 and 11). There is only one significant peak of the HRR profile during combustion stage which has similar characteristics to that of HCCI combustion mode. For both diesel injection timings of 46 and 50 °BTDC, the HRR profile is almost symmetric and SOC timing is very retarded. Combustion phasing (CA_{50}) is very close to TDC and most of the heat release happens during the expansion stroke (Figure 2-3 and Figure 2-4b). The expansion pressure and positive engine work are significantly improved when the CA_{50} occurs near TDC and combustion has a short duration. Therefore, the thermal efficiency is the highest for these injection timings (Figure 2-8a).

Figure 2-8b and Figure 2-8c depict the combustion rate and mass fraction of methane for three selected diesel injection timings. It can be seen that, for diesel injection timing of 46 °BTDC, the premixed natural gas combustion rate is higher with a greater utilization of natural gas compared to diesel injection timings of 38 °BTDC and 22 °BTDC. This leads to higher thermal efficiency and lower unburned methane emissions at the exhaust.

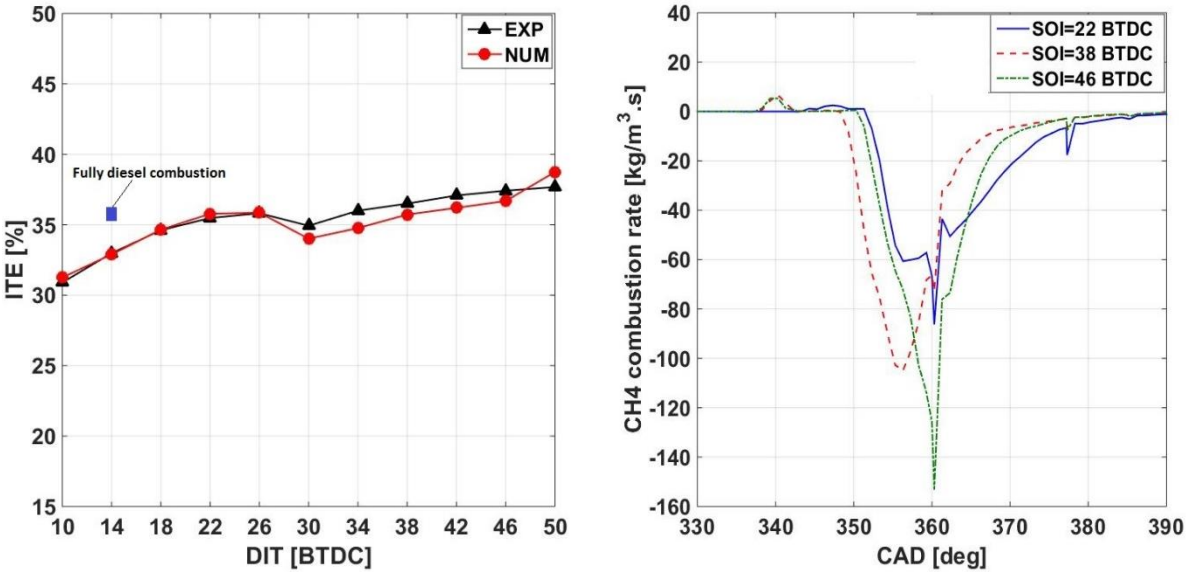

a) ITE b) CH_4 combustion rate

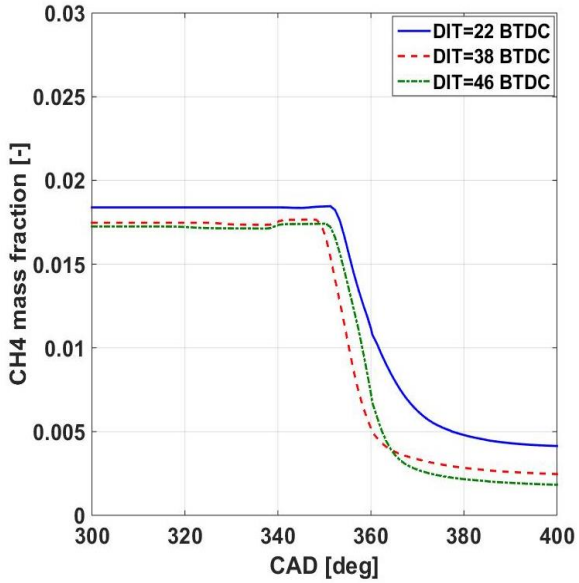

c) CH_4 mass fraction

Figure 2-8**.** ITE, CH_4 combustion rate, and CH_4 mass fraction profiles vs. diesel injection timing for natural gas/diesel dual-fuel mode at 25% engine load

2.5.2. Effect of diesel injection timing on emissions

It is well-known that natural gas/diesel dual-fuel combustion suffers from higher level of unburned methane and CO emissions at low engine load compared to that of diesel combustion. There are three possible reasons for the increase of unburned methane emissions of natural gas/diesel dual-fuel combustion mode at low load [55]. First, the premixed natural gas-air mixture is very lean, which results in sufficiently low chemical reactivity and consequently partial oxidation of the fuel. Second, the in-cylinder charge temperature is too low to oxidize the premixed natural gas fuel which has high specific heat capacity. The temperature required for completing the oxidation of UHC is not enough [56]. Finally, the extremely small amount of pilot diesel injected at a low engine load yields slower combustion rate and consequently premixed natural gas, which is located far away from diesel spray, avoids oxidation (combustion).

Figure 2-9a shows the experimental and numerical trends of the indicated unburned methane emissions versus different diesel injection timings. The experimental results show that methane emissions significantly decrease with advancing diesel injection timing. This trend is well reproduced

by the CFD model. However, the model quantitatively over-predicts unburned methane emissions at diesel injection timing between 26 and 34 °BTDC and also misses the slight increase trend at diesel injection timing between 30 and 38 °BTDC. Both calculated and measured results show that methane emissions are reduced by 6 times when diesel injection timing is advanced from 10 to 50 °BTDC. This is due to the relatively higher combustion rate and greater utilization of premixed natural gas at earlier injection timings (Figure 2-8b). Spatial and temporal distributions of unburned methane mass fraction for three selected diesel injection timings at frames of 5 and 60 °ASOC are shown in Figure 2-10. It can be observed that oxidation of CH_4 is more intense for diesel injection timing of 22 °BTDC during the first stage of combustion phase (at 5 °ASOC). However, at 60 °ASOC, CH_4 mass fraction of SOI = 46 °BTDC is lower than that of SOI=22 and 38 °BTD. This is due to the fact that, at SOI = 46 °BTDC, the premixed ignition of diesel-air mixture provides a significant wide ignition source for natural gas, resulting in a very fast combustion rate of natural gas-air mixture. As a result, the propagation of the flame front spreads into the portions of the charge situated far away from the pilot ignition nuclei (see Figure 2-7). Therefore, after an initial fast oxidation of the pilot injection, the combustion process is faster and complete, which yields low unburned methane emissions at the engine exhaust. It is worthwhile to note that, for all cases, the unburned methane is mainly found near the piston wall region where a cooler temperature makes it difficult to ignite local air-natural gas mixture.

The high level of CO emissions of dual-fuel combustion at low engine load is mainly due to very lean premixed fuel-air mixture and low in-cylinder mean charge temperature which control the rate of fuel decomposition and oxidation [34]. Figure 2-9b depicts the experimental and numerical trends of indicated specific CO (ISCO) emissions under different diesel injection timing. A good agreement of the CO emissions trends is found between the simulation and experimental data. The experimental data shows that CO emissions significantly drop with advancing diesel injection timing. The numerical simulation successfully captures the CO emissions trend of the experiments, except for

diesel injection timings between 30 and 42 °BTDC. As illustrated above, with advancing diesel injection timing, more premixed natural gas is entrained and the combustion process becomes faster and complete, which is probably the main reason of CO emissions decrease. Moreover, for very advanced diesel injection timings of 46 and 50 °BTDC, CO emissions tend to increase which is mainly due to lower in-cylinder temperature.

The experimental trend in Figure 2-9 shows that advancing diesel injection timing from 10 to 30 °BTDC significantly reduces the unburned methane and to less extent CO emissions. However, further advancing diesel injection timing between 46 and 50 °BTDC results in a further decrease in unburned methane emissions, whereas CO emissions exhibit a change of trend, that is, a slight increase. Based on these results, it can be concluded that, advancing diesel injection timing beyond 30 °BTDC does not significantly improve the unburned methane and CO emissions. This is mainly due to the lower in-cylinder charge temperature and also the more trapped premixed natural gas-air-diesel mixture in the crevice and squish volumes. The fact that the numerical simulation showed continual decrease in the unburned methane and CO emissions with further advancing diesel injection timing can be attributed to the crevice volume which is ignored in the CFD calculation.

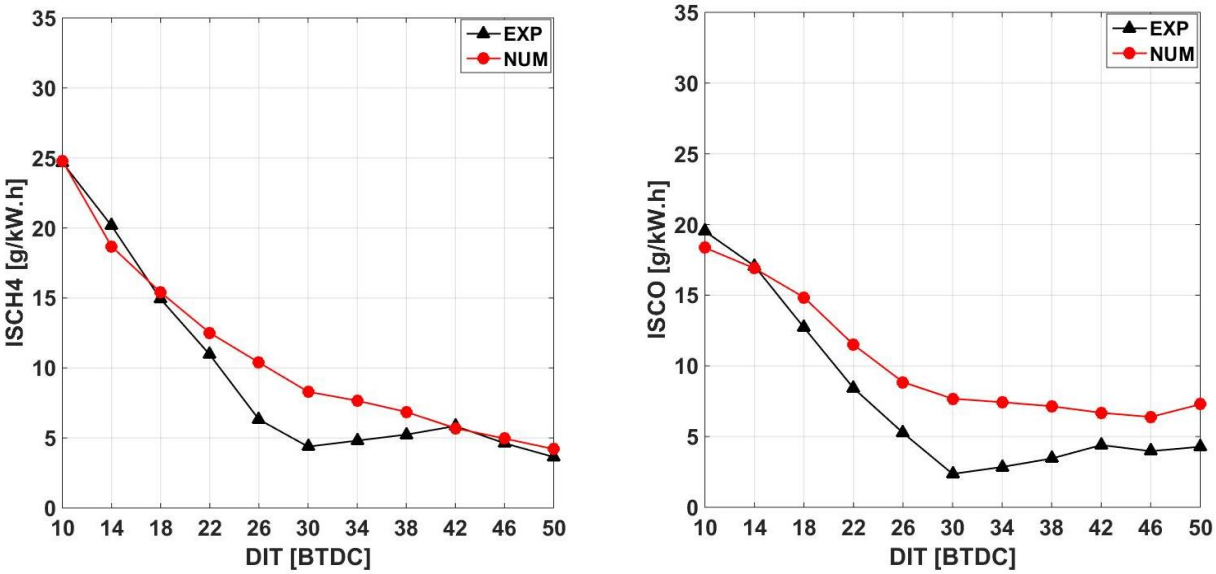

a) Indicated unburned methane b) Indicated CO

Figure 2-9. $ISCH_4$ and ISCO emissions of natural gas/diesel dual-fuel mode with different injection timings under 25% engine load

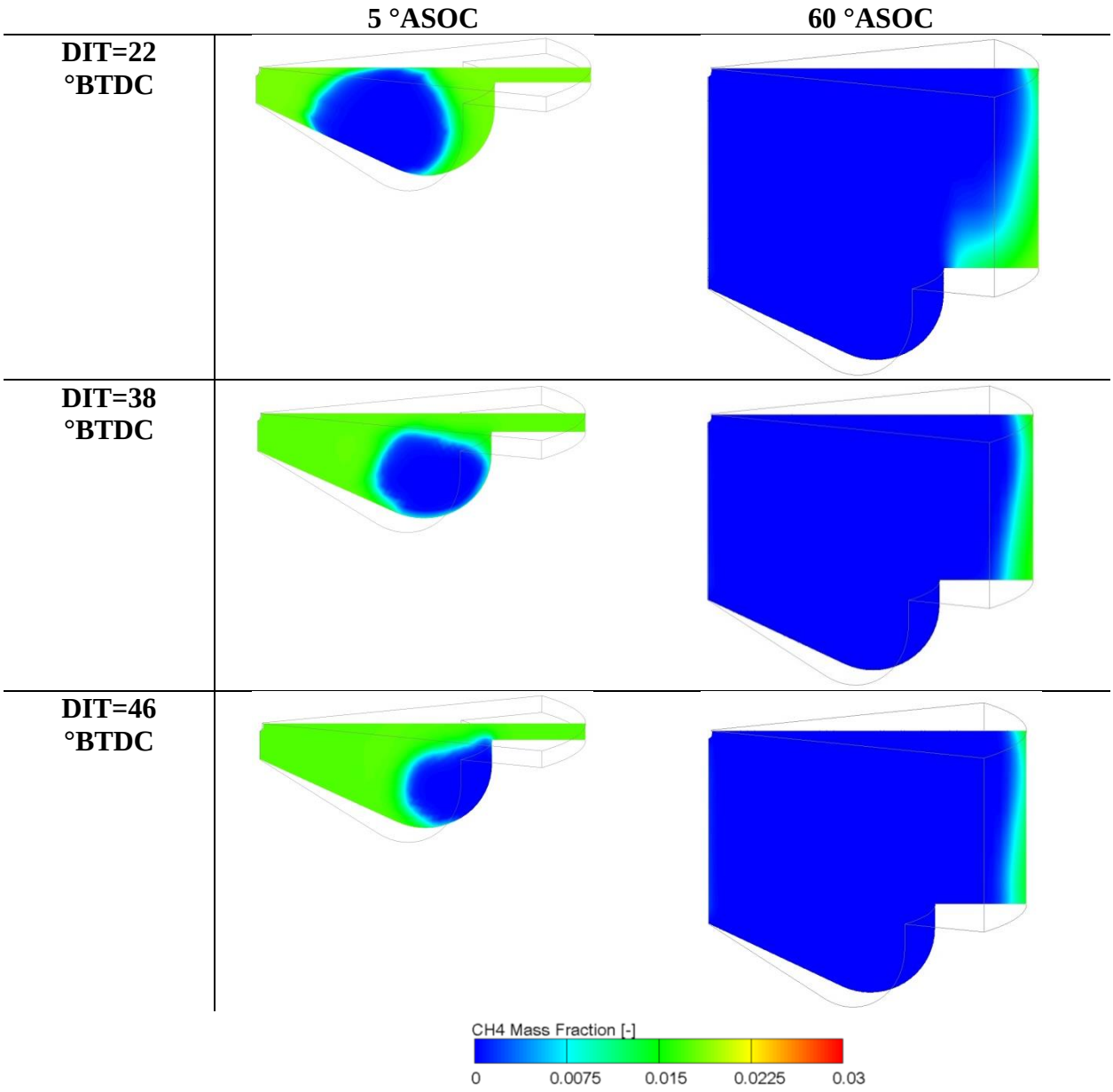

Figure 2-10. Spatial contours of CH_4 mass fraction of different diesel injection timings for natural gas/diesel dual-fuel mode under 25% engine load

Local gas temperature, oxygen concentration, and residence time are the three major factors affecting the formation of NO_x emissions. Figure 2-11a illustrates the indicated specific NO_x ($ISNO_x$) emissions at different diesel injection timings. It is observed that the experimental $ISNO_x$ trend is well captured numerically. However, the model quantitatively over-predicts NO_x emissions at diesel injection timings of 10 and 14 °BTDC. NO_x emissions consistently increase with advancing diesel

injection timing up to 30 °BTDC. This is due to the fact that the local gas temperature becomes higher and more homogeneous as diesel injection timing advances (Figure 2-12). With further advancing diesel injection timing from 30 °BTDC, more combustion reactions take place throughout in the combustion chamber, and the temperature field is more uniform as indicated by less local high temperature zones (Figure 2-12). This is due to the fact that the diesel fuel injection event is increasingly separated from the main combustion event (very long ignition delay). This separation implies that the diesel spray has more time to disperse into the surrounding natural gas-air mixture before the start of combustion. Thus, it is progressively less likely for a high-temperature diffusion flame to envelop the diesel spray during combustion, since most of NO_x emissions form in the high-temperature regions surrounding diesel sprays. Consequently, further advancing diesel injection timing up to 50 °BTDC significantly reduces NO_x emissions. At the same time, with advancing diesel injection timing, the total equivalence ratio shows a decreasing trend (Figure 2-2) which also contributes to a reduction in $ISNO_x$ emissions at very advanced diesel injection timings (DIT=50 °BTDC).

NO_x – CH_4 and NO_x – CO trade-off relationships are displayed in Figure 2-11b. While advancing diesel injection timing in the range of conventional dual-fuel combustion (i.e., 10-30 °BTDC) improves the emissions of unburned methane and CO, it produces high level of NO_x emissions. It can also be observed that diesel injection timing of 30 °BTDC is the conversion point for different combustion of conventional dual-fuel. Further advancing diesel injection timing beyond this point (30 °BTDC) drastically reduces NO_x emissions and to a less extent the unburned methane and CO emissions. However, it is clearly noticeable that very advanced diesel injection timings of 46 and 50 °BTDC reduce NO_x and methane emissions, whereas CO emissions exhibit a slight increase. Moreover, very advanced injection timings result in the highest ITE, as shown in Figure 2-8a. For instance, with advancing diesel injection timing from 10 °BTDC to 50 °BTDC, NO_x, methane and CO emissions are reduced, respectively, by 65.8%, 83%, and 60%, whereas ITE is increased by 7.5%.

However, for these very advanced diesel injection timings (46 and 50 °BTDC), the combustion process is very sensitive to the engine operating conditions where the coefficient of variation of IMEP (COVimep) exhibits an increasing trend (Figure 2-11c). Therefore, the engine operating conditions must be strictly controlled to improve the combustion performance and emissions.

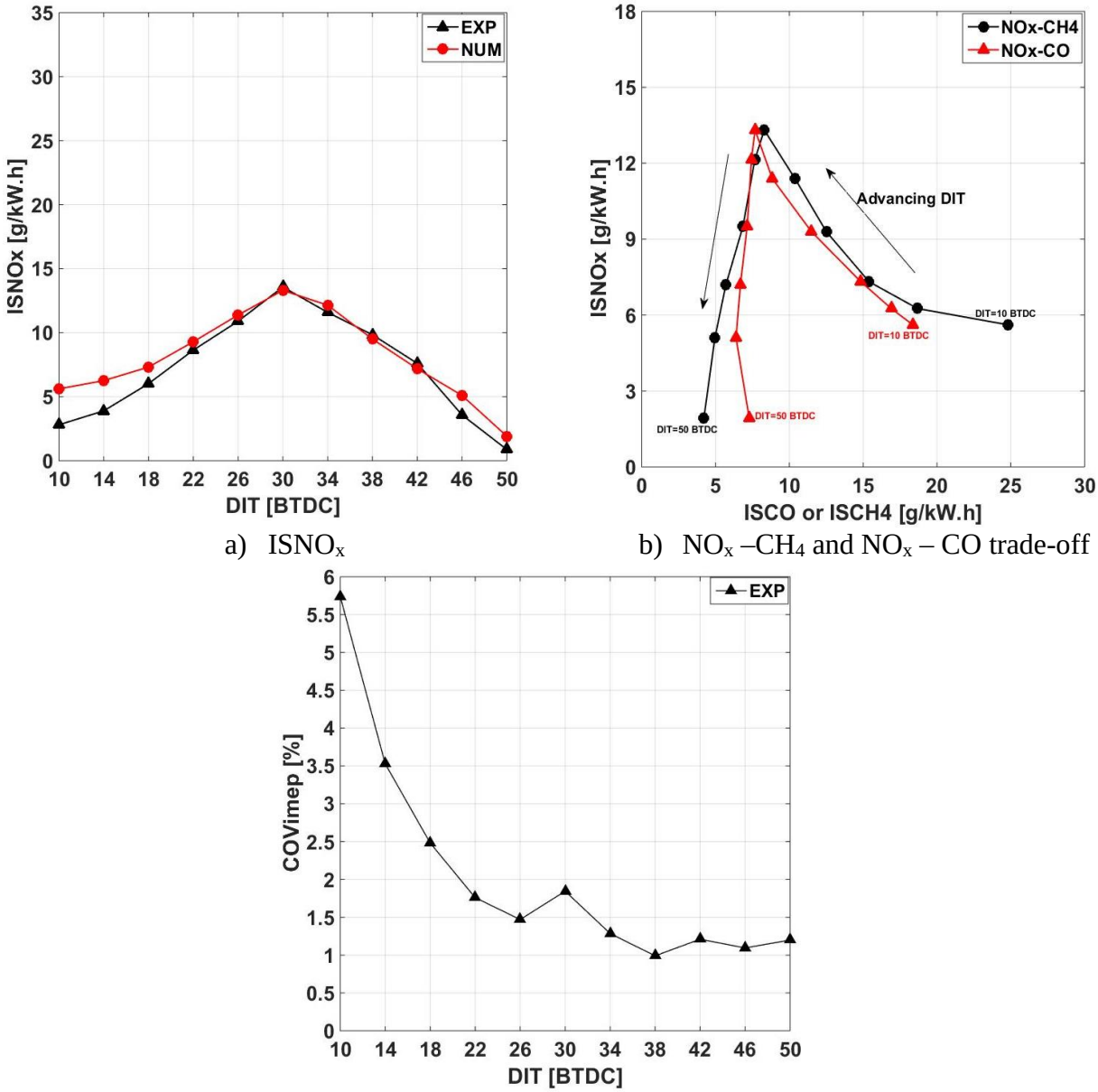

a) $ISNO_x$ b) NO_x –CH_4 and NO_x – CO trade-off

c) COV_{imep}

Figure 2-11. $ISNO_x$ emissions, NO_x-CH_4 and NO_x-CO trade-off , and COV_{imep} of natural gas/diesel dual-fuel mode with different injection timings under 25% engine load

	4 °ASOC	**10 °ASOC**	**15 °ASOC**

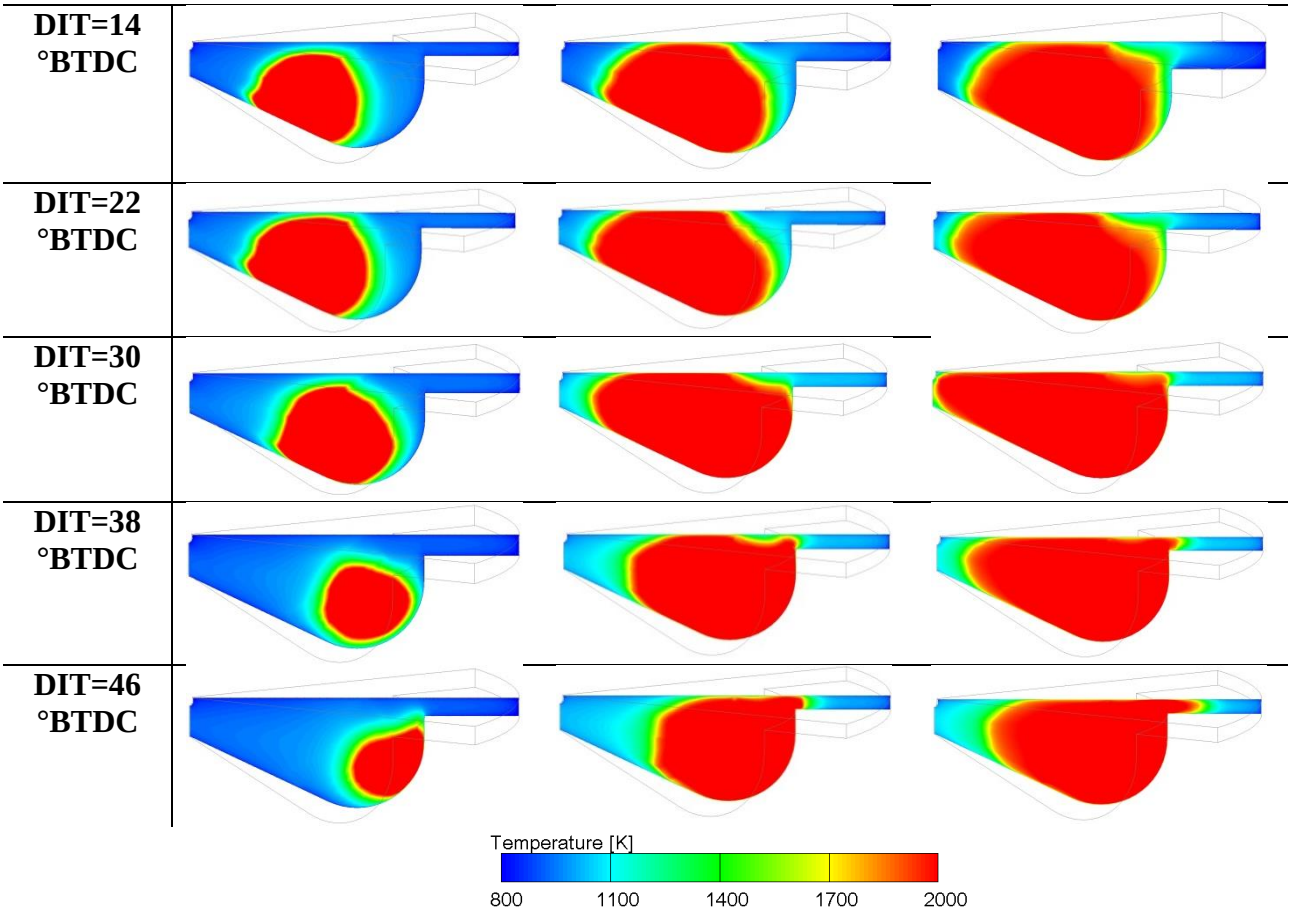

Figure 2-12**.** In-cylinder temperature contours (at 4, 10, and 15 °CA ASOC) of various diesel injection timings for natural gas/diesel dual-fuel mode under 25% engine load

2.6. Conclusions

The effect of a wide range of diesel injection timing, varying from 10 to 50 °BTDC, on the combustion performance and emissions of natural gas/diesel dual-fuel compression ignition engine at low load has been studied experimentally and numerically with the aim to reduce methane and CO emissions, and improve the engine thermal efficiency. The major concluding remarks are summarized below.

- Different combustion modes can be achieved with advancing diesel injection timing. Advancing the injection timing up to 30 °BTDC increases the maximum in-cylinder pressure and also allows the crank angle of the in-cylinder peak pressure to move closer to the TDC. This is due to the combined effect of prolonged ignition delay and higher in-cylinder charge

temperature which results in a larger number and wider space distribution of ignition kernel. With further advancing the diesel injection timing up to 50 °BTDC, the crank angle of the peak pressure is retarded and the maximum in-cylinder pressure is decreased mainly due to the lower in-cylinder temperature before SOC.

- Analysis of OH spatial distribution showed that OH radical distribution is wider for an injection timing of 30 °BTDC for the earlier stage of combustion. However, at very advanced diesel injection timing, the non-reactive zones are much narrower than other injection timings during the last stages of combustion, indicating that a greater premixed combustion takes place in these cases. For late diesel injection timings, the consumption of premixed fuel in the outer part of the charge is likely to be a significant challenge for dual-fuel combustion engine at low engine load. However, with advancing the diesel injection timing, the OH radical is more uniform throughout the combustion chamber which confirms that high temperature combustion reactions can occur in the central part of the charge.
- Natural gas/diesel dual-fuel combustion with diesel injection timings between 10 and 30 °BTDC (cases 1-6) experiences low combustion efficiency. However, advancing diesel injection timing from 10 to 30 °BTDC improves the combustion of natural gas, leading to an increase in ITE. For diesel injection timing between 34 and 42 °BTDC, diesel fuel experiences very long atomization and evaporation processes. The SOC timing is retarded and the combustion phasing continues into the expansion stroke. However, the late released heat of this combustion mode still positively affects the expansion pressure which leads to an increase in ITE. For both diesel injection timings of 46 and 50 °BTDC, combustion phasing mostly happens during the expansion stroke which increases the expansion pressure and positive engine work, and consequently yields the highest thermal efficiency.
- Unburned methane and CO emissions are reduced, respectively, by 6 and 5 times when diesel injection timing is advanced from 10 to 50 °BTDC. While advancing diesel injection timing

in the range of conventional dual-fuel combustion (10-30 °BTDC) improves the emissions of unburned methane and CO, it still produces high level of NO_x emissions. Diesel injection timing of 30 °BTDC is the conversion point for different combustion of conventional dual-fuel. Further advancing diesel injection timing beyond this point (30 °BTDC) drastically reduces NO_x emissions and to a less extent unburned methane and CO emissions. This is mainly due to the lower in-cylinder charge temperature and the trapped premixed natural gas-air-diesel mixture in the crevice and squish volumes.

Overall, very advanced diesel injection timings of 46 and 50 °BTDC simultaneously reduce NO_x, unburned methane, and CO emissions. Moreover, very advanced injection timings can lead to the highest ITE. The results revealed that with advancing diesel injection timing from 10 °BTDC to 50 °BTDC, NO_x, unburned methane, and CO emissions are reduced, respectively, by 65.8%, 83%, and 60% while ITE is increased by 7.5%.

2.7. References

[1] Pedrozo VB, May I, Dalla Nora M, Cairns A, Zhao H. Experimental analysis of ethanol dual-fuel combustion in a heavy-duty diesel engine: An optimisation at low load. Appl Energy 2016;165:166–82. doi:10.1016/j.apenergy.2015.12.052.

[2] Chen Z, Yao C, Wang Q, Han G, Dou Z, Wei H, et al. Study of cylinder-to-cylinder variation in a diesel engine fueled with diesel/methanol dual fuel. Fuel 2016;170:67–76. doi:10.1016/j.fuel.2015.12.019.

[3] Kumar S, Cho JH, Park J, Moon I. Advances in diesel-alcohol blends and their effects on the performance and emissions of diesel engines. Renew Sustain Energy Rev 2013;22:46–72. doi:10.1016/j.rser.2013.01.017.

[4] Britto RF, Martins CA. Emission analysis of a Diesel Engine Operating in Diesel-Ethanol

Dual-Fuel mode. Fuel 2015;148:191–201. doi:10.1016/j.fuel.2015.01.008.

[5] Krisman A, Hawkes ER, Kook S, Sjöberg M, Dec JE. On the potential of ethanol fuel stratification to extend the high load limit in stratified-charge compression-ignition engines. Fuel 2012;99:45–54. doi:10.1016/j.fuel.2012.04.001.

[6] Reitz RD, Duraisamy G. Review of high efficiency and clean reactivity controlled compression ignition (RCCI) combustion in internal combustion engines. Prog Energy Combust Sci 2015;46:12–71. doi:10.1016/j.pecs.2014.05.003.

[7] Aksu C, Kawahara N, Tsuboi K, Kondo M, Tomita E. Extension of PREMIER combustion operation range using split micro pilot fuel injection in a dual fuel natural gas compression ignition engine: A performance-based and visual investigation. Fuel 2016;185:243–53. doi:10.1016/j.fuel.2016.07.120.

[8] Yousefi A, Birouk M, Lawler B, Gharehghani A. Performance and emissions of a dual-fuel pilot diesel ignition engine operating on various premixed fuels. Energy Convers Manag 2015;106:322–36. doi:10.1016/j.enconman.2015.09.056.

[9] Yang B, Wei X, Xi C, Liu Y, Zeng K, Lai MC. Experimental study of the effects of natural gas injection timing on the combustion performance and emissions of a turbocharged common rail dual-fuel engine. Energy Convers Manag 2014;87:297–304. doi:10.1016/j.enconman.2014.07.030.

[10] Polk AC, Carpenter CD, Srinivasan KK, Krishnan SR. An investigation of diesel-ignited propane dual fuel combustion in a heavy-duty diesel engine. Fuel 2014;132:135–48. doi:10.1016/j.fuel.2014.04.069.

[11] Zhang Q, Li M, Shao S. Combustion process and emissions of a heavy-duty engine fueled with directly injected natural gas and pilot diesel. Appl Energy 2015.

doi:10.1016/j.apenergy.2015.08.021.

[12] Sahoo BB, Sahoo N, Saha UK. Effect of engine parameters and type of gaseous fuel on the performance of dual-fuel gas diesel engines-A critical review. Renew Sustain Energy Rev 2009;13:1151–84. doi:10.1016/j.rser.2008.08.003.

[13] Barik D, Murugan S. Effects of diethyl ether (DEE) injection on combustion performance and emission characteristics of Karanja methyl ester (KME)-biogas fueled dual fuel diesel engine. Fuel 2016;164:286–96. doi:10.1016/j.fuel.2015.09.094.

[14] Wang B, Li T, Ge L, Ogawa H. Optimization of combustion chamber geometry for natural gas engines with diesel micro-pilot-induced ignition. Energy Convers Manag 2016;122:552–63. doi:10.1016/j.enconman.2016.06.027.

[15] Nithyanandan K, Zhang J, Li Y, Meng X, Donahue R, Lee C-F, et al. Diesel-Like Efficiency Using Compressed Natural Gas/Diesel Dual-Fuel Combustion. J Energy Resour Technol 2016;138:52201. doi:10.1115/1.4032621.

[16] Nithyanandan K, Lin Y, Donahue R, Meng X, Zhang J, Lee CF. Characterization of soot from diesel-CNG dual-fuel combustion in a CI engine. Fuel 2016;184:145–52. doi:10.1016/j.fuel.2016.06.028.

[17] Mousavi SM, Saray RK, Poorghasemi K, Maghbouli A. A numerical investigation on combustion and emission characteristics of a dual fuel engine at part load condition. Fuel 2016;166:309–19. doi:10.1016/j.fuel.2015.10.052.

[18] Sahoo BB, Sahoo N, Saha UK. Effect of engine parameters and type of gaseous fuel on the performance of dual-fuel gas diesel engines-A critical review. Renew Sustain Energy Rev 2009. doi:10.1016/j.rser.2008.08.003.

[19] Hosmath RS, Banapurmath NR, Khandal S V., Gaitonde VN, Basavarajappa YH, Yaliwal VS.

Effect of compression ratio, CNG flow rate and injection timing on the performance of dual fuel engine operated on honge oil methyl ester (HOME) and compressed natural gas (CNG). Renew Energy 2016;93:579–90. doi:10.1016/j.renene.2016.03.010.

[20] Li W, Liu Z, Wang Z. Experimental and theoretical analysis of the combustion process at low loads of a diesel natural gas dual-fuel engine. Energy 2016;94:728–41. doi:10.1016/j.energy.2015.11.052.

[21] Di Iorio S, Magno A, Mancaruso E, Vaglieco BM. Performance, Gaseous and Particle Emissions of a Small Compression Ignition Engine Operating in Diesel/Methane Dual Fuel Mode 2016;180:613–23. doi:10.4271/2016-01-0771.

[22] Wang Z, Zhao Z, Wang D, Tan M, Han Y, Liu Z, et al. Impact of pilot diesel ignition mode on combustion and emissions characteristics of a diesel/natural gas dual fuel heavy-duty engine. Fuel 2016. doi:10.1016/j.fuel.2015.11.077.

[23] Xu M, Cheng W, Li Z, Zhang H, An T, Meng Z. Pre-injection strategy for pilot diesel compression ignition natural gas engine. Appl Energy 2016;179:1185–93. doi:10.1016/j.apenergy.2016.07.024.

[24] Yang B, Wang L, Ning L, Zeng K. Effects of pilot injection timing on the combustion noise and particle emissions of a diesel/natural gas dual-fuel engine at low load. Appl Therm Eng 2016;102:822–8. doi:10.1016/j.applthermaleng.2016.03.126.

[25] Abdelaal MM, Hegab AH. Combustion and emission characteristics of a natural gas-fueled diesel engine with EGR. Energy Convers Manag 2012;64:301–12. doi:10.1016/j.enconman.2012.05.021.

[26] Carlucci AP, Laforgia D, Saracino R, Toto G. Combustion and emissions control in diesel-methane dual fuel engines: The effects of methane supply method combined with variable in-

cylinder charge bulk motion. Energy Convers Manag 2011;52:3004–17. doi:10.1016/j.enconman.2011.04.012.

[27] Hockett A, Hampson G, Marchese AJ. A Reduced Chemical Kinetic Mechanism for CFD Simulations of Natural Gas / Diesel Dual Fuel Engines n.d.:1–11.

[28] Yousefi A, Birouk M. An Investigation of Multi-Injection Strategies for a Dual-Fuel Pilot Diesel Ignition Engine at Low Load. J Energy Resour Technol 2016;139:12201. doi:10.1115/1.4033707.

[29] Ryu K. Effects of pilot injection timing on the combustion and emissions characteristics in a diesel engine using biodiesel-CNG dual fuel. Appl Energy 2013;111:721–30. doi:10.1016/j.apenergy.2013.05.046.

[30] Srinivasan KK, Krishnan SR. Cyclic Combustion Variations in Dual Fuel Partially Premixed Pilot-Ignited Natural Gas Engines. J Energy Resour Technol 2014;136:1–10. doi:10.1115/1.4024855.

[31] Yang B, Xi C, Wei X, Zeng K, Lai MC. Parametric investigation of natural gas port injection and diesel pilot injection on the combustion and emissions of a turbocharged common rail dual-fuel engine at low load. Appl Energy 2015. doi:10.1016/j.apenergy.2015.01.037.

[32] Papagiannakis RG, Rakopoulos CD, Hountalas DT, Rakopoulos DC. Emission characteristics of high speed, dual fuel, compression ignition engine operating in a wide range of natural gas/diesel fuel proportions. Fuel 2010. doi:10.1016/j.fuel.2009.11.001.

[33] Papagiannakis RG, Hountalas DT. Combustion and exhaust emission characteristics of a dual fuel compression ignition engine operated with pilot diesel fuel and natural gas. Energy Convers Manag 2004;45:2971–87. doi:10.1016/j.enconman.2004.01.013.

[34] Rao BN, Prem Kumar BS, Kumar Reddy KV. Effect of CNG flow rate on the performance

and emissions of a Mullite-coated diesel engine under dual-fuel mode. Int J Ambient Energy 2015;750:1–8. doi:10.1080/01430750.2015.1023835.

[35] Mikulski M, Wierzbicki S, Śmieja M, Matijošius J. Effect of CNG in a fuel dose on the combustion process of a compression-ignition engine. Transport 2015;30:162–71. doi:10.3846/16484142.2015.1045938.

[36] Yousefi A, Birouk M. Investigation of natural gas energy fraction and injection timing on the performance and emissions of a dual-fuel engine with pre-combustion chamber under low engine load. Appl Energy 2017;189:492–505. doi:10.1016/j.apenergy.2016.12.046.

[37] Di Blasio G, Belgiorno G, Beatrice C, Fraioli V, Migliaccio M. Experimental Evaluation of Compression Ratio Influence on the Performance of a Dual-Fuel Methane-Diesel Light-Duty Engine. SAE Int J Engines 2015;8:2015-24–2460. doi:10.4271/2015-24-2460.

[38] Bora BJ, Saha UK. Experimental evaluation of a rice bran biodiesel - biogas run dual fuel diesel engine at varying compression ratios. Renew Energy 2016;87:782–90. doi:10.1016/j.renene.2015.11.002.

[39] Bora BJ, Saha UK. Optimisation of injection timing and compression ratio of a raw biogas powered dual fuel diesel engine. Appl Therm Eng 2016;92:111–21. doi:10.1016/j.applthermaleng.2015.08.111.

[40] Paul A, Panua RS, Debroy D, Bose PK. Effect of compressed natural gas dual fuel operation with diesel and Pongamia pinnata methyl ester (PPME) as pilot fuels on performance and emission characteristics of a CI (compression ignition) engine. Energy 2014;68:495–509. doi:10.1016/j.energy.2014.03.026.

[41] Tarabet L, Loubar K, Lounici MS, Khiari K, Belmrabet T, Tazerout M. Experimental investigation of di diesel engine operating with eucalyptus biodiesel/natural gas under dual

fuel mode. Fuel 2014;133:129–38. doi:10.1016/j.fuel.2014.05.008.

[42] Yang B, Wei X, Xi C, Liu Y, Zeng K, Lai MC. Experimental study of the effects of natural gas injection timing on the combustion performance and emissions of a turbocharged common rail dual-fuel engine. Energy Convers Manag 2014. doi:10.1016/j.enconman.2014.07.030.

[43] Hernandez JJ, Lapuerta M, Barba J. Separate effect of H2, CH4 and CO on diesel engine performance and emissions under partial diesel fuel replacement. Fuel 2016;165:173–84. doi:10.1016/j.fuel.2015.10.054.

[44] Mohan B, Yang W, Chou SK. Fuel injection strategies for performance improvement and emissions reduction in compression ignition engines—A review. Renew Sustain Energy Rev 2013;28:664–76. doi:10.1016/j.rser.2013.08.051.

[45] Guo H, Neill WS, Liko B. An experimental investigation on the combustion and emissions performance of a natural gas - Diesel dual fuel engine at low and medium loads 2015;1:130–7. doi:10.1115/ICEF2015-1041.

[46] http://www.tfd.chalmers.se/~valeri/MECH.html n.d.

[47] Aggarwal SK, Awomolo O, Akber K. Ignition characteristics of heptane-hydrogen and heptane-methane fuel blends at elevated pressures. Int J Hydrogen Energy 2011;36:15392–402. doi:10.1016/j.ijhydene.2011.08.065.

[48] Han Z, Reitz RD. Turbulence Modeling of Internal Combustion Engines Using RNG κ-ε Models. Combust Sci Technol 1995;106:267–95. doi:10.1080/00102209508907782.

[49] Kong S, Marriott CD, Reitz RD. Modeling and Experiments of HCCI Engine Combustion Using Detailed Chemical Kinetics with Multidimensional CFD. Society 2001:1–2. doi:10.4271/2001.

[50] Gmbh AVLL. AVL FIRE ® VERSION 2011 2011.

[51] Module LM. AVL FIRE ® VERSION 2011 2011.

[52] Beale JC., Reitz RD. Modeling Spray Atomization With the Kelvin-Helmotz/Rayleigh-Taylor Hybrid Model. At Sprays 1999;9:623–50. doi:10.1615/AtomizSpr.v9.i6.40.

[53] Butler T.D. & Cloutman LD& DJK& RDJ. Multidimensional numerical simulation of reactive flow in internal combustion engines 1981;7:293–315.

[54] J.D. Naber RDR. Modeling Engine Spray / Wall Impingement. Sae Tech Pap Ser 1988:880107. doi:10.4271/880107.

[55] Zhang C, Song J. Experimental study of co-combustion ratio on fuel consumption and emissions of NG–diesel dual-fuel heavy-duty engine equipped with a common rail injection system. J Energy Inst 2015:1–8. doi:10.1016/j.joei.2015.06.005.

[56] Liu J, Zhang X, Wang T, Zhang J, Wang H. Experimental and numerical study of the pollution formation in a diesel/CNG dual fuel engine. Fuel 2015;159:418–29. doi:10.1016/j.fuel.2015.07.003.

Chapter 3: An experimental and numerical study on diesel injection split of a natural gas/diesel dual-fuel engine at a low engine load

3.1.Abstract

Natural gas/diesel dual-fuel combustion is currently one of the most promising LTC strategies for the next generation of heavy-duty engines. While this concept is not new and it has been deliberated lengthily in the past two decades, several uncertainties still exist. A major shortcoming of this concept is associated with its low thermal efficiency and high level of unburned methane and CO emissions under low engine load conditions. The present paper reports an experimental and numerical study on the effect of different injection strategies (single and two pulses injection of pilot diesel fuel) on the combustion performance and emissions of a heavy duty natural gas/diesel dual-fuel engine at 25% engine load. The results of single diesel injection mode showed that advancing diesel injection timing from 10 to 30 °BTDC reduced unburned methane and CO emissions by 62% and 61% and increased thermal efficiency by 6%; however, NO_x emissions increased by 74%. In order to achieve NO_x – CH_4 and NO_x – CO trade-off and increased thermal efficiency at low load conditions, the effect of split injection strategy was experimentally and numerically examined. The results of split injection mode revealed that split injection strategy considerably increases the in-cylinder peak pressure compared to that of single injection (10 °BTDC). The results showed also that the heat release produced by the first injection of diesel fuel considerably increased the in-cylinder charge temperature before the start of the second injection. The flame zone of the split injection mode is markedly higher than that of the single injection due to larger heat release produced during the first injection which promotes the combustion of the second one. When the first injection timing is close to the second injection timing, the MPRR of split injection mode is higher than that of single injection (10 °BTDC). However, further

advancing of the first injection timing continuously decreased the MPRR. OH radical analysis showed that for advanced first injection timings (38-50 °BTDC), the overall growth rate of OH radical becomes slower and its distribution is narrower as indicated by the wider non-reactive blue zones compared with those observed at a late first injection timing in the initial stages of combustion. However, OH radicals gradually grow during last stages of combustion in the expansion stroke, indicating that a more premixed combustion takes place in these cases. For very advanced first injection timing of 55 °BTDC, the OH distribution is similar to that of the single injection mode with lower OH intensity at initial stages of combustion and they barely grow during the late expansion stroke. At this condition, the ignition of premixed mixture is mainly controlled by the second diesel fuel injection. The trade-off between NO_x – CH_4 and NO_x – CO is achieved when applying split injection. Compared to single injection (10 °BTDC), the first injection timing of 50 °BTDC decreased unburned methane and CO emissions by 60% and 63%, respectively, and increased the thermal efficiency by 8.9%. However, NO_x emissions were maintained at the same level as single injection mode (10 °BTDC).

Abbreviation			
ADIT	After Diesel Injection Timing	EVO	Exhaust Valve Opening
AMDIT	After Main Diesel Injection Timing	HCCI	Homogeneous Charge Compression Ignition
ASOC	After Start of Combustion	HRR	Heat Release Rate
ASOI	After Start of Injection	ITE	Indicated Thermal Efficiency
BMEP	Break Mean Effective Pressure	LHV	Lower Heating Value
BTDC	Before Top Dead Center	LTC	Low Temperature Combustion
BTE	Break Thermal Efficiency	MPRR	Maximum Pressure Rise Rate
CA	Crank Angle	NO_x	Nitrogen Oxides
CFD	Computational Fluid Dynamic	SOC	Start of Combustion
CI	Compression Ignition	SOI	Start of Injection
CO	Carbon monoxide	TDC	Top Dead Center
DIT	Diesel Injection Timing	THC	Total Hydrocarbon
EGR	Exhaust Gas Recirculation	UHC	Unburned Hydrocarbon
EOI	End of Injection	VCR	Variable Compression Ratio

3.2.Introduction

The usage of petroleum as an energy source is expected to decrease due to limited global oil reserves, its negative impact on the environment, and stringent emissions regulations. This will affect compression ignition (CI) diesel engines which play significant role in transportation and power

generation, where there is a need for cleaner, more economical, and reliable alternative fuels. Conventional diesel engines also suffer from high soot emissions due to the over-rich regions in the core area of the fuel spray and high nitrogen oxides (NO_x) emissions as a result of high flame temperature of the stoichiometric fuel-air mixture at the periphery of the fuel spray. In order to reduce both soot and NO_x emissions, fuel-rich and high temperature stoichiometric regions should be avoided simultaneously [1]. An effective approach is to employ low temperature combustion (LTC) strategies which are featured by improved fuel atomization, mixture preparation, lower local equivalence ratios, reduced local temperature, and alternative fuels [2]. Homogeneous charge compression ignition (HCCI) combustion is one of such strategies characterized by early fuel injection, which promotes fuel premixed charge, long ignition delay, and short combustion duration. Ignition timing is kinetically controlled and therefore decoupled from the timing of the fuel injection event [3,4]. However, the lack of direct control of ignition timing and combustion phasing, higher unburned hydrocarbon (UHC) and carbon monoxide (CO) emissions, as well as knock and misfiring under transient conditions, are the major drawbacks of HCCI combustion engines [5–8]. In contrast, some slightly more heterogeneous combustion strategies have been developed to overcome the majority of the aforementioned challenges. For example, the charge distribution is more heterogeneous than HCCI combustion as it consists of lean and rich regions at the time of ignition. Moreover, ignition timing is closely coupled to the fuel injection timing, though chemical kinetics still play an important role [3].

Natural gas/diesel dual-fuel combustion is one of these LTC strategies which allow a higher degree of combustion phasing control while maintaining low soot and NO_x emissions. In a dual-fuel engine, the primary method of fuel delivery is the port injection of natural gas which creates well-mixed charge of premixed fuel-air, while a small amount of diesel fuel is directly injected into the cylinder as the ignition source. Natural gas/diesel dual-fuel combustion tends to retain most and even surpasses occasionally the positive features of conventional diesel engines, and producing comparable power

output and efficiency at different engine loads [9–11]. In addition, natural gas/diesel dual-fuel mode has attracted much interests due to other advantages, such as simple modification from a diesel engine and the flexibility in switching back to fully diesel mode [12]. Moreover, this combustion concept relies on natural gas as the major energy source, which yields lower carbon dioxide (CO_2) emissions due to the higher hydrogen to carbon ratio. However, there still exist some issues that are limiting the application of natural gas/diesel dual-fuel engines. One of these issues is the low thermal efficiency and higher unburned methane and CO emissions at low engine load conditions. At low load conditions, a natural gas/diesel dual-fuel engine is fed with a very lean air-fuel mixture which is difficult to ignite and burn, leading to significant levels of unburned methane and CO emissions. This is because, at very lean air-methane mixtures, portions of the charge which resides far away from diesel fuel spray escape the combustion process [13–15]. Numerous studies have addressed these issues by examining the effect of combustion boundaries, such as diesel injection timing and pressure [16–20], natural gas energy fraction [20–23], variable compression ratio (VCR) [25–27], natural gas injection timing [20,28], and the use of exhaust gas recirculation (EGR) [29,30]. Among these strategies, diesel injection timing change is of great interest and usually regarded as a critical factor which has influence on the combustion performance and emissions characteristics.

Various researchers have examined the effect of conventional diesel injection timing (i.e., 5-30 ° before top dead center (BTDC)) on thermal efficiency and unburned methane and CO emissions of natural gas/diesel dual-fuel mode at low conditions [10,14,17,31–34]. For instance, Zhang et al. [34] examined the effect of diesel injection timing (DIT) sweep (DIT= 7-25 °BTDC with 2 °crank angle (CA) increment) on combustion performance and emissions of natural gas/diesel dual-fuel mode and found that total hydrocarbon (THC) and CO emissions reduced with advancing diesel injection timing. On the other hand, they noted increased NO_x emissions with advanced diesel injection timing due to higher in-cylinder temperature. Yang et al. [14] investigated various diesel injection timings (DIT=5-29 °BTDC with 4 °CA increment) in a natural gas/diesel dual-fuel engine at a low engine

load. They reported that advancing diesel injection timing from 5 to 29 °BTDC significantly increased break thermal efficiency (BTE). Moreover, they observed that, with advancing diesel injection timing, THC and CO emissions notably decreased due to the relatively higher combustion rate and greater utilization of premixed natural gas at earlier injection timings. Similar to the findings in [34], NO_x emission was observed to significantly increase with advancing diesel injection timing in [14]. Wang et al. [33] also observed that advancing diesel injection timing from -5 to 22.5 °BTDC drastically increased NO_x emissions, while decreased THC emissions.

Based on the briefly reviewed literature above, it is revealed that advancing diesel injection timing in the range of conventional diesel injection timing (i.e., 5-30 °BTDC) improved thermal efficiency as well as unburned methane and CO emissions but generated higher NO_x emissions. To address this issue, various single pulse conventional diesel injection timings (10-30 °BTDC with 4 °CA increment) are experimentally and numerically examined in the present paper using a natural gas/diesel dual-fuel combustion with 75% natural gas energy fraction under 25% engine load (break mean effective pressure (BMEP)= 4.05 bar). Afterwards, the effect of diesel injection split (two pulses injection) as a feasible method to decrease both NO_x and unburned methane emissions and increase thermal efficiency is examined under the same engine load condition. In particular, the effect of first pulse injection timing (28-55 °BTDC) with fixed split injection ratio of 60% and second pulse injection timing of 10 °BTDC on combustion performance and emissions of natural gas/diesel dual-fuel engine is investigated. This provides useful information for the optimization of diesel injection strategy for natural gas/diesel dual-fuel combustion at low load engine conditions.

3.3.Experiments

3.3.1. Test engine

The engine used in this investigation is a modified single-cylinder version of Caterpillar's 3400-series heavy-duty engine. More details about the experimental setup and engine configuration can be

found elsewhere [35]. Table 3-1 lists the specifics of the engine and Figure 3-1 depicts the schematic diagram of test setup.

Natural gas was injected into the intake port by a fuel injection manifold. Diesel fuel was directly injected into the cylinder using a prototype common-rail fuel injector system. The start of injection and injection pulse width for both diesel and natural gas were controlled by a driven system provided by National Instruments (model PXI-1031chassis, 8184 embedded controller, and 7813 R RIO card connected to cRIO-9151 expansion chassis) and LabVIEW-based software (Drivven Inc., Stand-Alone Direct Injector Drive System). The flow rates of diesel and natural gas were measured by two Bronkhorst mass flowmeters, respectively, and the flow rate of air was measured by a turbine mass flowmeter.

Table 3-1. Engine specifications

Engine type	Single cylinder-caterpillar 3400 heavy duty engine
Bore×Stroke	137.2 mm ×165.1 mm
Conn. rod length	261.62 mm
Displacement vol.	2.44 L
Compression ratio	16.25
Diesel fuel injector	Common rail injector
Injector tip length	1.51 mm
Number of nozzle hole×diameter	6×0.23 mm
Natural gas injection timing	-355 °ATDC
Inlet valve opening (IVO)	-358.3 °ATDC
Inlet valve closing (IVC)	-169.7 °ATDC
Exhaust valve opening (EVO)	145.3 °ATDC
Exhaust valve closing (EVC)	348.3 °ATDC

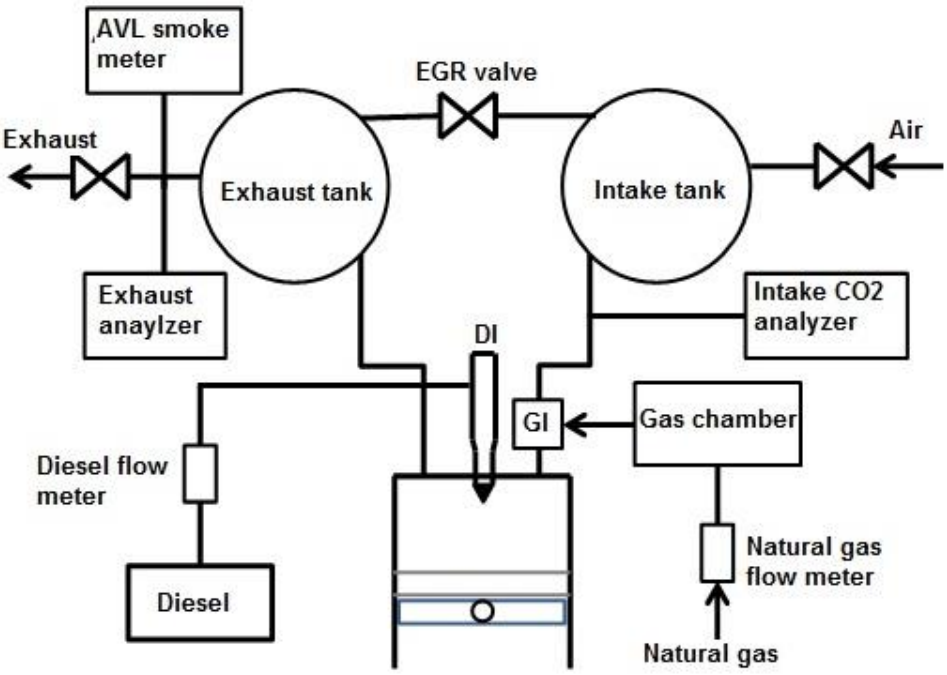

Figure 3-1. Schematic diagram of the experimental setup [35].

3.3.2. Fuels and their supply systems

Diesel fuel used in this study was a Canadian ultra-low-sulfur diesel (ULSD), and the natural gas used in this research was supplied by Enbridge Inc. Table 3-2 gives the properties of both diesel and natural gas used in this study. During the experiment, natural gas energy fraction, which is defined as the energy of natural gas divided by total energy of natural gas and diesel fuel, was kept constant at 75%.

Table 3-2. Fuel properties

Fuel type	**Natural gas**	**Diesel**
Density (kg/m^3)		814.8
Cetane number	-	44
LHV (MJ/kg)	48.4	44.64
Viscosity (cSt 40 °C)		1.483
H/C ratio	-	1.90
Component (% Vol.)	Methane: 96.186 Ethane: 1.741 Propane: 0.100 Hexanes: 0.012 Nitrogen: 1.372 Carbon dioxide: 0.589	

3.3.3. Test procedure and conditions

The experiments were conducted at an engine speed of 910 rpm and a brake mean effective pressure (BMEP) of 4.05 bar, which corresponded to 25% engine load. The intake temperature was kept constant at 40 ˚C during the experiments. The intake and exhaust manifold pressures were kept at 1.05 and 1.20 bar, respectively. The diesel injector rail pressure was 525 bar. EGR was not used in this study. During the tests, a sweep of diesel injection timing for both single injection and split injection modes was conducted.

3.3.4. Diesel injection strategies

The injection strategies employed in this study consisted of a single and two-pulse injections. For the two-pulse injection strategy, the first pulse injection timing was swept from 55 to 28 °BTDC, while the second pulse injection timing was kept constant at 10 °BTDC. The split ratio, which is defined as the mass of the diesel fuel injected in the first pulse over the total mass of the injected diesel fuel, was set at 60%. Table 3-3 shows details of the diesel injection strategies tested in the experiments.

Table 3-3. Experimental test cases- single and split injection strategies under 75% natural gas energy fraction and 25% engine load

Injection strategy	**Air flow (kg/h)**	**Diesel flow (kg/h)**	**NG flow (kg/h)**	**SOI (°BTDC)**	**EOI (°BTDC)**		
Single injection	66.93	0.5238	1.470	10	3.57	-	-
	67.21	0.4948	1.389	14	7.71		
	67.57	0.4710	1.306	18	11.81		
	67.45	0.4503	1.259	22	15.89		
	67.08	0.4370	1.237	26	19.95		
	66.7053	0.4552	1.2345	30	23.86		
				SOI1 (°BTDC)	**EOI1 (°BTDC)**	**SOI2 (°BTDC)**	**EOI2 (°BTDC)**
	63.89	0.4346	1.207	28	22.53	10	6.35
	63.81	0.4266	1.197	30	24.55		6.37
	63.91	0.4271	1.186	34	28.56		6.38
	63.03	0.4212	1.181	38	32.65		6.43
	64.15	0.4168	1.178	42	36.57		6.38

Split injection (60/40%)	64.14	0.4206	1.152	46	40.47	6.31
	64.16	0.4131	1.146	50	44.48	6.32
	64.02	0.4294	1.178	55	49.51	6.34

3.4.Numerical models

3.4.1. Flow and combustion modelling

Details of the model were reported in [36] and thus only a brief description is given here. Numerical simulations were performed using AVL-FIRE v2014 software coupled with CHEMKIN solver for flow and chemistry calculations. Both flow and combustion were modelled by solving the complete set of Navier-Stokes equations. CHEMKIN package was used to acquire reactions rates and thermal and transport properties of species. A reactions mechanism, consisting of 42 species and 168 reactions, developed at Chalmers University [37] and validated at engine relevant conditions by Aggarwal [38] was used in the calculation. In this chemical mechanism, n-heptane was used to represent diesel, and methane was used to represent natural gas. The Heywood original NO_x mechanism was used in this study to account for thermal and prompt NO_x formation [39]. To reduce the computational cost, soot emissions were not considered in the simulation, since soot prediction needs a more complex reaction mechanism. However, our experimental measurements showed that soot emissions for dual-fuel engine are very low [40]. Therefore, neglecting soot in the simulation should have insignificant effect on the results of other parameters. The ‘’Kong-Reitz’’ combustion model was used in the simulation. It assumes that the reaction rate of each species is determined by the kinetic process and the relative magnitude of mixing and reaction, which can be characterized by a local Damköhler number defined as the ratio of flow mixing to kinetic time scale [41]. Renormalization group (RNG) k-ε turbulence model, Reynolds Averaged Navier-Stokes (RANS), and pressure implicit with splitting of operators (PISO) algorithm were used to simulate the transient turbulent flow in the combustion chamber [42]. In the present study, the flow behaviour near the

cylinder wall and the heat transfer between the working fluid and the cylinder wall were modeled using the Hybrid Wall Treatment and Standard Wall Function models [39].

3.4.2. Spray modelling

The break-up process of diesel liquid fuel was simulated using WAVE model based on the physical properties (for the spray and mixing process) of diesel fuel [43]. In this model, the growth of an initial perturbation on the liquid surface is linked to its wavelength and other physical and dynamic parameters of the injected fuel and the in-cylinder gas. There exist two break-up regimes, one for high velocity Kevin-Helmholtz (KH) type and the other for low velocity Rayleigh-Taylor (RT) type break-up [44]. For the first case, the size of droplets is set equal to the wavelength of the fastest growing or most probable unstable surface wave. Rayleigh type break-up produces droplets that are larger than the original parent drops. This regime is not important for high pressure injection systems. The use of WAVE model in the present study, which was developed for KH instabilities, is an appropriate approach for high pressure injection system [43]. Primary parcels (blobs) are injected with a diameter similar to the nozzle orifice and a velocity which is a function of the injected mass flow rate. Particles passing through the flow interact with turbulent eddies. Such interaction results in deflecting particles by the instantaneous velocity of turbulent eddies and particles inertia. This additional turbulence effect on the spray particles could not be resolved by the flow field and consequently the O'Rourke turbulent dispersion model was used in the present study [43]. Moreover, Dukowicz model [45] was used for the heat-up and evaporation of droplets. It assumes that droplets evaporate in a non-condensable gas environment. Therefore, it uses a two-component system in the gas-phase which consists of vapor and non-condensable gas where each component may be composed of a mixture of different species.

3.4.3. Computational domain and initial conditions

The computational mesh was created by FIRE ESE-Diesel platform. Since the diesel injector has six equally spaced nozzle's orifices, a sector mesh of 60° was used to model one spray plume to take advantage of the axial symmetry. To ensure mesh independency, an optimized average cell size of 1.5 mm consisting of 28,833 control volumes at the top dead center (TDC) and 76,020 control volumes at the bottom dead center (BDC) was used. Further refinement of the mesh resolution up to 1 mm did not produce any significant improvement in the accuracy of the predictions, while the required computational runtime was 30% longer. The simulation time step was varied in the range from 0.25 to 0.5 crank angle (°CA) based on the temporal gradients of the computed parameters. Computation was performed in series using a 8-core processor and lasted approximately 6 hours CPU time. The computational domain at the TDC is shown in Figure 3-2. The boundary conditions at the engine head and piston surfaces were defined as impermeable wall boundary conditions. The cylinder geometry was assumed to be symmetric around the cylinder axis, and cyclic boundary conditions were applied to the cutting surfaces as shown in Figure 3-2. Simulation was initialized at IVC and terminated prior to EVO. The port fuel injected natural gas was considered to be homogeneously mixed with air at IVC. Table 3-4 provides the boundary and initial conditions for the numerically simulated cases.

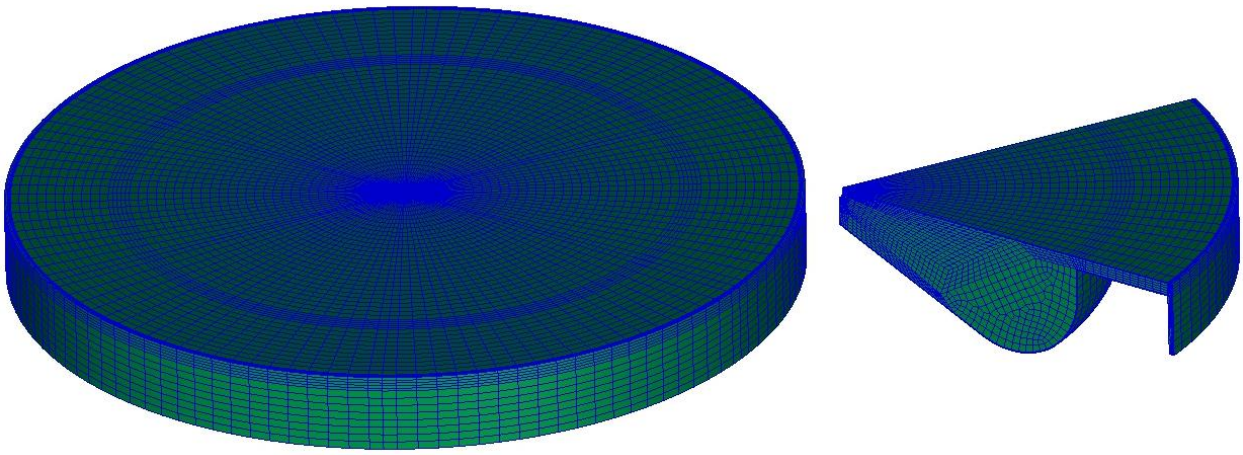

Figure 3-2**.** Computational domain of complete (left) and one-sixth (right) of the combustion chamber at TDC

Table 3-4**.** Initial and boundary conditions

Boundary conditions	**Boundary type/specific condition**
Cylinder head	Wall-temperature 400 K
Piston	Mesh movement-temperature 400 K
Segment cut	Periodic inlet/outlet
Liner	Wall-temperature 400 K
Initial conditions	
Pressure at IVC	1.02 bar
Temperature at IVC	360 K
Turb. kin. energy	10 m^2/s^2
Turb. length scale	0.003 m
Turb. diss. Rate	$1732^2/s^3$

3.4.4. Test conditions

According to the experimental test cases (Table 3-3), all test conditions, including engine load (25% load and BMEP=4.05 bar), speed (910 rpm), natural gas energy fraction (75%), diesel injector rail pressure (525 bar), and intake temperature and pressure (P_{intake} = 1.05 bar, T_{intake} = 313 K, and EGR=0%) were kept constant during the simulation and only the effect of different diesel injection strategies (i.e., single and double pulse injections) on the combustion performance and emissions of dual-fuel combustion was investigated.

3.5.Result and discussion

This section first reports the experimental and numerical results of the effect of conventional single injection timings (10-30 °BTDC) on combustion performance and emissions of natural gas/diesel dual-fuel combustion at 25% engine load (BMEP= 4.05 bar). All test conditions, including engine load (25% load and BMEP=4.05 bar), speed (910 rpm), natural gas energy fraction (75%), diesel injector rail pressure (525 bar), and intake temperature and pressure (P_{intake} = 1.05 bar, T_{intake} = 313 K, and EGR=0%) were kept constant and only diesel injection timing was swept in the range between 10 and 30 °BTDC with an increment of 4 °CA. Then the experimental and numerical results

of the effect of split injection (two pulses injection) on combustion performance and emissions of dual-fuel engine are provided. Numerical simulation results including in-cylinder pressure, heat release rate (HRR), thermal efficiency, emissions of NO_x, CO and unburned methane, and spatial and temporal contours of the mean charge temperature and OH radical are provided to help understand the behaviour of natural gas/diesel dual-fuel combustion process at low engine load conditions.

3.5.1. Single injection

Figure 3-3 shows the effect of conventional injection timing (10-30 °BTDC) on the in-cylinder pressure and HRR of natural gas/diesel dual-fuel mode at 25% engine load (BMEP=4.05 bar). In this study, the measured and calculated HRR was obtained from the average in-cylinder pressure based on the first law of thermodynamics and the ideal gas law. It can be seen that there is a good match between the measured and calculated in-cylinder pressure and HRR profiles, demonstrating the ability of the CFD model along with the adopted reaction mechanism. Advancing the injection timing up to 30 °BTDC increases the maximum in-cylinder pressure and shifts the in-cylinder peak pressure close to the TDC. The in-cylinder temperature during the diesel injection and before start of combustion (SOC) largely affects the premixed mixture formation. Figure 3-4 displays the in-cylinder temperature contours at 5 °CA after diesel injection timing (ADIT) and n-heptane mass fraction distribution at SOC for three selected diesel injection timings. As shown in this figure, at injection timing of 30 °BTDC the mixing process occurs earlier in the compression stroke and consequently lower temperature is present in the combustion chamber during the diesel injection and before SOC. This leads to a prolonged ignition delay and consequently more premixed mixture (diesel and premixed natural gas-air) is formed during the ignition delay period when advancing the diesel injection timing from 10 to 30 °BTDC (Figure 3-4). Earlier injection timing tends to advance the combustion phasing while prolonged ignition delay tends to retard combustion phasing. The effect of advancing diesel injection timing is more significant than that of prolonged ignition delay, leading

to the shift of combustion phasing toward TDC and thus higher maximum in-cylinder pressure when advancing diesel injection timing from 10 to 30 °BTDC.

Figure 3-5a displays the variation of the indicated thermal efficiency (ITE) as a function of diesel injection timing (single injection) under 25% engine load. Advancing the diesel injection timing from 10 to 30 °BTDC significantly increases the thermal efficiency (6%). This is due to the fact that advancing the diesel injection timing prolongs the ignition delay and thus more premixed natural gas-air and diesel mixture is formed before SOC which leads to larger number and wider space distribution of ignition kernel. As a result, combustion efficiency of natural gas is improved, which can be shown by Figure 3-5b and Figure 3-5c that show that advancing diesel injection timing from 10 to 30 °BTDC considerably reduces unburned methane and CO emissions, whereas increases NO_x emissions. Simulation results show that unburned methane and CO emissions are reduced by 62% and 61%, respectively. Advancing diesel injection timing enhanced the entrainment of premixed natural gas into the ignition kernels and consequently the combustion process becomes faster and complete, which is the main reason of the reduction in methane and CO emissions. However, NO_x emissions are increased by 61.3% when diesel injection timing is advanced from 10 to 30 °BTDC. This is due to the fact that the local gas temperature becomes higher and more homogeneous mixture is formed in the cylinder as diesel injection timing advances. Therefore, natural gas/diesel dual-fuel engine experiences improved thermal efficiency and unburned methane and CO emissions but at the expense of higher NO_x emissions when diesel injection is advanced from 10 to 30 °BTDC. This is not in line with LTC strategies which are generally centered on ultra-low NO_x emissions. In order to obtain NO_x – CH_4 and NO_x – CO trade-off, the effect of split injection strategy on natural gas/diesel dual-fuel combustion under similar engine load is investigated in the next section.

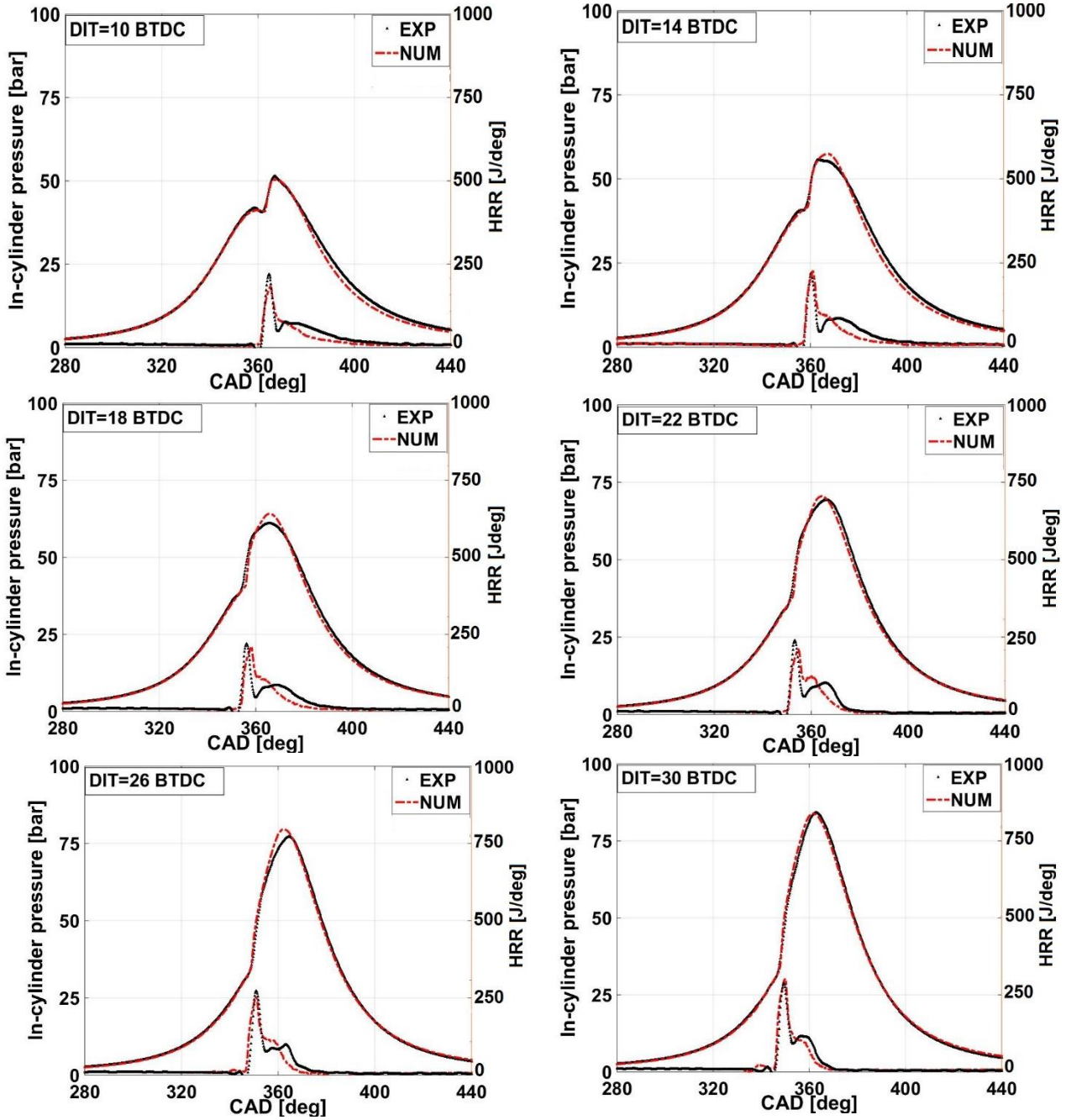

Figure 3-3**.** Comparison of experimental and numerical in-cylinder pressure and HRR of dual-fuel mode with single injection mode under 25% engine load.

Injection timing-single	**In-cylinder temperature at 5 °ADIT (K)**	**n-heptane at SOC**
DIT=10 °BTDC	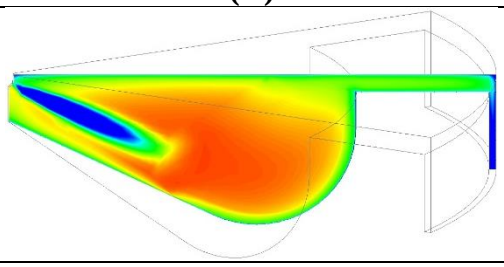	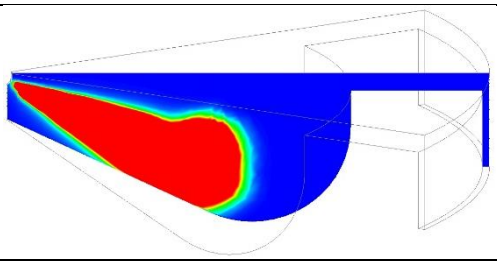

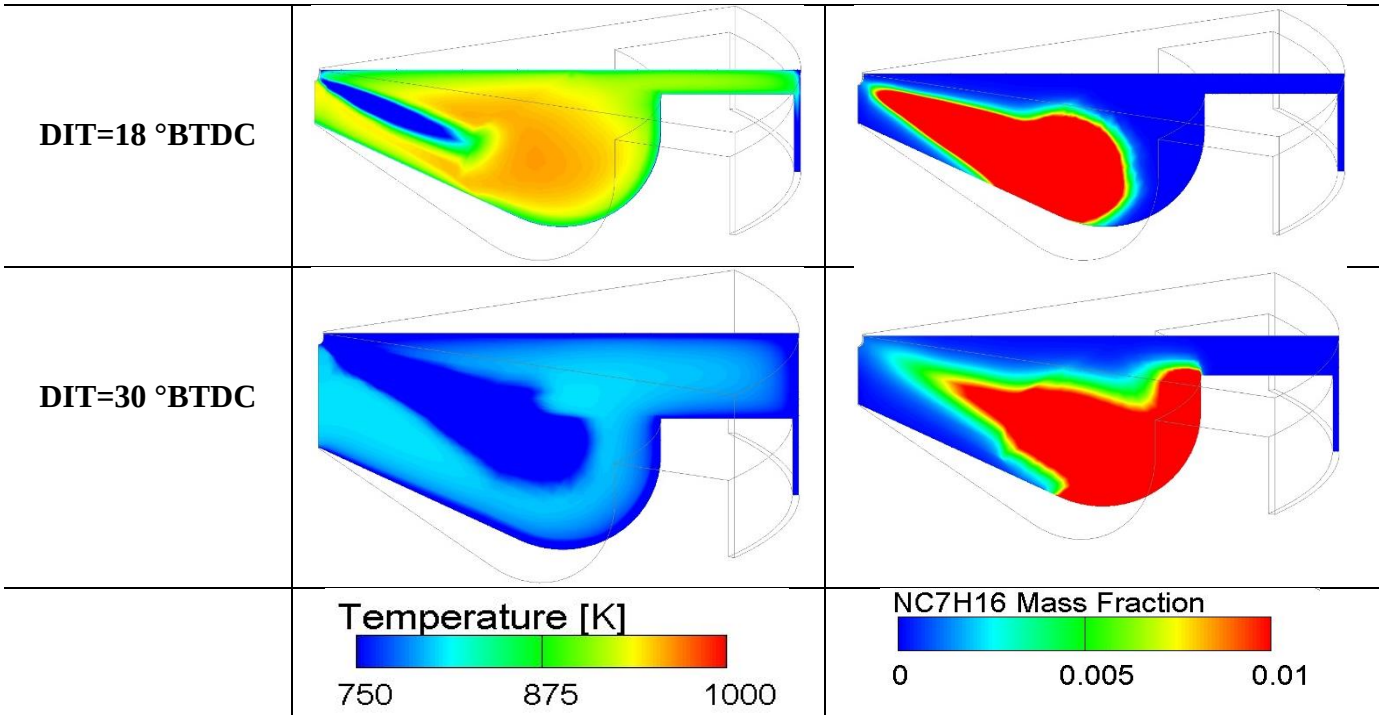

Figure 3-4. In-cylinder temperature (at 5 °CA ADIT) and n-heptane (at SOC) contours of dual-fuel mode with single injection under 25% engine load.

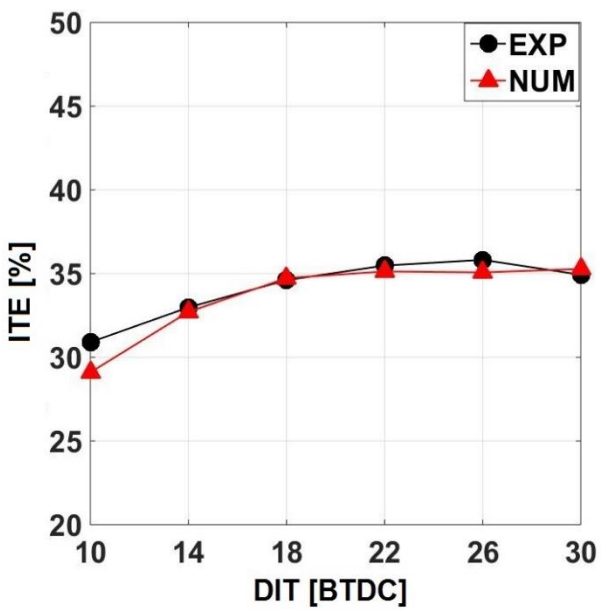

a) Thermal efficiency

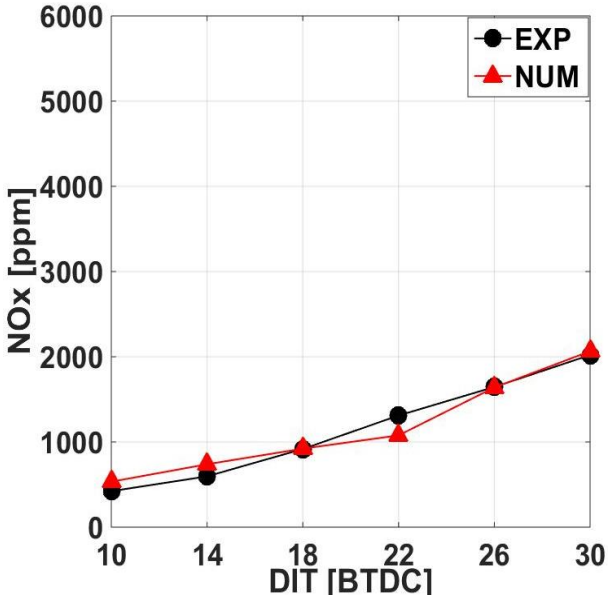

b) NO_x emission

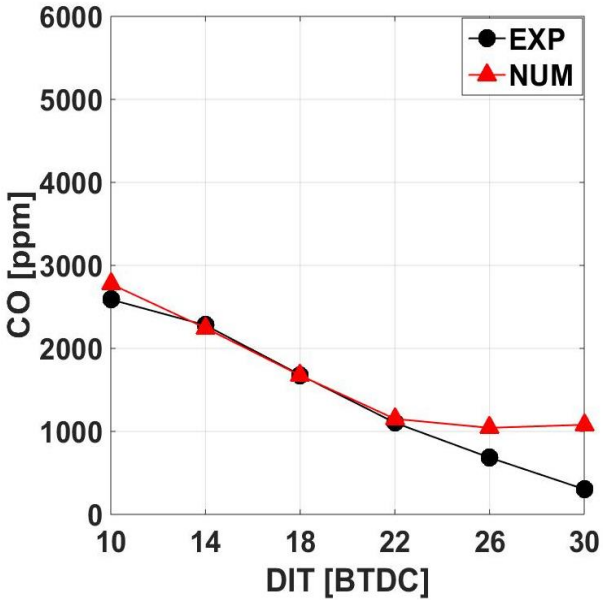

c) CH_4 emission

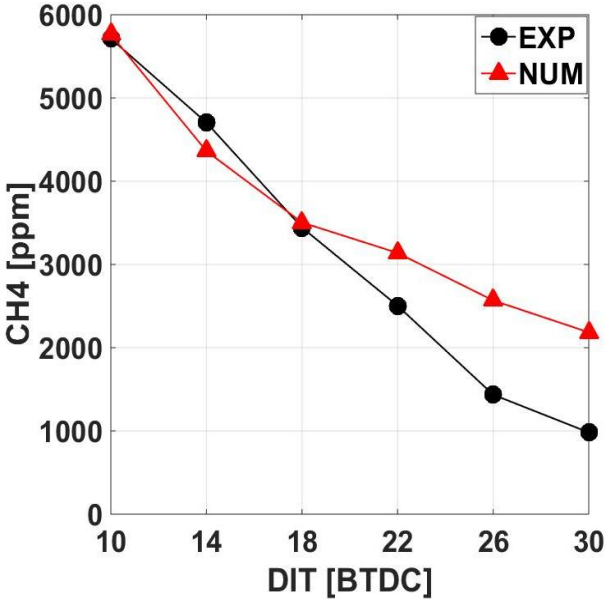

d) CO emission

Figure 3-5. Thermal efficiency and emissions of dual-fuel engine with single injection mode under 25% engine load.

3.5.2. Split injection

In this section the effect of first pulse injection timing (28-55 °BTDC) with a fixed second pulse injection timing of 10 °BTDC and split injection ratio of 60% on combustion performance and emissions under 25% engine load is studied. Split injection ratio is defined as the mass ratio of diesel fuel injected in the first pulse divided by the total amount of the injected diesel fuel. The operating conditions for different split injection strategies are listed in Table 3-3.

3.5.2.1.Effect of split injection on combustion characteristics

Figure 3-6 shows the experimental in-cylinder pressure and HRR of natural gas/diesel dual-fuel combustion of selected first injection timings under fixed split ratio of 60%, second injection timing of 10 °BTDC, and 25% engine load. Moreover, Figure 3-7 displays a comparison between the experimental and numerical in-cylinder pressure and HRR profiles for different first injection timings (28-55 °BTDC) and second injection timing of 10 °BTDC. It can be seen, from Figure 3-6a, that split injection mode considerably increases the in-cylinder peak pressure compared to that of single

injection (10 °BTDC). Figure 3-8 compares the in-cylinder temperature of different first injection timings with that of single injection (SOI=10 °BTDC) at frame contours of 10 and 7 °BTDC. It can be observed that, compared to single injection mode, the heat release produced by first injection of diesel fuel considerably increases the in-cylinder charge temperature before the start of the second injection. The flame zone of the split injection mode is markedly higher than that of the single injection due to larger heat release produced during the first injection which promotes the combustion of the second one.

As shown in Figure 3-6 and Figure 3-7, when the first injection timing is close to the second injection timing (first injection timings of 28, 30, and 34 °BTDC), the advancement of the first injection timing leads to increased peak in-cylinder pressure and HRR. This is mainly due to the advancement of combustion phasing toward TDC. Further advancing first injection timing (38-55 °BTDC) retards the SOC and shifts the combustion phasing away from TDC, leading to decreased peak in-cylinder pressure. Although the peak heat release rate happens slightly later for split injection than for single injection, the maximum pressure of split injection is higher than single injection when the first injection timing is 55 °BTDC. This is because of the significantly lower methane and CO emissions for split injection. As shown in Figure 3-8, when the first injection timing is close to the second injection (i.e., SOI1=30 °BTDC), the second injected diesel fuel spray is close to the high temperature region resulting from the first injection of diesel fuel (flame kernels of the first injection pulse). Thus, the spray of the second injection and the initial stages of flame kernels of the first injection interact with each other, as indicated in Figure 3-8 through the temperature distributions. Consequently, the effect of the first injection is more profound, which leads to increased ignition area of the in-cylinder mixture, earlier SOC (Figure 3-9a) and combustion phasing, and increased in-cylinder peak pressure. Further advancing the first injection timing (38-55 °BTDC) weakens its influence on the combustion of the second injected diesel fuel. This is due to the fact that under advanced first injection timings (i.e. 42 and 50 °BTDC in Figure 3-8), the second injected diesel fuel

spray is located far away from the high temperature region resulted from the first injection of diesel fuel. Under this condition, very advanced first injection timing leads to longer ignition delay, which promotes air-fuel mixing and the formation of leaner air-natural gas and diesel fuel mixture. Thus, SOC (Figure 3-9a) and combustion phasing are retarded which lead to reduced peak in-cylinder pressure.

In this study, the zero-crossing point of heat release curve is defined as SOC [46]. It can be seen from Figure 3-9a that SOC advances firstly and then gradually delays, with advancing the first injection timing. When the first injection timing is close to the second injection timing (first injection timings of 28, 30, and 34 °BTDC), advancing the first injection timing makes the mixing of diesel and natural gas/air mixture start earlier and therefore advances SOC. Further advancing the first injection timing (38-50 °BTDC) results in lower in-cylinder thermal environment at the time of first injection, which leads to longer ignition delay and retarded SOC. This is effective for improving the mixing of natural gas-air and the diesel fuel injected by the first injection and consequently the formation of leaner air-natural gas-diesel mixture. It also helps reduce methane and CO emissions and improve thermal efficiency. At very advanced first injection timing of 55 °BTDC, the premixed charge mixture (including the first injection of diesel fuel and natural gas-air) is too lean to be ignited in the compression stroke so that the ignition timing of the premixed charge is determined by the second injection of diesel fuel. In this case, the combustion starts very late (5.1 °BTDC) after the second injection of diesel fuel (Figure 3-9a).

Figure 3-9b shows the maximum pressure rise rate (MPRR) of single and split injection modes under 25% engine load. The MPRR is usually adopted as an index to describe the intensity of combustion roughness. Combustion noise is closely related to MPRR, which is a problem for highly premixed combustion like LTC. As shown in this figure, when the first injection timing is close to the second injection timing, the MPRR of split injection mode is much higher than that of single injection. However, further advancing first injection timing continuously decreases the MPRR. This

is due to the fact that advancing first injection timings weakens the effect of split injected fuel on premixed charge combustion. It retards the SOC and reduces the MPRR. For very advanced first injection timing of 55 °BTDC, the MPRR decreases significantly and is lower than that of single injection. As mentioned earlier, the SOC is very retarded (4.6 °BTDC) and occurs after the second injection timing. In this case the second injection of diesel fuel controls the ignition and combustion rate of the in-cylinder mixture.

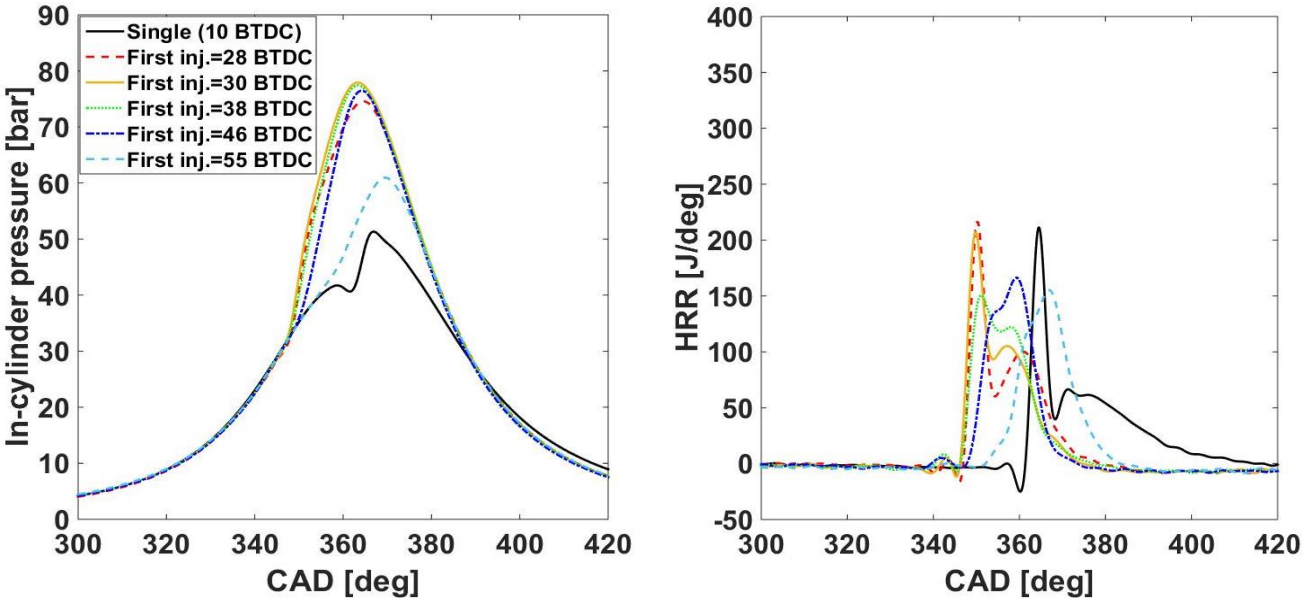

a) In-cylinder pressure b) HRR

Figure 3-6. Experimental in-cylinder pressure and HRR of dual-fuel mode with split injection under 25% engine load.

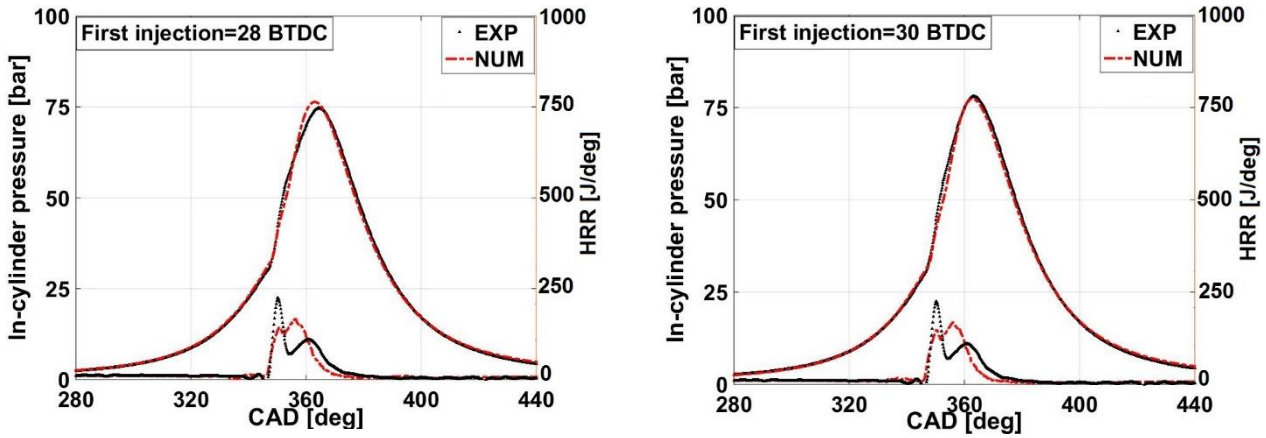

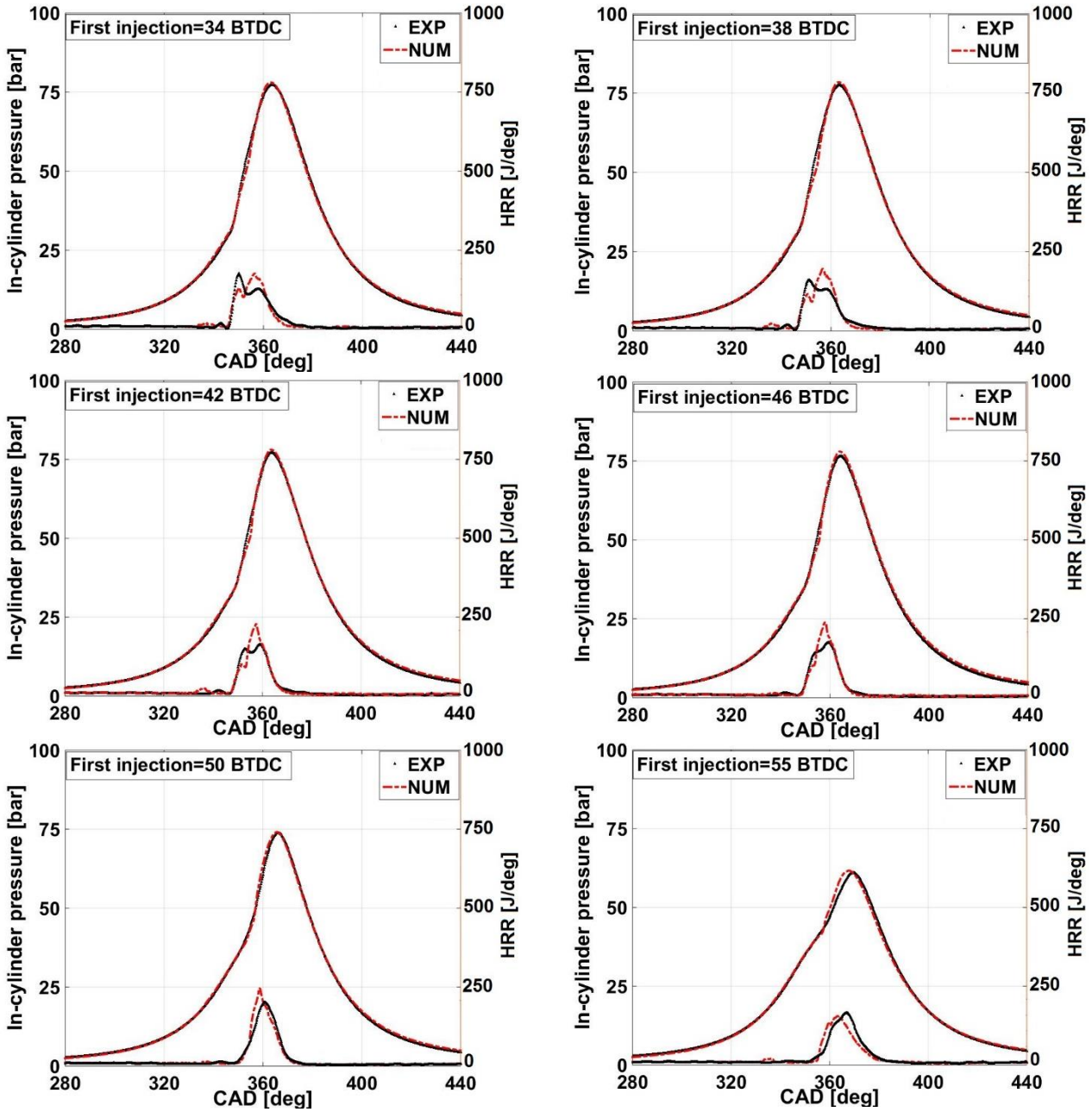

Figure 3-7**.** Experimental and numerical comparison of in-cylinder pressure and HRR of dual-fuel combustion with split injection mode (different first injection timings and second injection timing of 10 °BTDC) under 25% engine load.

	10 °BTDC	**7 °BTDC**
	Single injection	
SOI=10 °BTDC	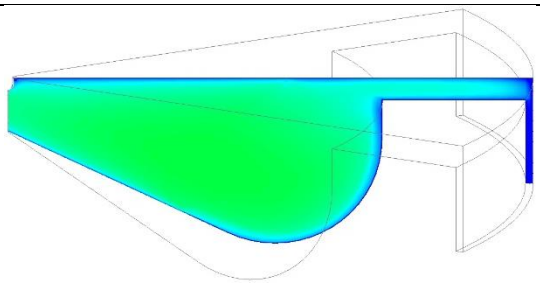	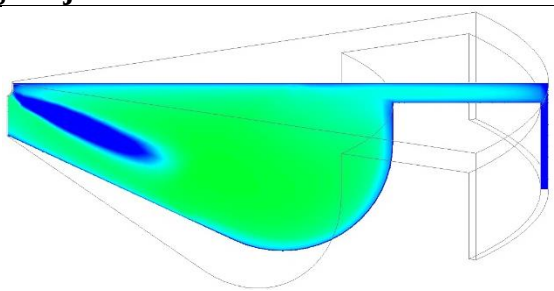

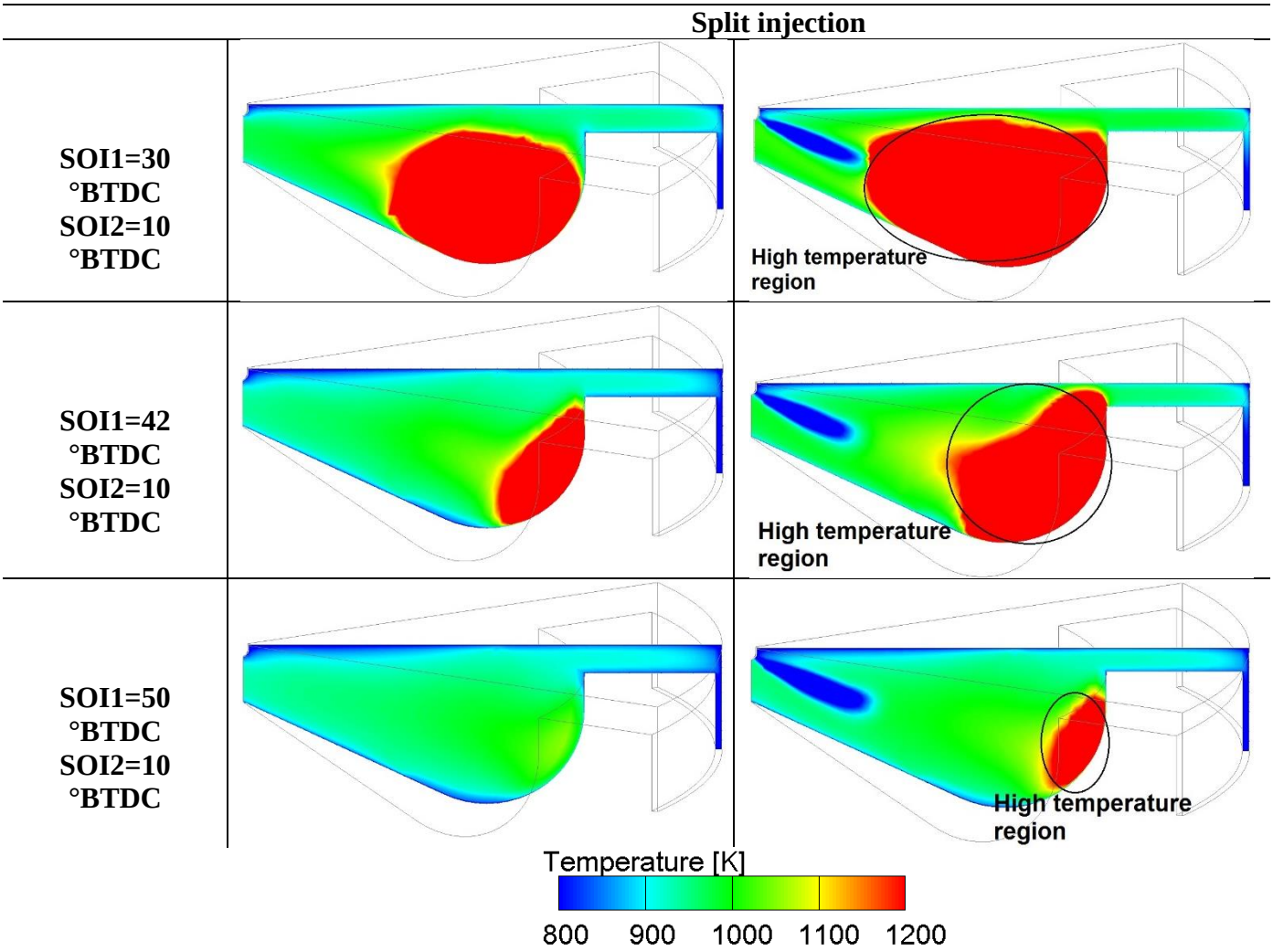

Figure 3-8**.** In-cylinder temperature contours for single injection and split injection modes under 25% engine load at frame contours of 7 and 10 °BTDC.

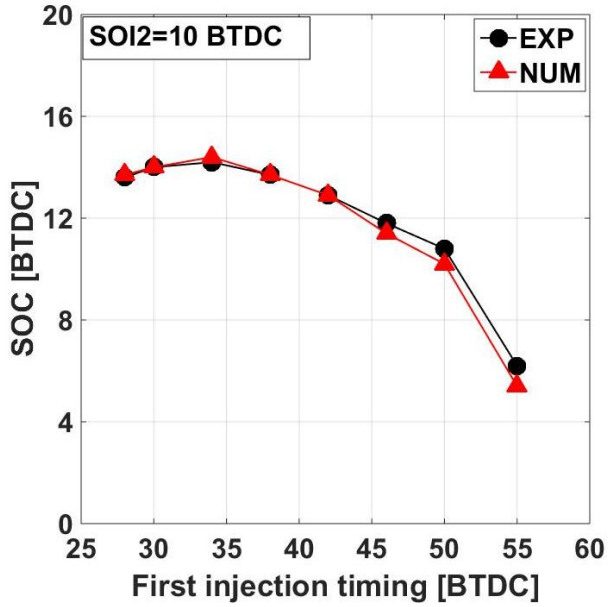

a) SOC

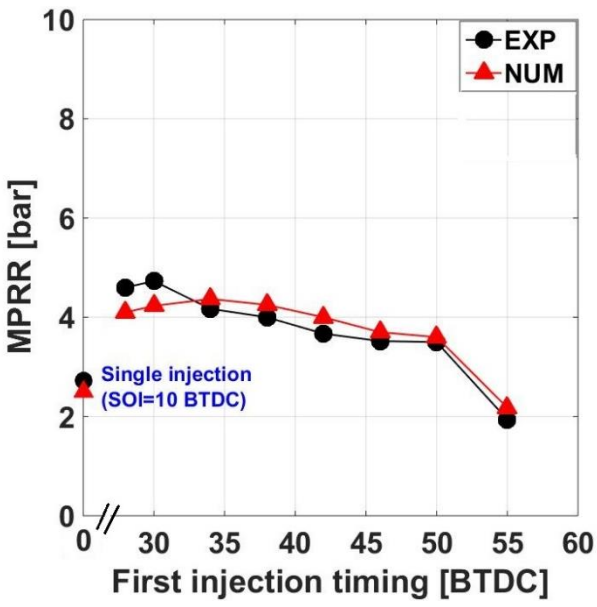

b) MPRR

Figure 3-9. Experimental and numerical comparison of SOC and MPRR of dual-fuel combustion with split injection mode under 25% engine load.

Figure 3-10 presents the spatial distribution of OH radical mass fraction for single injection timing of 10 °BTDC and selected first injection timings of 30, 42, 50, and 55 °BTDC at different crank angles of 3, 6, 10, and 15 ° after the start of combustion (ASOC). The contours plane is located at a vertical distance of 11 mm from the nozzle tip (top view). Moreover, Figure 3-11 depicts the in-cylinder charge temperature for these selected first injection timings at 8 °ASOC (side view). It can be observed, from Figure 3-10, that OH radical distribution is wider and more intense for the first injection timing of 30 °BTDC compared to single injection (10 °BTDC) and other first injection timings at initial stages of combustion (frame contours of 3 and 6 °ASOC). As shown in this figure, for this case, due to high temperature and pressure of premixed charge, the first injected diesel is directly ignited before the second injection timing. The second injected diesel fuel spray is close to the high temperature region resulting from the first injection of diesel fuel (flame kernels of the first injection pulse). Thus, the spray of the second injection and the initial stages of flame kernels of the first injection interact with each other and the second diesel injection undergoes auto-ignition instantly which leads to increased ignition area of the in-cylinder mixture in the directions of spray during the initial stages of combustion (Figure 3-11). However, OH radical distribution for this case appeared throughout the injection zones and their sizes do not change significantly during the last stages of combustion (frame contours of 10 and 15 °ASOC). With advancing first injection timing (i.e., 42 and 50 °BTDC), the overall growth rate of OH radical becomes slower, its distribution is narrower, and the blue non-reactive zones are wider than those observed with a late first injection timing in the initial stages of combustion. However, they gradually continue to grow during last stages of combustion in the expansion stroke, indicating that a more premixed combustion takes place in these cases (Figure 3-10 and Figure 3-11). It increases heat release during the expansion stroke which results in increased thermal efficiency. It is notable that for these cases (i.e., SOI1=42 and 50 °BTDC),

the OH radicals are detected in two zones at 10 °ASOC. The first zone is found near the wall region of piston bowl which corresponds to the high temperature fuel rich zones of first injected fuel and the second one is detected closer to the cylinder axis and nozzle tip which corresponds to the second diesel fuel injection (see Figure 3-11). Moreover, for very advanced injection timing of 55 °BTDC, the OH distribution is similar to that of the single injection mode with lower OH intensity at initial stages of combustion (3 °ASOC). For this case, the premixed charge (air-natural gas-first injected diesel) is very lean and the second injection of diesel fuel mostly controls the ignition of the premixed charge. It can be seen that the OH radicals are detected very close to cylinder axis and nozzle tip and they barely grow during the late expansion stroke (Figure 3-10). Moreover, the OH distribution is much narrower than that of the first injection timings of 30, 42, and 50 °BTDC, however, it is still wider than that of single injection (10 °BTDC).

	3 °ASOC	**6 °ASOC**	**10 °ASOC**	**15 °ASOC**
Single injection				
SOI=10 °BTDC	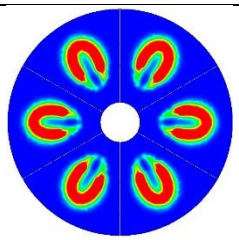	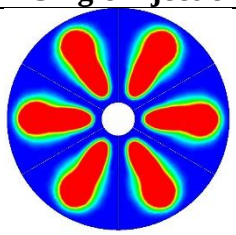	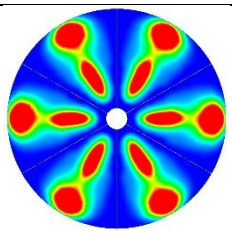	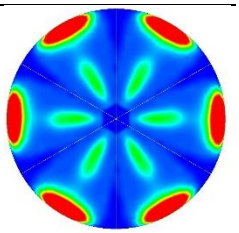
Split injection				
SOI1=30 °BTDC SOI2=10 °BTDC	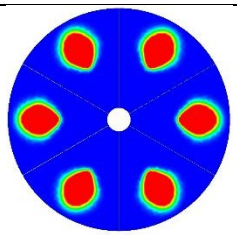	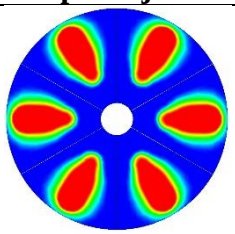	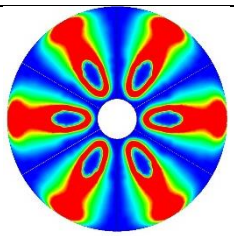	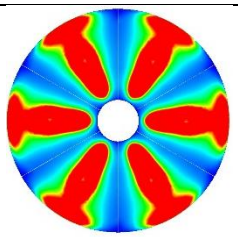
SOI1=42 °BTDC SOI2=10 °BTDC	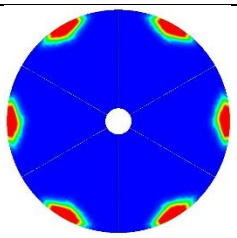	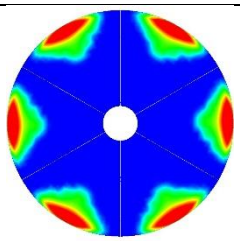	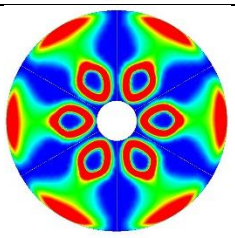	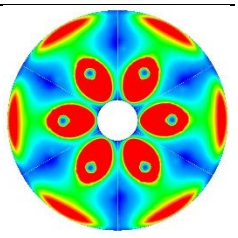

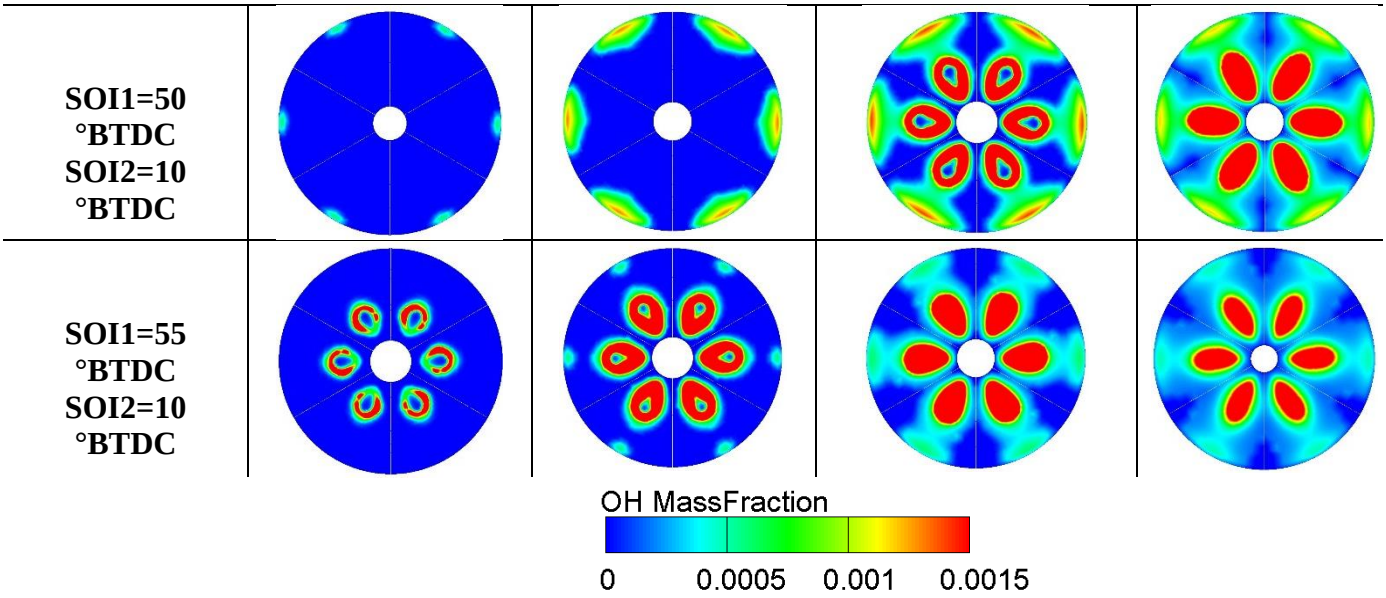

Figure 3-10. Spatial contours of OH radical for selected single and split injection modes under 25% engine load.

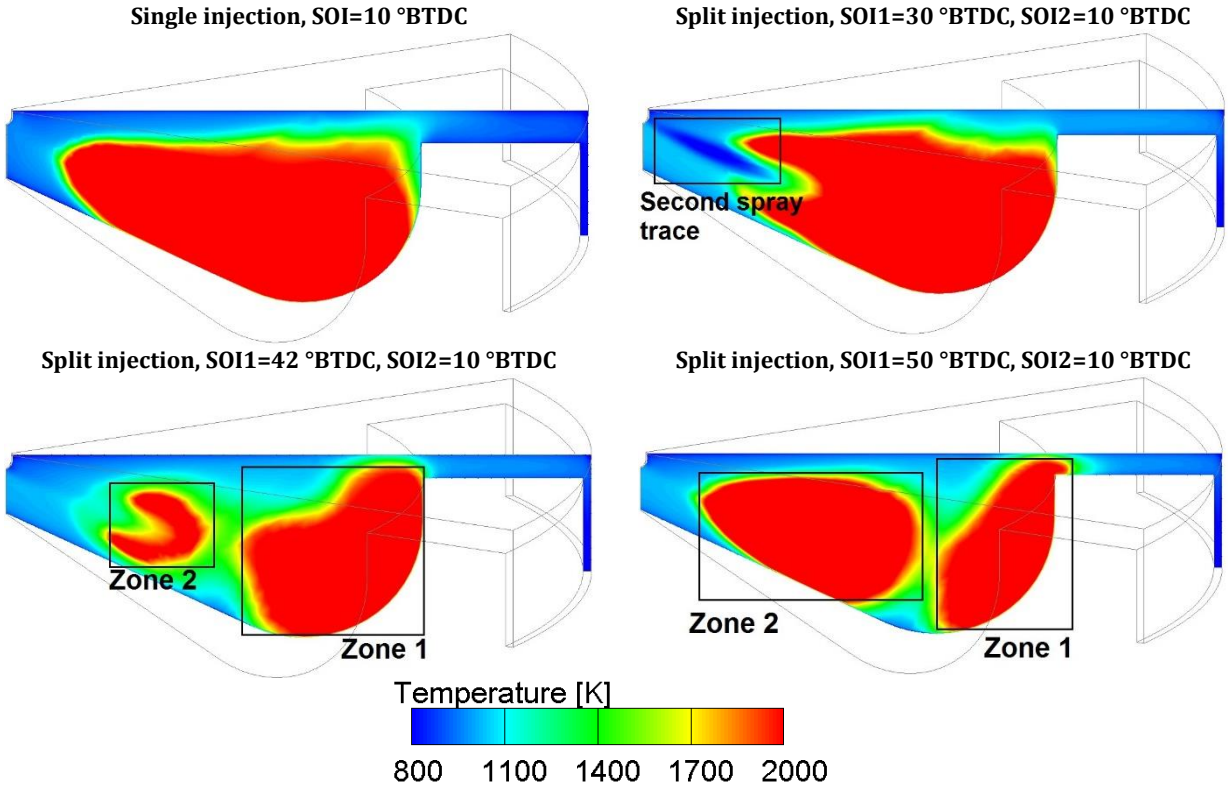

Figure 3-11. In-cylinder temperature contours (at 8 °ASOC) of single and split injection modes under 25% engine load.

3.5.2.2.Effect of split injection on engine performance and emissions

Figure 3-12 shows the ITE of natural gas/diesel dual-fuel combustion under single injection timing of 10 °BTDC and different first injection timings at 25% load condition. As shown in this figure, a considerable improvement in ITE can be observed when using split injection strategy. The ITE of dual-fuel combustion with split injection mode is increased (on average) by 7% compared to that of single injection mode. Moreover, the highest thermal efficiency (38.04%) is obtained at the first injection timing of 50 °BTDC. It can be seen that the ITE continuously increases with advancing the first injection timing from 28 to 50 °BTDC. As shown in Figure 3-10 and Figure 3-11, with advancing the first injection timing, the premixed ignition of diesel-air-natural gas mixture provides a significant wide ignition source for natural gas, resulting in a faster combustion rate of natural gas-air mixture. The multipoint premixed combustion dominated by natural gas occurs quickly after the premixed combustion of pilot diesel fuel which results in improved premixed combustion of natural gas and more released heat during the premixed combustion stage. This late released heat positively affects the expansion pressure which leads to an increase in ITE. However, the ITE starts to drop for very advanced first injection timing of 55 °BTDC. This is due to the late start of combustion which causes combustion process to be shifted into the expansion stroke which results in lower in-cylinder pressure during the expansion stroke. This yields an increase in unburned methane and CO emissions (Figure 3-13) which leads to a decrease in thermal efficiency.

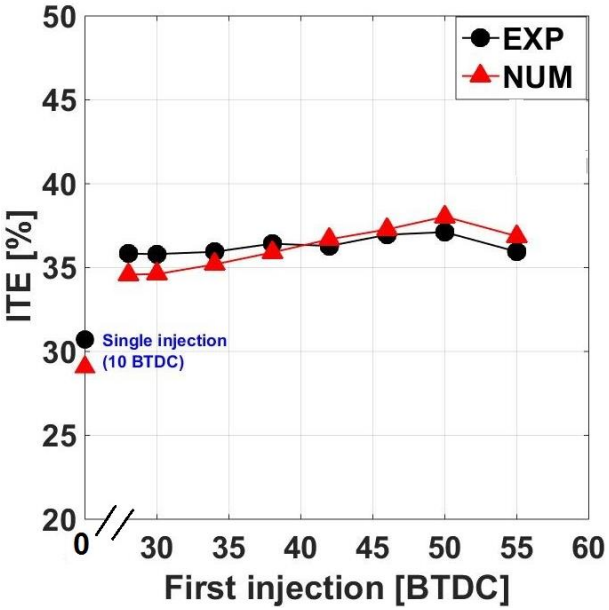

Figure 3-12**.** Experimental and numerical comparison of ITE under 25% engine load.

Figure 3-13a depicts the variation of NO_x emissions under different first injection timings and single injection timing of 10 °BTDC at 25% engine load. The formation of NO_x is related to combustion temperature and oxygen concentration. Higher in-cylinder charge temperature and oxygen concentration and longer reaction times result in more NO_x formation. It is observed that the experimental NO_x trend is well captured numerically. However, the model quantitatively over-predicts NO_x emissions. Moreover, it can be seen that a late first injection timing significantly increases NO_x emissions compared to that of single injection mode. This is because the first injected diesel is directly ignited due to high in-cylinder charge temperature. The second part of diesel fuel is injected during the combustion of the first injection, which leads to short interval time for sufficient air-fuel mixing. The local high combustion temperature regions are relatively wide (Figure 3-14) which results in relatively higher NO_x emissions. Advancing first injection timing leads to leaner diesel and natural gas-air mixture formation. The ignition effect of the first injection of diesel fuel on the second injection weakens, resulting in delayed SOC. It prompts better air-fuel mixing which provides local lean and low combustion temperature regions, and thereby decreases largely NO_x

formation. From Figure 3-13a, it can be seen that, at first injection timing of 50 °BTDC, the level of NO_x emissions becomes similar to that of single injection mode (10 °BTDC).

The high level of unburned methane emissions of natural gas/diesel dual-fuel combustion at low load is caused by very lean premixed natural gas-air mixture and low chemical reactivity, low combustion rate due to extremely small amount of injected diesel fuel, and low in-cylinder charge temperature for premixed natural gas fuel oxidation [47,48]. Figure 3-13b presents the unburned methane emissions for single injection timing of 10 °BTDC and different first injection timings under 25% engine load. The experimental results show that dual-fuel combustion with split injection mode significantly decreases unburned methane emissions compared to that of single injection mode (10 °BTDC). This trend is well reproduced by the CFD model. However, the numerical model over-predicts the unburned methane emissions under the examined first injection timings and misses the slight increase trend at first injection timings of 34-42 °BTDC. This might be due to the adopted reduced mechanism for natural gas/diesel dual-fuel combustion and also to the representation of diesel and natural gas by n-heptane and methane, respectively. Moreover, simulated methane emissions were predicted at EVO which may also contribute to the difference between the predicted and measured unburned methane emissions. It can be seen that the lowest methane emissions are achieved at very advanced first injection timing of 50 °BTDC. At this first injection timing, unburned methane emissions decrease by 60% compared to that of single injection. This is due to the improved premixed combustion and greater utilization of natural gas at earlier first injection timings. Further advancing first injection timing to 55 °BTDC increases the unburned methane emissions which are mainly due to a drop in combustion intensity during the expansion stroke.

The production of CO is mainly due to the incomplete combustion of fuels in the cylinder. Hence, CO is an intermediate product during the combustion process which can be formed in local oxygen deficit and low temperature regions. Excess air and combustion temperature greatly affect the oxidation reaction for converting CO to CO_2 [49]. Figure 3-13c displays the CO emissions for single

injection timing of 10 °BTDC and different first injection timings under 25% engine load. Due to the similar reason for the over-prediction of unburned methane emissions, the numerical model over-estimated the CO emissions under the examined first injection timings. However, its trend is well captured by the CFD model. It can be seen that compared to single injection mode, split injection considerably reduces the CO emissions. Compared to single injection, CO emissions are reduced by 63% at first injection timing of 50 °BTDC. Further advancing first injection timing (55 °BTDC) weakens the effect of first injected fuel on ignition and combustion intensity, and consequently leads to lower combustion temperature and increased CO emissions.

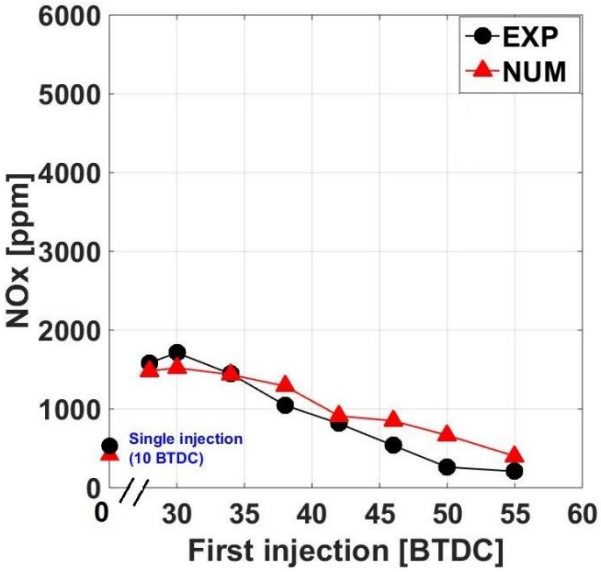

a) NO_x

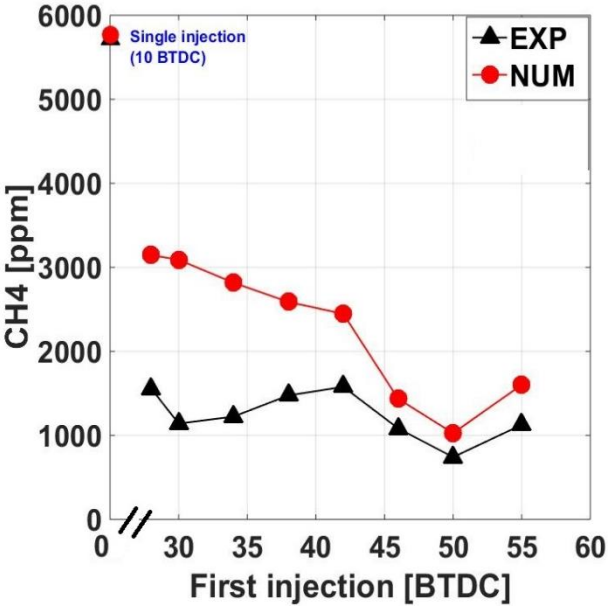

b) CH_4

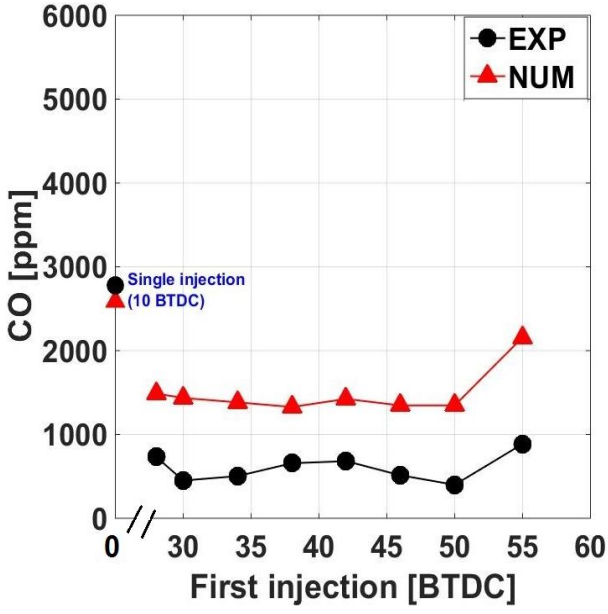

c) CO

Figure 3-13**.** Comparison between experimental and numerical emissions under 25% engine load.

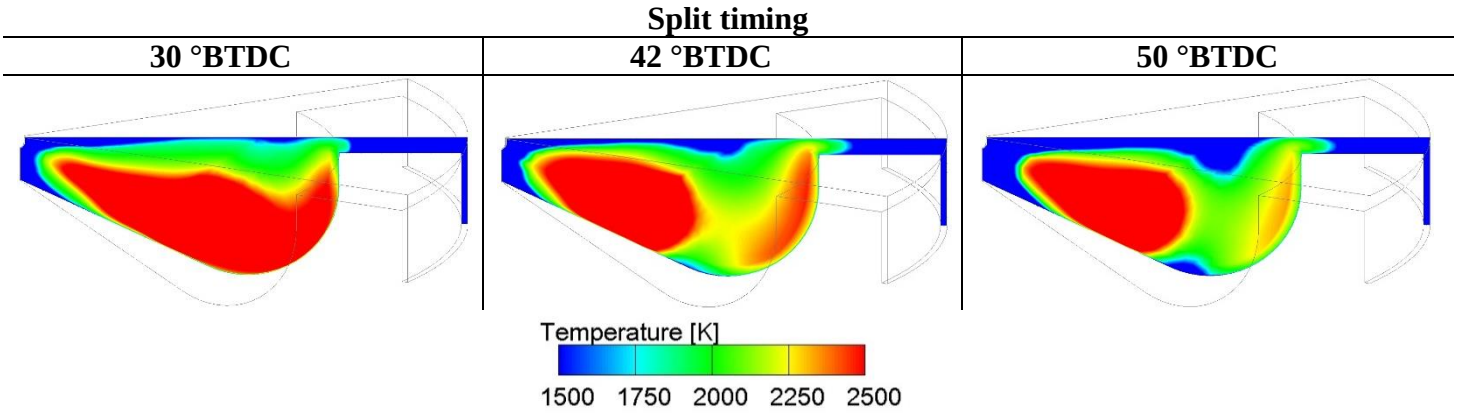

Figure 3-14. In-cylinder temperature (at TDC) of selected first injection timings under 25% engine load.

3.6.Conclusions

In this study, the effect of conventional single injection timing on the combustion and emissions characteristics of a natural gas/diesel dual-fuel combustion under low load conditions were investigated. Moreover, to achieve NO_x – CH_4 and NO_x – CO trade-off, the effect of split injection strategy under similar engine load was examined. The main conclusions of this study are summarized as follows:

- Natural gas/diesel dual-fuel engine at low loads experienced improved thermal efficiency and unburned methane and CO emissions at the expense of higher NO_x emissions when diesel injection is advanced from 10 to 30 °BTDC. Advancing single diesel injection timing from 10 to 30 °BTDC reduced unburned methane and CO emissions by 62% and 61% and increased thermal efficiency by 6%, but increased NO_x emissions by 74%.
- Split injection mode considerably increased the peak in-cylinder pressure compared to that of single injection (10 °BTDC). For late first injection timing, advancing the first injection timing led to increased peak in-cylinder pressure. Due to high temperature of premixed charge, first injected diesel directly ignited and the interaction between the spray of the second

injection and the initial stages of flame kernels led to increased ignition area of the in-cylinder mixture. Further advancing the first injection timing weakened the influence of the first injection of diesel fuel combustion on the second injection combustion. Moreover, at very advanced first injection timing of 55 °BTDC, the ignition of premixed charge is mainly controlled by the second diesel fuel injection.

- For advanced first injection timings (38-50 °BTDC), the overall growth rate of OH radical became slower with a narrower distribution, and a wider blue non-reactive zones than those observed with a late first injection timing in the initial stages of combustion. However, they exhibited a gradual growth during the last stages of combustion in the expansion stroke, indicating that a more premixed combustion occurred in these cases. For first injection timings of 42 and 50 °BTDC, the OH radicals were detected in the two zones during the last stages of combustion. Moreover, for very advanced injection timing of 55 °BTDC, the OH distribution is similar to that of the single injection mode with lower OH intensity at initial stages of combustion.
- The ITE of dual-fuel combustion with split injection mode increased (on average) by 7% compared to that of single injection mode. ITE continuously increased with advancing first injection timing from 28 to 50 °BTDC and the highest thermal efficiency of 38.04% was achieved at first injection timing of 50 °BTDC. However, the ITE started dropping for very advanced injection timing of 55 °BTDC as a result of late combustion phasing during the expansion stroke. Applying closely first injection timing significantly increased NO_x emissions compared to that of single injection mode. However, advancing first injection timing led to improved air-fuel mixing and lessened high combustion temperature regions, which consequently diminished NO_x formation. Moreover, the lowest methane and CO emissions were achieved at very advanced first injection timing of 50 °BTDC due to improved premixed combustion and greater utilization of natural gas at earlier first injection timings.

The trade-off between NO_x – CH_4 and NO_x – CO was accomplished with the application of split injection strategy. Compared to single injection, first injection timing of 50 °BTDC decreased unburned methane and CO emissions by, respectively, 60% and 63% and increased the thermal efficiency by 8.9%. However, NO_x emissions was maintained at the same level as that of single injection mode (10 °BTDC).

3.7.References

[1] Qiu L, Cheng X, Liu B, Dong S, Bao Z. Partially premixed combustion based on different injection strategies in a light-duty diesel engine. Energy 2016;96:155–65. doi:10.1016/j.energy.2015.12.052.

[2] Pedrozo VB, May I, Dalla Nora M, Cairns A, Zhao H. Experimental analysis of ethanol dual-fuel combustion in a heavy-duty diesel engine: An optimisation at low load. Appl Energy 2016;165:166–82. doi:10.1016/j.apenergy.2015.12.052.

[3] Musculus MPB, Miles PC, Pickett LM. Conceptual models for partially premixed low-temperature diesel combustion. vol. 39. Elsevier Ltd; 2013. doi:10.1016/j.pecs.2012.09.001.

[4] Yousefi A, Birouk M. Fuel suitability for homogeneous charge compression ignition combustion 2016;119:304–15.

[5] Jung D, Iida N. Closed-loop control of HCCI combustion for DME using external EGR and rebreathed EGR to reduce pressure-rise rate with combustion-phasing retard. Appl Energy 2015;138:315–30. doi:10.1016/j.apenergy.2014.10.085.

[6] Bendu H, Murugan S. Homogeneous charge compression ignition (HCCI) combustion: Mixture preparation and control strategies in diesel engines. Renew Sustain Energy Rev 2014;38:732–46. doi:10.1016/j.rser.2014.07.019.

[7] Saxena S, Bedoya ID. Fundamental phenomena affecting low temperature combustion and

HCCI engines, high load limits and strategies for extending these limits. Prog Energy Combust Sci 2013;39:457–88. doi:10.1016/j.pecs.2013.05.002 Review.

[8] Yousefi A, Gharehghani A, Birouk M. Comparison study on combustion characteristics and emissions of a homogeneous charge compression ignition (HCCI) engine with and without pre-combustion chamber. Energy Convers Manag 2015;100:232–41. doi:10.1016/j.enconman.2015.05.024.

[9] Sahoo BB, Sahoo N, Saha UK. Effect of engine parameters and type of gaseous fuel on the performance of dual-fuel gas diesel engines-A critical review. Renew Sustain Energy Rev 2009;13:1151–84. doi:10.1016/j.rser.2008.08.003.

[10] Yousefi A, Birouk M. Investigation of natural gas energy fraction and injection timing on the performance and emissions of a dual-fuel engine with pre-combustion chamber under low engine load. Appl Energy 2017;189:492–505. doi:10.1016/j.apenergy.2016.12.046.

[11] Yousefi A, Birouk M, Lawler B, Gharehghani A. Performance and emissions of a dual-fuel pilot diesel ignition engine operating on various premixed fuels. Energy Convers Manag 2015;106:322–36. doi:10.1016/j.enconman.2015.09.056.

[12] Hosmath RS, Banapurmath NR, Khandal S V., Gaitonde VN, Basavarajappa YH, Yaliwal VS. Effect of compression ratio, CNG flow rate and injection timing on the performance of dual fuel engine operated on honge oil methyl ester (HOME) and compressed natural gas (CNG). Renew Energy 2016;93:579–90. doi:10.1016/j.renene.2016.03.010.

[13] Carlucci AP, Laforgia D, Saracino R, Toto G. Combustion and emissions control in diesel-methane dual fuel engines: The effects of methane supply method combined with variable in-cylinder charge bulk motion. Energy Convers Manag 2011;52:3004–17. doi:10.1016/j.enconman.2011.04.012.

[14] Yang B, Wang L, Ning L, Zeng K. Effects of pilot injection timing on the combustion noise and particle emissions of a diesel/natural gas dual-fuel engine at low load. Appl Therm Eng 2016;102:822–8. doi:10.1016/j.applthermaleng.2016.03.126.

[15] Aksu C, Kawahara N, Tsuboi K, Kondo M, Tomita E. Extension of PREMIER combustion operation range using split micro pilot fuel injection in a dual fuel natural gas compression ignition engine: A performance-based and visual investigation. Fuel 2016;185:243–53. doi:10.1016/j.fuel.2016.07.120.

[16] Yousefi A, Birouk M. An Investigation of Multi-Injection Strategies for a Dual-Fuel Pilot Diesel Ignition Engine at Low Load. J Energy Resour Technol 2016;139:12201. doi:10.1115/1.4033707.

[17] Ryu K. Effects of pilot injection timing on the combustion and emissions characteristics in a diesel engine using biodiesel-CNG dual fuel. Appl Energy 2013;111:721–30. doi:10.1016/j.apenergy.2013.05.046.

[18] Srinivasan KK, Krishnan SR. Cyclic Combustion Variations in Dual Fuel Partially Premixed Pilot-Ignited Natural Gas Engines. J Energy Resour Technol 2014;136:1–10. doi:10.1115/1.4024855.

[19] Xu M, Cheng W, Li Z, Zhang H, An T, Meng Z. Pre-injection strategy for pilot diesel compression ignition natural gas engine. Appl Energy 2016;179:1185–93. doi:10.1016/j.apenergy.2016.07.024.

[20] Yang B, Xi C, Wei X, Zeng K, Lai MC. Parametric investigation of natural gas port injection and diesel pilot injection on the combustion and emissions of a turbocharged common rail dual-fuel engine at low load. Appl Energy 2015. doi:10.1016/j.apenergy.2015.01.037.

[21] Papagiannakis RG, Rakopoulos CD, Hountalas DT, Rakopoulos DC. Emission characteristics

of high speed, dual fuel, compression ignition engine operating in a wide range of natural gas/diesel fuel proportions. Fuel 2010. doi:10.1016/j.fuel.2009.11.001.

[22] Papagiannakis RG, Hountalas DT. Combustion and exhaust emission characteristics of a dual fuel compression ignition engine operated with pilot diesel fuel and natural gas. Energy Convers Manag 2004;45:2971–87. doi:10.1016/j.enconman.2004.01.013.

[23] Rao BN, Prem Kumar BS, Kumar Reddy KV. Effect of CNG flow rate on the performance and emissions of a Mullite-coated diesel engine under dual-fuel mode. Int J Ambient Energy 2015;750:1–8. doi:10.1080/01430750.2015.1023835.

[24] Mikulski M, Wierzbicki S, Śmieja M, Matijošius J. Effect of CNG in a fuel dose on the combustion process of a compression-ignition engine. Transport 2015;30:162–71. doi:10.3846/16484142.2015.1045938.

[25] Di Blasio G, Belgiorno G, Beatrice C, Fraioli V, Migliaccio M. Experimental Evaluation of Compression Ratio Influence on the Performance of a Dual-Fuel Methane-Diesel Light-Duty Engine. SAE Int J Engines 2015;8:2015-24–2460. doi:10.4271/2015-24-2460.

[26] Bora BJ, Saha UK. Experimental evaluation of a rice bran biodiesel - biogas run dual fuel diesel engine at varying compression ratios. Renew Energy 2016;87:782–90. doi:10.1016/j.renene.2015.11.002.

[27] Bora BJ, Saha UK. Optimisation of injection timing and compression ratio of a raw biogas powered dual fuel diesel engine. Appl Therm Eng 2016;92:111–21. doi:10.1016/j.applthermaleng.2015.08.111.

[28] Yang B, Wei X, Xi C, Liu Y, Zeng K, Lai MC. Experimental study of the effects of natural gas injection timing on the combustion performance and emissions of a turbocharged common rail dual-fuel engine. Energy Convers Manag 2014. doi:10.1016/j.enconman.2014.07.030.

[29] Abdelaal MM, Hegab AH. Combustion and emission characteristics of a natural gas-fueled diesel engine with EGR. Energy Convers Manag 2012;64:301–12. doi:10.1016/j.enconman.2012.05.021.

[30] Hernandez JJ, Lapuerta M, Barba J. Separate effect of H2, CH4 and CO on diesel engine performance and emissions under partial diesel fuel replacement. Fuel 2016;165:173–84. doi:10.1016/j.fuel.2015.10.054.

[31] Li W, Liu Z, Wang Z. Experimental and theoretical analysis of the combustion process at low loads of a diesel natural gas dual-fuel engine. Energy 2016;94:728–41. doi:10.1016/j.energy.2015.11.052.

[32] Liu J, Yang F, Wang H, Ouyang M, Hao S. Effects of pilot fuel quantity on the emissions characteristics of a CNG/diesel dual fuel engine with optimized pilot injection timing. Appl Energy 2013;110:201–6. doi:10.1016/j.apenergy.2013.03.024.

[33] Wang Z, Zhao Z, Wang D, Tan M, Han Y, Liu Z, et al. Impact of pilot diesel ignition mode on combustion and emissions characteristics of a diesel/natural gas dual fuel heavy-duty engine. Fuel 2016;167:248–56. doi:10.1016/j.fuel.2015.11.077.

[34] Zhang Q, Li N, Li M. Combustion and emission characteristics of an electronically-controlled common-rail dual-fuel engine. J Energy Inst 2015:1–16. doi:10.1016/j.joei.2015.03.012.

[35] Guo H, Neill WS, Liko B. An experimental investigation on the combustion and emissions performance of a natural gas - Diesel dual fuel engine at low and medium loads 2015;1:130–7. doi:10.1115/ICEF2015-1041.

[36] Yousefi A, Birouk M, Guo H. An experimental and numerical study of the effect of diesel injection timing on natural gas/diesel dual-fuel combustion at low load. Fuel 2017;203:642–57. doi:10.1016/j.fuel.2017.05.009.

[37] http://www.tfd.chalmers.se/~valeri/MECH.html n.d.

[38] Aggarwal SK, Awomolo O, Akber K. Ignition characteristics of heptane-hydrogen and heptane-methane fuel blends at elevated pressures. Int J Hydrogen Energy 2011;36:15392–402. doi:10.1016/j.ijhydene.2011.08.065.

[39] Gmbh AVLL. AVL FIRE ® VERSION 2011 2011.

[40] H. Guo, B. Liko, W.S. Neil. Effect of Diesel Injection Split on Combustion and Emissions Performance of Natural Gas – Diesel Dual Fuel Engine at a Low Load Condition. Proc ASME 2017 Intern Combust Engine Div Fall Tech Conf, ICEF2017-3584, October 15-18, 2017, Seattle, Washington, USA.

[41] Kong S, Marriott CD, Reitz RD. Modeling and Experiments of HCCI Engine Combustion Using Detailed Chemical Kinetics with Multidimensional CFD. SAE Int J Engines 2001:1–2. doi:10.4271/2001.

[42] Han Z, Reitz RD. Turbulence Modeling of Internal Combustion Engines Using RNG κ-ε Models. Combust Sci Technol 1995;106:267–95. doi:10.1080/00102209508907782.

[43] Module LM. AVL FIRE ® VERSION 2011 2011.

[44] Beale JC., Reitz RD. Modeling Spray Atomization With the Kelvin-Helmotz/Rayleigh-Taylor Hybrid Model. At Sprays 1999;9:623–50. doi:10.1615/AtomizSpr.v9.i6.40.

[45] Butler T.D. & Cloutman LD& DJK& RDJ. Multidimensional numerical simulation of reactive flow in internal combustion engines. Prog Energy Combust Sci 1981;7:293–315.

[46] Gao G, Yang F, Ouyang M, Fang C. SOC Detection of Diesel Engines Based on Online Estimation of Motored Pressure. Vol 1 Large Bore Engines; Adv Combust Emiss Control Syst Instrumentation, Control Hybrids 2013:V001T05A002. doi:10.1115/ICEF2013-19030.

[47] Zhang C, Song J. Experimental study of co-combustion ratio on fuel consumption and emissions of NG–diesel dual-fuel heavy-duty engine equipped with a common rail injection system. J Energy Inst 2015:1–8. doi:10.1016/j.joei.2015.06.005.

[48] Liu J, Zhang X, Wang T, Zhang J, Wang H. Experimental and numerical study of the pollution formation in a diesel/CNG dual fuel engine. Fuel 2015;159:418–29. doi:10.1016/j.fuel.2015.07.003.

[49] Huang H, Wang Q, Shi C, Liu Q, Zhou C. Comparative study of effects of pilot injection and fuel properties on low temperature combustion in diesel engine under a medium EGR rate. Appl Energy 2016;179:1194–208. doi:10.1016/j.apenergy.2016.07.093.

Chapter 4: Effect of diesel injection timing on the combustion of natural gas/diesel dual-fuel engine at low-high load and low-high speed conditions

4.1. Abstract

Past research has shown that advancing diesel injection timing is a promising approach to decrease the unburned methane and greenhouse gas (GHG) emissions of natural gas/diesel dual-fuel engines at lower engine loads. However, this benefit may not persist under medium to high load-low speed conditions. To explore this, the present paper uses experiments and detailed computational fluid dynamic (CFD) modeling to investigate the impacts of diesel injection timing on the combustion and emissions performance of a heavy-duty natural gas/diesel dual-fuel engine under four different engine load-speed conditions. The results showed that advancing diesel injection timing increases the peak pressure, thermal efficiency, and NO_x emissions for all examined engine load-speed conditions. Advancing diesel injection timing also significantly decreases the unburned methane and CO_2-equivalent (GHG) emissions of the dual-fuel engine under low load-low speed and medium load-high speed conditions. The concentration of OH and CH_4 revealed that the central part of the combustion chamber is the main source of the unburned methane emissions under low load-low speed and medium load-high speed conditions, and advancing diesel injection timing significantly improves the combustion of natural gas-air mixture in this region. However, advancing diesel injection timing slightly increases the unburned methane emissions trapped in the crevice volume. However, this slight increase in the unburned methane emissions in the crevice volume is much lower than its significant decrease in the central region of the combustion chamber. At medium to high load-low

speed conditions, there is almost no unburned methane in the central part of the combustion chamber, and the crevice region is considered as the main source of unburned methane emissions. As a result, advancing diesel injection timing does not improve the combustion of natural gas-air mixture in the central part of the combustion chamber but slightly increases the unburned methane trapped in the crevice region. This is the main reason that advancing diesel injection timing slightly increases the unburned methane emissions under medium to high load-low speed conditions. Overall, advancing diesel injection timing significantly increases thermal efficiency and decreases the unburned methane and GHG emissions under low load-low speed and medium load-high speed conditions. It improves the thermal efficiency under medium to high load-low speed conditions, but comes at the expense of increased methane and unchanged GHG emissions.

Nomenclature

AMR	Adaptive Mesh Refinement	GHG	Greenhouse Gas
ASOC	After Start of Combustion	IMEP	Indicated Mean Effective Pressure
ATDC	After Top Dead Center	IVC	Intake Valve Closing
BMEP	Break Mean Effective Pressure	IVO	Intake Valve Opening
CAD	Crank Angle Degree	$ISCH_4$	Indicated Specific CH_4
CFD	Computational Fluid Dynamic	$ISNO_x$	Indicated Specific NO_x
CO	Carbon monoxide	$ISCO_2$	Indicated Specific CO_2
COV	Coefficient of Variation	LTC	Low Temperature Combustion
DIT	Diesel Injection Timing	NO_x	Nitrogen Oxides
EGR	Exhaust Gas Recirculation	RPM	Revolution per Minute
EVC	Exhaust Valve Closing	SOC	Start of Combustion
EVO	Exhaust Valve Opening	TDC	Top Dead Center

4.2.Introduction

Low temperature combustion (LTC) concept is recognized as a viable strategy to overcome the challenge of simultaneously suppressing the nitrogen oxides (NO_x) and soot emissions in compression ignition diesel engines. The two key features of LTC strategies consist of low combustion temperature and long ignition delay time [1]. Low temperature inhibits NO_x formation while a long ignition delay time promotes an enhanced mixing that reduces the propensity of soot formation by avoiding locally fuel-rich zones, and consequently ultra-low level of NO_x and soot below the current emissions limits may be achieved. LTC strategies have been demonstrated to result in high thermal efficiency through a combination of lean mixture, optimal combustion phasing near

the top dead center (TDC), short combustion duration, and reduced heat transfer [2]. Recently, the LTC strategies have been examined by blending two fuels with different reactivity, i.e., dual-fuel combustion. Dual-fuel combustion uses direct injection of a high reactivity fuel to ignite a premixed low reactivity fuel and air mixtures [3]. Diesel is usually used as the high reactivity fuel because of its high cetane number. Natural gas is great candidate for the low reactivity fuel due to its high ignition temperature. In the dual-fuel combustion, the ignition process is initiated in the high reactivity regions where the liquid fuel is directly injected. Owing to the premixed charge of lower reactivity fuel-air mixture, the combustion process is controllable, which sequentially progresses from the higher reactivity to the lower reactivity regions.

Dual-fuel mode not only is a fuel flexible approach, but also has the potential to lead to high efficiency clean combustion in compression ignition engines. In recent years, natural gas has drawn substantial interest as a low reactivity fuel in dual-fuel combustion and some of the original versions of diesel engine have been commercialized to operate as a dual-fuel engine based on premixed natural gas [4–6]. Natural gas/diesel dual-fuel combustion tends to retain most positive features of conventional diesel engines, and is capable of producing comparable power output and efficiency at different engine loads [7]. Moreover, this strategy can be achieved via the installation of a low cost port fuel injection system for the formation of a low reactivity mixture of air and fuel (e.g., natural gas), while, the stock diesel fuel injection system can be retained in the dual-fuel mode. However, the greatest challenge of natural gas/diesel dual-fuel engine is the high level of unburned methane emissions which contribute to the GHG by about 25 times greater than CO_2 over a 100 year period [8]. Past research has shown that advancing diesel injection timing reduces the unburned methane and CO emissions of natural gas/diesel dual-fuel engine under low-medium engine load conditions [9–12]. It is shown that advancing diesel injection timing under low load-low speed and medium load-high speed conditions significantly decreases the unburned methane and GHG emissions [13–16]. However, according to the experimental data of the present study, advancing diesel injection

timing under medium to high load-low speed conditions increases the unburned methane emissions and does not change the GHG emissions. Finding the reasons behind this phenomenon is the main objective of the present study.

Accordingly, four typical cases of drive cycle in heavy-duty diesel engine are selected to investigate the effect of diesel injection timing on natural gas/diesel dual-fuel engine. Cases 1 and 2 represent the low load-low speed (Case 1, BMEP=4.05 bar, RPM=910) and medium load-high speed (Case 2, BMEP=11.24 bar, RPM=1750) conditions, respectively. Advancing diesel injection timing under these conditions significantly reduces the unburned methane and GHG emissions. Cases 3 and 4 represent the medium load-low speed (BMEP=12.15 bar, RPM=910) and high load-low speed (BMEP=17.15 bar, RPM=1120) conditions, respectively. The opposite scenario manifests under these cases where advancing diesel injection timing increases the unburned methane emissions. A computational fluid dynamic (CFD) model based on CONVERGE 2.4 software is developed to examine and hence understand the reasons behind the underlying phenomenon. Cylinder pressure, engine out emissions, and OH and CH_4 distributions are all analyzed in order to investigate the effect of diesel injection timing on natural gas/diesel dual-fuel engine under different engine load-speed conditions.

4.3.Methodology

4.3.1. Experimental setup

The engine used in this investigation is a modified single-cylinder heavy-duty engine. Detailed description of the experimental setup and methodology is reported elsewhere [17], and only a brief summary is provided here. Specifications of the engine are provided in Table 4-1. Natural gas port fuel injector was fed by a low-pressure line which included eight gas fuel injectors manufactured by Alternative Fuel Systems Inc. The diesel, natural gas, and air flow rates were measured by means of a TRICOR, a Bronkhorst, and a turbine mass flowmeters, respectively. Engine loading was

accomplished by an eddy-current dynamometer. The engine speed and load were controlled by an electronic control module and an AVL Digalog Testmate. The in-cylinder pressure was measured by means of a water-cooled pressure transducer (Krister Corp.,) fitted inside the cylinder head and acquired with a resolution of 0.2 crank angle degree. The averaged pressure signal for the calculation of the indicated mean effective pressure (IMEP) and heat release rate (HRR) were averaged over 100 consecutive cycles using an AVL real-time combustion analysis system. The emitted smoke was measured using a commercialized laser-induced incandescence system. The engine-out gaseous emissions such as CH_4, NOx, CO, and CO_2 were measured using a California Analytical Instruments' series 600 gas analyzers.

The experiments were conducted at four different engine load-speed conditions including low load-low speed (BMEP=4.05 bar and 910 RPM), medium load-high speed (BMEP=11.24 bar and 1750 RPM), medium load-low speed (BMEP=12.15 bar and 910 RPM), and high load-low speed (BMEP=17.6 bar and 1120 RPM). A diesel injection timing (DIT) test was conducted during the investigation for each case. For all cases, the intake temperature was kept constant at 40 $^{\circ}$C during the experiments and no exhaust gas recirculation (EGR) was used in this study. Table 4-2 gives the experimental test conditions.

Table 4-1. Test setup specifications

Engine type	Single cylinder-CAT 3400
Bore×Stroke	137.2 mm ×165.1 mm
Conn. rod length	261.62 mm
Displacement vol.	2.44 L
Compression ratio	16.25
Diesel fuel injector	Common rail injector
Number of nozzle hole×diameter	6×0.23 mm
Maximum Speed	2100 rpm
Low idle speed	600 rpm
Rated power BMEP @1800 rpm	20.6 bar
IVO	-358.3 °ATDC
IVC	-169.7 °ATDC
EVO	145.3 °ATDC
EVC	348.3 °ATDC

Table 4-2**.** Experimental test conditions

	Case 1, low load-low speed	**Case 2, medium load-high speed**	**Case3, medium load-low speed**	**Case 4, high load-low speed**
BMEP (bar)	4.05	11.24	12.15	17.60
Engine speed (RPM)	910	1750	910	1120
Intake temperature (°C)	40	40	40	40
Intake pressure (bar)	1.05	2.02	1.8	2.2
%NG (energy fraction)	75	80	90	65
Injection timing (°BTDC)	10-30 (4 CA step)	26, 28, 29	10.5, 12, 14, 15	12, 13, 14, 15, 16
IP (bar)	525	525	525	800
ϕ_{NG}	~0.32	~0.4	~0.6	~0.45
ϕ_{Tot}	~0.43	~0.48	~0.66	~0.73

4.3.2. Numerical model

The CFD solver CONVERGE 2.4 [18] was used in this study. Detailed description of the numerical model is reported elsewhere [19] and thus only a brief summary is presented here. CONVERGE has an integrated chemistry solver (SAGE model [18]), which performs the detailed chemistry calculations in each computational cell. The chemical properties of diesel and natural gas are represented by n-heptane and methane, respectively. The adopted mechanism includes 76 species and 464 reactions [20].

Adaptive mesh refinement (AMR) is used to resolve flow and flame propagation in the engine cylinder. The use of AMR with small enough cell sizes (0.25-0.5 mm) in the flame region adequately resolves the turbulent flame front and the species gradients without the need of any sub-grid model [21,22]. The largest grid size used in the simulation is 2 mm and the smallest is 0.25 mm, which adequately resolves diesel spray and turbulent flame fronts. Since the diesel injector has six equally spaced orifices, a sector mesh of 60° is used to model one spray plume with periodic boundaries from intake valve closing (IVC) to exhaust valve opening (EVO).

The atomization of the liquid fuel and subsequent droplets were simulated based on the Kelvin-Helmholtz and Rayleigh-Taylor instability mechanisms without the use of a breakup length [23]. The liquid phase was modeled as a single component with the thermodynamic properties of diesel fuel obtained from the CONVERGE liquids property library (denoted as "DIESEL2") [18].

4.3.3. Model validation

The numerical model was validated by comparing the calculated data with those measured using the test engine. The measured and predicted cylinder pressure and HRR for four different cases are compared in Figure 4-1. For each case, the results of two DITs are selected for comparison. More validation can be found elsewhere [24]. It can be seen that, in general, for all examined cases, good agreement between the model and experiments is observed for the start of combustion, peak pressure, combustion duration, and shape of the heat release rate. However, the predicted peak pressure and HRR do not perfectly match the measured data. This could be due to the fact that the measured data is taken as the average of 100 cycles and there is a small cycle to cycle variation for each case. However, the calculated data is only one cycle simulation based on the average inputs (e.g., air, natural gas, and diesel mass flow rates) where no inputs variation is considered. This validation is a demonstration that the present numerical simulation is capable of reproducing the experimental results with a reasonable error. Therefore, the validated numerical model is used to investigate the effect of diesel injection timing on dual-fuel engine under different engine load-speed conditions.

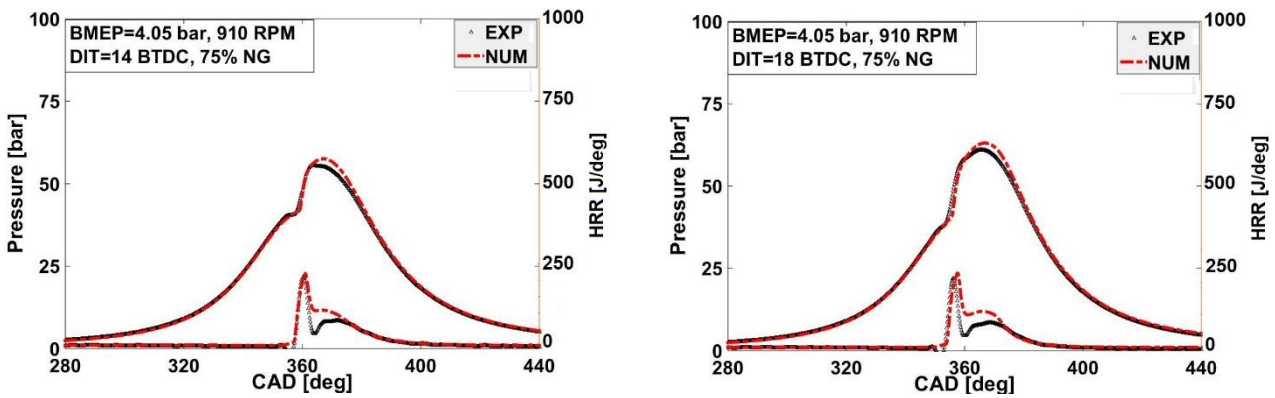

a) Case 1, low load-low speed

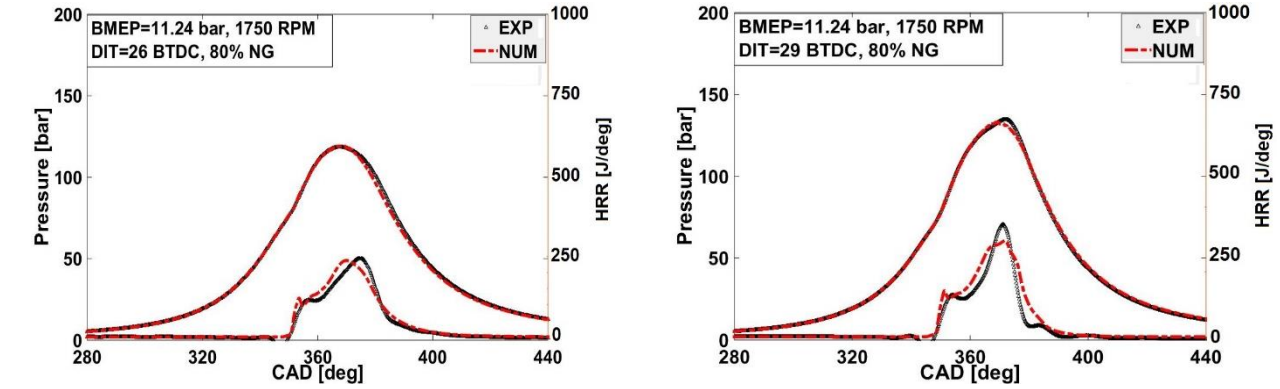

b) Case 2, medium load-high speed

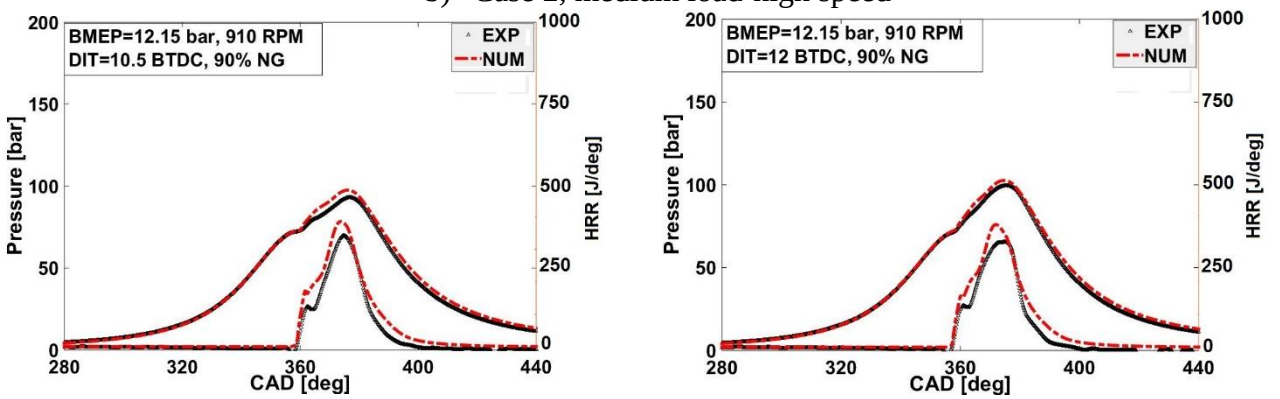

c) Case 3, medium load-low speed

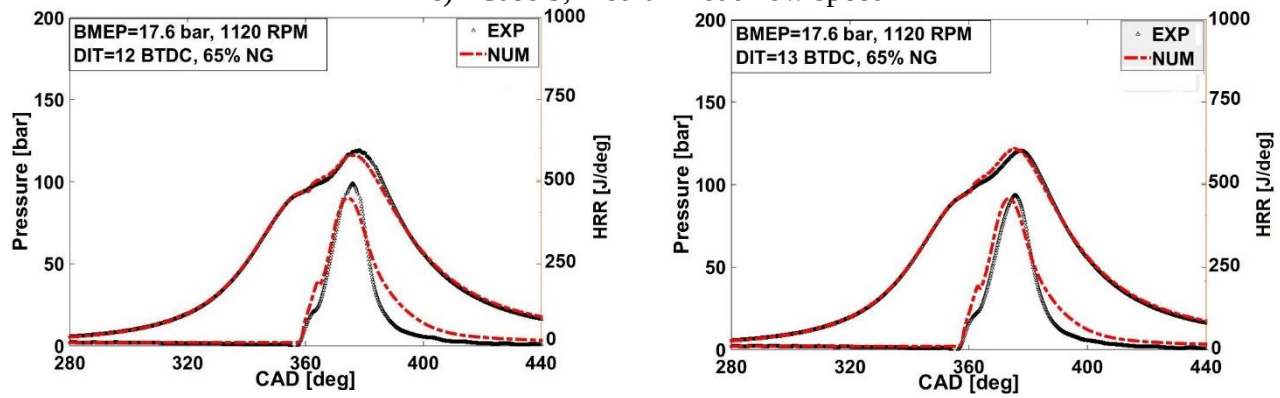

d) Case 4, high load-low speed

Figure 4-1. Cylinder pressure and HRR of natural gas/diesel dual-fuel engine under different engine load-speed conditions.

4.4.Result and discussions

Figure 4-2 show the effect of diesel injection timing on the peak pressure, indicated thermal efficiency (ITE), and emissions (NO_x and CH_4) of natural gas/diesel dual-fuel engine under the four investigated engine load-speed conditions. The solid and dashed lines represent the experimental and numerical results, respectively. It is well-known in the literature [10,25–27] that advancing diesel

injection timing in the range of conventional diesel injection strategy (i.e., 10 to 30 °BTDC) leads to an increase in peak pressure, thermal efficiency, and NO_x emissions. These trends are also noticeable in Figure 4-2a-c. Advancing diesel injection timing prolongs the ignition delay, and thus more premixed natural gas-air and diesel mixture forms before the start of combustion (SOC). This shifts the combustion phasing towards the TDC, increases the local cylinder gas temperature during the combustion phasing, and improves the combustion efficiency. This consequently leads to increased peak pressure, NO_x emissions, and thermal efficiency. Moreover, it can be seen from Figure 4-2d that advancing diesel injection timing significantly decreases the unburned methane emissions of natural gas/diesel dual-fuel engine under low load-low speed (Case 1) and medium load-high speed (Case 2) conditions. However, unburned methane emissions increase when advancing diesel injection timing under medium load-low speed (Case 3) and high load-low speed (Case 4) conditions. In order to understand the fundamental mechanism behind this behaviour, the OH and CH_4 distributions of Cases 1 and 3 are compared in Figure 4-3 to Figure 4-6, where the top-view contour plane is located at a vertical distance of 10 mm from the nozzle tip and the side-view contours plane is cut from one of the six injector's orifices. Due to the similarity of Cases 1 and 2, and Cases 3 and 4, the contours of Case 2 and Case 4 are not presented in this study.

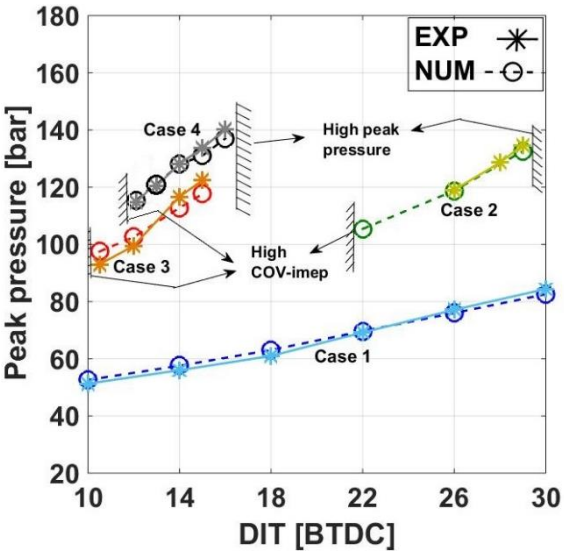

a) Peak pressure

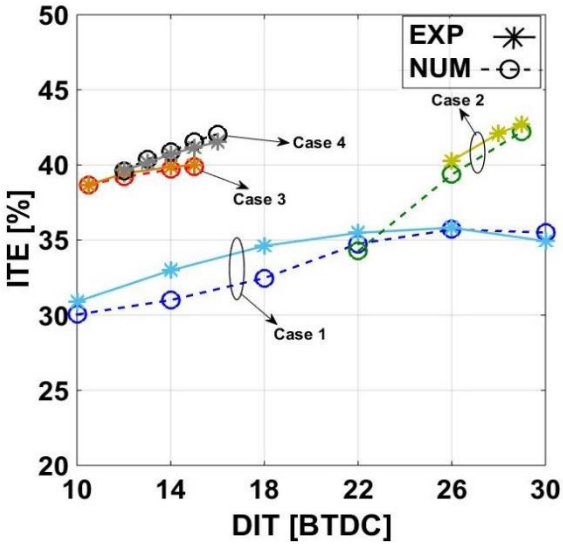

b) ITE

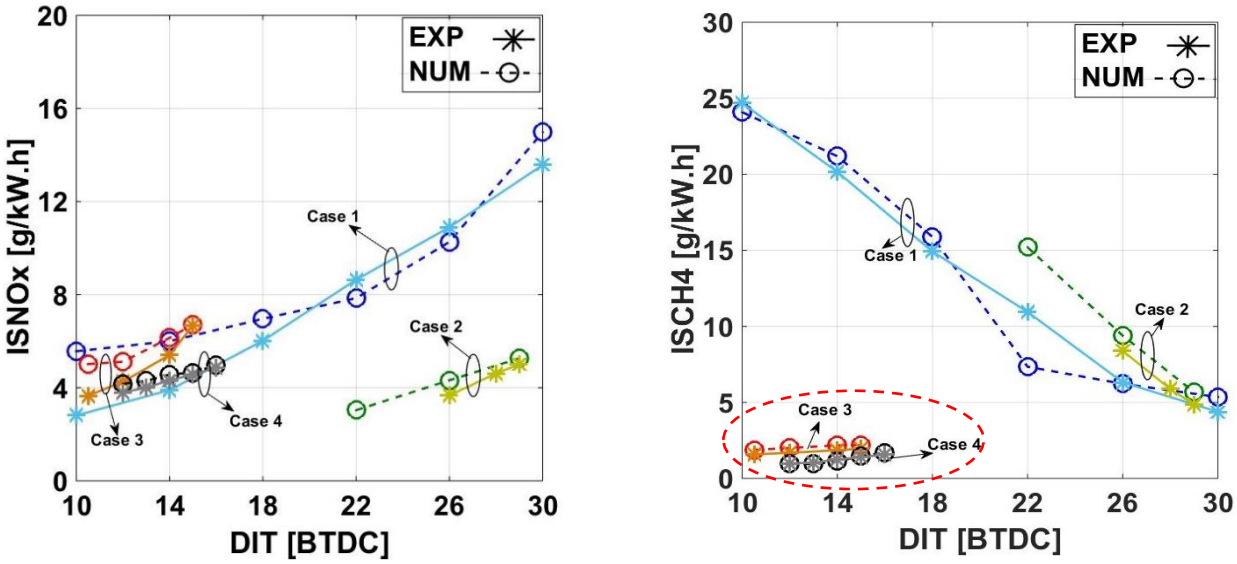

c) $ISNO_x$ d) $ISCH_4$

Figure 4-2. Effect of diesel injection timing on peak pressure, ITE, and emissions of natural gas/diesel dual-fuel engine under different engine load-speed conditions.

Figure 4-3 depicts OH distribution of natural gas/diesel dual-fuel engine under low load-low speed condition (Case 1) at two different diesel injection timings of 10 and 18 °BTDC. At low engine loads, with very lean natural gas-air fuel mixtures, no consistent flame propagation takes place from the ignition centres and the pilot fuel dominates the burning region [28]. As can be observed in this figure, combustion is initiated near the wall of the piston bowl and then extends rapidly towards the center of the combustion chamber (crank angle degree (CAD) =+3-8° after the start of combustion (°ASOC)). However, the central region within the bowl is marked by a blue non-reactive zone where almost no OH radical can be observed. It can be seen that the reaction zones extend from richer to leaner regions and the combustion progresses within each jet only in the radial direction towards the center of the cylinder. The absence of OH radical in the central region of the bowl is an indication that very limited high temperature oxidation reactions take place in this zone (11-25 °ASOC). Therefore, the combustion of natural gas in the central part of the charge is a significant challenge for dual-fuel combustion strategy under the examined low load condition. However, by advancing diesel injection timing, more premixed mixture (diesel and natural gas-air) forms before the onset of ignition which improves the combustion process in the central region of the combustion chamber. The same

scenario is also observed for medium load-high speed conditions (Case 2, contours not presented here), under which the premixed equivalence ratio is closer to or even lower than the flammability limit of natural gas/air mixture [28]. Therefore, premixed combustion of diesel fuel is followed by diesel diffusion and flame propagation of natural gas. However, the engine speed is high (1750 RPM) and there is no enough time for the flame to propagate and to burn all the premixed air-natural gas mixture in the central region of the combustion chamber. Similar to Case 1, advancing diesel injection timing significantly improves the combustion process in the central region of the combustion chamber under medium load-high speed condition (Case 2).

Figure 4-4 shows CH_4 distribution of natural gas/diesel dual-fuel engine under low load-low speed condition (Case 1) at two different diesel injection timings of 10 and 18 °BTDC. It can be observed that, for both diesel injection timings, the central region within the bowl (marked by green arrow) is the main source of unburned methane emissions (+10°ASOC). However, advancing diesel injection timing significantly decreases the unburned methane emissions in this region (+25 °ASOC). At the engine's crank angle of CAD=+50 °ASOC, unburned methane is also spotted in the crevice region. It can be seen that, when advancing diesel injection timing, the amount of unburned methane trapped in the crevice volume slightly increases. This is due to the fact that advancing diesel injection timing leads to a higher cylinder pressure during the combustion phasing (Figure 4-1a and Figure 4-1b) which forces more premixed air-natural gas into the crevice region. However, this slight increase in the unburned methane emissions in the crevice volume is still insignificant compared with its level of decrease in the central region of combustion chamber. This is the reason that advancing diesel injection timing significantly decreases the unburned methane emissions under low load-low speed (Case 1) and medium low-high speed (Case 2, contours not presented) conditions, as shown in Figure 4-2d.

DIT=10 °BTDC		**DIT=18 °BTDC**	
+3 °ASOC	**+15 °ASOC**	**+3 °ASOC**	**+15 °ASOC**

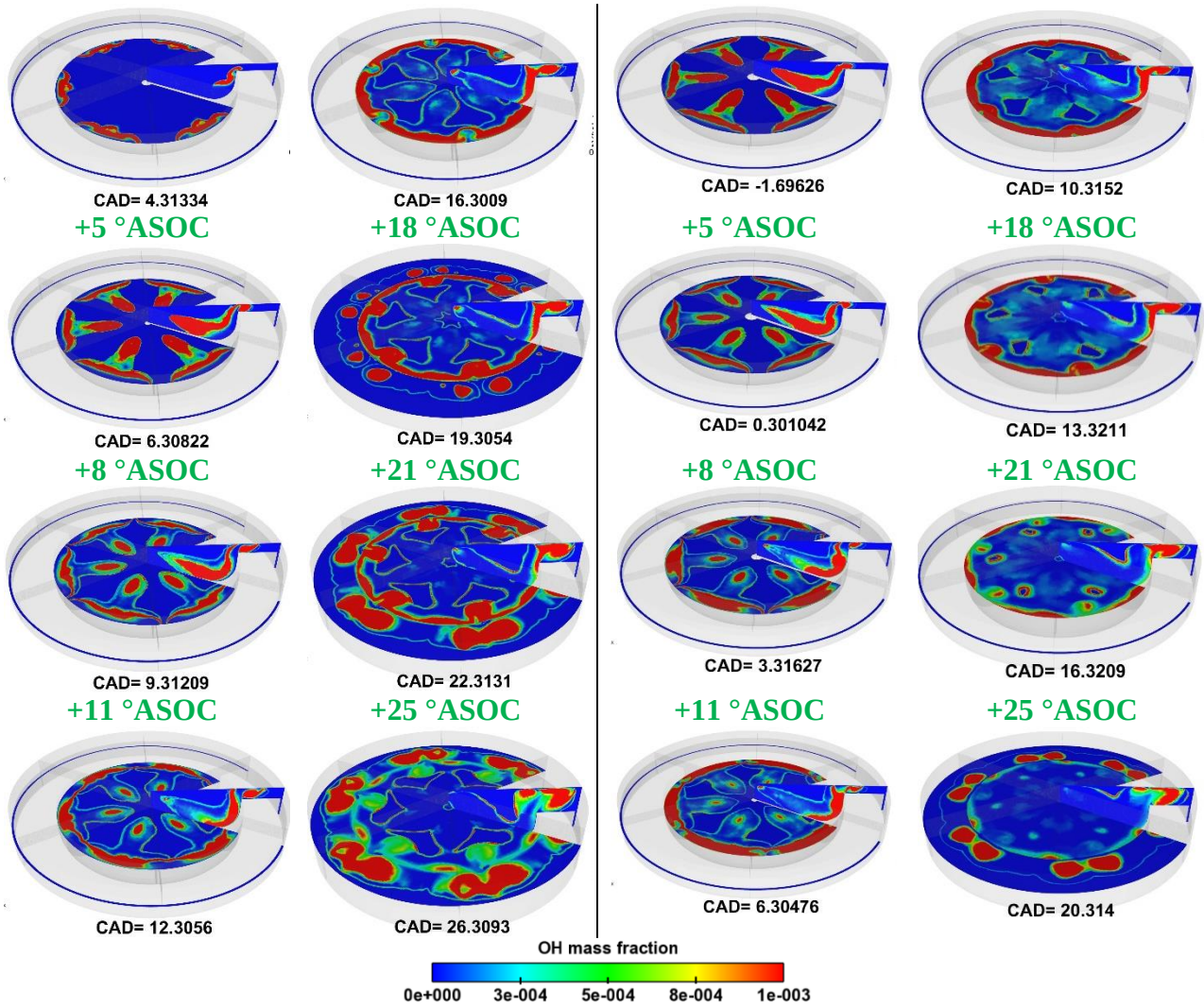

Figure 4-3. OH distribution of natural gas/diesel dual-fuel engine under low load-low speed conditions (Case 1) and DITs of 10 and 18 °BTDC.

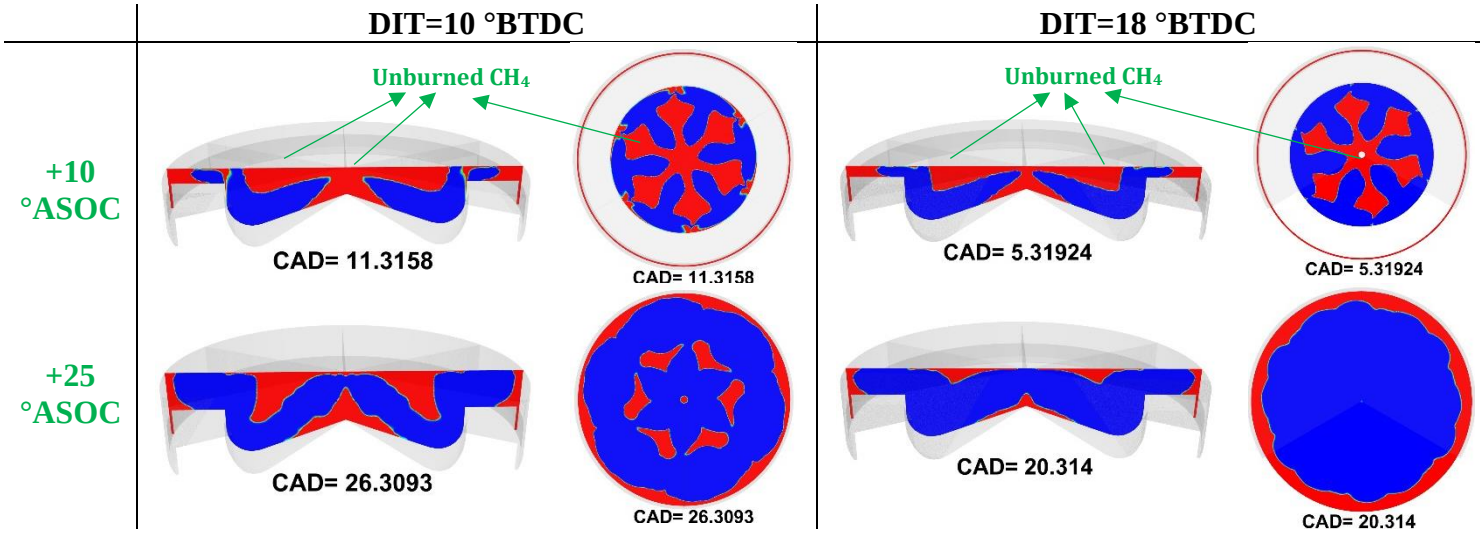

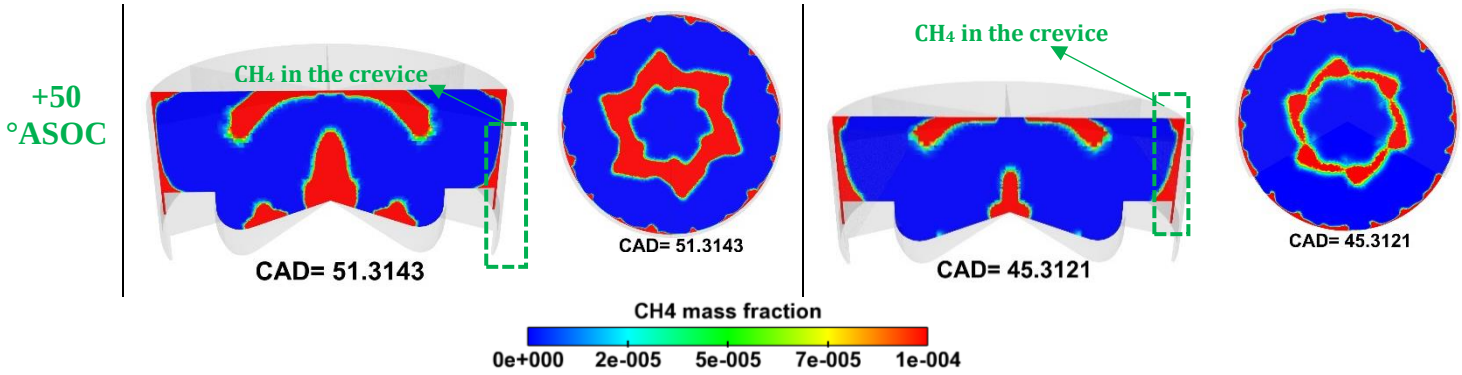

Figure 4-4. Unburned methane distribution of natural gas/diesel dual-fuel engine under low load-low speed conditions (Case 1) and DITs of 10 and 18 °BTDC.

Figure 4-5 presents OH distribution of natural gas/diesel dual-fuel engine under medium load-low speed condition (Case 3) at two different diesel injection timings of 10.5 and 15 °BTDC. It can be observed that, similar to Case 1, combustion is initiated near the piston wall. After the initiation of chemical reaction near the point of impingement onto the bowl wall, combustion rapidly progresses within each jet in both the azimuthal and radial directions (11 °ASOC). It can be observed that multiple flames propagate simultaneously within the piston bowl along the spray axes, and progressively consume the fresh charge. OH radical is observed throughout the entire piston bowl at 18 °ASOC. This behavior suggests that flame propagation could be the predominant combustion mode under this engine condition. As shown in this figure, advancing diesel injection timing slightly increases the OH intensity in the central region of the combustion chamber. As mentioned above, even with a retarded injection timing (DIT=10 °BTDC), almost all of the premixed natural gas-air mixture in the central region of the combustion chamber is burned, and that the combustion of natural gas-air mixture does not significantly improve when advancing further the diesel injection timing to 15 °BTDC. However, advancing diesel injection timing advances the combustion phasing which increases the peak pressure and thermal efficiency (shown in Figure 4-2). It is important to highlight the fact that, for both diesel injection timings, shown in Figure 4-5, there still exist small blue non-reactive zones in the crevice volume where limited high temperature oxidation reactions occur. These

regions are the main source of unburned methane emissions under medium to high load-low speed conditions, as shown in Figure 4-6. The results of case 4 are qualitatively similar to those of case 3.

Figure 4-6 shows CH_4 distribution of natural gas/diesel dual-fuel engine under medium load-low speed condition (Case 3) at two different diesel injection timings of 10.5 and 15 °BTDC. In contrast to the observations presented in Figure 4-3, for these diesel injection timings, the reaction zones propagate into the central region of the piston bowl, and progressively consume all of the fresh charge such that almost no unburned CH_4 is detected throughout the entire combustion chamber at an engine crank of +50 °ASOC. It can be seen that the crevice region is the main source of unburned methane emissions under this condition. As shown in Figure 4-4 and at an engine crank angle of 100 °ASOC, the maximum limit of CH_4 mass fraction, which is rescaled to 10^{-6}, clearly shows the CH_4 emissions distribution with advancing diesel injection timing. Similar to the results presented in Figure 4-4, the unburned methane emissions trapped in the crevice region increase when advancing the diesel injection timing. During compression and combustion, unburned charge is pushed into the crevice region, and more premixed air-natural gas is be trapped in the crevice volume at higher peak pressure (for advanced injection timing). The gases in the crevice volume begin to flow back into the cylinder during the expansion stroke where the combustion temperature is not high enough to oxidize the unburned gases. As shown in Figure 4-6, there is no major source of unburned methane emissions in the combustion chamber and consequently all methane emissions result from the crevice regions. This is the main reason that advancing diesel injection timing slightly increases the unburned methane emissions under medium to high load-low speed conditions (Cases 3 and 4).

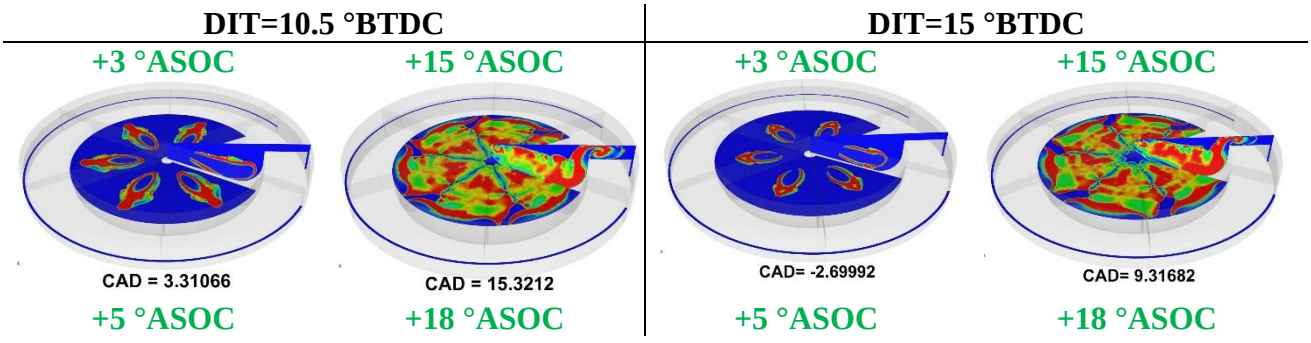

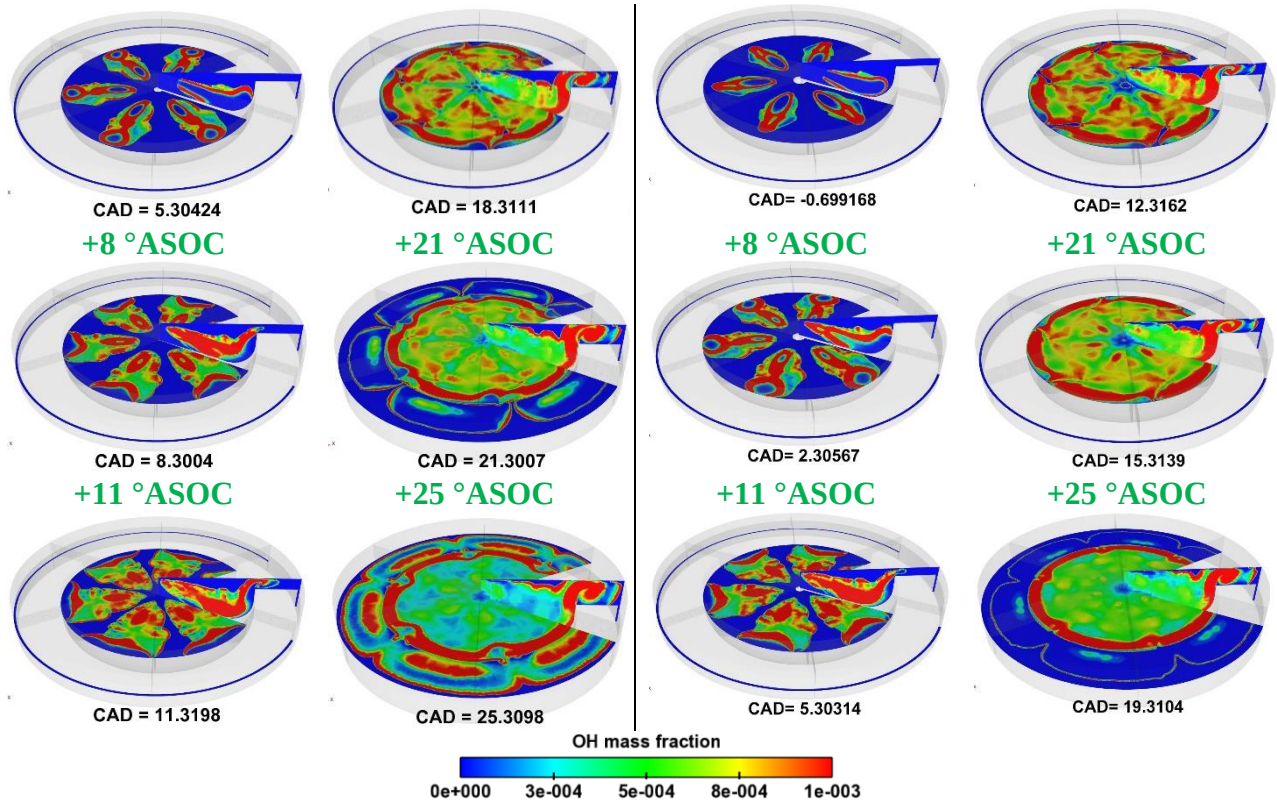

Figure 4-5. OH distribution of natural gas/diesel dual-fuel engine under low load-low speed conditions (Case 3) and DITs of 10 and 18 °BTDC.

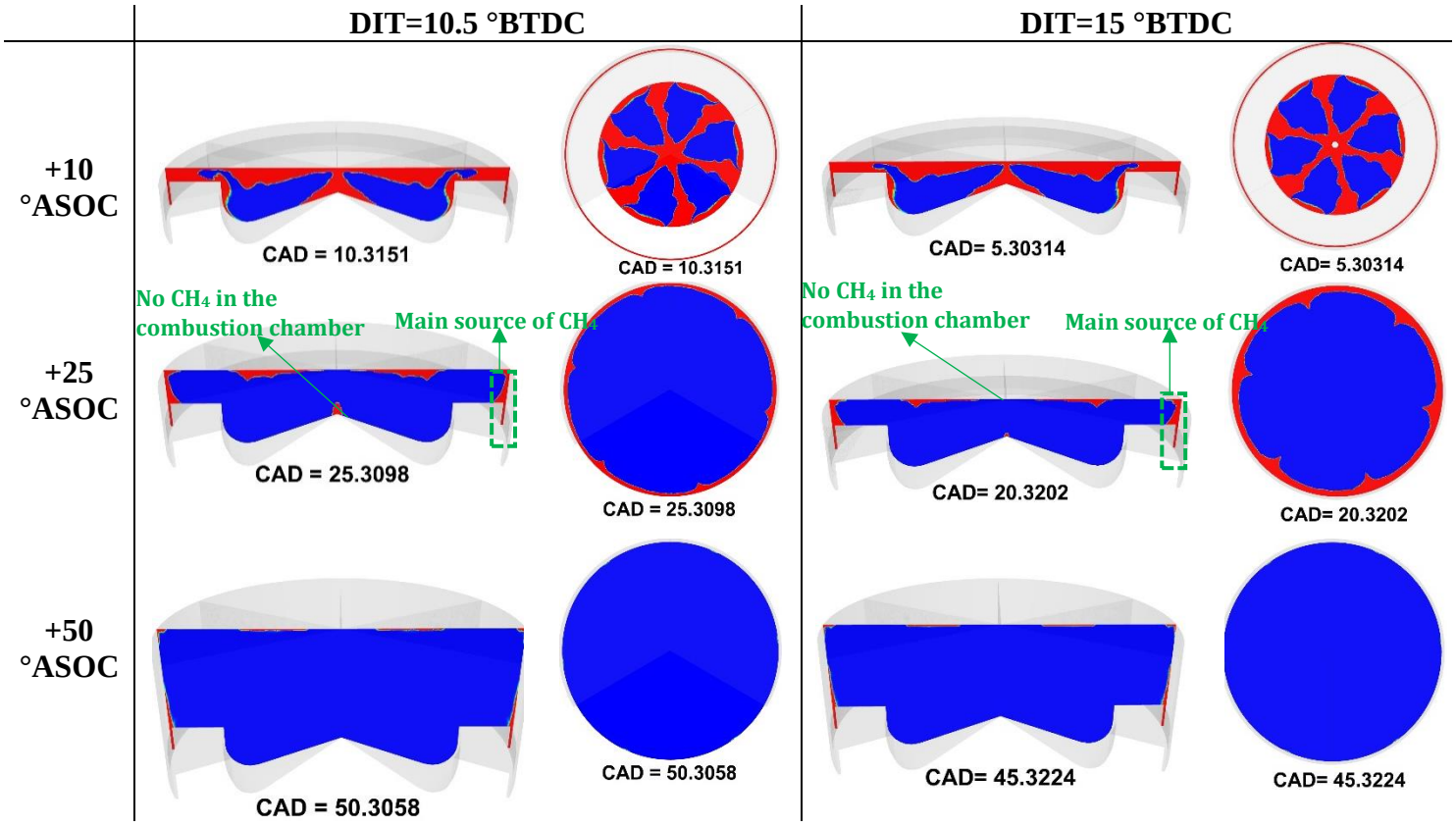

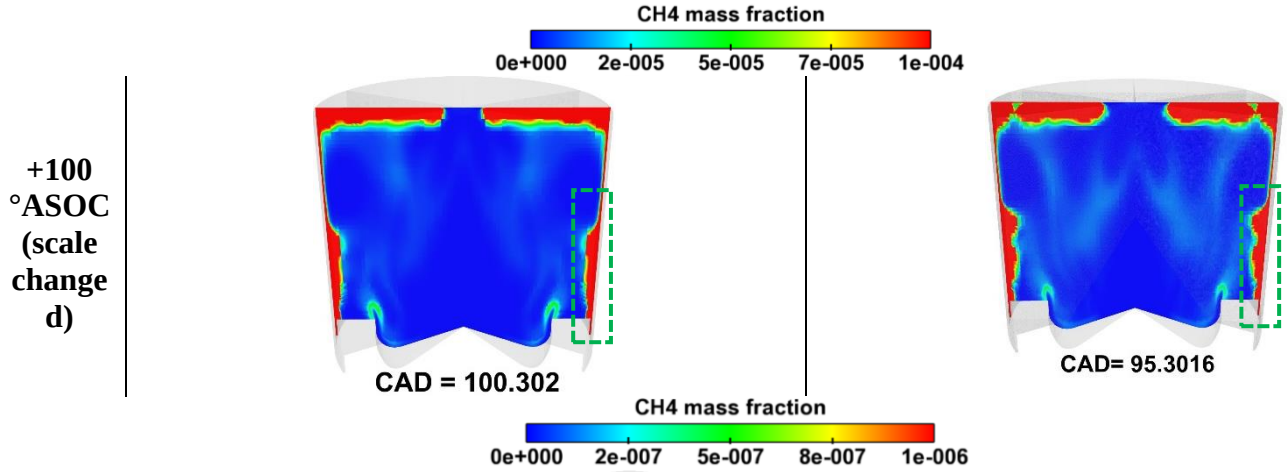

Figure 4-6. Unburned methane distribution of natural gas/diesel dual-fuel engine under medium load-low speed conditions (Case 3) and DITs of 10.5 and 15 °BTDC.

Figure 4-7 depicts the effect of diesel injection timing on the overall greenhouse gas emissions, ISCO_2-equivalent, of natural gas/diesel dual-fuel engine under different engine load-speed conditions. The CO_2 equivalent is defined as the summation of CO_2 emissions and CH_4 emissions multiplied by 25, which is the global warming potential of CH_4 over 100 year period [29]. As shown in Figure 4-7, advancing diesel injection timing significantly decreases the CO_2-equivalent emissions for Cases 1 and 2. This is mainly due to the significant reduction of unburned methane emissions (Figure 4-2d, Cases 1 and 2) accompanied by an improvement in the thermal efficiency (Figure 4-2b, Cases 1 and 2) while advancing diesel injection timing. However, advancing diesel injection timing does not significantly improve CO_2-equivalent emissions under medium to high load-low speed conditions (Cases 3 and 4). As shown in Figure 4-2b (Cases 3 and 4), although advancing diesel injection timing improves the thermal efficiency which leads to a decrease in CO_2 emissions, this benefit is offset by a slight increase in methane emissions (Figure 4-2d, Cases 3 and 4) which results in an almost constant trend of ISCO_2-equivalent when advancing diesel injection timing under medium to high load-low speed conditions (Cases 3 and 4).

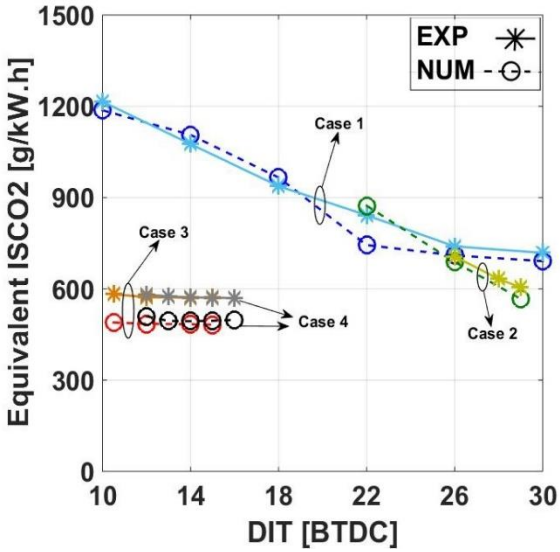

Figure 4-7. Effect of diesel injection timing on GHG emissions (CO_2 equivalent) of natural gas/diesel dual-fuel engine under different engine load-speed conditions.

4.5.Conclusions

The effect of diesel injection timing on the combustion performance and emissions of natural gas/diesel dual-fuel engine under four different engine load-speed conditions (BMEP=4.05 bar and 910 RPM, BMEP=11.24 bar and 1750 RPM, BMEP=12.15 and 910 RPM, and BMEP=17.6 bar and 1150 RPM) is experimentally and numerically investigated. The main findings can be summarized as follows:

- Advancing diesel injection timing within the range of conventional diesel increases the peak pressure, thermal efficiency, and NO_x emissions for all examined engine load-speed conditions. Moreover, advancing the diesel injection timing significantly decreases the unburned methane and CO_2-equivalent emissions of natural gas/diesel dual-fuel engine under low load-low speed and medium load-high speed conditions. However, unburned methane emissions increase while CO_2-equivalent emissions do not significantly change when advancing diesel injection timing under medium to high load-low speed conditions.
- The central region of the combustion chamber is the main source of unburned methane emissions under low load-low speed and medium load-high speed conditions. Advancing

diesel injection timing significantly improves the combustion of natural gas-air mixture in this region. However, advancing diesel injection timing slightly increases the unburned methane trapped in the crevice volume. This slight increase in the unburned methane in the crevice volume is much lower compared to the significant decrease of the unburned methane in the central region of combustion chamber. This is the reason that advancing diesel injection timing significantly decreases the unburned methane emissions under low load-low speed and medium load-high speed conditions.

- At medium to high load-low speed conditions, almost all of the premixed natural gas-air mixture in the central region of the combustion chamber burns even with a retarded injection timing (e.g., DIT=10.5 °BTDC). Further advancing diesel injection timing does not improve the combustion of natural gas-air mixture in this region. However, the unburned methane trapped in the crevice region, which is considered as the main source of CH_4 emissions, slightly increases when advancing the diesel injection timing. This is why advancing diesel injection timing slightly increases the unburned methane emissions under medium to high load-low speed conditions.

Overall, advancing diesel injection timing within the range of conventional diesel increases the thermal efficiency and decreases the unburned methane and GHG emissions under low load-low speed and medium load-high speed conditions. It also improves the thermal efficiency under medium to high load-low speed conditions, but this benefit comes at the expense of increased methane emissions.

4.6.References

[1] Kavuri C, Kokjohn SL. Computational optimization of a reactivity controlled compression ignition (RCCI) combustion system considering performance at multiple modes simultaneously. Fuel 2017;207:702–18. doi:10.1016/j.fuel.2017.06.071.

[2] Roberts G, Rousselle CM, Musculus M, Wissink M, Curran S, Eagle E. RCCI Combustion Regime Transitions in a Single-Cylinder Optical Engine and a Multi-Cylinder Metal Engine. SAE Int J Engines 2017;10:2017-24-0088. doi:10.4271/2017-24-0088.

[3] Yousefi A, Guo H, Birouk M. An experimental and numerical study on diesel injection split of a natural gas/diesel dual-fuel engine at a low engine load. Fuel 2018;212. doi:10.1016/j.fuel.2017.10.053.

[4] Dual-Fuel Management - HEINZMANN GmbH & Co. KG. Http://WwwHeinzmannCom/En/Engine-Turbine/Dual-Fuel-Management n.d.

[5] JINAN DIESEL ENGINE CO., LTD. Http://WwwJinanengineCom/ n.d.

[6] Cummins Engines Ltd. Cummins Dual Fuel Engines for Drilling - Cummins Engines. Https://CumminsenginesCom/Dual-Fuel n.d.

[7] Sahoo BB, Sahoo N, Saha UK. Effect of engine parameters and type of gaseous fuel on the performance of dual-fuel gas diesel engines-A critical review. Renew Sustain Energy Rev 2009;13:1151–84. doi:10.1016/j.rser.2008.08.003.

[8] Yousefi A, Birouk M, Guo H. An experimental and numerical study of the effect of diesel injection timing on natural gas/diesel dual-fuel combustion at low load. Fuel 2017;203:642–57. doi:10.1016/j.fuel.2017.05.009.

[9] Verma S, Das LM, Bhatti SS, Kaushik SC. A comparative exergetic performance and emission analysis of pilot diesel dual-fuel engine with biogas, CNG and hydrogen as main fuels. Energy Convers Manag 2017;151:764–77. doi:10.1016/j.enconman.2017.09.035.

[10] Yang B, Wang L, Ning L, Zeng K. Effects of pilot injection timing on the combustion noise and particle emissions of a diesel/natural gas dual-fuel engine at low load. Appl Therm Eng 2016;102:822–8. doi:10.1016/j.applthermaleng.2016.03.126.

[11] Guido C, Napolitano P, Fraioli V, Beatrice C, Del N, Istituto G. Assessment of Engine Control Parameters Effect to Minimize GHG Emissions in a Dual Fuel NG/Diesel Light Duty Engine 2018:1–14. doi:10.4271/2018-01-0266.Abstract.

[12] Ahmad Z, Aryal J, Ranta O, Kaario O, Vuorinen V. An Optical Characterization of Dual-Fuel Combustion in a Heavy-Duty Diesel Engine. SAE Tech Pap 2018;2018-1–2:1–10. doi:10.4271/2018-01-0252.Abstract.

[13] Zhang C, Zhou A, Shen Y, Li Y, Shi Q. Effects of combustion duration characteristic on the brake thermal efficiency and NOx emission of a turbocharged diesel engine fueled with diesel-LNG dual-fuel. Appl Therm Eng 2017;127:312–8. doi:10.1016/j.applthermaleng.2017.08.034.

[14] Li W, Liu Z, Wang Z. Experimental and theoretical analysis of the combustion process at low loads of a diesel natural gas dual-fuel engine 2016. doi:10.1016/j.energy.2015.11.052.

[15] Srinivasan KK, Krishnan SR. Cyclic Combustion Variations in Dual Fuel Partially Premixed Pilot-Ignited Natural Gas Engines. J Energy Resour Technol 2014;136:1–10. doi:10.1115/1.4024855.

[16] Ryu K. Effects of pilot injection timing on the combustion and emissions characteristics in a diesel engine using biodiesel-CNG dual fuel. Appl Energy 2013;111:721–30. doi:10.1016/j.apenergy.2013.05.046.

[17] Guo H, Neill WS, Liko B. An experimental investigation on the combustion and emissions performance of a natural gas - Diesel dual fuel engine at low and medium loads. Proc ASME 2015 Intern Combust Engine Div Fall Tech Conf ICEF2015 Novemb 8-11, 2015, Houston, TX, USA ICEF2015-1041 2015;1:130–7. doi:10.1115/ICEF2015-1041.

[18] Richards K.J. SPK and PE. Converge Manual. Converg (Version 24) Manual," Converg Sci

Inc, Madison, Wisconsin, USA 2017.

[19] Yousefi A, Guo H, Birouk M. Effect of swirl ratio on NG/diesel dual-fuel combustion at low to high engine load conditions 2018. doi:10.1016/j.apenergy.2018.08.017.

[20] Rahimi A, Fatehifar E, Saray RK. Development of an optimized chemical kinetic mechanism for homogeneous charge compression ignition combustion of a fuel blend of *n*-heptane and natural gas using a genetic algorithm. Proc Inst Mech Eng Part D J Automob Eng 2010;224:1141–59. doi:10.1243/09544070JAUTO1343.

[21] Jupudi RS, Finney CEA, Primus R, Wijeyakulasuriya S, Klingbeil AE, Tamma B, et al. Application of High Performance Computing for Simulating Cycle-to-Cycle Variation in Dual-Fuel Combustion Engines 2016. doi:10.4271/2016-01-0798.

[22] Wijeyakulasuriya S. Multidimensional Modeling and Validation of Dual-Fuel Combustion in a Large Bore Medium Speed Diesel Engine. Proc ASME 2015 Intern Combust Engine Div Fall Tech Conf ICEF2015 Novemb 8-11, 2015, Houston, TX, USA 2015:1–14.

[23] Senecal PK, Richards KJ, Pomraning E, Yang T, Dai MZ, McDavid RM, et al. A New Parallel Cut-Cell Cartesian CFD Code for Rapid Grid Generation Applied to In-Cylinder Diesel Engine Simulations 2007;2007:776–90. doi:10.4271/2007-01-0159.

[24] Amin Yousefi, Hongsheng Guo MB. Effect of swirl ratio on natural gas/diesel dual-fuel combustion under low to high engine load conditions. Appl Energy 2018.

[25] Song H, Liu C, Li F, Wang Z, He X, Shuai S, et al. A comparative study of using diesel and PODEn as pilot fuels for natural gas dual-fuel combustion. Fuel 2017;188:418–26. doi:10.1016/j.fuel.2016.10.051.

[26] Wang Z, Zhao Z, Wang D, Tan M, Han Y, Liu Z, et al. Impact of pilot diesel ignition mode on combustion and emissions characteristics of a diesel/natural gas dual fuel heavy-duty

engine. Fuel 2016;167:248–56. doi:10.1016/j.fuel.2015.11.077.

[27] Qi Y, Srinivasan KK, Krishnan SR, Yang H, Midkiff KC. Effect of hot exhaust gas recirculation on the performance and emissions of an advanced injection low pilot-ignited natural gas engine. Int J Engine Res 2007;8:289–303. doi:10.1243/14680874JER02306.

[28] Rochussen J, Kirchen P. Characterization of reaction zone growth in an optically accessible heavy-duty diesel / methane dual-fuel engine 2018. doi:10.1177/1468087418756538.

[29] Forster, P., V. Ramaswamy, P. Artaxo, T. Berntsen, R. Betts, D.W. Fahey, J. Haywood, J. Lean, D.C. Lowe, G. Myhre, J. Nganga, R. Prinn, G. Raga MS and RVD. Changes in Atmospheric Constituents and in Radiative Forcing (IPCC 2007). Clim Chang 2007 Phys Sci Basis 2007;30:129–234. doi:10.1103/PhysRevB.77.220407.

Chapter 5: On greenhouse gas emissions and thermal efficiency of natural gas/diesel dual-fuel engine at low load conditions: Coupled effect of injector rail pressure and split injection

5.1.Abstract

Natural gas/diesel dual-fuel (NDDF) engine has lower thermal efficiency and produces higher greenhouse gas (GHG) emissions than its counterpart diesel engine at low load conditions when conventional diesel combustion strategy is used. This is due to the higher methane emissions. The present paper experimentally and numerically investigates the coupling of two strategies; namely increasing diesel injector rail pressure and splitting diesel injection, in order to overcome this drawback of NDDF engine at low engine load conditions. The results revealed that, compared to NDDF engine with a single injection, using diesel fuel split injection strategy significantly decreases pressure rise rate (PPR), especially at higher split ratios. Increasing the injection rail pressure advances the combustion phasing of both diesel and NDDF engines with a single injection. Increasing the injection rail pressure is also found to advance the combustion phasing of NDDF engine with split injection at split ratios of 45, 50, and 55%; while it retards the combustion phasing under split ratios of 60 and 65%. Increasing the injection rail pressure decreases thermal efficiency of NDDF engine with split injection as a result of overly advanced combustion phasing. However, a higher thermal efficiency (37.2%), than that of diesel and NDDF engines with a single injection, can be achieved under optimized combustion phasing. Increasing the injection rail pressure significantly reduces the unburned methane emissions of NDDF engine with split injection, especially at lower split ratios. However, increasing the injection rail pressure does not affect the unburned methane emissions under

a split ratio of 65%. This is due to the fact that a larger portion of diesel fuel impinges onto the cylinder wall surface. The optimum methane emissions of NDDF engine with split injection is reduced by 50% compared to the best condition of NDDF engine with a single injection. Moreover, the indicated specific carbon dioxide (ISCO2) equivalent emissions of NDDF engine with split injection are reduced by 11% compared to those of NDDF engine with a single injection and diesel engines. Increasing the injection rail pressure significantly decreases soot emissions of NDDF engine when using split injection strategy. Moreover, using split injection can significantly reduce nitrogen oxide (NOx) emissions even at high injection rail pressure. All in all, thermal efficiency and GHG emissions can be further improved using NDDF engine when simultaneously varying diesel fuel injection split ratio and rail pressure increase. This strategy is also found to help reducing PRR and, NOx and soot emissions.

Nomenclature

AMR	Adaptive Mesh Refinement	HRR	Heat Release Rate
ATDC	After Top Dead Center	IMEP	Indicated Mean Effective Pressure
ASOC	After Start of Combustion	ISCH4	Indicated Specific CH4
ASODI	After Start of Diesel Injection	ISCO2	Indicated Specific CO2
BMEP	Break Mean Effective Pressure	$ISNO_x$	Indicated Specific NOx
CA50	Crank Angle of 50% Cumulative Heat Release	ITE	Indicated Thermal Efficiency
CAD	Crank Angle Degree	IVC	Intake Valve Closing
CFD	Computational Fluid Dynamic	IVO	Intake Valve Opening
CI	Compression Ignition	NDDF	Natural gas/Diesel Dual-Fuel
CO	Carbon Monoxide	NO_x	Nitrogen Oxide
CO_2	Carbon Dioxide	PM	Particulate Matter
COV	Coefficient of Variation	PRR	Pressure Rise Rate
EGR	Exhaust Gas Recirculation	RNG	Re-Normalization Group
EPA	Environmental Protection Agency	RPM	Revolution Per Minute
EVC	Exhaust Valve Closing	SODI	Start of Diesel Injection
EVO	Exhaust Valve Opening	SMD	Sauter Mean Diameter
GHG	Greenhouse Gas		

5.2.Introduction

Environmental pollution and energy scarcity fuelled further motivations to put more focus towards alternative clean fuels for internal combustion engines. Compression ignition (CI) diesel engine has been favoured due to its higher fuel efficiency and lower carbon dioxide (CO_2) emissions compared to spark ignition engine. However, soot and NO_x emissions have been a challenge for diesel fueled CI engines due to the nature of heterogeneous and high temperature combustion. Moreover, there is

a serious concern over the extent of GHG emissions produced from the combustion of diesel fuel [1]. For instance, the U.S. Environmental Protection Agency (EPA) has regulated GHG emissions and fuel efficiency standards for light-duty vehicles by 2018, and heavy-duty vehicles by 2025 [2]. Substituting diesel fuel by natural gas is a good approach to resolve environmental issues of diesel engines, since natural gas is a low carbon fuel which produces less soot and CO_2 emissions compared to diesel fuel. Using natural gas in dual-fuel CI engines has drawn more and more research interest in recent years [3–5]. In a typical NDDF engine, natural gas is introduced into the intake manifold, and a small quantity of diesel fuel is directly injected into the cylinder to ignite the natural gas-air mixture. A conventional diesel engine can be easily converted to a NDDF engine, which reduces the engine development cost and allows the engine to switch back to full diesel combustion when needed [6]. However, using natural gas in CI diesel engine causes lower thermal efficiency and higher unburned methane and carbon monoxide (CO) emissions compared to diesel engine at low load conditions [7]. This drawback can significantly offset the advantage of lower CO_2 emissions of natural gas combustion in terms of the overall GHG emissions, since methane has a global warming potential that is about 20 ~ 34 times greater than that of CO_2 over a 100 year period [8]. A variety of strategies have been investigated in order to improve the performance of NDDF engines [9–12]. For instance, Guo et al. [11] found that advancing SODI in the range of conventional diesel injection timing reduces the unburned methane and GHG emissions and improves thermal efficiency of NDDF engine under a low load condition. They found that advancing SODI lengthens the ignition delay, which allows more natural gas to be mixed with diesel during the premixed combustion phase. This helps more premixed natural gas to be burned during the combustion process, which results in significantly reduced methane and GHG emissions and improved thermal efficiency. Ryu et al. [10] studied the effect of diesel injection rail pressure on natural gas/biodiesel dual-fuel engine at a low load condition. They demonstrated that increasing the injection rail pressure significantly improves the thermal efficiency and unburned hydrocarbon and CO emissions. They stated that this is mainly

due to the improved pilot fuel atomization and decreased ignition delay. Therefore, both advanced SODI and increased injection rail pressure promote a better mixing between diesel fuel and premixed natural gas. However, advancing SODI (in the range of conventional diesel injection timing, i.e., -10 to -30 °ATDC) and/or increasing the injection rail pressure usually causes high pressure rise rate (PRR) and increased NO_x emissions [9–14].

In addition to studies on diesel injection timing and injection rail pressure, several studies have examined the effect of diesel split injection on NDDF engine [15–21]. Aksu et al. [16] examined the effect of the start of the second diesel injection timing (SODI2) on combustion and emissions of NDDF engine. They revealed that diesel split injection significantly improves the indicted mean effective pressure (IMEP) and thermal efficiency. They noted that combustion progresses earlier when the first part of the injected diesel auto-ignites during the second injection. Xu et al. [17] studied the effect of the start of the first diesel injection timing (SODI1) on the combustion and emissions of NDDF engine under low load conditions. They indicated that using very advanced SOD1 could decrease combustion intensity and NOx and unburned hydrocarbon emissions as well as improve thermal efficiency. Guo et al. [20] investigated the effect of diesel injection split ratio and timings (SODI1 and SODI2) on natural gas/diesel dual-fuel engine at low load conditions. They found that split injection improves the thermal efficiency and methane and equivalent CO2 emissions.

The briefly reviewed literature above revealed that advancing SODI (in the range of conventional injection timing) and/or increasing diesel injection rail pressure improves thermal efficiency and unburned methane emissions of NDDF engine (with a single injection) at low load conditions. The drawback of this strategy is the resultant high PRR and NOx emissions. On the other hand, using diesel split injection helps reducing both PRR and NOx emissions and can also improve thermal efficiency and unburned methane emissions. However, the outcome of an investigation of the coupled effect of both strategies, diesel split injection and diesel injection rail pressure, on the combustion of NDDF engine is still unknown. This is the focus of the present study. In the present study, the effect

of increasing injection rail pressure on combustion performance and emissions of both NDDF and diesel engines with single injection is studied first to develop baseline data. . The coupled effect of diesel split injection and injection rail pressure increase is then experimentally investigated, which is the focus of this paper. In addition to the experimental study, a computational fluid dynamic (CFD) model is used to further explain experimental results.

5.3.Experimental setup and test methodology

5.3.1. Engine test cell

A modified single cylinder heavy-duty engine was employed to carry out the experiments. A schematic of the experimental test setup is shown in Figure 5-1 and the engine specifications are listed in Table 5-1. The diesel fuel used in the study was a Canadian ultra-low-sulfur diesel fuel, and the natural gas was supplied by Enbridge Inc. Natural gas was injected by a injector block which consist of eight gas fuel injectors manufactured by Alternative Fuel Systems Inc. Natural gas and diesel injection parameters (start and width of injection pulse) were controlled by a LabVIEW-based software (Drivven Inc.). The diesel and natural gas fuel measurements were realized by means of two Bronkhorst mass flowmeters. A turbine mass flowmeter was used to measure air flow rate. Engine loading was carried out by an eddy-current dynamometer. Engine speed was sensed by a Hall-effect transducer. More details can be found in [22].

The in-cylinder pressure was measured by means of a water-cooled pressure transducer (Krister Corp.,), which sampled over 100 cycles at intervals of 0.2 crank angle degree (CAD) using an AVL real-time combustion analysis system. Soot emissions were measured by an AVL smoke meter [22]. California Analytical Instruments gas analyzers was used to measure engine-out emissions such as CH_4, NOx, CO, and CO_2.

5.3.2. Test conditions and procedure

Tests were conducted at a constant engine load-speed condition (BMEP=4.05 bar, RPM=910) using both diesel-only and NDDF mode under steady state. The tested condition was a representative of low speed and low load conditions of a real heavy-duty diesel engine. The intake manifold pressure and temperature were kept constant at 105 kPa and 40 °C, respectively. Exhaust gas recirculation (EGR) was not used in the experiments. The natural gas energy fraction in dual-fuel mode, which is defined as the energy fraction coming from natural gas, was kept constant at 70%.

A maximum PRR of 13 bar/CAD and a coefficient of variation of IMEP (COV_{IMEP}) of 5% were considered as the engine operating limits during the test. Four sets of experiment were conducted in this study as shown in Table 5-2. The goal of this test matrix was to test the possibility to decrease PRR, NOx, CH_4, and GHG emissions and increase thermal efficiency of NDDF engine mode with respect to diesel engine using the combination of increasing diesel injection rail pressure and splitting diesel injection. For diesel combustion mode, only single injection strategy was examined, while both single and split (double) injection strategies were tested for NDDF combustion mode. For diesel combustion mode, different starts of diesel injection (SODI) were examined. At each SODI, three different injection rail pressures (P-rail) were tested (Test 1). The same procedure was adopted for NDDF mode with single injection strategy (Test 2). Due to the high PRR, the start of diesel injection timing was limited to conventional diesel injection regime (i.e., not earlier than -32 °ATDC) in NDDF mode with single injection. Test 3 was carried out to optimize split ratio under three different injection rail pressures and fixed SODI1 and SODI2 (optimized points). Test 4 was performed to optimize CA50 (by retarding SODI2) while keeping thermal efficiency at high level with a constant injection rail pressure of 800 bar and split ratio of 55% (best point of Test 3). The split ratio is the mass of diesel fuel injected in the first pulse divided by the total mass of the injected diesel fuel.

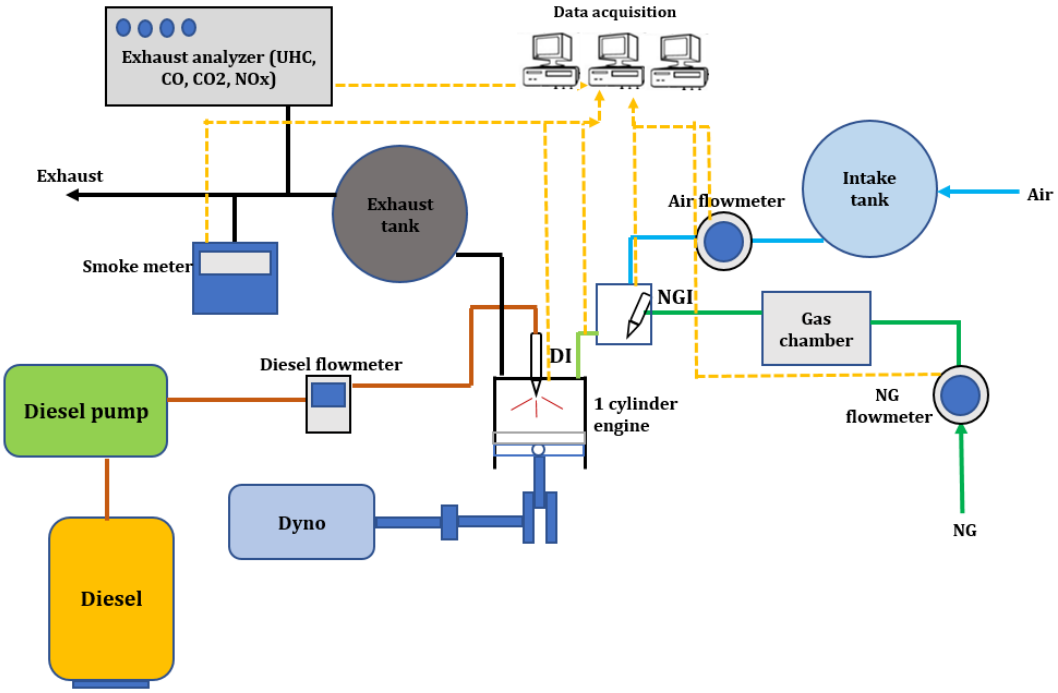

Figure 5-1. Schematic of the experimental setup

Table 5-1. Engine specifications.

Engine type	Single cylinder-caterpillar 3400
Bore×Stroke	137.2 mm ×165.1 mm
Conn. rod length	261.62 mm
Displacement vol.	2.44 L
Compression ratio	16.25
Diesel fuel injector	Common rail injector
Natural gas injection timing	-355 °ATDC
Inlet valve opening (IVO)	-358.3 °ATDC
Inlet valve closing (IVC)	-169.7 °ATDC
Exhaust valve opening (EVO)	145.3 °ATDC
Exhaust valve closing (EVC)	348.3 °ATDC

Table 5-2. Test matrix.

Test No.	Combustion mode	Injection strategy	P-rail(bar)	SODI or SODI1 (ATDC)	SODI2 (ATDC)	Split ratio (%)
1	Diesel	Single	525	-14 to -26		
			650	-14 to -22	-	-
			800	-14 to -18		
2	Dual-fuel	Single	525	-16 to -32		
			650	-14 to -28	-	-
			800	-14 to -22		
3	Dual-fuel		525	-54	-24	45 to 65
			650	-54	-24	45 to 65

		Split-optimized split ratio	800	-54	-24	45 to 65
4	Dual-fuel	Split-optimized CA50	800	-54	-24 to -16	55

5.4.Numerical simulation setup

A computational CFD model based on CONVERGE 2.4 [23] was employed to simulate the physical and chemical processes (e.g., turbulent flow, spray, combustion, heat transfer, and emissions formation) in the engine cylinder. The details of the developed CFD model can be found in [7,8] and a brief description is presented here. In order to implement the chemistry calculation, a transient chemistry solver, named as SAGE [23], was used in the simulation. The chemical reactions of diesel fuel were represented by n-heptane, whereas natural gas oxidation was represented by methane. It was assumed that the methane and air mixture is homogeneous at the start of the simulation immediately after the intake valve closing (IVC). The merged natural gas/diesel mechanism consisted of 76 species and 464 reactions [24]. Adaptive mesh refinement (AMR) was used to resolve flow and flame propagation in the cylinder. AMR provides adequate resolution of temperature and velocity fields only when and where a fine mesh is needed. Moreover, using AMR with fine enough cell sizes (0.25–0.5 mm) in the flame region adequately resolves the turbulent flame front and the species gradients without the need of any sub-grid model [23]. Renormalization Group (RNG) k-ε turbulence model was used to simulate the turbulent flow within the combustion chamber. The Kelvin-Helmholtz/Rayleigh-Taylor breakup model was employed to simulate the spray atomization and breakup.

5.5.Results and discussion

A comparison of the combustion performance and emissions of diesel and NDDF engines with single injection is made with NDDF engine with split injection strategy. Numerical simulation results

(i.e., diesel spray and OH radical distribution) are also presented for some cases to gain insight into the combustion process. The developed CFD model was validated under different engine load-speed conditions as reported elsewhere [7,8]; however, further validation cases are presented in this paper.

5.5.1. Combustion characteristics

Figure 5-2 shows the experimental results of the effect of injection rail pressure on PRR of diesel and NDDF engines with single injection (Figure 5-2a and Figure 5-2b, respectively) and NDDF engine with split injection (Figure 5-2c) under a low load-low speed condition. It is noteworthy to mention that based on CO_2 equivalent emissions, as presented later on, the SODI1=-54 °ATDC and SODI2=-24 °ATDC are found to be the optimized diesel injection timings at P-rail=525 bar and split ratio of 60%. Therefore, these diesel split injection timings were chosen to study the effects of injection rail pressure under different split ratios when using split injection strategy. As shown in Figure 5-2a and Figure 5-2b, PRR quickly increases with increasing the injection rail pressure for both diesel and NDDF engines with single injection. Increasing the injection rail pressure makes the examined range of SODI narrower due to increased PPR. For example, in diesel engine at P-rail=525 bar, the most advanced SODI is -26 °ATDC. However, the most advanced SODI of -18 °ATDC is achieved under injection rail pressure of 800 bar (Figure 5-2a). It can be seen, from Figure 5-2b, that NDDF engine with a single injection exhibits lower PRR compared to diesel engine under the same engine load-speed condition. This is the main reason why a wider range of SODI is examined for NDDF engine with a single injection compared to diesel engine. Figure 5-2c shows the experimental results of the effect injection rail pressure at different split ratios. It can be seen that similar to a single injection, increasing the injection rail pressure increases the PRR of NDDF engine. However, diesel split injection significantly decreases PPR of NDDF engine compared to single injection, especially at higher split ratios. The maximum registered PRR is below the limit (13 bar/deg) for all examined cases of NDDF engine with diesel split injection.

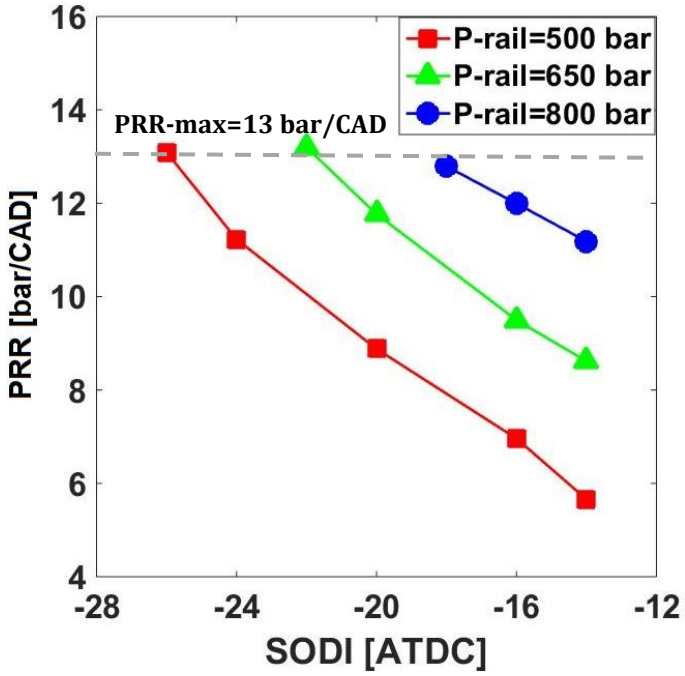

a) Diesel-single injection

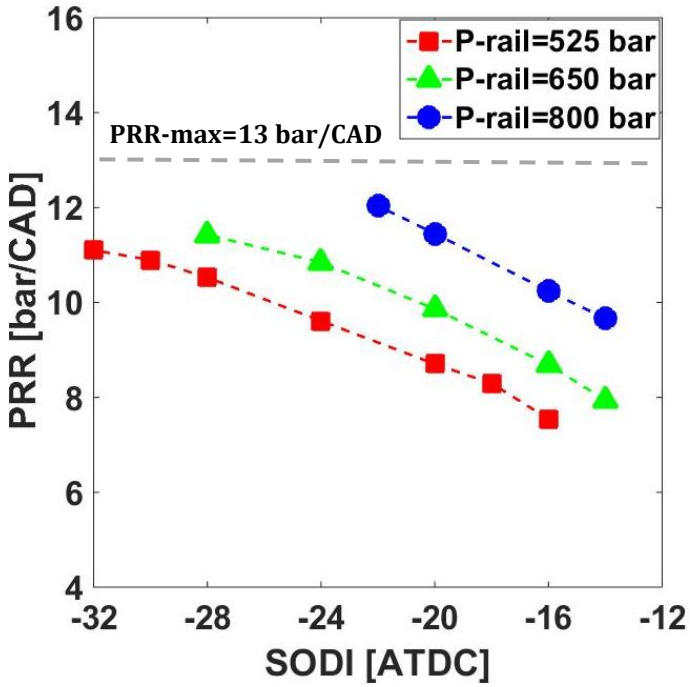

b) NDDF-single injection

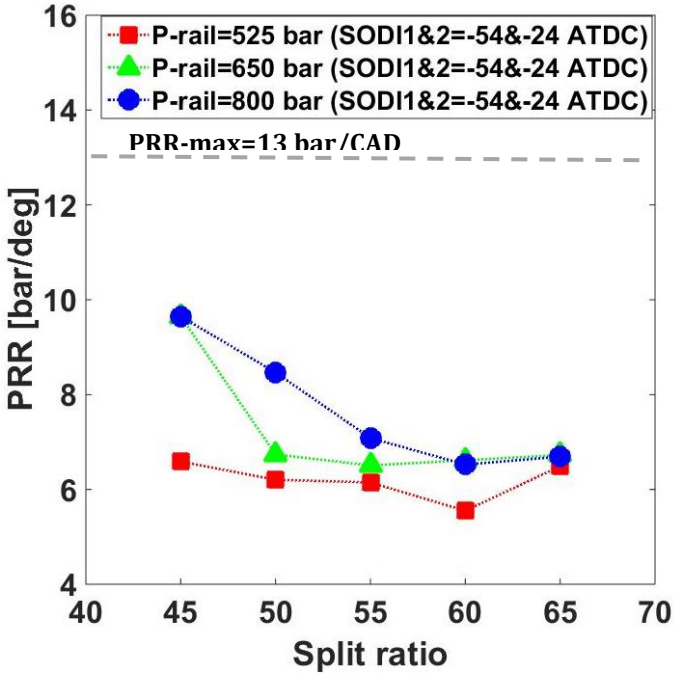

c) NDDF-split injection

Figure 5-2. Effect of the injection rail pressure on PRR of diesel and NDDF engines.

Figure 5-3 shows the experimental results of the effect of injection rail pressure on combustion phasing (CA50) of diesel and NDDF engines with a single injection and NDDF engine with split injection under a low load-low speed condition. As shown in this figure, increasing the injection rail pressure advances the combustion phasing of both diesel and NDDF engines with single injection.

Increasing the injection rail pressure leads to prolonged ignition delay and consequently more premixed mixture (diesel/air or diesel/air-natural gas) is formed before the start of combustion which results in the advancement of combustion phasing (Figure 5-3a and Figure 5-3b). However, as shown in Figure 5-3c, increasing the injection rail pressure advances combustion phasing of NDDF engine with split injection for split ratios of 45%, 50%, and 55%, but it slightly retards the combustion phasing for split ratios of 60 and 65%.

To gain insight into the effect of injection rail pressure on the combustion process, a CFD simulation was carried out for two different injection rail pressures of 525 and 800 bar. It is noteworthy to mention that the effect of injection rail pressure on combustion phasing of both diesel and NDDF engines with a single injection is almost similar and, therefore, the CFD result of diesel combustion engine is not presented in this paper. Figure 5-4 displays the measured and predicted cylinder pressure and HRR of NDDF engine with a single injection under a low load condition at different injection rail pressures (constant SODI of -20 °ATDC). It can be observed that increasing the injection rail pressure increases the cylinder peak pressure and HRR and also advances the start of combustion. Figure 5-5 depicts OH radical distribution, spray penetration, and local equivalence ratio contours of NDDF engine with a single injection under constant SODI and two injection rail pressures of 525 and 800 bar. For both injection rail pressures, the combustion initiates near the piston bowl and expands toward the center of cylinder. The OH intensity significantly increases and extends more rapidly with increasing the injection rail pressure. The maximum spray penetration of P-rail=525 bar is 36 mm, while the maximum spray penetration of P-rail=800 bar is 42 mm. Increasing the injection rail pressure accelerates the break-up and atomization of droplets, more droplets with smaller Sauter Mean Diameters (SMD) are generated, which consequently promotes liquid fuel evaporation. This provides a longer time for fuel to spread in the cylinder where a more homogenous mixture (diesel-air-natural gas) can be formed within a shorter period of time. It promotes a faster

formation of a combustible mixture, advances the start of combustion, and increases the cylinder peak pressure.

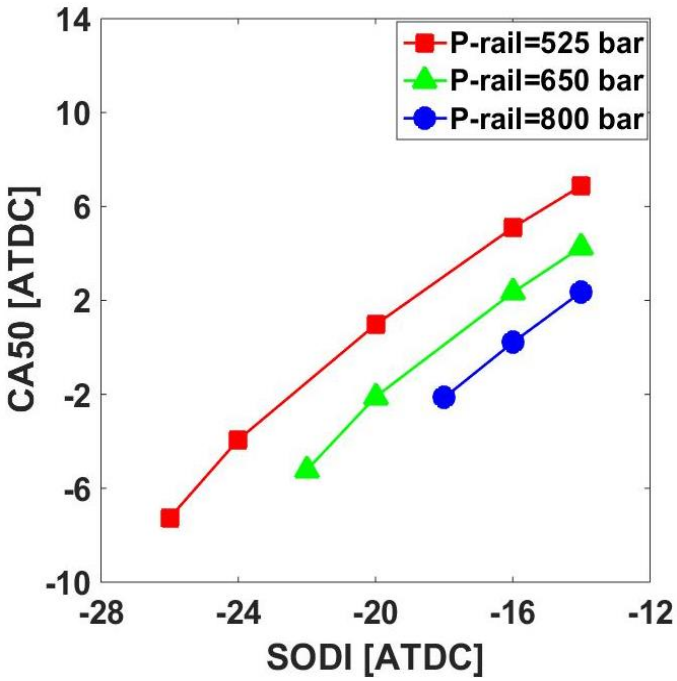

a) Diesel-single injection

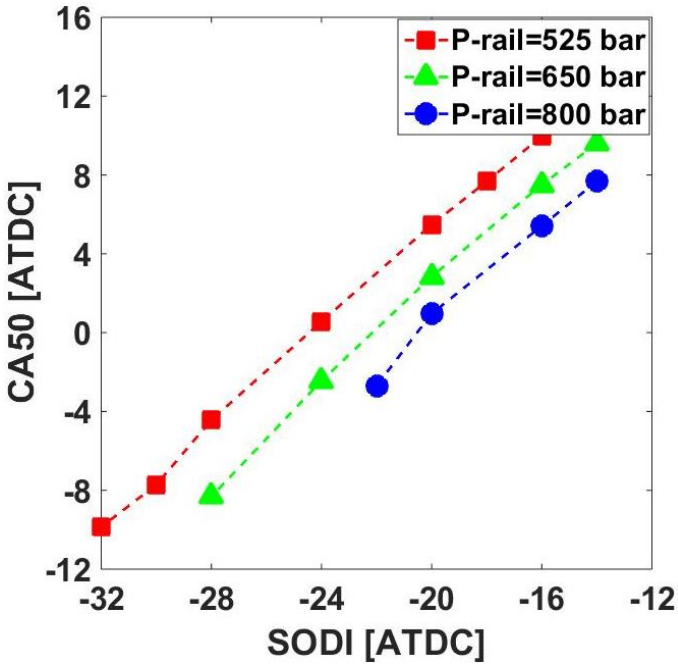

b) NDDF-single injection

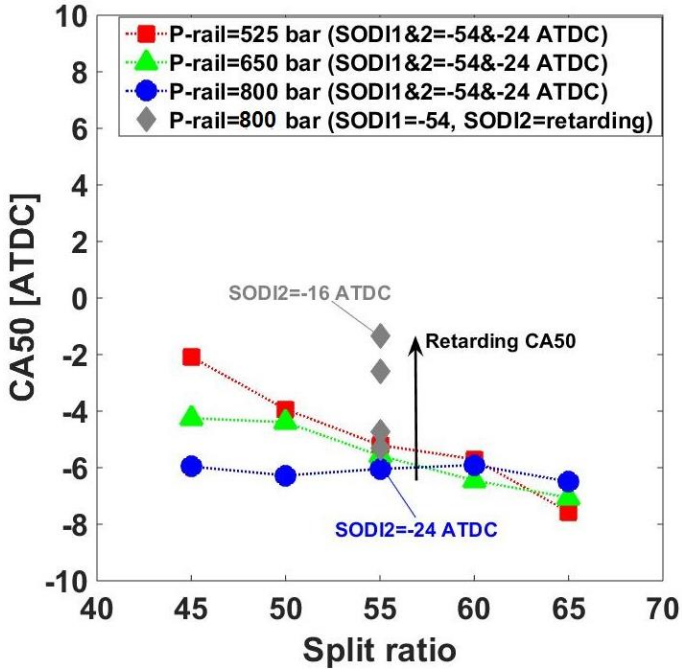

c) NDDF-split injection

Figure 5-3**.** Effect rail pressure on combustion phasing of diesel and NDDF engines.

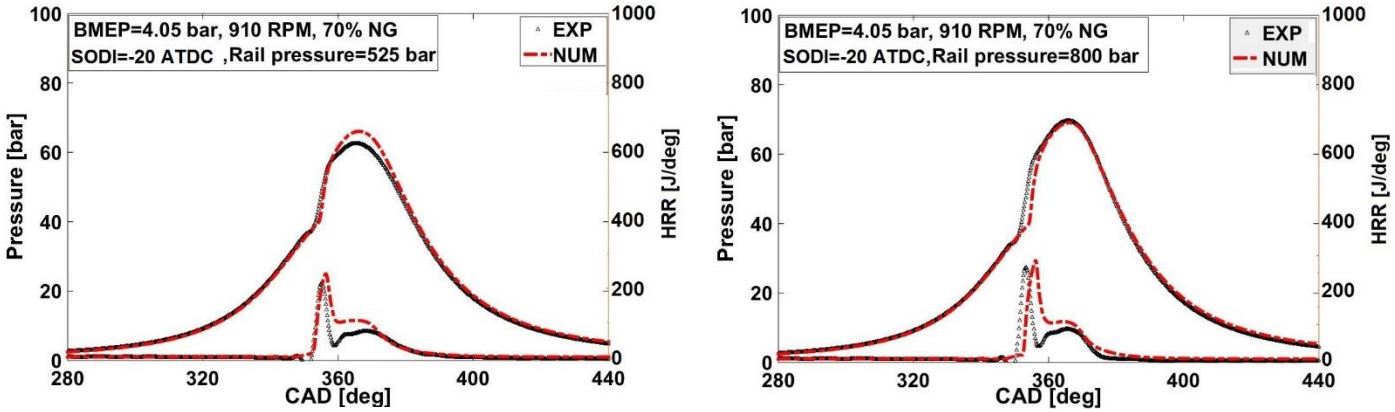

Figure 5-4**.** Effect of injection rail pressure on cylinder pressure and HRR of NDDF engine with single injection (measured and predicted data).

SODI=-20 °ATDC, P-rail=525 bar

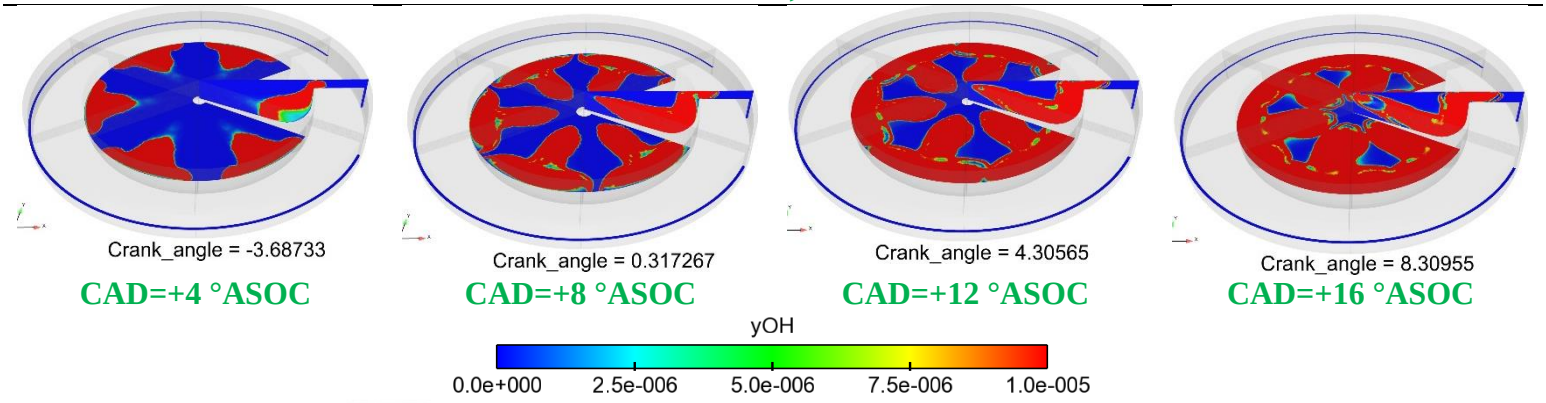

CAD=+4 °ASOC **CAD=+8 °ASOC** **CAD=+12 °ASOC** **CAD=+16 °ASOC**

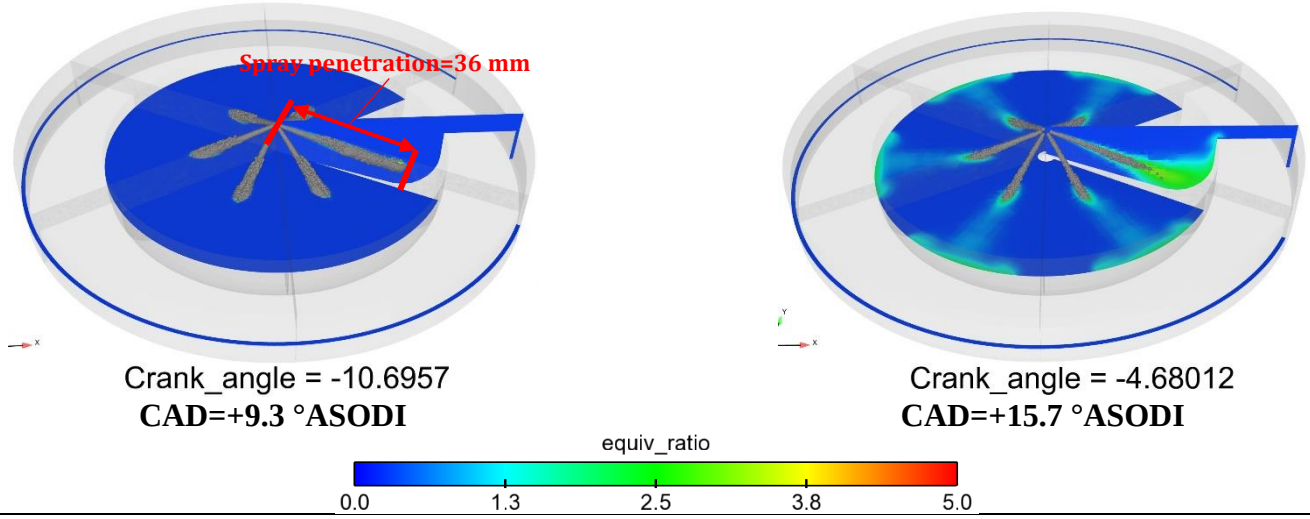

CAD=+9.3 °ASODI **CAD=+15.7 °ASODI**

SODI=-20 °ATDC, P-rail=800 bar

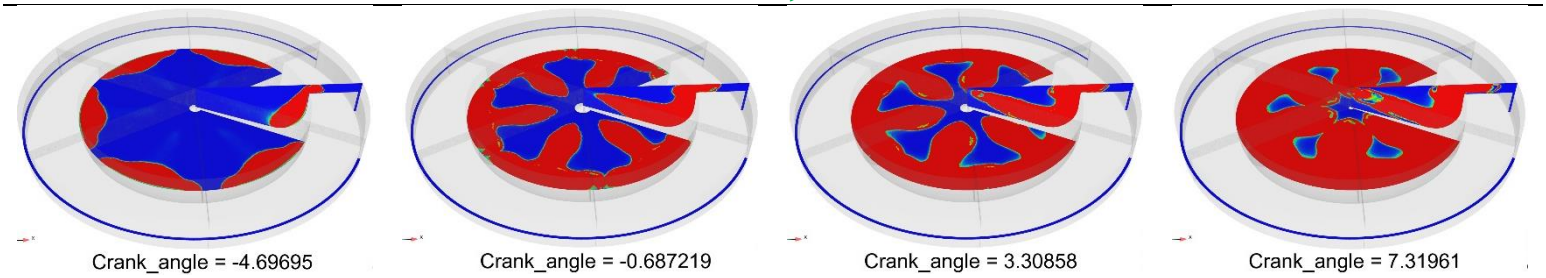

CAD=+4 °ASOC **CAD=+8 °ASOC** **CAD=+12 °ASOC** **CAD=+16 °ASOC**

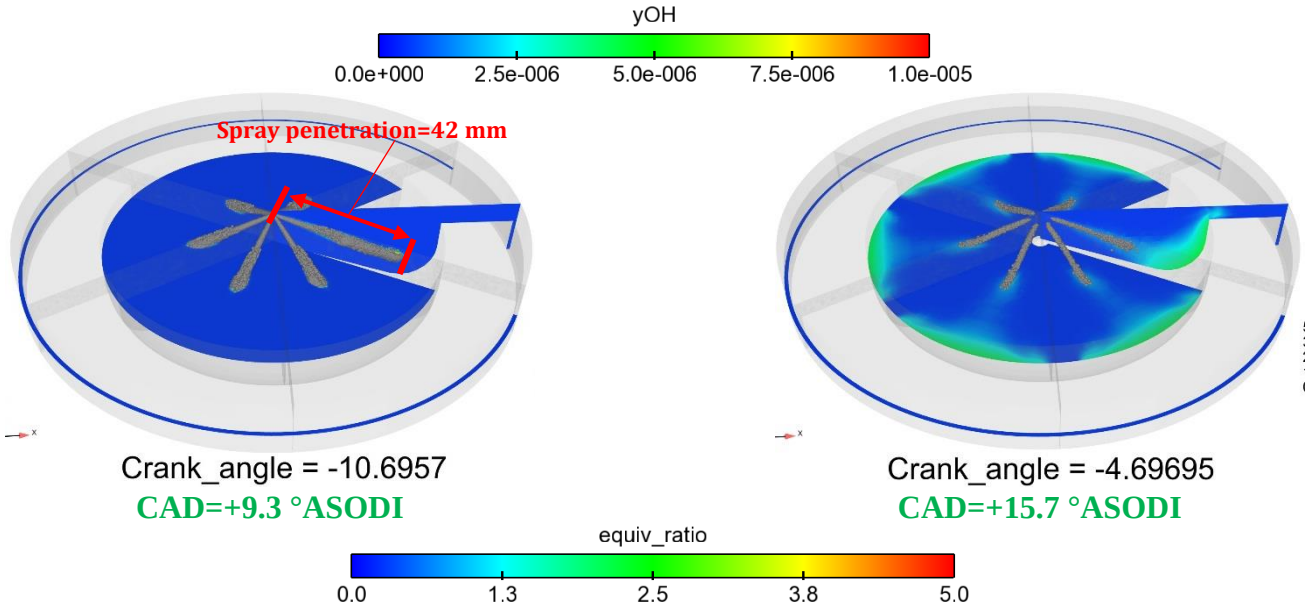

Figure 5-5**.** Effect of injection rail pressure on OH distribution, spray penetration, and equivalence ratio of NDDF engine with single injection.

Figure 5-6a and Figure 5-6b depict the effect of injection rail pressure on cylinder pressure and HRR of NDDF engine with split injection at two split ratios of 45% and 65%, respectively. As shown in Figure 5-6a (split ratio of 45%), increasing the injection rail pressure advances the start of combustion and increases the cylinder peak pressure. However, under split ratio of 65%, increasing the injection rail pressure retards the start of combustion and slightly decreases the cylinder peak pressure (Figure 5-6b). To explain the reason behind this, the spray penetration and OH distribution contours are presented in Figure 5-7 and Figure 5-8, respectively. It can be observed from Figure 5-7a and Figure 5-7b that increasing the injection rail pressure increases the evaporation rate and reduces liquid parcels hiding in the squish region (first pulse of diesel). Moreover, it also enhances the atomization and evaporation processes of the second pulse of diesel injection (similar to a single injection shown above). These are beneficial for diesel-air-natural gas mixing process which shortens the ignition delay and advances the combustion phasing. In addition, a high injection pressure can increase the initial velocity and momentum of the droplets which results in that diesel fuel droplet (first pulse of injected diesel) is pushed towards and dispersed into the cylinder wall and squish regions where the lower temperature exists. The mixture temperature decreases as the diesel fuel

approaches the cylinder wall, increasing the ignition delay and retarding the combustion phasing. For a split ratio of 45%, less diesel fuel reaches the cylinder wall and squish regions during the first pulse. Thus, the effect of increased injection rail pressure on atomization and evaporation process is more significant which shortens the ignition delay and advances the combustion phasing (shown in Figure 5-3c). With increasing the split ratio (e.g., split ratio of 65%), a larger amount of diesel fuel locates in the region close to the low temperature wall surface. Thus, increasing the injection rail pressure leads to a slower evaporation process during the first pulse of injected diesel. This lengthens the ignition delay and retards the combustion phasing, as shown in Figure 5-3c.

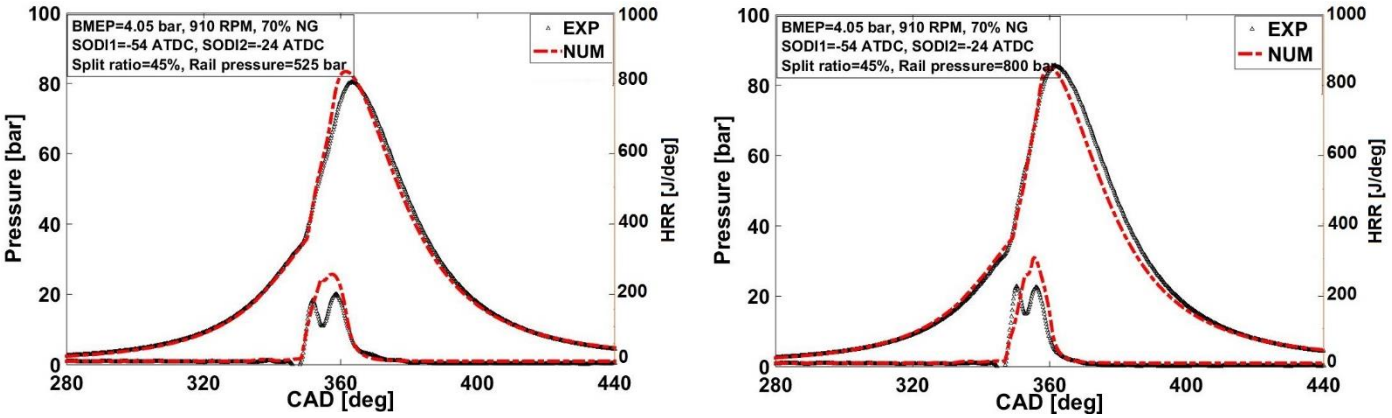

a) Measured and predicted cylinder pressure and HRR of NDDF engine with split injection-split ratio of 45% and increased rail pressure

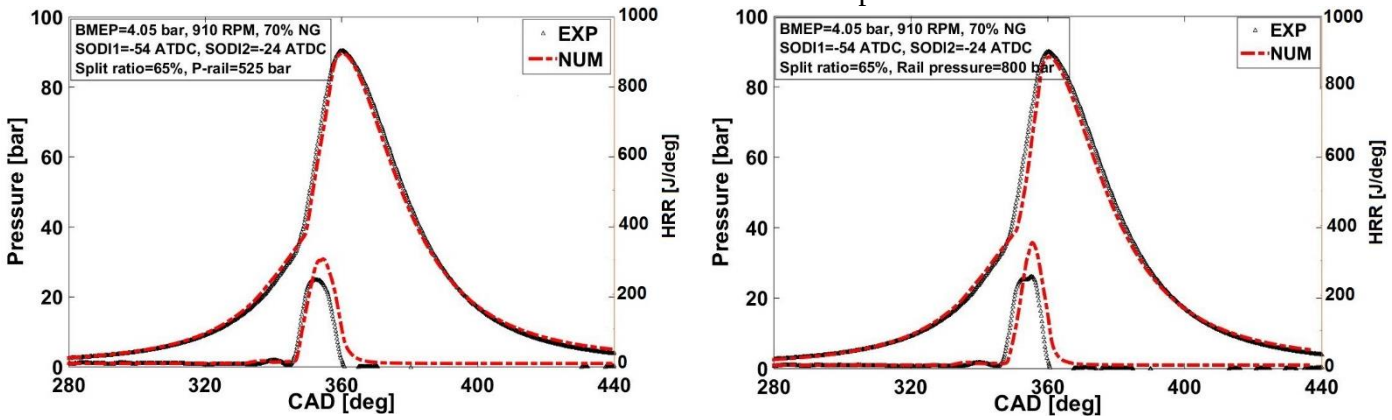

b) Measured and predicted cylinder pressure and HRR of NDDF engine with split injection-split ratio 60% and increased rail pressure

Figure 5-6 Effect of injection rail pressure on cylinder pressure and HRR of NDDF engine with split injection at two split ratios of 45 and 65% (measured and predicted data).

Split ratio=45%, P-rail=525 bar	Split ratio=45%, P-rail=800 bar

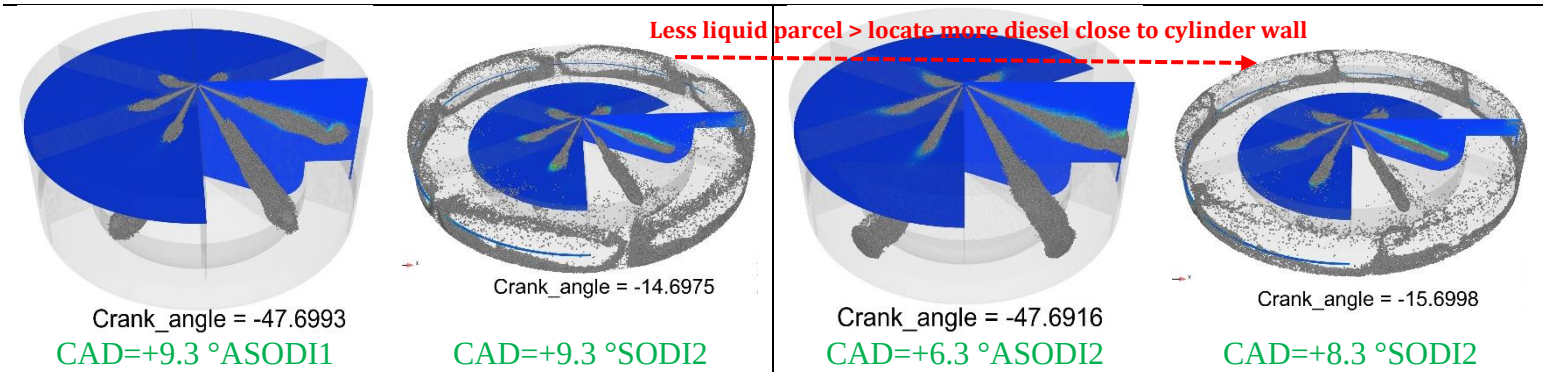

a) Diesel spray penetration at constant split ratio of 45% and different injection rail pressures

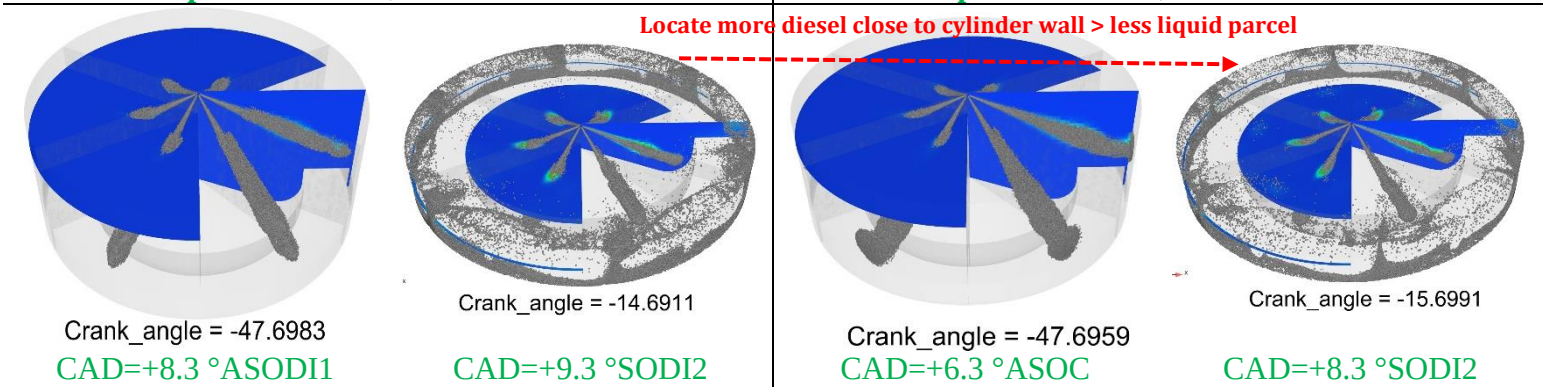

b) Diesel spray penetration at constant split ratio of 65% and different injection rail pressures

Figure 5-7**.** Effects of injection rail pressure on spray penetration of NDDF engine with split injection at two split ratios of 45 and 65%.

Figure 5-8 shows OH radical distribution of NDDF engine with split ratios of 45 and 65% and injection rail pressures of 525 and 800 bar. This figure shows that, for all cases, the combustion starts after the second pulse of injected diesel. Moreover, the combustion starts from two zones; namely piston bowl and piston squish regions. As shown in Figure 5-8a (a split ratio of 45%), increasing the injection rail pressure significantly advances the start of combustion and increases the combustion rate (frame contours of CAD=+10 °ATDC). However, increasing the injection rail pressure at a split ratio of 65% slightly retards the start of combustion and decreases the combustion rate (Figure 5-8b). As mentioned earlier, this is mainly due to the fact that a larger amount of diesel fuel impinges onto the cylinder wall which results in a lengthened ignition delay and retarded combustion phasing. It can be concluded that increasing the injection rail pressure under advanced SODI1 and high split ratio

(i.e., 65%) may not significantly improve the combustion rate and unburned methane emissions (as shown Figure 5-11b).

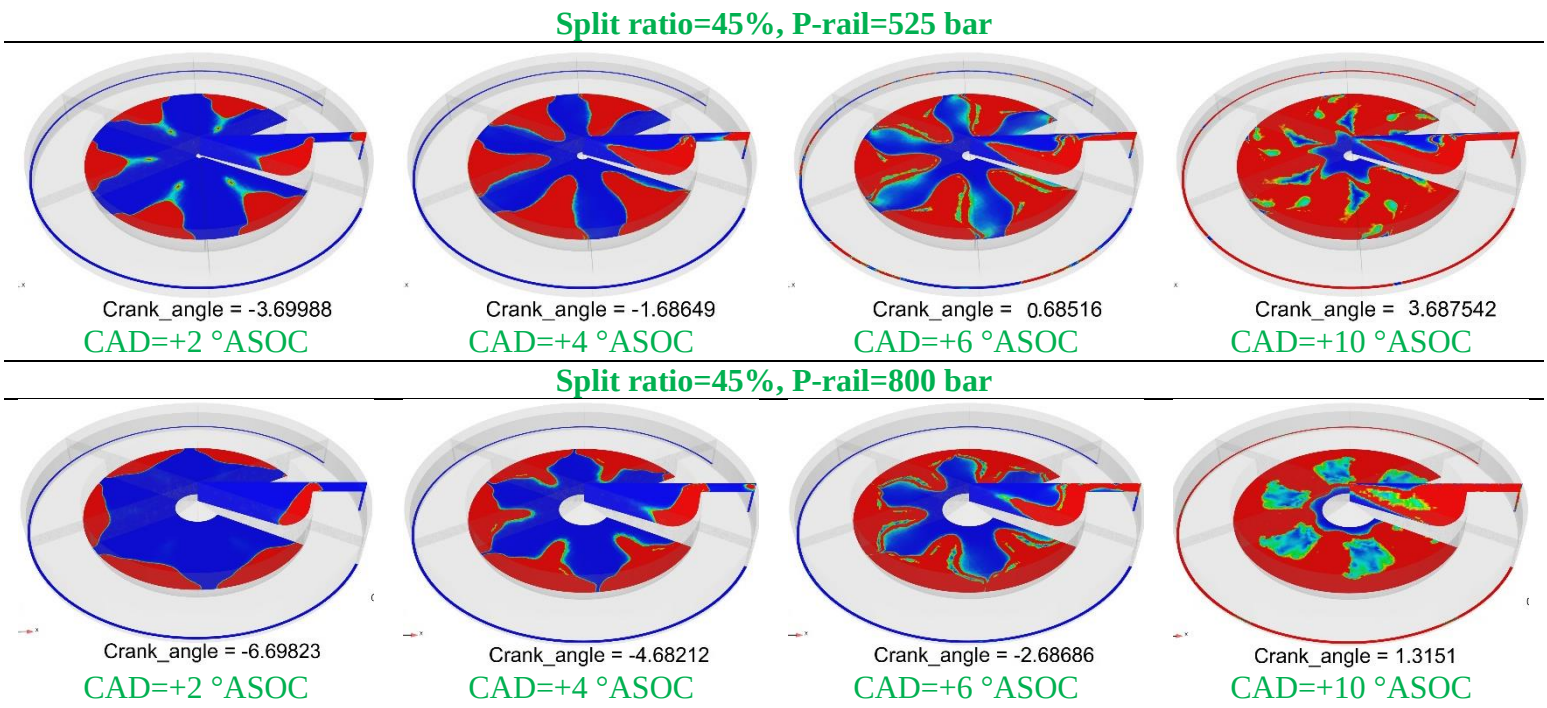

a) OH distribution at constant split ratio of 45% and different injection rail pressures

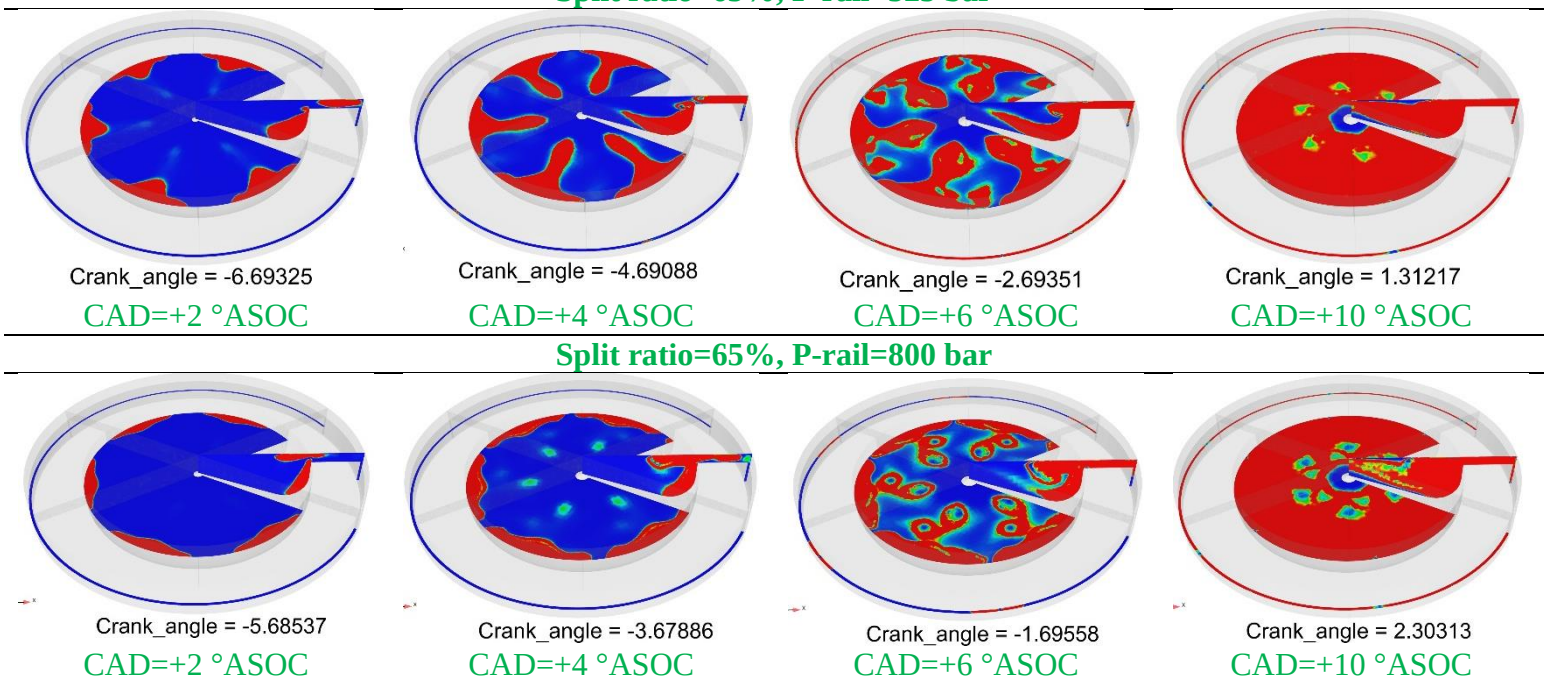

b) OH distribution at constant split ratio of 65% and different injection rail pressures

Figure 5-8**.** Effects of injection rail pressure on OH radical distribution of NDD F engine with split injection at two split ratios of 45 and 65%.

Figure 5-9 shows the experimental results of the effect of injection rail pressure on thermal efficiency of diesel and NDDF engines with a single injection and NDDF engine with split injection under a low load-low speed condition. It can be seen that increasing the injection rail pressure do not significantly affect thermal efficiency of diesel engine. Thermal efficiency starts slightly decreasing after SODI=-18 °ATDC for injection rail pressures of 525 and 650 bar (Figure 5-9a). This is mainly due to an overly advanced combustion phasing, as shown in Figure 5-3a. The diesel engine maximum thermal efficiency of 36.6% is achieved at SODI=-14 °ATDC and P-rail=800 bar. Thermal efficiency of NDDF engine with a single injection is much lower than that of diesel engine (Figure 5-9b) at retarded injection timing and low injection rail pressure (e.g., SODI=-14 °ATDC and P-rail=525 bar). However, increasing the injection rail pressure and/or advancing the SODI significantly improves NDDF engine thermal efficiency. A maximum thermal efficiency of 36.7% is attained at SODI=-24 °ATDC and P-rail=525 bar, which is comparable to the highest ITE of diesel engine (i.e., ITE=36.6 %). Similarly thermal efficiency starts to decrease with further advancing SODI due to the overly advanced combustion phasing. As shown in Figure 5-9c (experimental results), NDDF engine with split injection and injection rail pressure of 800 bar has the lowest thermal efficiency compared to the injection rail pressures of 650 and 525 bar. This is mainly due to the overly advanced combustion phasing (Figure 5-3c). To find an optimum point (retarding the combustion phasing), the second injection timing is slightly retarded from -24 to -16 °ATDC while the SODI1 and split ratio are fixed at -54 °ATDC and 55%, respectively, when the rail pressure is 800 bar. The grey diamond symbols in Figure 5-3c and Figure 5-9c show the variations of CA50 and ITE when SODI2 is retarded from -24 to -16 °ATDC at SODI1 = -54 °ATDC at split ratio of 55%, and P-rail of 800 bar. As shown in Figure 5-9c, retarding SODI2 significantly increases thermal efficiency at P-rail of 800 bar. The highest thermal efficiency of 37.2% is achieved at operating conditions of SODI1=-54 °ATDC, SODI2=-16 °ATDC, P-rail=800 bar, and split ratio of 55%. This is the optimum condition of NDDF engine with split injection. It can be seen that using split injection (optimum condition) increases

thermal efficiency by about 1.34% and 1.88% compared to the highest ITE of NDDF and diesel engines with a single injection, respectively.

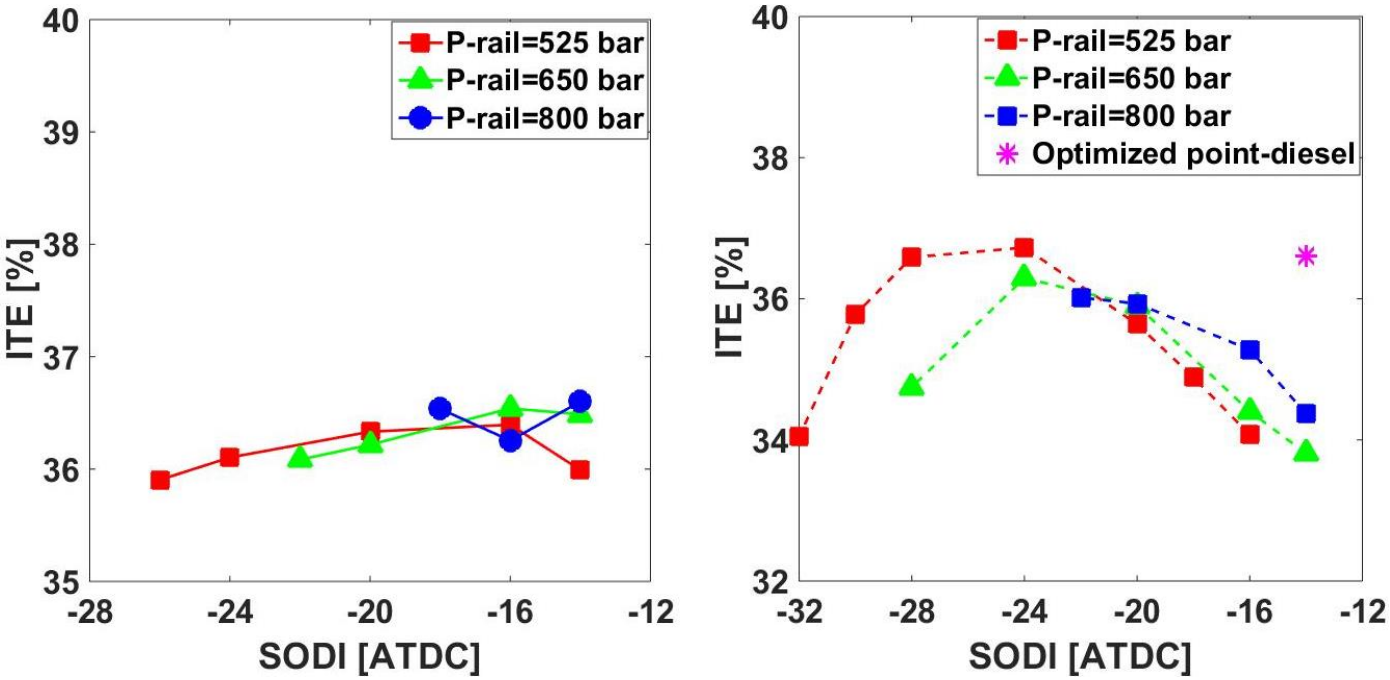

a) Diesel-single injection b) NDDF-single injection

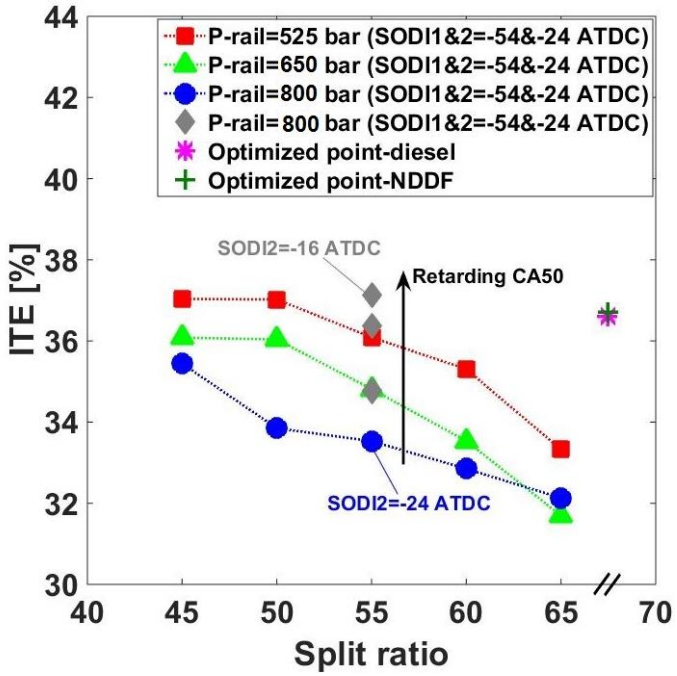

c) NDDF-split injection

Figure 5-9**.** Effect of injection rail pressure on ITE of diesel and NDDF engines.

5.5.2. Emissions

Many studies have reported that less CO_2 emissions are produced during the combustion process of NDDF engine compared to that of diesel. This is mainly due to the reduced carbon to hydrogen ratio of natural gas [25–28]. However, unburned methane emissions can significantly offset its greenhouse gas benefits if natural gas does not burn to completion. According to EPA's GHG Phase (I) regulation, the GHG impact of 25 is assigned to any tailpipe methane emissions when computing the total CO_2 equivalent or GHG emissions from the engine [29]. Thus, in the present study, the factor of 25 is considered for the calculation of GHG emissions. Figure 5-10 depicts the experimental results of the effect of rail pressure on indicated specific CO_2 equivalent ($ISCO_2$-equivalent) of diesel and NDDF engines with a single injection and NDDF engine with split injection. As shown in Figure 5-10a, advancing SODI and/or increasing the injection rail pressure does not significantly affect the $ISCO_2$-equivalent emissions of diesel engine. The lowest $ISCO_2$-equivalent emissions of 719 g/kW-hr is achieved at SODI=-14 °ATDC and P-rail=800 bar. It is obvious that under advanced injection timing, the $ISCO_2$-equivalent emissions slightly increase for injection rail pressures of 525 and 650 bar, which is mainly due to the drop in thermal efficiency. As shown in Figure 5-10b, compared to diesel engine, NDDF engine with a single injection produces higher level of CO2 equivalent emissions at lower injection pressure and retarded injection timings under this engine load-speed condition (e.g., GHG=1082 g/kW-hr at SODI=-16 ATDC and P-rail=525 bar). This is mainly due to the high level of unburned methane emissions (Figure 5-11a). However, advancing SODI and/or increasing the injection rail pressure significantly decreases the unburned methane and CO_2 equivalent emissions. It can be seen, from Figure 5-10b, that the lowest CO_2 equivalent emissions achieved under this engine load-speed condition is 721 g/kW-hr, which is almost similar to that of diesel engine (the lowest CO_2 equivalent emissions of 719 g/kW-hr).

Figure 5-11c shows that increasing the injection rail pressure significantly reduces the unburned methane emissions of NDDF engine with split injection, especially at lower split ratios. On the other

hand, increasing the injection rail pressure does not affect the unburned methane emissions under a split injection ratio of 65%. The optimum methane emissions of NDDF engine with split injection is reduced by 50% compared to the best condition of NDDF engine with a single injection. Moreover, the lowest ISCO2 equivalent emissions (optimum point) of NDDF engine with split injection is 640 g/kW-hr (Figure 5-10c). The ISCO2 equivalent emissions of NDDF engine with split injection are reduced by 11% compared to those of NDDF engine with a single injection (ISCO2 equ.$_{min}$=721 g/kW-hr) and diesel engine (ISCO2 equ.$_{min}$=719 g/kW-hr).

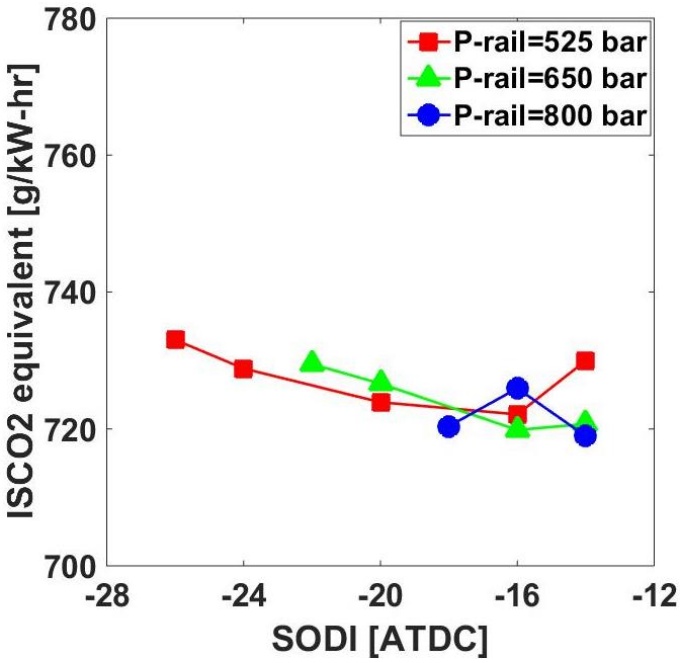

a) Diesel-single injection

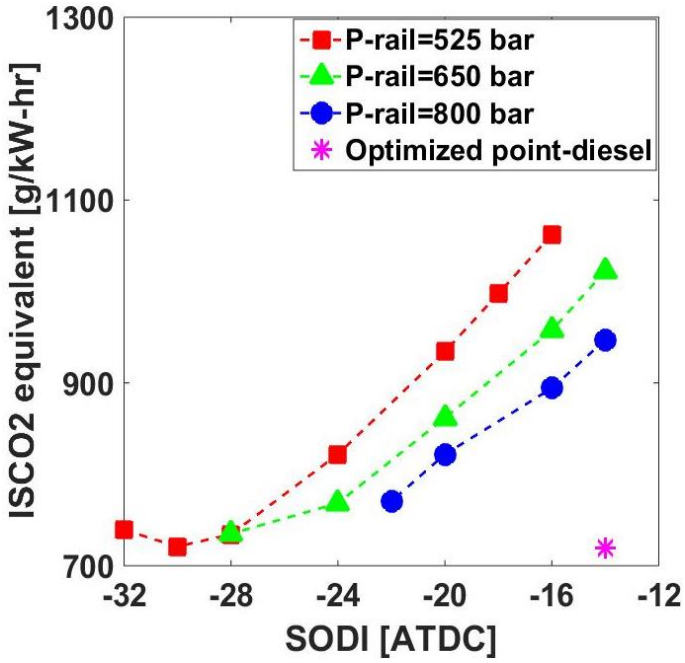

b) NDDF-single injection

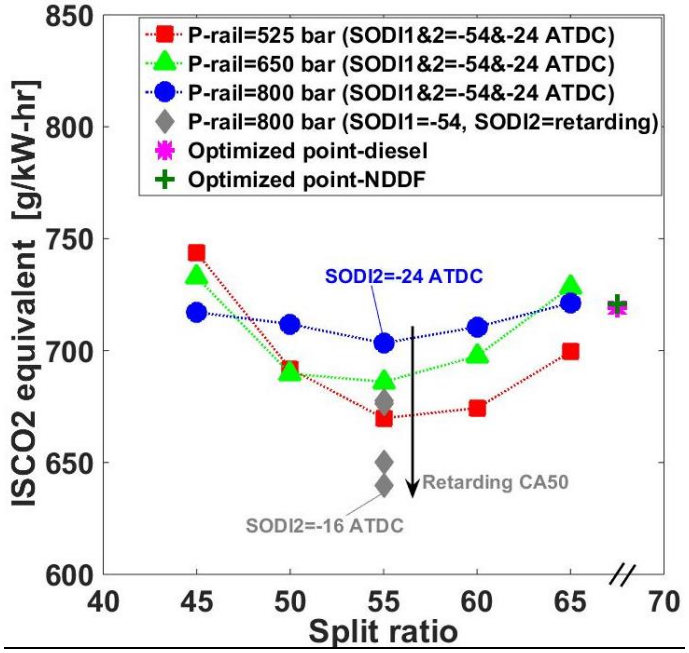

c) NDDF-split injection

Figure 5-10. Effect of injection rail pressure on ISCO2 equivalent emissions of diesel and NDDF engines.

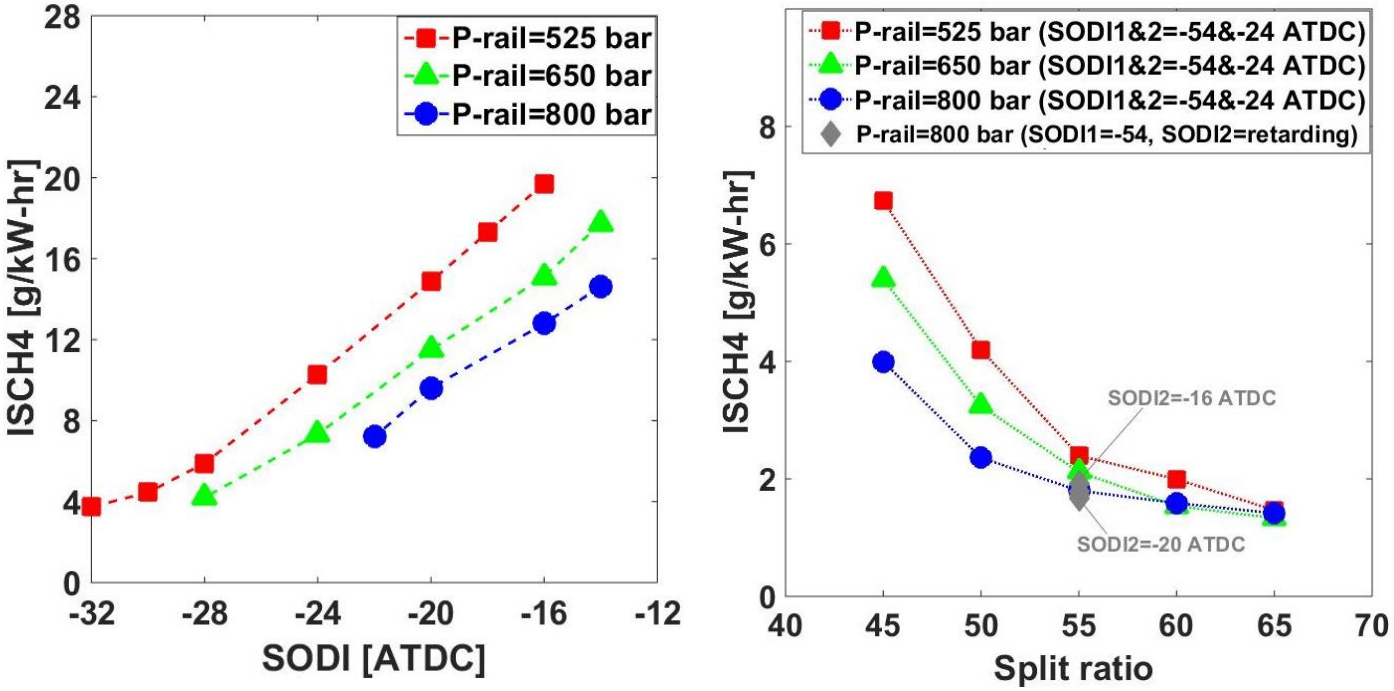

a) NDDF-single injection b) NDDF-split injection

Figure 5-11. Effects of injection rail pressure on CH_4 emissions of NDDF engine with single and split injection strategies.

Figure 5-12 depicts the experimental results of the effect of rail pressure on soot and NOx emissions of diesel and NDDF engines with a single injection and NDDF engine with split injection.

It can be seen that advancing SODI and/or increasing the injection rail pressure significantly decreases soot emissions of diesel engine. For instance, advancing SODI from -14 to -26 °ATDC (at P-rail=525 bar) decreases soot emissions by 96%. Increasing the injection rail pressure from 525 to 800 bar (at SODI=-14 °ATDC) decreases soot emissions by 91.6%. However, the decrease in soot emissions is achieved at the expenses of increased NO_x emissions. It can be observed, from Figure 5-12a, that either advancing SODI and/or increasing injection rail pressure significantly increases NO_x emissions. For example, advancing SODI from -14 to -26 °ATDC (P-rail=525 bar) and increasing the injection pressure from 525 to 800 bar (SODI=-14 °ATDC) increase NO_x emissions by 67% and 44%, respectively. Similar trend is observed for NDDF engine with a single injection. It can be seen that achieving low level of CO2 equivalent emissions comes at the expense of an increased NO_x emissions (Figure 5-10b and Figure 5-12b). It is noted that NDDF engine produces much lower soot emissions compared to diesel engine, as shown in Figure 5-11b. However, NDDF engine with a single injection can still meet the 2015 EPA particulate matter (PM) emissions standard for heavy-duty diesel engines under this load-speed condition even at retarded injection timings and low injection rail pressure.

Figure 5-12c display the experimental results of the effects of injection rail pressure on NOx and soot emissions of NDDF engine with split injection at different split ratios under a low load condition. It can be seen that increasing the injection rail pressure significantly decreases soot emissions of NDDF engine using split injection strategy. Moreover, using split injection can significantly reduce NOx emissions even at high injection rail pressure of 800 bar. The lowest NOx emissions (4.9 g/kW-hr) occurs at the optimum operating condition (SODI1=-54 °ATDC, SODI2=-16 °ATDC, split ratio=55%, and P-rail=800 bar), which is comparable to the best point of diesel engine.

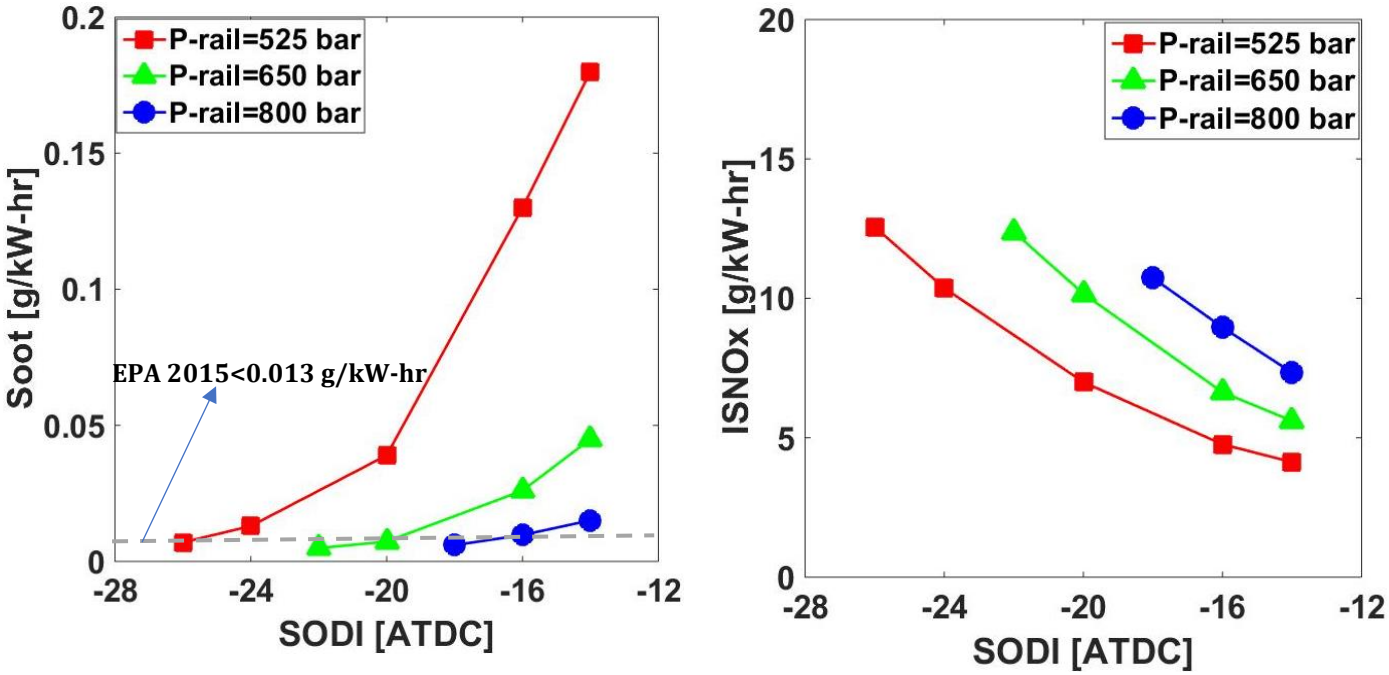

a) Diesel-single injection

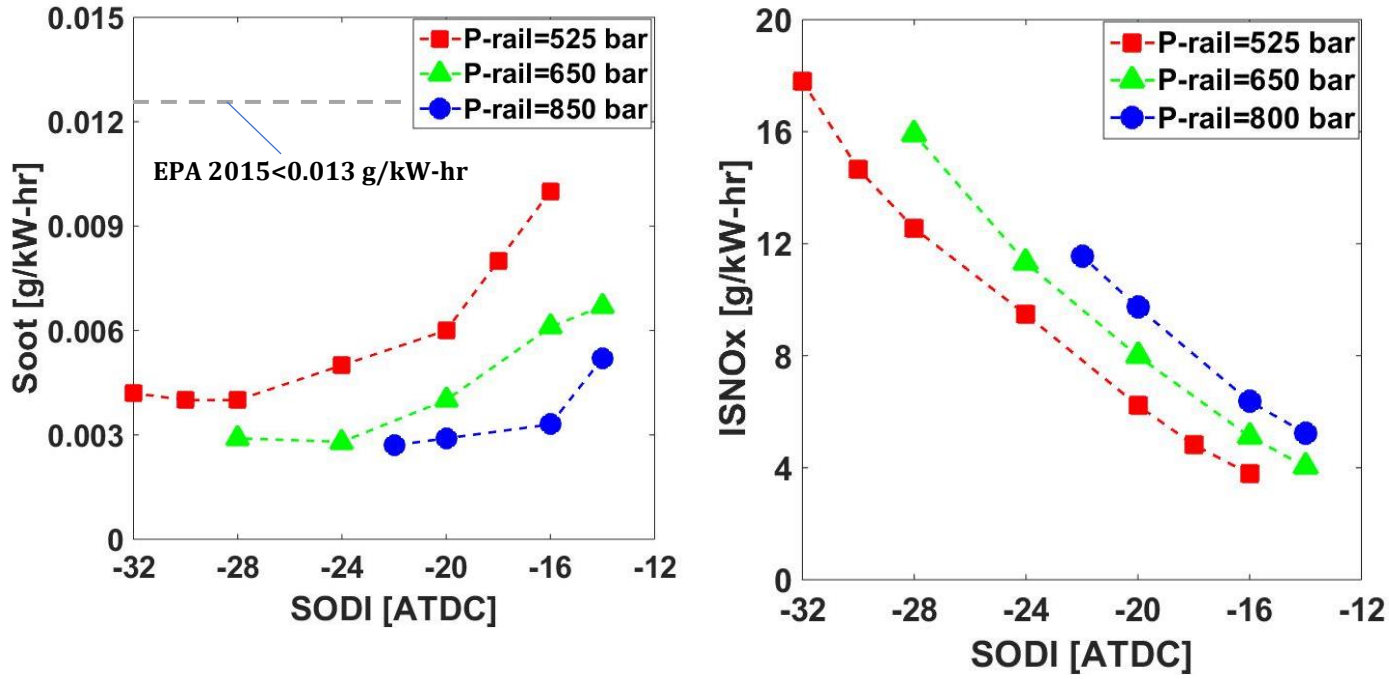

b) NDDF-single injection

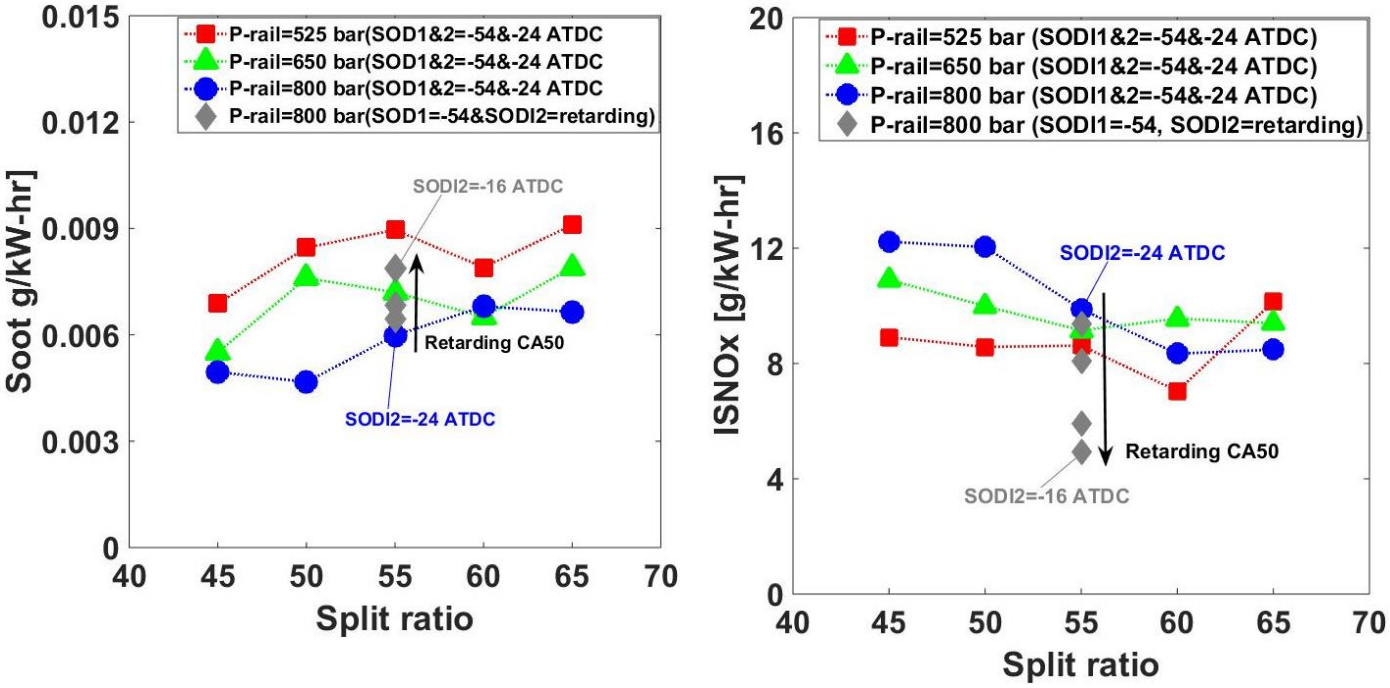

c) NDDF-split injection

Figure 5-12**.** Effects of injection rail pressure on NOx and soot emissions of diesel and NDDF engines.

From the above discussion it can be concluded that NDDF engine with the combination of split injection and rail pressure increase can reduce GHG and soot emissions and improve thermal efficiency compared to diesel engine. This is achieved with a lower pressure rise rate compared to diesel engine but with similar NOx emissions.

5.6.Conclusions

An experimental investigations has been performed to investigate the combined effect of injection rail pressure increase and diesel injection split on the combustion performance and GHG, unburned methane, NOx, and soot emissions of NDDF engine at low load-low speed conditions. The results of NDDF engine when combining the effect of split injection and injector rail pressure increase were compared with those of NDDF engine with a single injection and diesel engines at the same engine load-speed condition. A CFD model was used to support the experimental results and shed light on the combustion of diesel and NDDF (with single and split injection strategies) engines. The main findings are summarized as follows.

- Compared to NDDF engine with a single injection, using diesel split injection strategy significantly decreases PPR, especially at higher split ratios. Increasing the injection rail pressure advances the combustion phasing of both diesel and NDDF engines with a single injection. However, it advances the combustion phasing of NDDF engine with split injection at split ratios of 45, 50, and 55% and retards the combustion phasing under split ratios of 60 and 65%. At lower split ratios, less diesel fuel reaches the cylinder wall and squish regions during the first pulse. Thus, the effect of increased injection rail pressure on the atomization and evaporation process is more significant which shortens the ignition delay and advances the combustion phasing. At high split ratio (e.g., split ratio of 65%), a large portion of diesel fuel is located in the region close to the cylinder's low temperature wall surface. Thus increasing the injection rail pressure leads to a slower evaporation process of the first pulse of injected diesel, which lengthens the ignition delay and retards the combustion phasing.
- Increasing the injection rail pressure does not significantly affect thermal efficiency of diesel engine. The maximum thermal efficiency of 36.6% is achieved at SODI=-14 °ATDC and P-rail=800 bar. Increasing the injection rail pressure and/or advancing the SODI significantly improves thermal efficiency of NDDF engine with a single injection. Increasing the injection rail pressure decreases the thermal efficiency of NDDF engine with split injection. This is mainly due to the overly advanced combustion phasing. However, when optimizing the combustion phasing, a thermal efficiency of 37.2% is achieved at operating conditions of SODI1=-54 °ATDC, SODI2=-16 °ATDC, P-rail=800 bar, and a split ratio of 55%, which is higher than that of diesel and NDDF engines with a single injection.
- Increasing the injection rail pressure significantly reduces the unburned methane emissions of NDDF engine with split injection, especially at lower split ratios. However, increasing the injection rail pressure does not affect the unburned methane emissions under a split ratio of 65%. This is due to the fact that a larger portion of diesel fuel impinges onto the cylinder wall

surface which retards the combustion phasing and may not significantly improve the combustion rate and unburned methane emissions. The optimum methane emissions of NDDF engine with split injection is reduced by 50% compared to the best condition of NDDF engine with a single injection. Moreover, the lowest ISCO2 equivalent emissions of NDDF engine with split injection is 640 g/kW-hr. The ISCO2 equivalent emissions of NDDF engine with split injection are reduced by 11% compared to those of NDDF engine with a single injection and diesel engines.

- Increasing the injection rail pressure significantly decreases soot emissions of NDDF engine using split injection strategy. Moreover, using split injection can significantly reduce NOx emissions even with a P-rail of 800 bar. The lowest NOx emissions (4.9 g/kW-hr) occurs at the optimum operating condition (SODI1=-54 °ATDC, SODI2=-16 °ATDC, split ratio=55%, and P-rail=800 bar), which is comparable to the best of diesel engine.

Overall, thermal efficiency and GHG emissions can be further improved using NDDF engine when simultaneously varying diesel fuel injection split ratio and rail pressure increase. This strategy is also found to help reducing PRR and, NOx and soot emissions.

5.7.References

[1] Pedrozo VB, May I, Guan W, Zhao H. High efficiency ethanol-diesel dual-fuel combustion: A comparison against conventional diesel combustion from low to full engine load. Fuel 2018;230:440–51. doi:10.1016/j.fuel.2018.05.034.

[2] Hockett A, Hampson G, Marchese AJ. Development and Validation of a Reduced Chemical Kinetic Mechanism for Computational Fluid Dynamics Simulations of Natural Gas/Diesel Dual-Fuel Engines. Energy & Fuels 2016;30:2414–27. doi:10.1021/acs.energyfuels.5b02655.

[3] Dual-Fuel Management - HEINZMANN GmbH & Co. KG. Http://WwwHeinzmannCom/En/Engine-Turbine/Dual-Fuel-Management n.d.

[4] JINAN DIESEL ENGINE CO., LTD. Http://WwwJinanengineCom/ n.d.

[5] Cummins Engines Ltd. Cummins Dual Fuel Engines for Drilling - Cummins Engines. Https://CumminsenginesCom/Dual-Fuel n.d.

[6] Hosmath RS, Banapurmath NR, Khandal S V., Gaitonde VN, Basavarajappa YH, Yaliwal VS. Effect of compression ratio, CNG flow rate and injection timing on the performance of dual fuel engine operated on honge oil methyl ester (HOME) and compressed natural gas (CNG). Renew Energy 2016;93:579–90. doi:10.1016/j.renene.2016.03.010.

[7] Yousefi A, Guo H, Birouk M. Effect of swirl ratio on NG/diesel dual-fuel combustion at low to high engine load conditions. Appl Energy 2018;229:375–88. doi:10.1016/j.apenergy.2018.08.017.

[8] Yousefi A, Guo H, Birouk M. Effect of diesel injection timing on the combustion of natural gas / diesel dual-fuel engine at low-high load and low-high speed conditions. Fuel 2019;235:838–46.

[9] Zhang C, Zhou A, Shen Y, Li Y, Shi Q. Effects of combustion duration characteristic on the brake thermal efficiency and NOx emission of a turbocharged diesel engine fueled with diesel-LNG dual-fuel. Appl Therm Eng 2017;127:312–8. doi:10.1016/j.applthermaleng.2017.08.034.

[10] Ryu K. Effects of pilot injection pressure on the combustion and emissions characteristics in a diesel engine using biodiesel-CNG dual fuel. Energy Convers Manag 2013;76:506–16. doi:10.1016/j.enconman.2013.07.085.

[11] Guo H, Liko B, Luque L, Littlejohns J. COMBUSTION PERFORMANCE AND UNBURNED HYDROCARBON EMISSIONS OF A NATURAL GAS – DIESEL DUAL FUEL ENGINE AT A LOW LOAD CONDITION Hongsheng. Proc ASME 2017 Intern

Combust Engine Div Fall Tech Conf ICEF2017 Oct 15-18, 2017, Seattle, Washington, USA 2017:1–9.

[12] Guerry ES, Raihan MS, Srinivasan KK, Krishnan SR, Sohail A. Injection timing effects on partially premixed diesel-methane dual fuel low temperature combustion. Appl Energy 2016;162. doi:10.1016/j.apenergy.2015.10.085.

[13] Xu L, Bai XS, Jia M, Qian Y, Qiao X, Lu X. Experimental and modeling study of liquid fuel injection and combustion in diesel engines with a common rail injection system. Appl Energy 2018;230:287–304. doi:10.1016/j.apenergy.2018.08.104.

[14] Yang B, Xi C, Wei X, Zeng K, Lai MC. Parametric investigation of natural gas port injection and diesel pilot injection on the combustion and emissions of a turbocharged common rail dual-fuel engine at low load. Appl Energy 2015. doi:10.1016/j.apenergy.2015.01.037.

[15] Poorghasemi K, Saray RK, Ansari E, Irdmousa BK, Shahbakhti M, Naber JD. Effect of diesel injection strategies on natural gas/diesel RCCI combustion characteristics in a light duty diesel engine. Appl Energy 2017;199:430–46. doi:10.1016/j.apenergy.2017.05.011.

[16] Aksu C, Kawahara N, Tsuboi K, Kondo M, Tomita E. Extension of PREMIER combustion operation range using split micro pilot fuel injection in a dual fuel natural gas compression ignition engine: A performance-based and visual investigation. Fuel 2016;185:243–53. doi:10.1016/j.fuel.2016.07.120.

[17] Xu M, Cheng W, Zhang H, An T, Zhang S. Effect of diesel pre-injection timing on combustion and emission characteristics of compression ignited natural gas engine. Energy Convers Manag 2016;117:86–94. doi:10.1016/j.enconman.2016.02.054.

[18] May I, Cairns A, Zhao H, Pedrozo V, Wong HC, Whelan S, et al. Reduction of Methane Slip Using Premixed Micro Pilot Combustion in a Heavy-Duty Natural Gas-Diesel Engine. SAE

Tech Pap 2015. doi:10.4271/2015-01-1798.

[19] Ishiyama T, Kang J, Ozawa Y, Sako T. Improvement of Performance and Reduction of Exhaust Emissions by Pilot-Fuel-Injection Control in a Lean-Burning Natural-Gas Dual-Fuel Engine. SAE Int J Fuels Lubr 2011;5:2011-01-1963. doi:10.4271/2011-01-1963.

[20] H. Guo, B. Liko WSN. Effect of Diesel Injection Split on Combustion and Emissions Performance of Natural Gas – Diesel Dual Fuel Engine at a Low Load Condition. Proc ASME 2017 Intern Combust Engine Div Fall Tech Conf n.d.

[21] Yousefi A, Guo H, Birouk M. An experimental and numerical study on diesel injection split of a natural gas/diesel dual-fuel engine at a low engine load. Fuel 2018;212. doi:10.1016/j.fuel.2017.10.053.

[22] Guo H, Neill WS, Liko B. An experimental investigation on the combustion and emissions performance of a natural gas - Diesel dual fuel engine at low and medium loads. Proc ASME 2015 Intern Combust Engine Div Fall Tech Conf ICEF2015 Novemb 8-11, 2015, Houston, TX, USA ICEF2015-1041 2015;1:130–7. doi:10.1115/ICEF2015-1041.

[23] Richards K.J. SPK and PE. Converge Manual. Converg (Version 24) Manual," Converg Sci Inc, Madison, Wisconsin, USA 2017.

[24] Rahimi A, Fatehifar E, Saray RK. Development of an optimized chemical kinetic mechanism for homogeneous charge compression ignition combustion of a fuel blend of *n*-heptane and natural gas using a genetic algorithm. Proc Inst Mech Eng Part D J Automob Eng 2010;224:1141–59. doi:10.1243/09544070JAUTO1343.

[25] Di Blasio G, Belgiorno G, Beatrice C. Parametric Analysis of Compression Ratio Variation Effects on Thermodynamic, Gaseous Pollutant and Particle Emissions of a Dual-Fuel CH<inf>4</inf>-Diesel Light Duty Engine. SAE Tech Pap 2017;2017–March.

doi:10.4271/2017-01-0764.

[26] Barro C, Nani C, Hutter R, Boulouchos K, Zurich ETH. Spray Model Based Phenomenological Combustion Description and Experimental Validation for a Dual Fuel Engine 2017. doi:10.4271/2017-24-0098.Copyright.

[27] Nithyanandan K, Gao Y, Wu H, Lee C-F, Liu F, Yan J. An Optical Investigation of Multiple Diesel Injections in CNG/Diesel Dual-Fuel Combustion in a Light Duty Optical Diesel Engine. SAE Tech Pap 2017;2017–March. doi:10.4271/2017-01-0755.

[28] García Valladolid P, Tunestål P, Monsalve-Serrano J, García A, Hyvönen J. Impact of diesel pilot distribution on the ignition process of a dual fuel medium speed marine engine. Energy Convers Manag 2017;149:192–205. doi:10.1016/j.enconman.2017.07.023.

[29] Neely GD, Florea R, Miwa J, Abidin Z. Efficiency and Emissions Characteristics of Partially Premixed Dual-Fuel Combustion by Co-Direct Injection of NG and Diesel Fuel (DI 2) - Part 2. SAE Tech Pap 2016-01-0779 2017. doi:10.4271/2017-01-0766.

Chapter 6: Effect of swirl ratio on NG/diesel dual-fuel combustion at low to high engine load conditions

6.1.Abstract

Recent regulation in pollutant and greenhouse gas (GHG) emissions has exerted great pressure on diesel engine industries which generate significant amount of GHG and pollutants. The concept of lean burn pilot ignited natural gas/diesel dual-fuel (NDDF) combustion is thought as one of the most suitable engine platforms to meet the emissions and fuel economy regulations in short to medium term. However, a major challenge is the slightly lower fuel efficiency and high level of methane (CH4) and carbon monoxide (CO) emissions, especially under low to medium load conditions. This paper numerically investigates the influence of swirl ratio on the combustion performance and emissions of a NDDF engine under low to high load conditions. The results at a low load-low speed condition and retarded injection timing of 14 crank angle degrees before top dead center (BTDC) suggest that increasing swirl ratio from 0.5 to 1.5 significantly improves the fuel efficiency and CH4 and CO emissions. However, under the same engine load-speed condition but at advanced injection timing of 30 crank angle degrees BTDC, increasing swirl ratio deteriorates the fuel efficiency and CH4 and CO emissions. Under a medium load-high speed condition, swirl ratio significantly improves the diffusion combustion and turbulent flame propagation of natural gas. The distribution of OH radical shows that OH propagates more rapidly in the azimuthal direction when increasing swirl ratio from 0.5 to 1.5. Further increasing the swirl ratio causes the peak pressure to exceed the limit (160 bar). At a high load-low speed condition, increasing the swirl ratio significantly improves the diesel diffusion and flame propagation of natural gas, which leads to an increase in fuel efficiency. Under this engine load-speed condition, the OH radical distribution shows that the combustion progresses rapidly within each jet in both the azimuthal and radial directions. Considering fuel

efficiency and emissions, a swirl ratio of 1.5 is found to be the best. Overall, it is concluded that swirl motion may provide better mixture preparation, diesel diffusion, and natural gas flame propagation, but this benefit may not persist under very high swirl ratio (swirl ratio>1.5) due to higher heat losses.

Abbreviations			
AMR	Adaptive Mesh Refinement	IVC	Intake Valve Closing
ATDC	After Top Dead Center	IVO	Intake Valve Opening
BMEP	Break Mean effective Pressure	LTC	Low Temperature Combustion
BTDC	Before Top Dead Center	NDDF	Natural Gas/Diesel Dual-Fuel
CAD	Crank Angle Degree	NG	Natural Gas
CFD	Computational Fluid Dynamic	NO_x	Nitrogen Oxides
CO	Carbon Monoxide	NTC	No Time Counter
DIT	Diesel Injection Timing	RANS	Reynolds-Averaged Navier-Stokes
EGR	Exhaust Gas Recirculation	RCCI	Reactivity Controlled Compression Ignition
EVC	Exhaust Valve Closing	RNG	Re-Normalization Group
EVO	Exhaust Valve Opening	Rpm	Revolution Per Minute
HCCI	Homogeneous Charge Compression Ignition	SOC	Start of Combustion
HRR	Heat Release Rate	SR	Swirl Ratio
IMEP	Indicated Mean Effective Pressure	TDC	Top Dead Center
IFE	Indicated Fuel Efficiency	UHC	Unburned Hydrocarbon

6.2.Introduction

Compression ignition is the most common combustion strategy in heavy-duty diesel engine market due to its higher fuel efficiency. However, diesel engines are facing challenges meeting stringent emission regulations while retaining their fuel efficiency benefit. NO_x and soot emission limits imposed by the emission regulations for diesel engines have become more and more stringent over the years, which consequently fuelled further motivations to develop advanced combustion strategies to achieve at the same time high efficiency and low emissions. The advanced low temperature combustion (LTC) strategies offer attractive combustion and emission characteristics and have the potential to meet the emissions and fuel economy regulations of the future. Two key features of the LTC strategies are low combustion temperature and long ignition delay time [1]. The low combustion temperature inhibits NO_x formation and the long ignition delay provides sufficient time for air-fuel mixing, reduces fuel-rich zones, and prevents soot formation. Moreover, the LTC strategies have been shown to be well-suited for operation using alternative fuels (e.g. natural gas [2,3]). Compression ignition LTC modes have been demonstrated to result in high fuel efficiencies through

a combination of lean operation, optimal combustion phasing near top dead center (TDC), short combustion duration, and reduced heat transfer [4]. LTC strategies can be governed by different mechanisms depending on the timing of fuel injection event [5]. When the injection timing is early in the cycle (or port fuel injection), ignition timing is kinetically controlled, which is often termed as homogeneous charge compression ignition (HCCI) combustion. Practical operation of HCCI combustion is still challenging due to the lack of control of the combustion phasing or duration. Dual-fuel combustion can achieve control of the combustion phasing and duration by adjusting global fuel reactivity and cylinder stratification of mixture reactivity using the differences in fuel's physical and chemical properties [4]. In dual-fuel combustion, a low reactivity fuel is premixed with the intake air and a second fuel with higher reactivity (usually diesel) is directly injected. The charge distribution of dual-fuel combustion is more heterogeneous than HCCI, as it consists of lean and rich regions at the time of ignition. The combustion phasing and duration are controlled by the ratio of the two fuels and injection strategy of the high reactivity fuel. Because of the higher ignition temperature, natural gas is a great candidate serving as the low reactivity fuel in dual-fuel combustion.

The main constituent of natural gas, which is CH4, has lower carbon content and offers a significant reduction of CO_2 emissions (if burnt completely) compared to diesel fuel. A 20 to 30% CO_2 emissions reduction is achievable, and this number can be further improved if natural gas comes from a renewable source such as biogas [6], compared to diesel. Therefore, one of the major targets for developing NDDF combustion is to minimize the injected pilot fuel quantity in order to reduce diesel fuel dependency. In recent years, natural gas has drawn substantial interest as a low reactivity fuel in dual-fuel combustion and some original engine manufacturers have commercialized dual-fuel engine based on premixed natural gas [7]. NDDF combustion tends to retain most positive features of conventional diesel engines [8]. In addition, NDDF mode has drawn much attention due to other advantages. For instance, dual-fuel combustion can be achieved without major engine hardware modifications, which not only reduces the engine development costs but also means that the engine

can revert to fully diesel combustion once needed [9]. However, higher CH4 and CO emissions and lower fuel efficiency (particularly at low engine loads) compared to fully diesel combustion strategy are the main drawbacks of NDDF engines [10]. Many studies have been conducted to improve efficiency and CH4 and CO emissions of NDDF combustion. Most of them have been focused on advancing diesel injection timing (DIT) [11,12], applying hot exhaust gas recirculation (EGR) [13], and increasing diesel injection pressure [14]. A much smaller subset was focused on the effect of swirl ratio on NDDF combustion. For instance, Jha et al. [15] numerically investigated the effect of different initial swirl ratios (0.05-1.5) on NDDF combustion under low engine load conditions (BMEP= 3.3 bar and rpm=1500). They found that increasing swirl ratio from 0.05 to 1.2 decreased the unburned hydrocarbon (UHC) and CO emissions by 60% and 50%, respectively. However, the reductions in HC and CO emissions were accompanied by 26% increase in NO_x emissions. Carlucci et al. [16] examined the effect of three different intake ports including swirl, tumble, and swirl/tumble on CH4/diesel dual-fuel combustion under low load (IMEP=4 bar and rpm=1500) and high load (IMEP=8 bar and rpm=2000) conditions. They noted that the charge bulk flow induced by the swirl intake port helped improve the charge mixing of the diesel spray and the propagation of the turbulent flame fronts, and thus was capable of enhancing the oxidation of air-natural gas mixtures located farther away from the pilot ignition nuclei, which resulted in lower unburned hydrocarbon emissions. Similar to the study in [15], they also found that NO_x emissions slightly increased when swirl intake port was used.

Introducing swirl flow to the combustion chamber increases the burning rate and extends the flammability limit. An appropriate strength of swirl improves the fuel efficiency and smoke emissions due to increased rates of fuel-air mixing [17]. The disadvantages of swirl ratio include higher heat loss, higher peak pressure (especially at high engine load conditions), and higher pressure rise rate (PRR) which may lead to greater engine noise [18]. Although NO_x emissions have been observed to increase with increasing swirl, the increase in NO_x emissions can be overcome by slightly retarding

the injection timing and adding EGR. The overall benefits of swirl flow may be achieved by an optimum swirl intensity, depending on the engine operating conditions.

From the above discussion, a limited number of studies have attempted to examine the effect of initial swirl ratio on NDDF combustion. However, to achieve an optimum swirl ratio, an extensive study should be performed under different engine load-speed conditions. In the present study, a computational optimization based on CONVERGE 2.4 software was conducted by considering the combustion and emissions under three engine load/speed conditions, a low load-low speed (BMEP=4.05 bar and rpm=910), a high load-low speed (BMEP=17.6 bar and rpm=1120), and a medium load-high speed (BMEP=11.24 bar and rpm=1750) in order to identify an optimal swirl ratio. In addition to the pressure, heat release rate (HRR) and engine out emissions, the heat losses, OH radical distribution, and charge temperature were all analyzed to investigate how significant the impact of swirl on mixing, combustion process, and heat losses at each operating condition.

6.3.Experimental setup

6.3.1. Test engine

Tests were conducted using a modified single-cylinder engine. A detailed description of the experimental setup and methodology is reported elsewhere [19], and thus only a brief summary is provided here. Geometric specifications for the engine are given in Table 6-1, and a schematic diagram of the test setup is shown in Figure 6-1.

The experiments were conducted at three different engine load-speed conditions including a low load-low speed (BMEP=4.05 bar and 910 rpm) condition, a medium load-high speed (BMEP=11.24 bar and 1750 rpm) condition, and a high load-low speed (BMEP=17.6 bar and 1120 rpm). For all three conditions, the intake temperature was kept constant at 40 $^{\circ}$C during the experiments. The diesel injector rail pressure (IP) was 525 bar for the low load-low speed and medium load-high speed

conditions, and 800 bar for the high load-low speed condition. EGR was not used in this study. To avoid the risk of engine damage, the maximum allowable peak pressure and pressure rise rate were kept below 160 bar and 13 bar/CAD, respectively, during all experiments. Table 6-2 summarizes the experimental conditions for all the examined cases. These selected operating conditions will be used to examine the effect of swirl ratio on dual-fuel combustion presented in section 6.5. Cases 1 and 2 are the typical low load-low speed conditions. Two diesel injection timings of 14 and 30 °BTDC were investigated at this condition. The reason for investigating advanced injection timing of 30 °BTDC is that the ignition delay is long and increasing the swirl ratio may not significantly improve the diesel-air-natural gas mixing process. Case 3 shows the medium load-high speed condition with an injection timing of 29 °BTDC. Further advancing the injection timing beyond this point causes the peak pressure to exceed the limit (160 bar) under this condition. Moreover, the engine speed is high compared to cases 1 and 2, which means that there is a shorter time for diesel-air-natural gas mixing process. Case 4 presents the high load-low speed condition with an injection timing of 11.4 °BTDC. This is the most advanced injection timing under this condition and further advancing the injection timing beyond this point results in a high peak pressure (>160 bar).

Table 6-1. Engine specifications

Engine type	Caterpillar heavy duty engine
Bore×Stroke	137.2 mm ×165.1 mm
Conn. rod length	261.62 mm
Compression ratio	16.25
Diesel fuel injector	Common rail injector
Nozzle hole×diameter	6×0.23 mm
Natural gas injection timing	-355 °ATDC
IVO	-358.3 °ATDC
IVC	-169.7 °ATDC
EVO	145.3 °ATDC
EVC	348.3 °ATDC

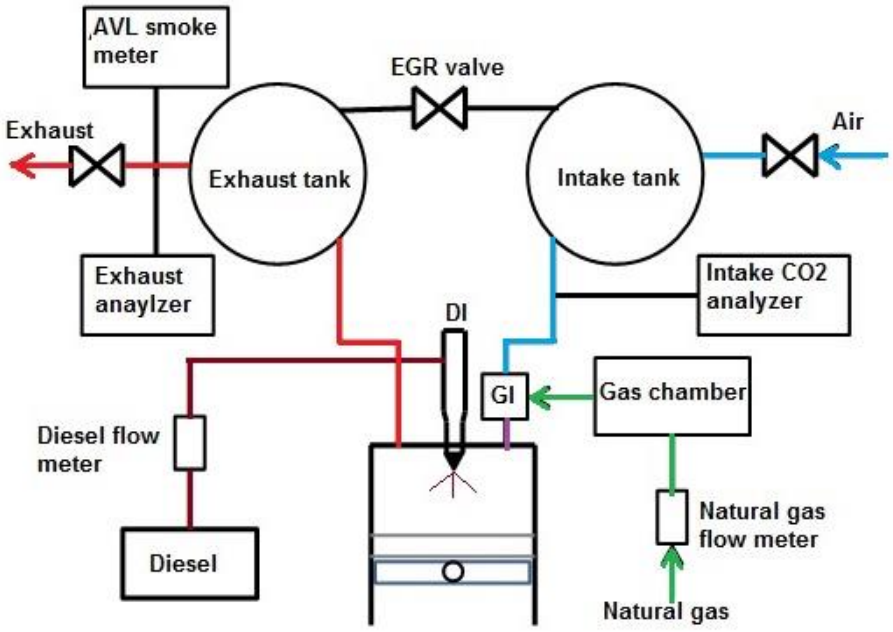

Figure 6-1. Schematic diagram of the experimental setup [19].

Table 6-2. Experimental test conditions.

	Case 1	Case 2	Case 3	Case 4
BMEP (bar)	4.05	4.05	11.24	17.6
Speed (rpm)	910	910	1750	1120
Intake temperature (°C)	40	40	40	40
Intake pressure (bar)	1.05	1.05	2	2.19
%NG (energy fraction)	75	75	80	75
DIT (°BTDC)	14	30	29	11.4
IP (bar)	525	525	525	800
NG (kg/hr)	1.39	1.23	6.05	5.26
Diesel (kg/hr)	0.49	0.455	1.6	1.93
Air (kg/hr)	67.21	66.70	273.73	186.36

6.4.Computational setup

6.4.1. Numerical model

The CFD solver CONVERGE 2.4 [20] was used in this study. Han and Reitz model was used to calculate wall heat transfer [21]. The renormalization group (RNG) k-ε turbulence model [22] was used to model turbulence. In this investigation, the largest grid size used in the simulation is 2 mm

and the smallest is 0. 25 mm, which adequately resolves diesel spray and turbulent flame front. Local grid refinement (fixed embedding with the cell size of 0.25 mm) was applied for piston bowl, cylinder head, cylinder wall, and the exit of the diesel jet into the combustion chamber to accurately resolve velocity and temperature gradients (Figure 6-2). Since diesel injector has six equally spaced nozzle's orifices, 1/6 of the combustion chamber was modeled with periodic boundaries from intake valve closing (IVC) to exhaust valve opening (EVO). The maximum cell in the simulation was 1.5 million which occurred when spray embedding and AMR were in action during the diesel spray. Figure 6-2 show the different grid refinements by CONVERGE adaptive mesh refinement (AMR) tool at -4.69 and +15.3 °ATDC, respectively.

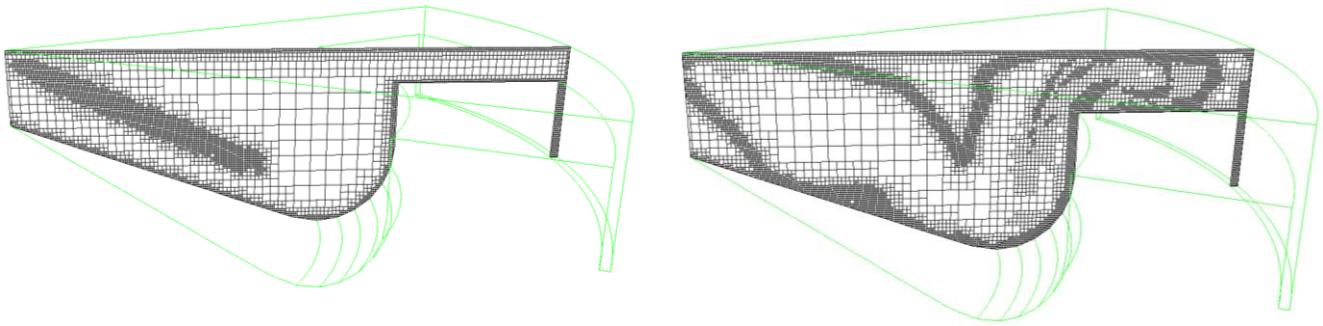

Figure 6-2. Different grid refinements by CONVERGE adaptive mesh refinement, on the left: computational grid at -4.69 °ATDC and on the right: computational grid at +15.3 °ATDC

6.4.2. Spray and combustion models

The atomization of the liquid fuel and subsequent droplets was simulated based on the Kelvin-Helmholtz and Rayleigh-Taylor instability mechanisms without the use of a breakup length [23]. The no time-counter (NTC) collision [24] was used for the collision of fuel droplets.

SAGE model [20] was used in this study which performs the detailed chemistry calculations on each computational cell. The use of AMR with small enough cell sizes (0.25-0.5 mm) in the flame region adequately resolves the turbulent flame front and the species gradients without the need of any sub-grid model [25]. Performing detailed chemistry calculations on each mesh cell can be computationally expensive. To accelerate the computations, an adaptive-zoning strategy was utilized

[26]. In this strategy, cells having similar temperature and composition were grouped into zones, and the chemistry calculations were conducted on zones rather than on individual cells.

The diesel fuel injection rate profile and duration strongly affect the velocity of injected parcels, which has a significant effect on the rate of droplet break up and vaporization. In this study, diesel injection profiles based on experimental measurements and regression analysis were used in the simulation. Figure 6-3 displays the fuel injection map at different injection pressures. This figure shows that the diesel fuel injection rate profiles, used in the simulation, are in perfect agreement with the measurements.

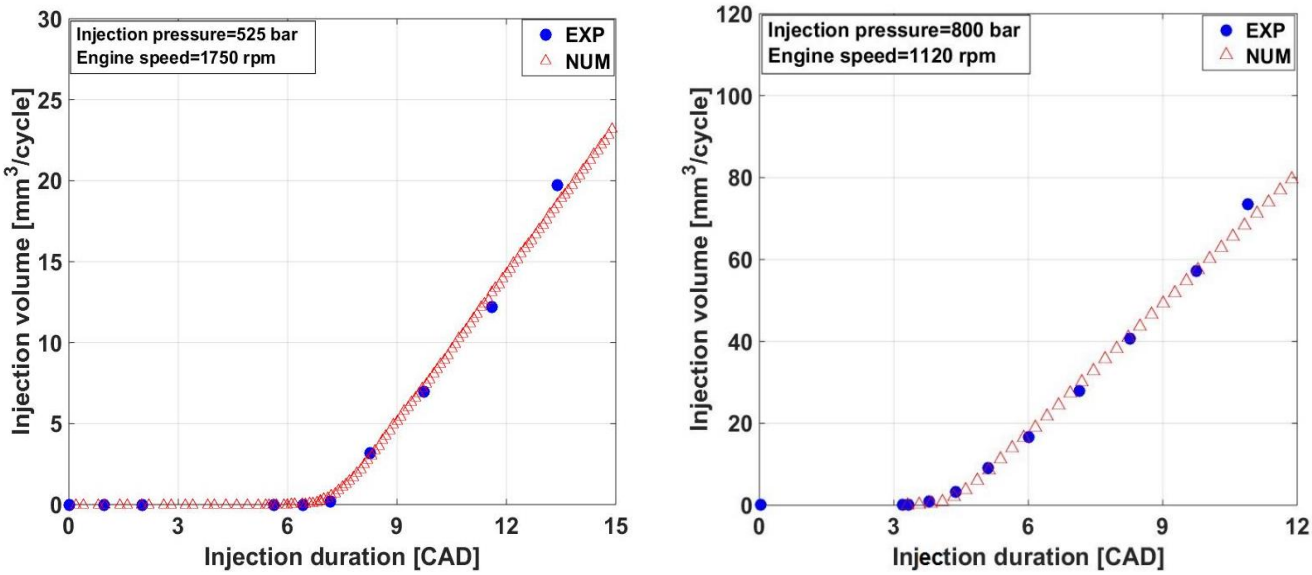

Figure 6-3. Diesel fuel injection map at two different conditions.

The closed engine cycle simulation (from IVC to EVO) assumed homogeneous composition, temperature, and pressure of the gas at IVC. Since the test engine is a heavy-duty engine, there is a low swirl ratio at IVC which is estimated to be 0.5. The IVC temperatures for low load-low speed (case 1 and 2), medium load-high speed (case 3), and high load-low speed (case 4) are 367 K, 380 K, and 370 K, respectively. While the trapped mass was kept fixed, the IVC pressure used in the simulations were slightly adjusted ($\pm$5 kPa) in order to obtain closer agreement with the experimental pressure during the compression stroke. The chemical properties of diesel and natural gas were

represented by n-heptane and CH4, respectively. The adopted mechanism includes 76 species and 464 reactions [27]. It can be noted that n-heptane has higher cetane number compared to diesel fuel which caused shorter ignition delay and more advanced start of combustion (SOC) during the experiment. Hence, an appropriate value of injection delay was established by comparing the SOC of CFD predictions to that of the experiments. In this investigation, an injection delay of 4.5 CAD was used consistently for all other cases.

6.4.3. Model validation

The numerical model was validated by comparing the calculated data with those measured using the test engine. The measured and predicted pressure and heat release rate (HRR) for four different cases are compared in Figure 6-4. In both cases, HRR was determined based on the first law of thermodynamics. It is noted that good agreement between the model and experimental results were achieved for the start of combustion, pressure rise rate, peak pressure, combustion duration, and shape of the heat release rate for all examined cases. Figure 6-5 compares the predicted and measured emissions (CH_4, NO_x, and CO) and indicated fuel efficiency (IFE) results. It is observed that the predicted CH4, NO_x, and fuel efficiency are in good agreement with the measured data in both trend and magnitude at all investigated conditions. Although CO emissions are significantly under-predicted, its trend is in line with the experimental data. Similar results of CO emissions were observed by Sameera et al. [25] who found that the predicted CO are closer to the experimentally measured values considering the uncertainties in the amount of injected diesel and wall temperature [25]. However, in the present study, the wall temperature was kept constant for all examined cases (piston bowl=530 K, cylinder head=500 K, cylinder wall=430 K). Overall, the validation demonstrates the capability of the present numerical simulation to reproduce the experimental combustion and emissions with an acceptable error. Therefore, this validated numerical model is used to investigate the effect of swirl ratio.

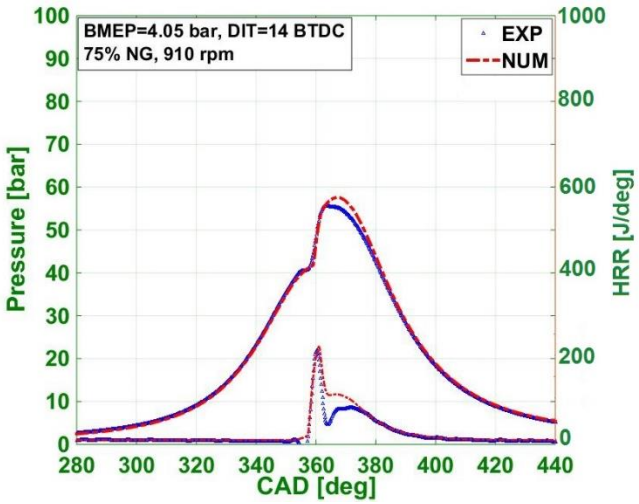

Case 1 (low load-low speed)

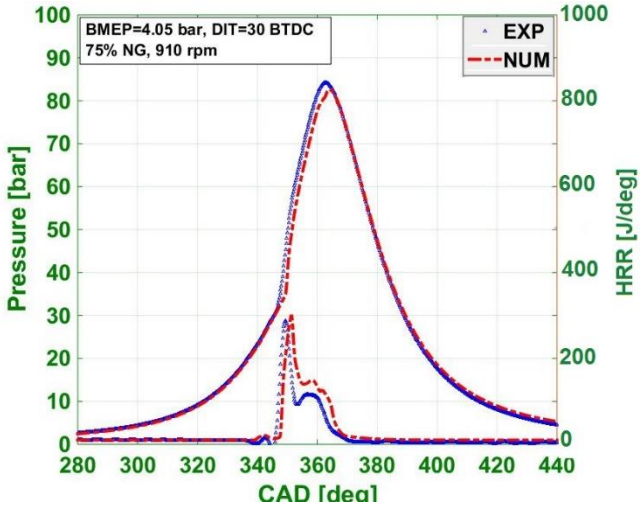

Case 2 (low load-low speed)

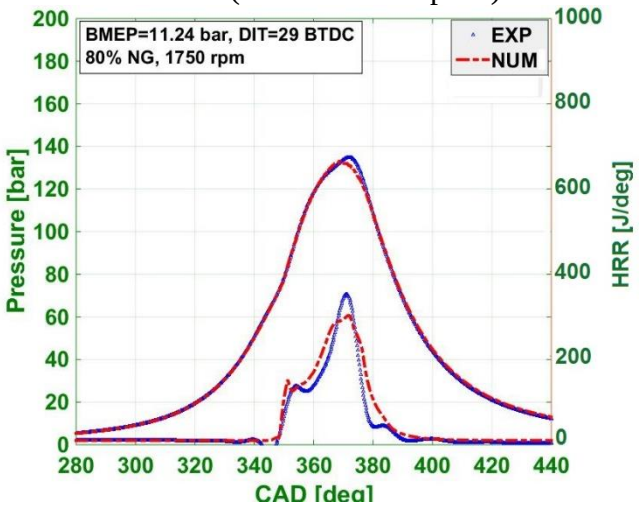

Case 3 (medium load-high speed)

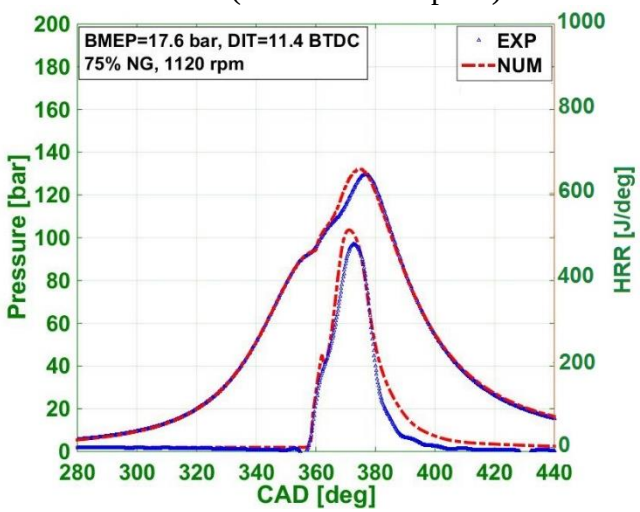

Case 4 (high load-low speed)

Figure 6-4. Comparisons of measured and predicted pressure and HRR for cases 1-4.

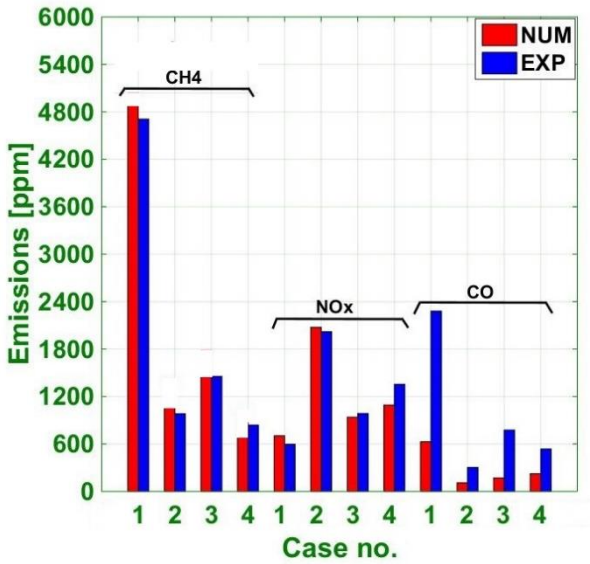

a) Emissions

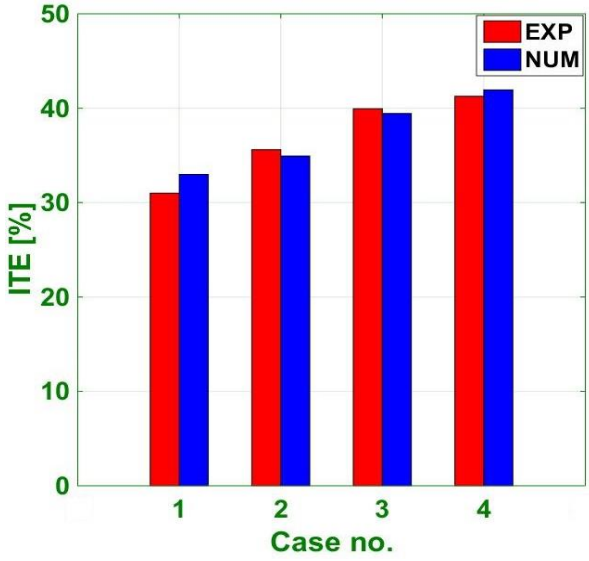

b) Fuel efficiency

Figure 6-5. Comparison of measured and predicted emissions (CH_4, NO_x, and CO) and fuel efficiency for cases 1-4

6.5.Results and discussion

6.5.1. Effect of swirl ratio on dual-fuel combustion

Usually the combustion process in dual-fuel engine takes place in three stages. The first stage is the premixed combustion of the pilot diesel and a small portion of entrained natural gas fuel. The second stage involves diffusion combustion of pilot diesel along with the initiation of flame propagation of natural gas. The third stage involves diffusion combustion of the residual pilot diesel and subsequent turbulent flame propagation (and sometimes auto-ignition) of natural gas [28]. These three stages often occur under medium to high load conditions. However, at low engine loads, with very lean natural gas-air fuel mixtures, the bulk of energy release comes from the ignition and subsequent rapid combustion of pilot diesel and a small fraction of entrained natural gas-air mixture where higher temperatures and relatively richer mixture regions prevail. Within the very lean mixtures, no consistent flame propagation takes place from the ignition centres and pilot fuel influences the burning region [28].

In the following sections, the impact of swirl ratio on the mixing and combustion processes of NDDF engine under different load-speed conditions is investigated. Swirl ratio is defined as the average angular velocity of the rotating flow normalized by the angular velocity of the engine crankshaft.

6.5.1.1.Low load-low speed condition (BMEP=4.05 bar and 910 rpm)

Figure 6-6a shows the effect of different swirl ratios on the pressure and HRR of NDDF combustion at low load-low speed condition (BMEP=4.05 bar and 910 rpm) under retarded diesel injection timing of 14 °BTDC. It is noted that swirl ratio does not seem to significantly affect the onset of ignition. However, increasing the swirl ratio enhances the mixing of premixed natural gas-

air and diesel due to higher charge velocity which implies higher turbulence. This increases the heat release rate during the early mixing controlled combustion stage. As a result, the pressure curves are nearly identical from IVC to approximately +0.3 °ATDC. Beyond this time, however, the pressure curves diverge, where higher swirl ratio generally induces higher pressure. The value of the peak pressure is 57.5, 59.2, 61.3, 62.5, and 63 bar for swirl ratios of 0.5, 1.0, 1.5, 2.0, and 3.0, respectively. Increasing the swirl ratio from 0.5 to 1.0 increases the peak pressure by 3%. However, the peak pressure is only increased by 0.8% when the swirl ratio increases from 2.0 to 3.0.

The reason for the above observed variation in the heat release rate and peak pressure is due to the effect of swirl ratio on the combustion process and heat loss. Increasing the swirl ratio enhances the combustion efficiency due to a better mixing process of diesel and premixed natural gas-air mixture, which tends to enhance the combustion rate and consequently increases the peak pressure. On the other hand, due to the higher tangential charge velocity and displacement of high combustion temperature region towards the piston, the total heat loss increases when increasing the swirl ratio, which has a negative impact on combustion efficiency. As shown in Figure 6-6b, with increasing the swirl ratio from 0.5 (base case) to 3.0, the total heat loss increases by 4.7%. The heat loss through the piston and cylinder wall increases but that through the cylinder head decreases when increasing the swirl ratio. Further details about this will be discussed later in Figure 6-8 and Figure 6-9. To better understand the effect of swirl on the mixing process and heat loss, the OH radical distribution and the cylinder temperature contours are presented in Figure 6-7 and Figure 6-8, respectively, where the top-view contour plane is located at a vertical distance of 10 mm from the nozzle tip and the side-view contours plane is cut from one of the six injector holes.

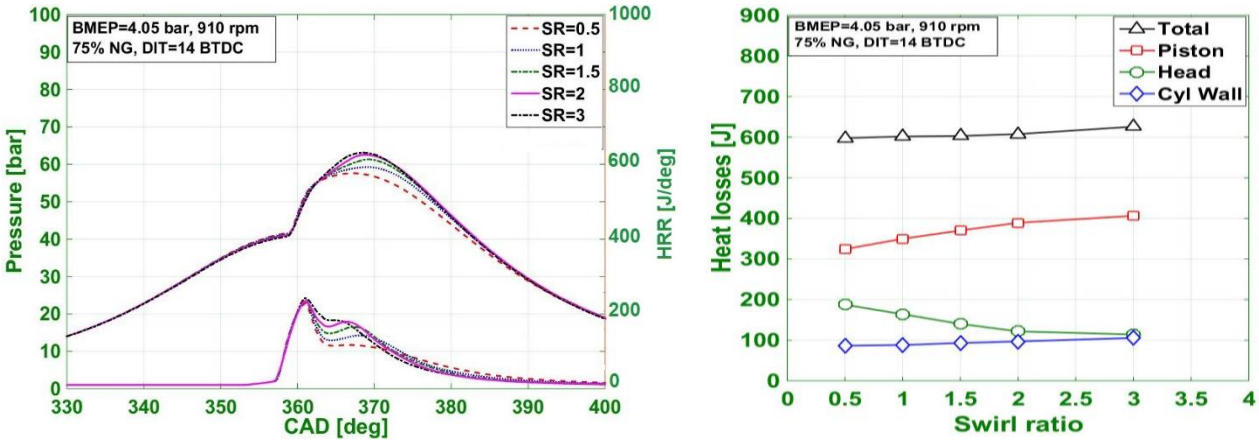

a) Pressure and HRR b) Heat loss

Figure 6-6**.** Effect of the swirl ratio on the pressure, HRR, and heat loss of NDDF combustion under low load-low speed conditions and DIT=14 °BTDC

Figure 6-7 presents the OH spatial distribution of dual-fuel combustion under the low load-low speed condition for diesel injection timing of 14 °BTDC and three different values of the swirl ratio. The top-view contours in Figure 6-7 indicate that the initial OH radical appears in the high reactivity regions (downstream of diesel fuel jets) at about +0.3 °ATDC for all examined swirl ratios. The OH radical intensity does not change significantly with increasing swirl ratio at CAD=+0.3 °ATDC. However, at CAD=+3.3 °ATDC, a higher swirl ratio leads to a wider and more intense OH distribution. For the swirl ratio of 0.5, OH radical does not progress farther toward the center of combustion chamber and very limited high temperature oxidation reactions occur in this zone until CAD= +6.3 and +10.3 °ATDC. The blue non-reactive zones tend to become narrower for the values of the swirl ratio of 2.0 and 3.0 in the second stage of combustion. This behavior is also apparent with HRR curves (Figure 6-6a) where the highest swirl ratio is associated with the largest heat release rate during the diffusion combustion stage. At CAD=+10.3 °ATDC and a swirl ratio of 0.5, there is almost no OH radicals in the central region within the piston bowl. The intensity of OH radical inside the piston bowl becomes more significant with increasing the swirl ratio. Swirl effect remains important during the final stage of combustion (CAD= +20.3 °ATDC), but the overall mass of the remaining fuel becomes the dominant factor for determining the heat release rate. This can be clearly seen in Figure 6-6a, where the heat release rate for a swirl ratio of 3.0 drops rapidly, and exhibits the lowest

heat release rate for all examined swirl ratios. As shown in Figure 6-7, at CAD= +20.3 °ATDC and the swirl ratio of 0.5, the high reactive zones reside far away from the piston bowl and close to squish area (shown by black arrow). However, when increasing the swirl ratio, the high reactive zones shift to the piston bowl. This can be observed in Figure 6-8 where the temperature distribution of dual-fuel combustion is displayed under three different swirl ratios.

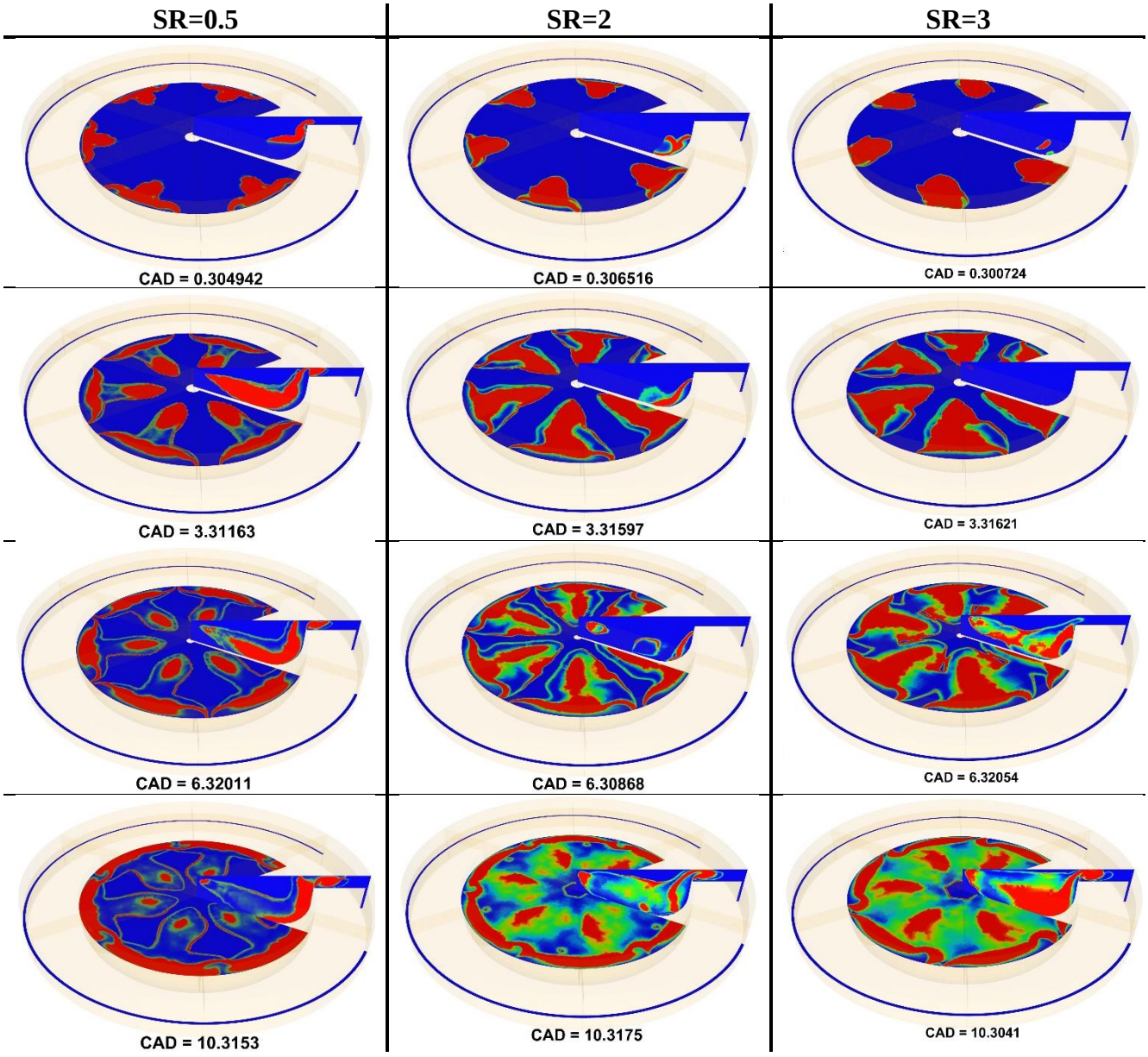

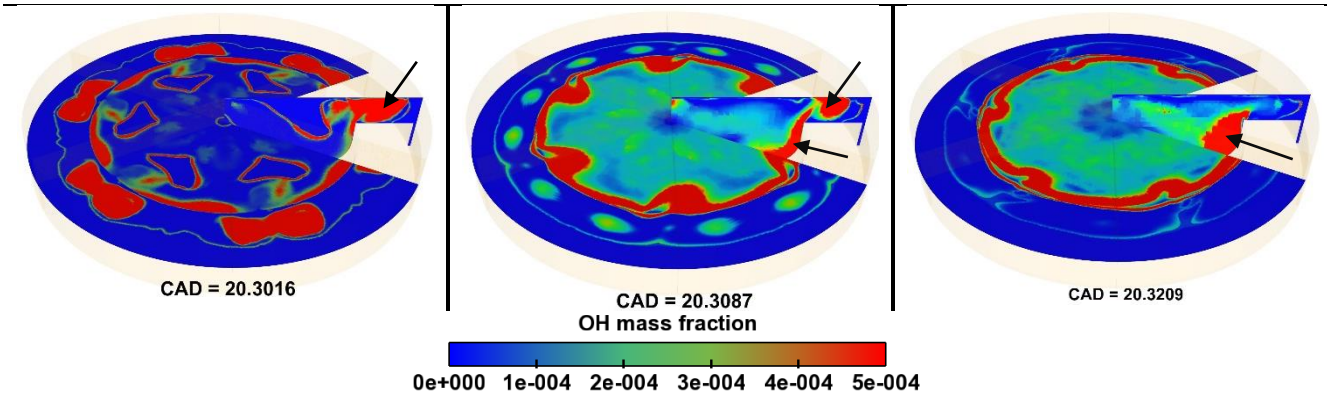

Figure 6-7. OH* distribution of NDDF combustion at low load-low speed conditions for three different swirl ratios and DIT=14 °BTDC.

On the other side, increasing the swirl ratio affects the heat losses. Based on Han and Reitz model [21], which was used in this investigation, the wall heat transfer depends on the shear velocity, u_τ, and fluid temperature near the wall T_f, as expressed by Equations 6-1 and 6-2.

$$q_w = \begin{cases} \dfrac{\mu C_P (T_f - T_w)}{Pr_m y} & y^+ < 11.5 \\ \dfrac{\rho C_P u_\tau T_f Ln\left(\frac{T_f}{T_w}\right)}{2.1\, Ln(y^+) + 2.5} & y^+ > 11.5 \end{cases} \qquad \text{Eq. (6-1)}$$

$$y^+ = \frac{\rho u_\tau y}{\mu} \qquad \text{Eq. (6-2)}$$

where μ is the dynamic viscosity, C_P is the specific heat in constant pressure, Pr_m is the molecular Prandtl number, ρ is the density, T_w is the wall temperature, and y is the effective distance between the boundary cell center and the boundary itself.

Increasing the swirl ratio increases the shear velocity which increases the heat loss. However, the temperature distribution near the combustion chamber walls may significantly change while increasing the swirl ratio. To explain the effect of the swirl ratio on the heat loss (Figure 6-6b), the temperature distribution contours at crank angles of +15.3 and +24.3 °ATDC are presented in Figure 6-8. Moreover, the velocity field at crank angle of +24.3 °ATDC is displayed in Figure 6-9. It is noted that increasing swirl ratio displaces the high temperature regions (combustion) towards the

piston bowl. When the swirl ratio increases, a stronger centrifugal force causes the lower temperature and higher density gases to move outward. It can be observed, from Figure 6-8, that at a swirl ratio of 3.0, the high temperature gases remain in the middle of combustion chamber and away from the cylinder head, while the lower temperature moves toward the cylinder head (shown by black arrow). The combination of the higher near piston wall temperature and higher shear velocity caused an increased heat loss through the piston. However, the effect of lower near-cylinder head temperature is more significant than that of the higher shear velocity, which yields a reduced heat loss through the cylinder head (Figure 6-6b). It is notable that the average fluid temperature near the cylinder wall decreases slightly with increasing the swirl ratio. However, the higher shear velocity (Figure 6-9) resulting from high swirl motion increases the heat loss. It seems that the effect of the latter is more significant, which causes an increased heat loss from the cylinder wall when increasing the swirl ratio. However, as depicted in Figure 6-6b, the total heat loss through the combustion chamber walls increases when increasing the swirl ratio which negatively affects the combustion efficiency.

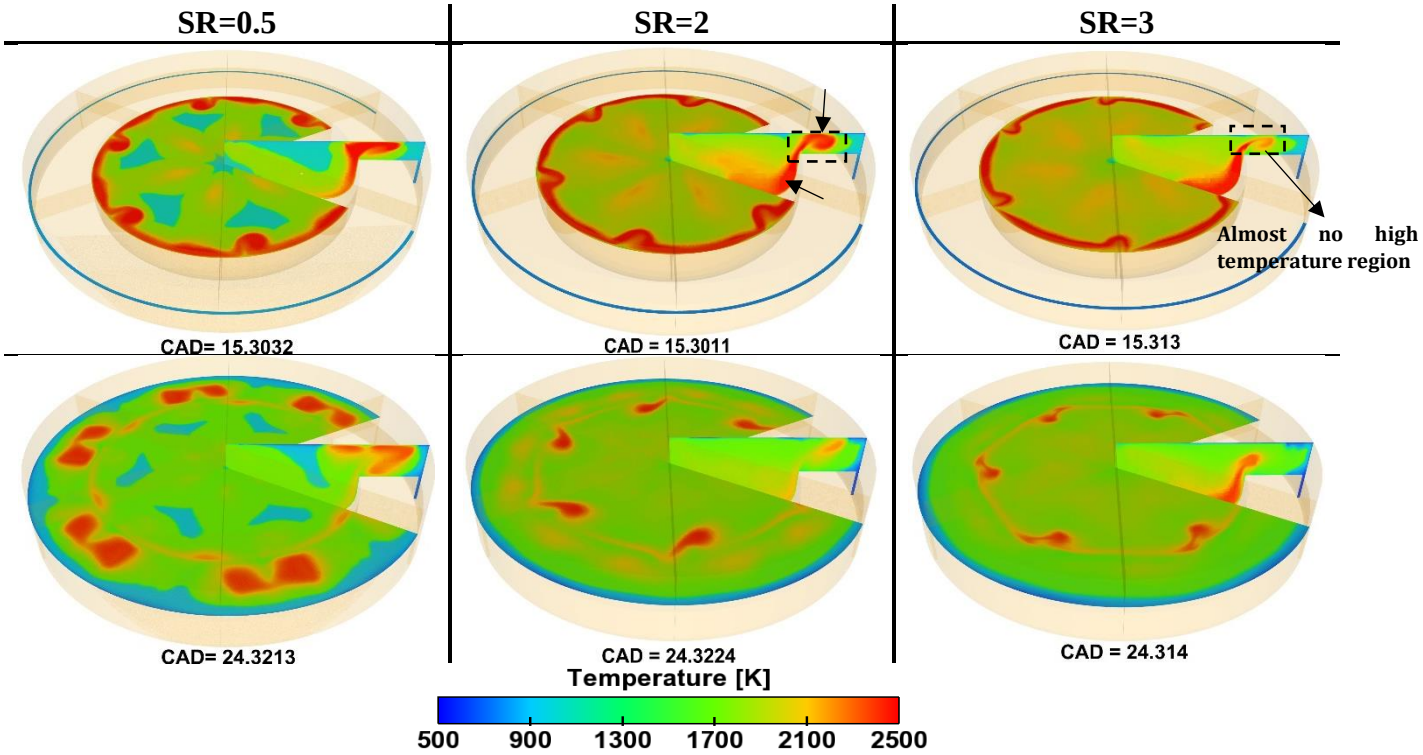

Figure 6-8. Temperature distribution of NDDF combustion at low load-low speed conditions for three different swirl ratios and DIT= 14 °BTDC.

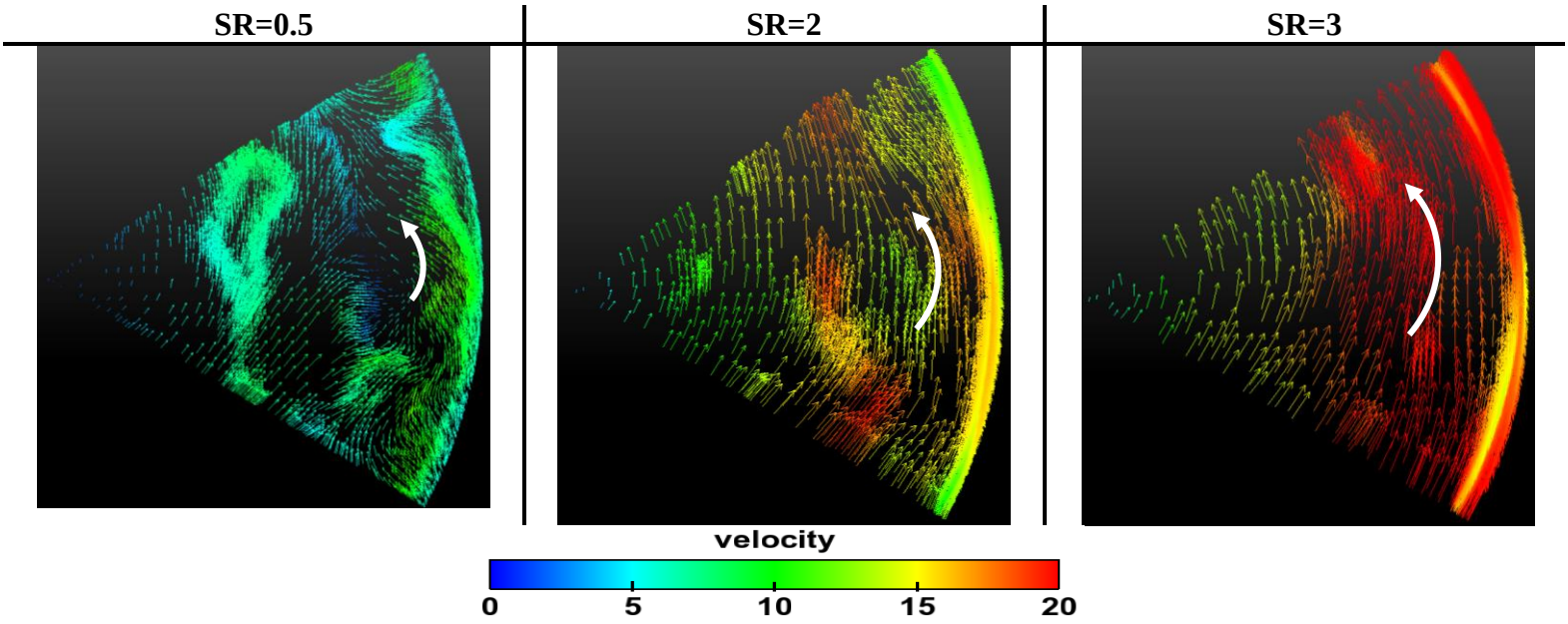

Figure 6-9. Velocity field of NDDF combustion at low load-low speed conditions for three different swirl ratios and DIT=14 °BTDC

In order to reduce the CH4 and CO emissions in dual-fuel engine, numerous studies focused on advanced diesel injection timings [11,14,29]. In the present study, the effect of the swirl ratio on dual-fuel engine at low load-low speed condition (BMEP=4.05 bar and 910 rpm) and an advanced injection timing of 30 °BTDC is also examined. Figure 6-10 displays the effect of different swirl ratios on the pressure, HRR, and heat loss of NDDF combustion at the low load-low speed condition under the advanced injection timings of 30 °BTDC. In contrast to the pressure shown in Figure 6-6a, it is interesting to note that the peak pressure decreases with increasing the swirl ratio (Figure 6-10a). The value of the peak pressure is 82.6, 82.3, 81.6, 80.6, and 80.3 bar for a swirl ratio of 0.5, 1.0, 1.5, 2.0, and 3.0, respectively. Although increasing the swirl ratio enhances the premixed charge and diesel fuel mixing, this improvement is insufficient to compensate for the increased heat loss. The OH radical distribution in Figure 6-11 shows that increasing the swirl ratio slightly improves the mixing-controlled and diffusion combustion as shown at the contours of +4.3 °ATDC where OH radical intensity inside the piston bowl is almost similar for all examined swirl ratios. Under the advanced

injection timing of 30 °BTDC, the premixed natural gas-air mixture and diesel fuel have enough time to mix together before combustion. Thus, increasing the swirl motion does not significantly enhance the mixing process. However, increasing the swirl ratio increases the heat loss (Figure 6-10b), which results in lower combustion efficiency. It can be seen from Figure 6-10b that increasing the swirl ratio from 0.5 to 3.0 increases the total heat loss by 15.8%. Similar to the results for DIT=14 °BTDC, increasing the swirl ratio increases the piston and cylinder wall heat losses and decreases the cylinder head heat loss.

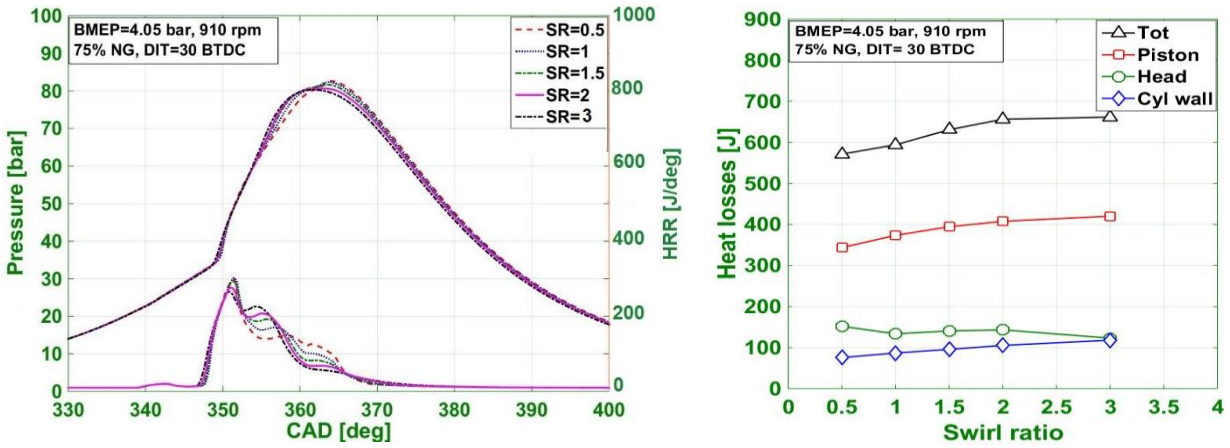

a) Pressure b) Heat losses

Figure 6-10. Effect of the swirl ratio on the pressure, HRR, and heat loss of NDDF combustion under low load-low speed conditions and DIT=30 °BTDC

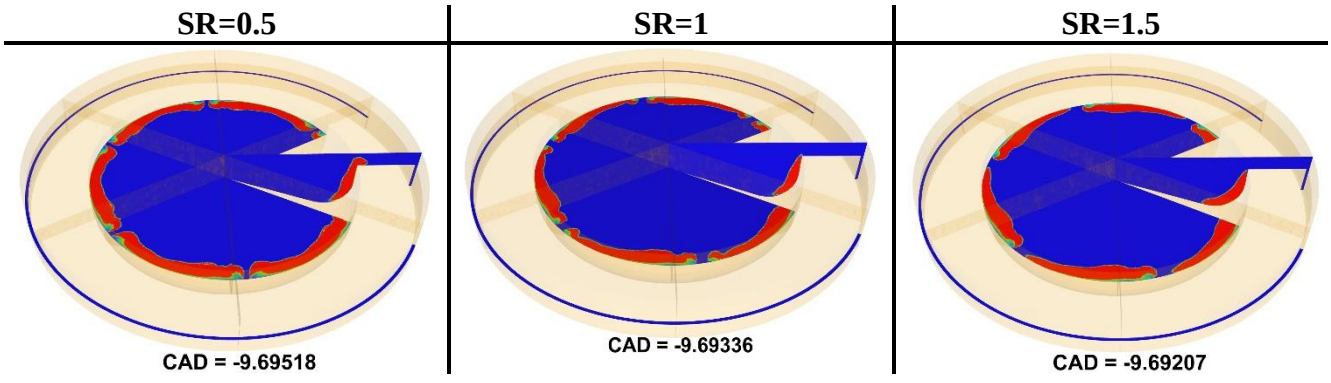

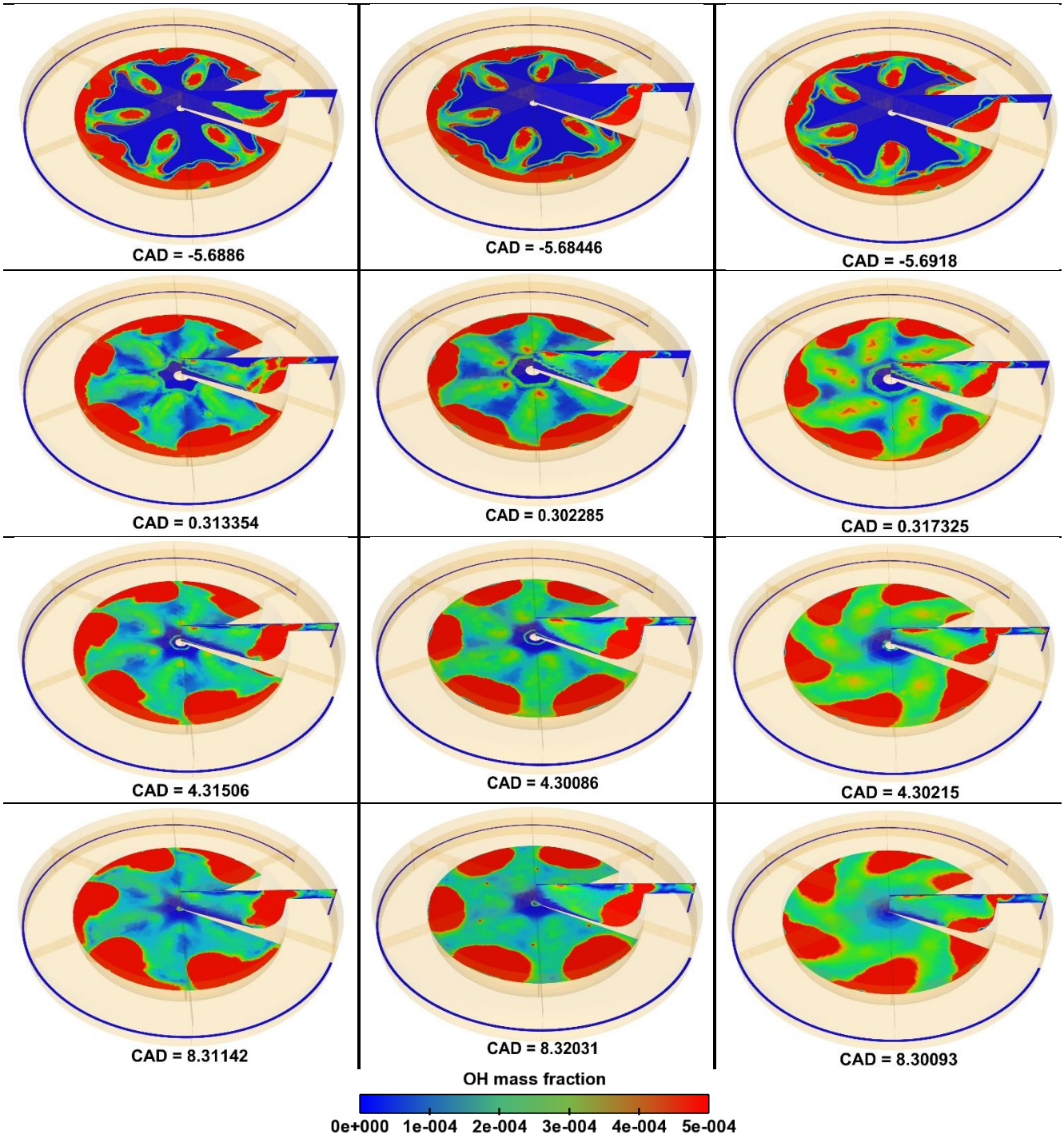

Figure 6-11. OH* distribution of NDDF combustion at low load-low speed conditions for three different swirl ratios and DIT=30 °BTDC.

Figure 6-12 displays the indicated fuel efficiency and emissions (CH_4, CO, and NO_x) of NDDF engine at the low load-low speed condition of BMEP = 4.05 bar with different swirl ratios and two diesel injection timings of 14 and 30 °BTDC. As mentioned above, increasing the swirl ratio has

different effects on retarded (DIT=14 °BTDC) and advanced injection timings (DIT=°30 BTDC). As shown in Figure 6-12a, under retarded injection timing, increasing the swirl ratio from 0.5 to 1.5 increases the fuel efficiency by 4.5% and decreases the CH4 and CO emissions by 20% and 27.6%, respectively. NO_x emissions slightly increase with increasing the swirl. However, further increasing the swirl ratio (swirl ratio=3.0) deteriorates the fuel efficiency and increases the CH4 and CO emissions. It can be seen that, for retarded injection timing (i.e., DIT=14 °BTDC), an optimum swirl ratio (SR=1.5) exists for achieving the highest fuel efficiency. However, under advanced injection timing of 30 °BTDC, increasing the swirl ratio monotonically decreases the fuel efficiency and increases the CH4 and CO emissions (Figure 6-12b). As mentioned above, increasing the swirl ratio slightly improves the premixed charge and diesel fuel mixing, which, in turn, enhances the combustion efficiency. However, increasing the swirl ratio increases the heat loss, which affects negatively the combustion efficiency. The combination of the two effects can be negative in some cases leading to decreased fuel efficiency and increased CH4 and CO emissions.

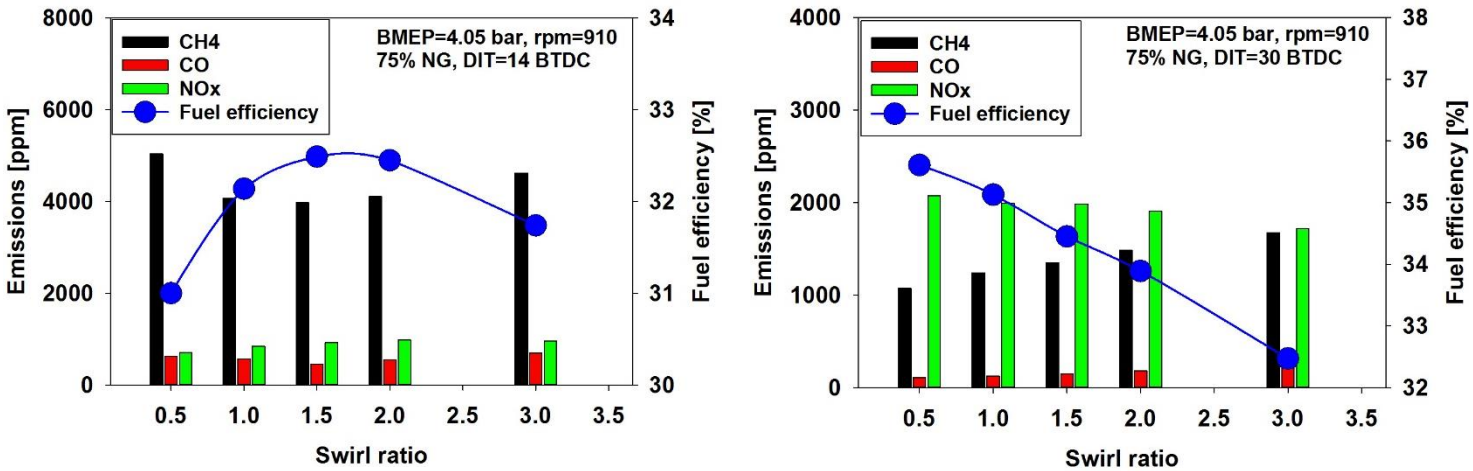

a) DIT=14 °BTDC b) DIT=30 °BTDC

Figure 6-12. Effect of the swirl ratio on fuel efficiency and CH_4, CO, and NO_x emissions of NDDF combustion under low load-low speed conditions and DITs=14 and 30 °BTDC.

6.5.1.2.Medium load-high speed condition (BMEP=11.24 bar and 1750 rpm)

Figure 6-13 shows the effect of different swirl ratios on the pressure, HRR, and heat loss of NDDF combustion at a medium load-high speed condition (BMEP=11.24 bar and 1750 rpm) under an

advanced injection timing of 29 °BTDC. Under this condition, the heat release rate profile (Figure 6-13a) shows that premixed combustion of diesel fuel is followed by diesel diffusion and flame propagation of natural gas for all examined swirl ratios. It can be observed that the peak pressure significantly increases with increasing the swirl ratio even under advanced injection timing of 29 °BTDC (case 3), which is different from what observed at low load-low speed condition and injection timing of 30 °BTDC (case2). It is notable that because of the higher engine speed (1750 rpm), the natural gas-air-diesel mixing time (or ignition delay) of case 3 is much shorter than case 2. The ignition delay under this condition is similar to the case with retarded injection timing and low engine speed condition (e.g., case 1). As shown in Figure 6-13a, the value of the peak pressure is 132.6, 145, and 158.2 bar for the swirl ratios of 0.5, 1.0, and 1.5, respectively. Further increasing the swirl ratio results in that the peak pressure exceeds the limit (160 bar). The heat release rate profile also shows that increasing the swirl ratio significantly improves the diffusion combustion and turbulent flame propagation of natural gas. Further details about this will be discussed later in Figure 6-14. As shown in Figure 6-13b, similar to the results obtained under the low load condition, the piston and cylinder wall heat losses increase and the cylinder head heat loss decreases when increasing the swirl ratio. However, the total heat loss increases by 20.8% when increasing the swirl ratio from 0.5 (base case) to 1.5.

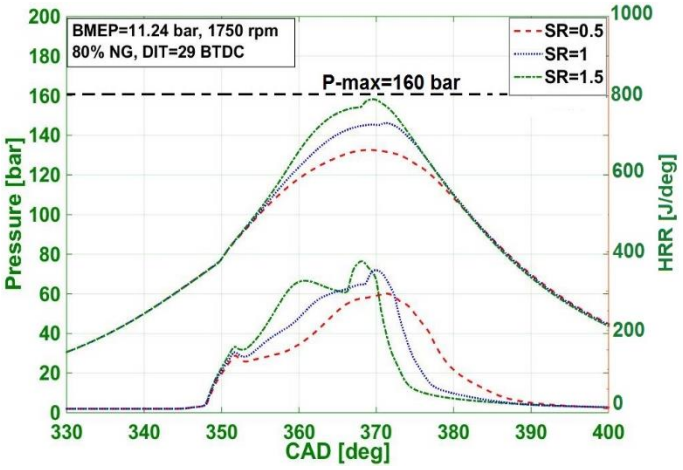

a) Pressure

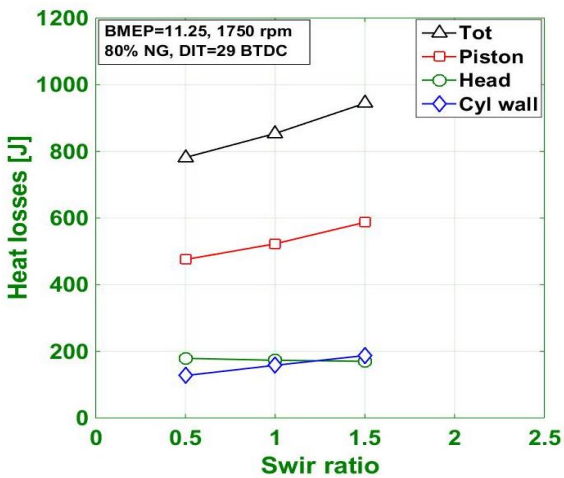

b) Heat loss

Figure 6-13**.** Effect of the swirl ratio on the pressure, HRR, and heat loss of NDDF combustion under medium load-high speed conditions and DIT= 29 °BTDC.

Figure 6-14 shows OH radical distribution contours of NDDF engine under the medium load-high speed condition at three different swirl ratios. It can be seen that OH radical initially appears around the diesel spray that is away from the center of the cylinder and the distribution is similar for all swirl ratios (CAD=-8.7 °ATDC). However, at the premixed combustion stage (CAD=-4.7 °ATDC), the OH distribution becomes slightly wider at higher swirl ratios. This is mainly due to the enhancement in the mixing of premixed natural gas/air mixture and diesel fuel. This is also observed in HRR profile (Figure 6-13a) where the first peak of HRR for the swirl ratio of 1.5 is slightly higher than that for the swirl ratio of 0.5. As diesel atomization and evaporation proceed, more premixed mixture is formed which results in a growth of the ignition zones. At CAD=-0.7 °ATDC, the combustion starts to progress within each jet in both the azimuthal (connecting one jet to the next) and the radial directions. The OH radical propagates more strongly in the radial direction than in azimuthal direction for the swirl ratio of 0.5 (base case). However, with increasing the swirl ratio to 1.5, the OH radical propagates more rapidly in the azimuthal direction compared to the swirl ratio of 0.5 (CAD=+4.3 °ATDC). As shown in the contours of CAD=+10 °ATDC, for a swirl ratio of 0.5, there are still void regions of OH radical in the region between the jets, the very central region of piston bowl, and the squish area. These regions could be the main source of CH4 emissions. With increasing the swirl ratio (SR=1.5), the piston bowl is nearly filled with high temperature reaction zone and a very small blue non-reactive zone located in the piston squish area.

Figure 6-15 depicts the fuel efficiency and emissions (CH_4, CO, and NO_x) of NDDF engine at medium load-high speed conditions with different swirl ratios. As shown in this figure, increasing the swirl ratio from 0.5 to 1.5 increases the fuel efficiency by 2.4%, decreases the CH4 and CO emissions by 13.5% and 11.8%, respectively, and increases NO_x emissions by 50%. It can be seen

that at medium load-high speed conditions and considering the fact that the maximum allowable peak pressure is 160 bar, the highest fuel efficiency and lowest CH4 and CO emissions are achieved at a swirl ratio of 1.5. It can be concluded that under a medium load-high speed condition, the enhancement of diesel diffusion and flame propagation of natural gas due to the increase of the swirl ratio is more significant than that of increased heat loss which consequently leads to improved fuel efficiency.

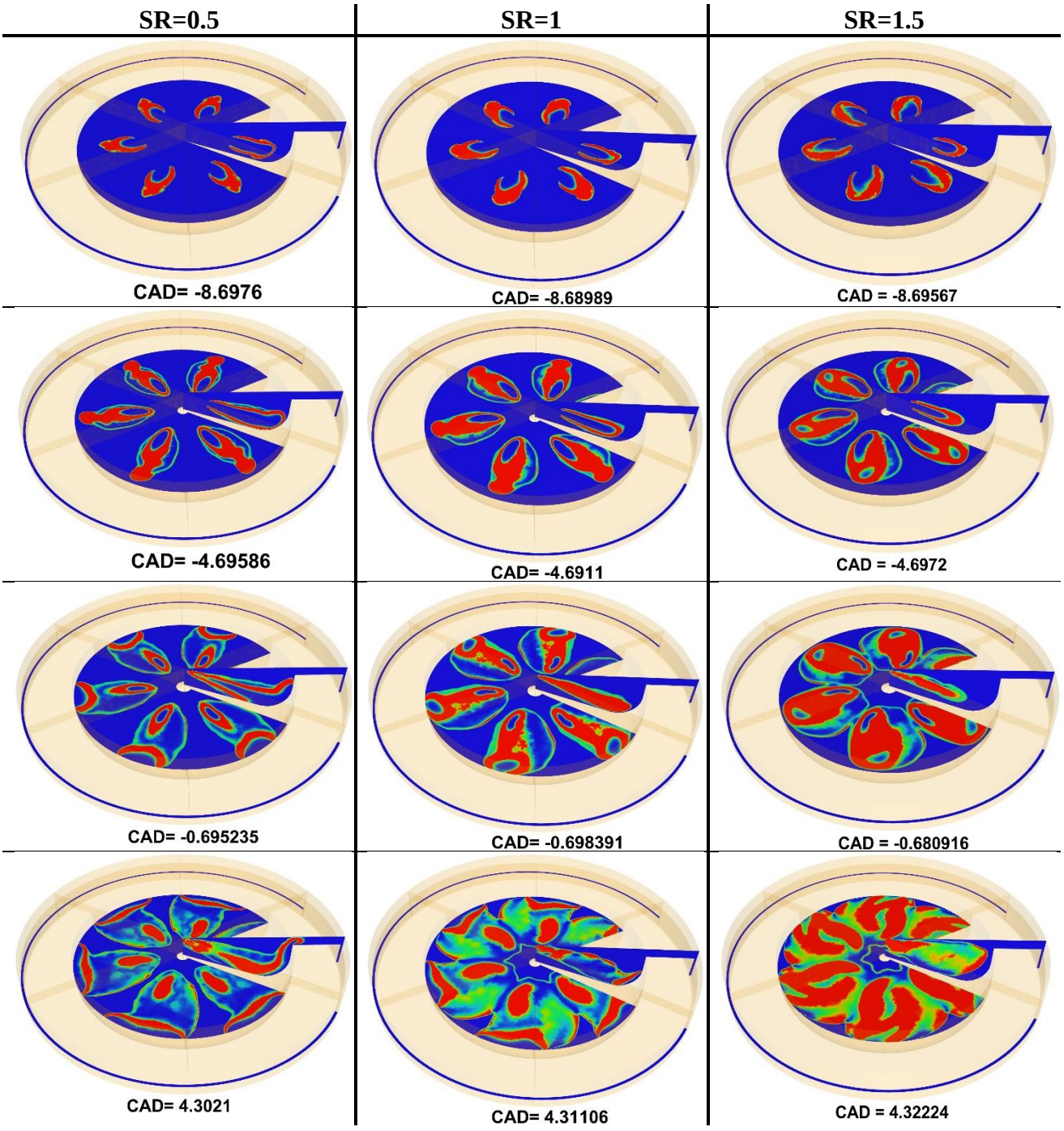

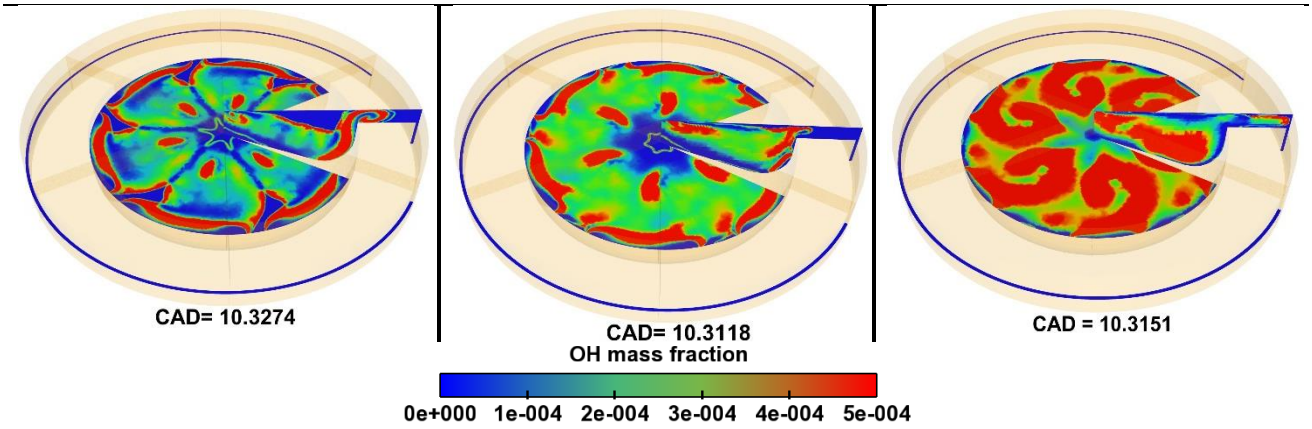

Figure 6-14. OH* distribution of NDDF combustion at medium load-high speed conditions for three different swirl ratios and DIT=29 °BTDC.

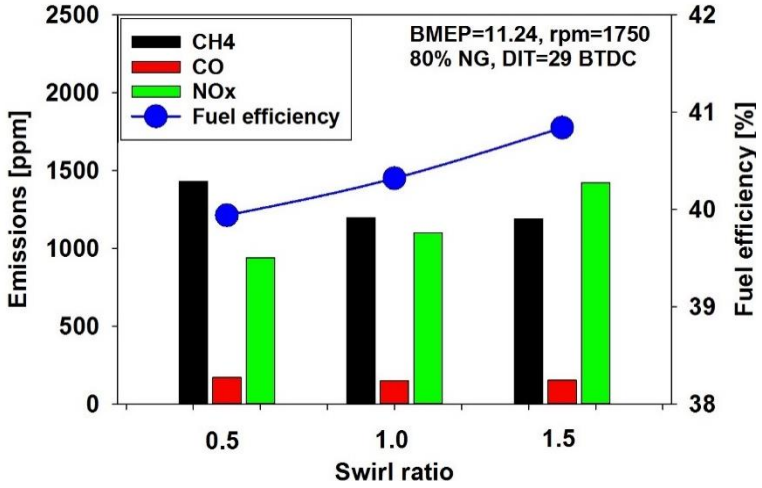

Figure 6-15**.** Effect of the swirl ratio on fuel efficiency and CH_4, CO, and NO_x emissions of NDDF combustion under medium load-high speed conditions and DIT= 29 °BTDC.

6.5.1.3.High load-low speed condition (BMEP=17.6 bar and 1120 rpm)

Figure 6-16 shows the pressure, HRR, and heat loss of NDDF combustion at a high load-low speed condition (BMEP=17.6 bar and 1120 rpm) under different swirl ratios and a diesel injection timing of 11.4 °BTDC. It can be seen that there is noticeable differences in the heat release rate at high load condition compared to the two other cases. It is observed that the combustion duration is significantly reduced and the profile of HRR resembles to a bell shape with a single peak. Similar to the results obtained under medium load conditions, increasing the swirl ratio significantly improves the diesel diffusion and flame propagation of natural gas which leads to an increase in the peak of the pressure

and heat release rate (Figure 6-16a). As shown in this figure, the value of the peak pressure is 132, 141.4, 149.3, and 155.1 bar for a swirl ratio of 0.5, 1, 1.5, and 2, respectively. It is noteworthy to mention that further increasing the swirl ratio also results in that the peak pressure exceeds the limit (160 bar). Moreover, similar to the results at low and medium load conditions, the piston and cylinder wall heat losses increase, and the cylinder head heat loss decreases when increasing the swirl ratio. However, the total heat loss increases by 6% when increasing swirl ratio from 0.5 (base case) to 2 (Figure 6-16b).

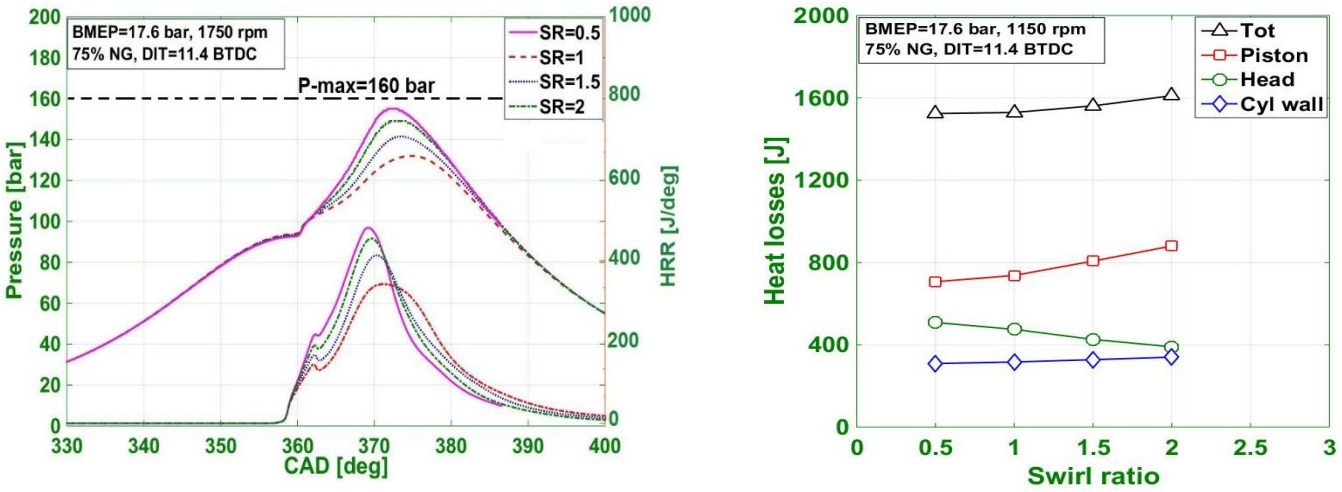

a) Pressure and HRR b) Heat loss

Figure 6-16**.** Effect of the swirl ratio on pressure, HRR, and heat loss of NDDF combustion under high load-low speed conditions and DIT=11.4 °BTDC.

Figure 6-17 shows the OH radical distribution contours of NDDF engine under high load-low speed conditions for three different swirl ratios. As displayed in this figure, combustion is initiated near the piston walls (CAD=+1.3 °ATDC) and the flame shape is similar to the diesel spray shape for all swirl ratios. After initiating near the point of impingement onto the bowl wall, combustion progresses within each jet in both the azimuthal and radial direction where the higher swirl ratio exhibits the widest and strongest OH radical distribution (CAD=+5.3 °ATDC). However, in contrast to the contours presented in Figure 6-5, the progression in the azimuthal direction is more rapid with a greater intensity of OH radical. It can be observed that increasing the swirl ratio significantly improves the flame propagation (CAD=+9.3 °ATDC). With increasing the swirl ratio (SR=1.5), the

flame propagates more rapidly within the piston bowl along the spray axes, and progressively consumes the fresh charge such that burned gases are detected throughout the entire piston bowl at CAD=+13 °ATDC. Looking at the contours of +21.3 °ATDC for a swirl ratio of 0.5, the blue non-reactive zones can be seen in the central region of the piston bowl. However, with increasing the swirl ratio (SR=1.5), the piston bowl completely fills with high temperature reaction zones.

Figure 6-18 shows the effect of the swirl ratio on fuel efficiency and emissions at high load-low speed condition. It is observed that increasing the swirl ratio from 0.5 to 1.5 decreases the CH4 and CO emissions by 22% and 59%, respectively, and increases the fuel efficiency by 2.5%. However, NO_x emissions increase with increasing the swirl ratio. Further increasing the swirl ratio to 2 decreases the fuel efficiency and increases the CH4 and CO emissions due to increased heat losses.

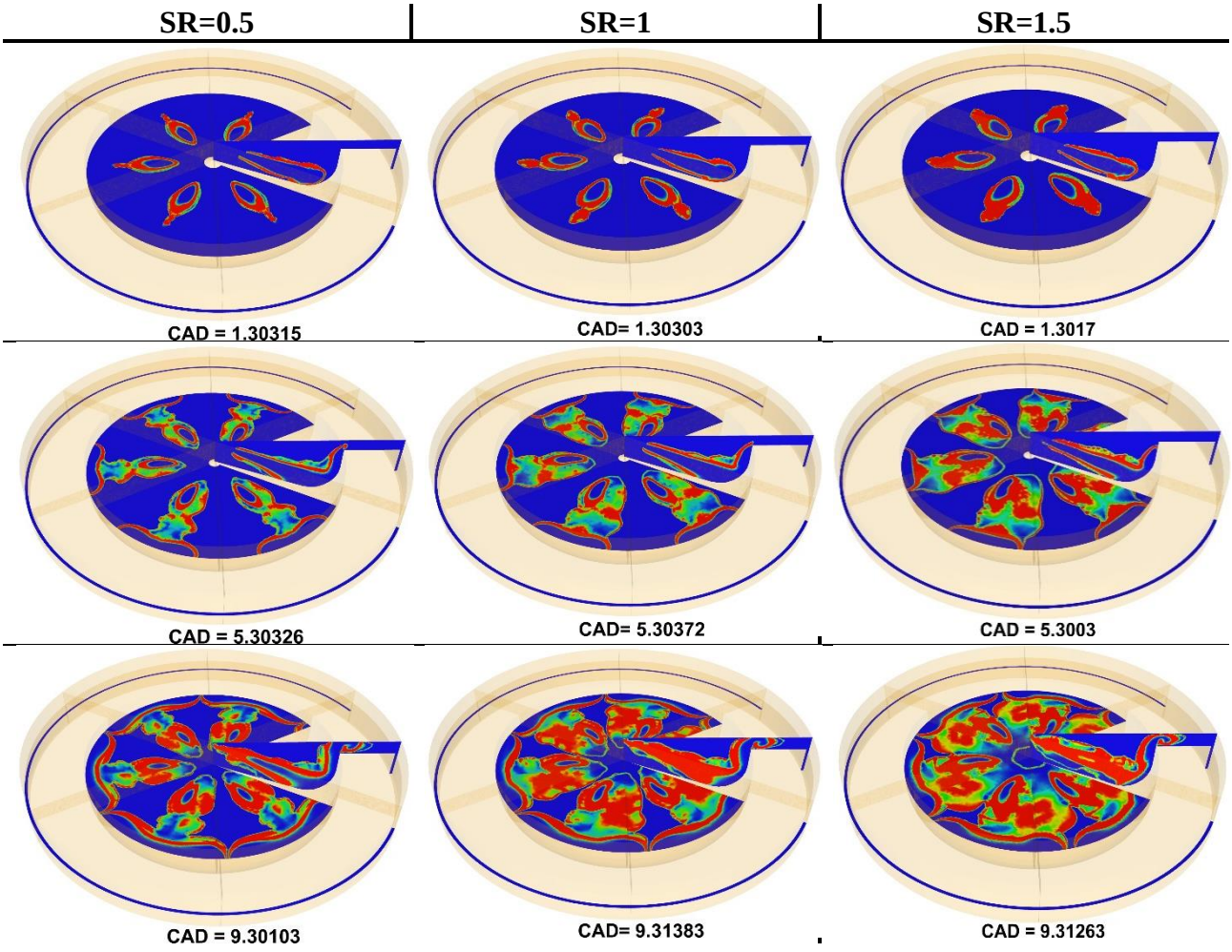

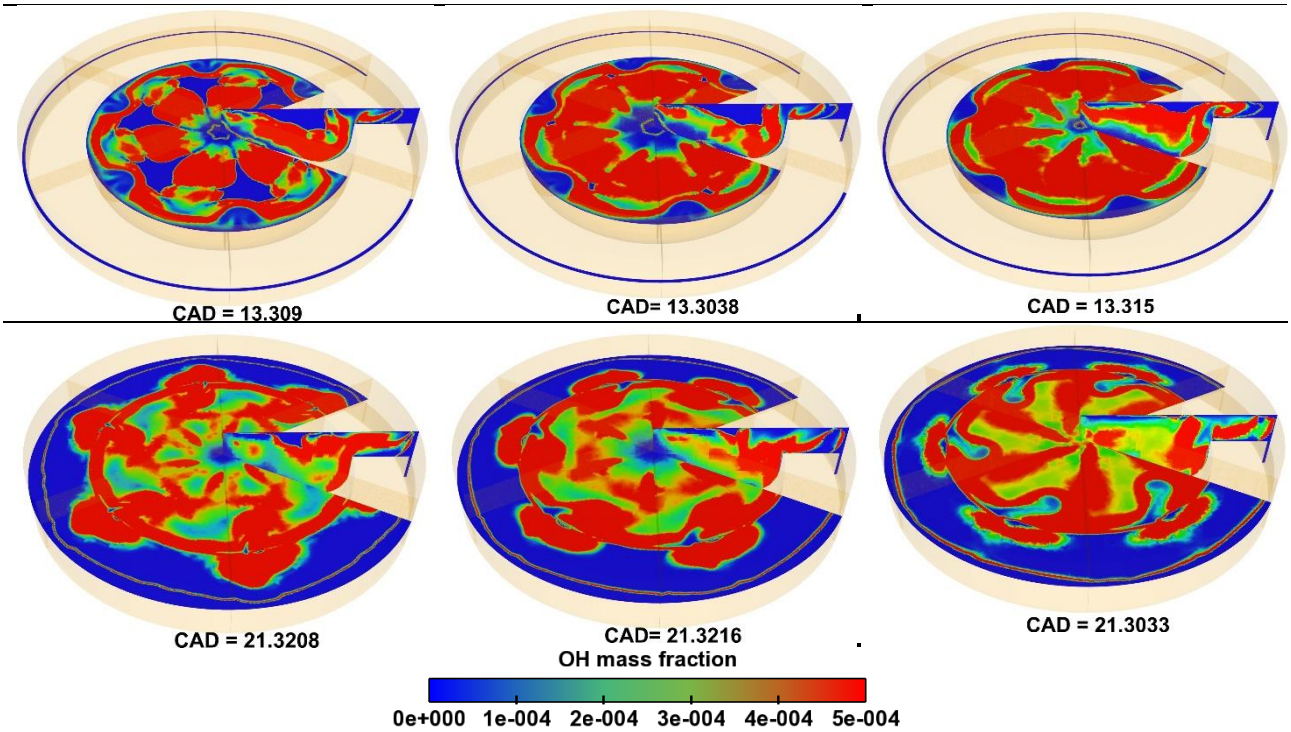

Figure 6-17. OH* distribution of NDDF combustion at medium load-high speed conditions for three different swirl ratios and DIT=11.4 °BTDC.

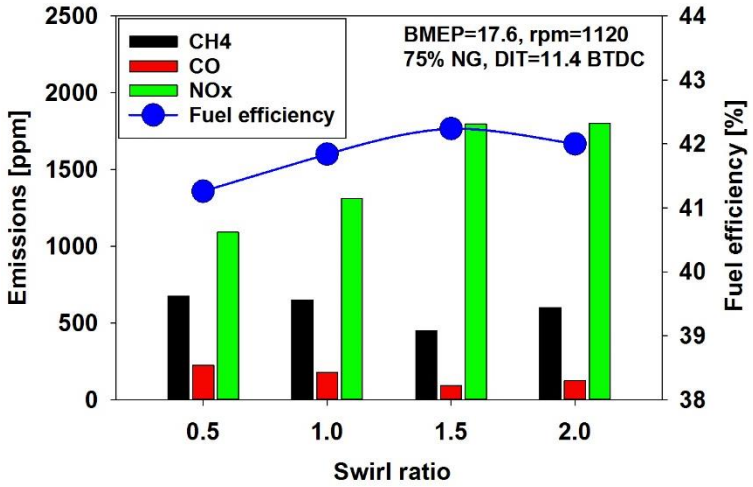

Figure 6-18**.** Effect of the swirl ratio on fuel efficiency and CH_4, CO, and NO_x emissions of NDDF combustion under high load-low speed conditions and DIT= 11.4 °BTDC.

6.6.Conclusions

The effect of swirl ratio on the combustion performance and emissions of a NDDF engine under three different load-speed conditions (BMEP=4.05 bar and 910 rpm, BMEP=11.24 bar and 1750 rpm,

and BMEP=17.6 bar and 1150 rpm) were numerically investigated. The main results can be summarized as follows:

- Increasing swirl ratio affected differently on the combustion performance at later and earlier diesel injection timings under low load-low speed condition. At the injection timing of 14 °BTDC, increasing the swirl ratio from 0.5 to 1.5 enhanced the early stage of the premixed-controlled combustion. The OH radical distribution revealed that the non-reactive zones tend to become narrower for higher swirl ratios in the second stage of combustion. The highest fuel efficiency and lowest CH4 and CO emissions were achieved at a swirl ratio of 1.5 at the retarded injection timing of 14 °BTDC. However, under an injection timing of 30 ° BTDC, increasing the swirl ratio slightly improved the mixing-controlled diffusion combustion, but this improvement was insufficient to compensate for the effect of the increased heat loss. An increase in the swirl ratio at advanced injection timing resulted in a decrease in fuel efficiency.
- At medium load-high speed condition, it was found that increasing swirl ratio significantly improves the diffusion combustion and turbulent flame propagation of natural gas. The OH distribution contours showed that OH radical propagated more rapidly in the azimuthal direction when increasing the swirl ratio from 0.5 to 1.5. Further increase in the swirl ratio led the peak pressure to exceed the limit (160 bar). Moreover, increasing the swirl ratio from 0.5 to 1.5 increased the fuel efficiency by 2.4% and decreased the CH4 and CO emissions by 13.5% and 11.8%, respectively. However, NO_x emissions increased by 50%.
- At high load-low speed condition, increasing the swirl ratio significantly improved the diesel diffusion and flame propagation of natural gas which led to an increase in the peak of the pressure. The OH radical distribution showed that the combustion progressed within each jet in both the azimuthal and radial direction. It was found that increasing the swirl ratio from 0.5 to 1.5 decreased the CH4 and CO emissions by 22% and 59%, respectively, while increased the fuel efficiency by 2.5%. However, this was achieved at high NO_x emissions. It was

observed that further increase in the swirl ratio to 2 decreased the fuel efficiency and increased the CH4 and CO emissions.

Overall, swirl motion may provide better mixture preparation, diesel diffusion, and natural gas flame propagation; however, this benefit is offset by higher (increased) heat loss under very high swirl ratio. Out of the examined engine load-speed conditions and accounting for fuel efficiency and emissions, a swirl ratio of 1.5 is found to be the optimum.

6.7.References

[1] Kavuri C, Kokjohn SL. Computational optimization of a reactivity controlled compression ignition (RCCI) combustion system considering performance at multiple modes simultaneously. Fuel 2017;207:702–18. doi:10.1016/j.fuel.2017.06.071.

[2] Yousefi A, Birouk M, Guo H. An experimental and numerical study of the effect of diesel injection timing on natural gas/diesel dual-fuel combustion at low load. Fuel 2017;203:642–57. doi:10.1016/j.fuel.2017.05.009.

[3] Yousefi A, Birouk M. Investigation of natural gas energy fraction and injection timing on the performance and emissions of a dual-fuel engine with pre-combustion chamber under low engine load. Appl Energy 2017;189. doi:10.1016/j.apenergy.2016.12.046.

[4] Roberts G, Rousselle CM, Musculus M, Wissink M, Curran S, Eagle E. RCCI Combustion Regime Transitions in a Single-Cylinder Optical Engine and a Multi-Cylinder Metal Engine. SAE Int J Engines 2017;10:2017-24-0088. doi:10.4271/2017-24-0088.

[5] Chuahy FDF, Kokjohn SL. High efficiency dual-fuel combustion through thermochemical recovery and diesel reforming. Appl Energy 2017;195:503–22. doi:10.1016/j.apenergy.2017.03.078.

[6] Dronniou N, Kashdan J, Lecointe B, Sauve K, Soleri D. Optical Investigation of Dual-fuel

CNG / Diesel Combustion Strategies to Reduce CO 2 Emissions. SAE Int J Engines 2014:1–2. doi:10.4271/2014-01-1313.

[7] Cummins Engines Ltd. Cummins Dual Fuel Engines for Drilling - Cummins Engines. Https://CumminsenginesCom/Dual-Fuel n.d.

[8] Sahoo BB, Sahoo N, Saha UK. Effect of engine parameters and type of gaseous fuel on the performance of dual-fuel gas diesel engines-A critical review. Renew Sustain Energy Rev 2009;13:1151–84. doi:10.1016/j.rser.2008.08.003.

[9] Hosmath RS, Banapurmath NR, Khandal S V., Gaitonde VN, Basavarajappa YH, Yaliwal VS. Effect of compression ratio, CNG flow rate and injection timing on the performance of dual fuel engine operated on honge oil methyl ester (HOME) and compressed natural gas (CNG). Renew Energy 2016;93:579–90. doi:10.1016/j.renene.2016.03.010.

[10] Johnson DR, Heltzel R, Nix AC, Clark N, Darzi M. Greenhouse gas emissions and fuel efficiency of in-use high horsepower diesel, dual fuel, and natural gas engines for unconventional well development. Appl Energy 2017;206:739–50. doi:10.1016/j.apenergy.2017.08.234.

[11] Yang B, Wang L, Ning L, Zeng K. Effects of pilot injection timing on the combustion noise and particle emissions of a diesel/natural gas dual-fuel engine at low load. Appl Therm Eng 2016;102:822–8. doi:10.1016/j.applthermaleng.2016.03.126.

[12] Yousefi A, Guo H, Birouk M. An experimental and numerical study on diesel injection split of a natural gas/diesel dual-fuel engine at a low engine load. Fuel 2018;212. doi:10.1016/j.fuel.2017.10.053.

[13] Abdelaal MM, Hegab AH. Combustion and emission characteristics of a natural gas-fueled diesel engine with EGR. Energy Convers. Manag., 2012.

doi:10.1016/j.enconman.2012.05.021.

[14] Yang B, Xi C, Wei X, Zeng K, Lai MC. Parametric investigation of natural gas port injection and diesel pilot injection on the combustion and emissions of a turbocharged common rail dual-fuel engine at low load. Appl Energy 2015;143:130–7. doi:10.1016/j.apenergy.2015.01.037.

[15] Jha PR, Srinivasan KK, Krishnan SR. Influence of Swirl Ratio on Diesel-Methane Dual Fuel Combustion – A CFD Investigation. Proc ASME 2017 Intern Combust Engine Div Fall Tech Conf ICEF2017 Oct 15-18, 2017, Seattle, Washington, USA 2017.

[16] Carlucci AP, Laforgia D, Saracino R, Toto G. Combustion and emissions control in diesel-methane dual fuel engines: The effects of methane supply method combined with variable in-cylinder charge bulk motion. Energy Convers Manag 2011;52:3004–17. doi:10.1016/j.enconman.2011.04.012.

[17] Miles PC. The Influence of Swirl on HSDI Diesel Combustion at Moderate Speed and Load. SAE Techinical Pap 2000-01-1829 2000. doi:10.4271/2000-01-1829.

[18] Hill PG, Zhang D. The effects of swirl and tumble on combustion in spark-ignition engines. Prog Energy Combust Sci 1994;20:373–429. doi:10.1016/0360-1285(94)90010-8.

[19] Guo H, Neill WS, Liko B. An experimental investigation on the combustion and emissions performance of a natural gas - Diesel dual fuel engine at low and medium loads. Proc ASME 2015 Intern Combust Engine Div Fall Tech Conf ICEF2015 Novemb 8-11, 2015, Houston, TX, USA ICEF2015-1041 2015;1:130–7. doi:10.1115/ICEF2015-1041.

[20] Richards K.J. SPK and PE. Converge Manual. Converg (Version 24) Manual," Converg Sci Inc, Madison, Wisconsin, USA 2017.

[21] Han Z, Reitz RD. A temperature wall function formulation for variable-density turbulent

flows with application to engine convective heat transfer modeling. Int J Heat Mass Transf 1997;40:613–25. doi:10.1016/0017-9310(96)00117-2.

[22] Yakhot V, Orszag SA, Thangam S, Gatski TB, Speziale CG. Development of turbulence models for shear flows by a double expansion technique. Phys Fluids A 1992;4:1510–20. doi:10.1063/1.858424.

[23] Senecal PK, Richards KJ, Pomraning E, Yang T, Dai MZ, McDavid RM, et al. A New Parallel Cut-Cell Cartesian CFD Code for Rapid Grid Generation Applied to In-Cylinder Diesel Engine Simulations 2007;2007:776–90. doi:10.4271/2007-01-0159.

[24] Schmidt DP, Rutland CJ. A New Droplet Collision Algorithm. J Comput Phys 2000;164:62–80. doi:10.1006/jcph.2000.6568.

[25] Wijeyakulasuriya S. Multidimensional Modeling and Validation of Dual-Fuel Combustion in a Large Bore Medium Speed Diesel Engine. Proc ASME 2015 Intern Combust Engine Div Fall Tech Conf ICEF2015 Novemb 8-11, 2015, Houston, TX, USA 2015:1–14.

[26] Lucchini T, D'Errico G, Ettorre D, Ferrari G. Numerical Investigation of Non-Reacting and Reacting Diesel Sprays in Constant-Volume Vessels. SAE Int J Fuels Lubr 2009;2:966–75. doi:10.4271/2009-01-1971.

[27] Rahimi A, Fatehifar E, Saray RK. Development of an optimized chemical kinetic mechanism for homogeneous charge compression ignition combustion of a fuel blend of *n*-heptane and natural gas using a genetic algorithm. Proc Inst Mech Eng Part D J Automob Eng 2010;224:1141–59. doi:10.1243/09544070JAUTO1343.

[28] Karim GA. Combustion in Gas Fueled Compression: Ignition Engines of the Dual Fuel Type. J Eng Gas Turbines Power 2003;125:827. doi:10.1115/1.1581894.

[29] Wang X, Qian Y, Zhou Q, Lu X. Modulated diesel fuel injection strategy for efficient-clean

utilization of low-grade biogas. Appl Therm Eng 2016;107:844–52.
doi:10.1016/j.applthermaleng.2016.07.057.

Chapter 7: Conclusions and recommendations for future studies

7.1. Research summary and major findings

In this study a combination of experiment and numerical simulation were used to explore the combustion performance and emissions of a natural gas/diesel dual-fuel engine under different engine load-speed conditions. Engine experiments were conducted using a modified single cylinder heavy-duty Caterpillar's 3401 diesel engine. The engine was modified to accommodate port injection of natural gas. A CFD model has been developed for natural gas/diesel dual-fuel engine and validated across a wide range of engine loads-speeds, natural gas energy fractions, and diesel injection timings, pressures and split ratios. The CFD model developed was able to reasonably capture the experimental data under various load-speed conditions, including ignition, flame propagation, combustion duration and emissions, etc.

This thesis primarily focused on low engine load conditions under which the dual fuel engine has relatively lower thermal efficiency and generates higher unburned methane and CO_2 equivalent emissions compared to diesel engine. Different strategies are examined and/or developed in this thesis to reduce unburned methane emissions and improve thermal efficiency under low load conditions. Although natural gas/diesel dual-fuel engine offers similar (or sometimes better) thermal efficiency and lower CO_2 equivalent emissions compared to diesel engine under medium to high load conditions, the thesis also studied the effect of advancing diesel injection timing and swirl ratio on dual-fuel engine to further improve the combustion performance and emissions under medium to high load conditions. The major findings and contributions of this research are summarized below.

7.1.1. Typical low load condition (BMEP=4.05 bar and RPM=910)

a) Single injection (75% NG, diesel injector rail pressure=525 bar)

- Both experimental and numerical results showed that different combustion modes can be achieved with advancing diesel injection timing. Diesel injection timing of 30 °BTDC is the critical timing for different combustion modes. The combustion is similar to conventional diesel engine (diffusion combustion) for diesel injection timings between 10-30 °BTDC (late diesel injection timings). However, a greater premixed combustion takes place by advancing diesel injection timing to 30-50 °BTDC. The simulation results demonstrated that OH radical distribution is more uniform throughout the combustion chamber, which makes the combustion look like similar to that in a HCCI engine. While advancing diesel injection timing in the range of conventional diesel injection (10-30 °BTDC) improves thermal efficiency and emissions of unburned methane, it leads to high PRR and NO_x emissions. However, further advancing diesel injection timing retards the start of combustion and results in that most of the heat release occurs during the expansion stroke, which yields the highest thermal efficiency and ultra-low NO_x emissions.
- Advancing diesel injection timing significantly decreases the unburned methane and CO_2-equivalent emissions of natural gas/diesel dual-fuel engine under low load-low speed conditions. Simulation results showed that the central region of the combustion chamber is the main source of unburned methane emissions. Advancing diesel injection timing significantly improves the combustion of natural gas-air mixture in the central region of the combustion chamber. However, advancing diesel injection timing slightly increases the unburned methane trapped in the crevice volume. This slight increase in the unburned methane in the crevice volume is much lower compared to the significant decrease of the unburned methane in the central region of combustion chamber when diesel injection timing

is advanced. This is the reason that advancing diesel injection timing significantly decreases the unburned methane emissions under low load-low speed conditions.

b) Split injection (first pulse timing sweep, SODI2=10 °BTDC, Split ratio=60%, diesel injector rail pressure=525 bar, 75% NG)

- Comparing the results of diesel split injection with that of single injection timing of 10 °BTDC reveals that the heat release produced by first injection of diesel fuel considerably increases the in-cylinder charge temperature before the start of the second injection. The flame zone of the split injection mode is markedly higher than that of the single injection (10 °BTDC) due to larger heat release produced during the first injection which promotes the combustion of the second one. When the first injection timing is close to the second injection timing (first injection timings of 28, 30, and 34 °BTDC), the advancement of the first injection timing leads to increased peak of the in-cylinder pressure and HRR. This is mainly due to the advancement of combustion phasing. Further advancing first injection timing (38-55 °BTDC) retards the SOC and shifts the combustion phasing away from TDC, leading to decreased peak of the in-cylinder pressure.
- Numerical simulation results show that when the first injection timing is close to the second injection (i.e., SOI1=30 °BTDC), the second injected diesel fuel spray is close to the high temperature region resulting from the first injection of diesel fuel. Thus, the spray of the second injection and the initial stages of flame kernels of the first injection interact with each other. Consequently, the effect of the first injection is more profound, which leads to increased ignition area of the in-cylinder mixture, advanced SOC, and increased in-cylinder peak pressure. Further advancing the first injection timing (38-55 °BTDC) weakens its influence on the combustion of the second injected diesel fuel. This is due to the fact that under advanced first injection timings (i.e. 42 and 50 °BTDC), the second injected diesel fuel spray is located far away from the high temperature region that results from the first injection of

diesel fuel. Under this condition, very advanced first injection timing leads to longer ignition delay, which promotes air-fuel mixing and the formation of leaner air-natural gas and diesel fuel mixture. Thus, SOC and combustion phasing are retarded which lead to reduced peak in-cylinder pressure.

- Under low load-low speed conditions, the highest thermal efficiency of 38.04% was achieved at an optimum condition (SODI1=50 °BTDC, fixed SODI2=10 °BTDC, and split ratio of 60%). This shows an increase of 8.9% in thermal efficiency compared to single diesel injection timing of 10 °BTDC. Moreover, compared to single injection of 10 °BTDC, using diesel split injection (optimum point mentioned above) decreases the unburned methane and CO emissions by 60% and 63%, respectively. However, NOx emission was maintained at the same level as that of single injection timing of 10 °BTDC.

c) Combination of injection rail pressure increase and diesel split injection (sweep of first and second pulse timings and split ratio, increase of rail pressure, 70% NG)

- The experimental results show that increasing the injection rail pressure advances the combustion phasing of dual-fuel engine with split injection at split ratios of 45, 50, and 55% but retards the combustion phasing under split ratios of 60 and 65%. The numerical results further reveal the mechanism behind this observation. According to the simulation results, at lower split ratios, less diesel fuel reaches the cylinder wall and squish regions during the first pulse. Thus, the effect of increased injection rail pressure on the atomization and evaporation process is more significant which shortens the ignition delay and advances the combustion phasing. At high split ratio (e.g., split ratio of 65%), a larger portion of diesel fuel is located in the region close to the cylinder's low temperature wall region. Thus increasing the injection rail pressure leads to a slower evaporation process of the first pulse of injected diesel, which lengthens the ignition delay and retards the combustion phasing.

- Increasing the injection rail pressure significantly reduces the unburned methane emissions of dual-fuel engine with split injection, especially at lower split ratios. However, increasing the injection rail pressure does not affect the unburned methane emissions under a higher split ratio (such as 65%). This is due to the fact that at a higher split ratio, a larger portion of diesel fuel impinges onto the cylinder wall which retards the combustion phasing and may not significantly improve the combustion rate and unburned methane emissions. The optimum methane emissions with split injection is 50% lower compared to the best condition of dual-fuel engine with a single injection. Moreover, the lowest ISCO2 equivalent emissions of dual-fuel engine with split injection is 640 g/kW-hr, which is 11% lower compared to those of dual-fuel engine with a single injection and diesel engine.

d) Swirl ratio increase (diesel injection timings of 14 and 30 °BTDC, rail pressure=525 bar, 75% NG).

- Numerical simulation results reveal that increasing swirl ratio affected differently the combustion performance at later and earlier diesel injection timings under low load-low speed condition. At an injection timing of 14 °BTDC, increasing the swirl ratio from 0.5 to 1.5 enhances the early stage of the premixed-controlled combustion. OH radical distribution reveal that the non-reactive zones tend to become narrower for higher swirl ratios in the second stage of combustion. The highest fuel efficiency and lowest CH4 and CO emissions are achieved at a swirl ratio of 1.5 at a retarded injection timing of 14 °BTDC. However, under an injection timing of 30 °BTDC, increasing the swirl ratio slightly improve the mixing-controlled diffusion combustion, but this improvement is insufficient to compensate for the effect of the increased heat loss. An increase in the swirl ratio at an advanced injection timing of 30 °BTDC decreases fuel efficiency.

7.1.2. Medium to high load conditions (BMEP=12.15 bar, RPM=910 and BMEP=17.6 bar, RPM=1120)

a) Single injection (injection timing sweep, 65% and 90% NG, Rail pressures of 525 and 800 bar)

- Numerical simulation results show that, under medium to high load-low speed conditions after the initiation of chemical reaction near the point of impingement onto the bowl wall, combustion rapidly progresses within each jet in both the azimuthal and radial directions. It can be observed that multiple flames propagate simultaneously within the piston bowl along the spray axes and progressively consume the fresh charge. This behavior suggests that flame propagation could be the predominant combustion mode under this engine condition.
- Under these conditions, unburned methane emissions increase while CO_2-equivalent emissions do not significantly change when advancing diesel injection timing. Almost all of the premixed natural gas-air mixture in the central region of the combustion chamber burns even with a retarded injection timing (e.g., DIT=10.5 °BTDC) under these conditions. Further advancing diesel injection timing does not significantly improve the combustion of natural gas-air mixture in the central region of combustion chamber. The unburned methane trapped in the crevice region, which is considered as the main source of CH_4 emissions under these conditions, slightly increases when advancing the diesel injection timing. This is why advancing diesel injection timing slightly increases the unburned methane emissions under medium to high load-low speed conditions.

b) Swirl ratio increase (diesel injection timing of 11.4 °BTDC, rail pressure=800 bar, 75% NG)

- Numerical simulation results reveal that, under high load-low speed conditions (BMEP=17.6 bar and RPM=1120), increasing the swirl ratio significantly improves diesel diffusion combustion and flame propagation of natural gas, which leads to an increase in the peak cylinder pressure. OH radical distribution shows that combustion progresses very rapidly

within each jet in both the azimuthal and radial direction when increasing the swirl motion. It is found that increasing the swirl ratio from 0.5 to 1.5 decreases CH4 and CO emissions by 22% and 59%, respectively, while increases fuel efficiency by 2.5%. However, this is achieved at high NO_x emissions. It is observed that further increase in the swirl ratio to 2 decreases fuel efficiency and increases CH4 and CO emissions. Swirl motion may provide better mixture preparation, diesel diffusion combustion, and natural gas flame propagation; however, this benefit can be offset by higher heat loss under very high swirl ratio.

7.2. Recommendations for future studies

Although various advanced combustion strategies have been developed and examined for natural gas/diesel dual fuel combustion, there are still certain areas which need further research. Some of these areas are outlined as follows:

1. In order to achieve ultra-low NOx emissions while improving thermal efficiency and GHG and soot emissions of natural gas/diesel dual-fuel engine, a combined application of EGR and other strategies (e.g., advanced diesel injection, increased injection rail pressure, and diesel split injection) are necessary. For example, the results of this study revealed that even when using diesel split injection, the generated NOx emissions is still higher than the limit set by the current emissions regulation (i.e. EPA Tier 4, Engine 130-560 kW, NOx=2 g/kW-hr [1]). Although many experimental studies have investigated the effect of EGR on dual-fuel combustion [2–6], the fundamental impact of EGR on combustion and emissions of natural gas/diesel dual-fuel engine has not been yet examined. Moreover, the interaction between EGR rates, EGR temperature, engine load-speed and the resultant emissions are highly complex. Therefore, further experimental and numerical studies are needed to develop an understanding of the EGR effects on the NOx and GHG emissions at different engine load-speed conditions and injection strategies.

2. As revealed by the results of the study of the combined diesel split injection and increased injection rail pressure of dual-fuel combustion, usually very early diesel injection timing with high split ratio and injection rail pressure can cause fuel impingement, which results in incomplete combustion. Thus, more effort should be devoted to the control of the spray to alleviate fuel deposits. The effect of varying the number of injector holes and spray angles can be taken into consideration.
3. It is found that advancing diesel injection timing does not decrease CO2 equivalent emissions of natural gas/diesel dual-fuel engine at medium to high load conditions. Moreover, it significantly increases NOx, cylinder peak pressure, and PRR. Therefore, examining diesel split injection strategy are needed to achieve high thermal efficiency as well as to determine a trade-off between NOx-CH4 and NOx-CO2 emissions under medium to high load conditions.
4. It is revealed that the crevice regions are the main source of unburned methane emissions under medium to high load conditions. As shown in this study, advancement of diesel injection timing slightly increases unburned methane emissions. However, the trapped unburned gas flows back during expansion stroke where the combustion temperature is not high enough to burn it. Therefore, using post injection could help in decreasing the trapped unburned gas in the crevice region. There is almost no study in the literature that examine the effect of post injection (e.g., triple injections: two pulses before TDC and one post injection) in natural gas/diesel dual-fuel engine. Therefore, more experimental and numerical works are needed to test the post injection strategies under medium to high load conditions.

7.3. References

[1] United States Nonroad Diesel Engines, https://www.dieselnet.com/standards/us/nonroad.php#tier4. DieselNet 2016;1990:1–7. doi:10.1002/j.1532-2149.2012.00255.x.

[2] Basavarajappa YH, Banapurmath NR. Effect of Exhaust Gas Recirculation on the Performance and Emissions of A Dual Fuel Engine Operated on CNG-Biodiesel-Ethanol Blends 2013;2:449–58.

[3] Qi Y, Srinivasan KK, Krishnan SR, Yang H, Midkiff KC. Effect of hot exhaust gas recirculation on the performance and emissions of an advanced injection low pilot-ignited natural gas engine. Int J Engine Res 2007;8:289–303. doi:10.1243/14680874JER02306.

[4] Abdelaal MM, Hegab AH. Combustion and emission characteristics of a natural gas-fueled diesel engine with EGR. Energy Convers Manag 2012;64:301–12. doi:10.1016/j.enconman.2012.05.021.

[5] Guo H, Neill WS, Liko B. The Effect of EGR on Combustion and Emissions of a Natural Gas– Diesel Dual Fuel Engine Hongsheng. Proc Combust Inst – Can Sect Spring Tech Meet Univ Waterloo May 10-12, 2016 2016;1. doi:10.1115/ICEF2015-1041.

[6] Zhou L, Liu Y, Sun L, Hou H, Zeng K, Huang Z. Effect of Hot Exhaust Gas Recirculation on the Combustion Characteristics and Particles Emissions of a Pilot-Ignited Natural Gas Engine. SAE Int J Engines 2013;6:1116–25. doi:10.4271/2013-01-1341.

Appendix

Two CFD models were developed based on AVL-FIRE and CONVERGE software. The former was used in Chapter 2 and Chapter 3, and the latter was employed in Chapter 4 to Chapter 6. As shown in this study, both models predicted well the combustion behavior and emissions of natural gas/diesel dual-fuel engine under low load conditions. However, AVL-FIRE was not able to predict flame propagation under medium to high engine load conditions. This was the main reason that CONVRGE software was introduced as a more reliable CFD tool for the rest of this thesis. It was noted that all of the used models and sub-models were similar for both developed CFD models except the meshing procedure. As shown in Chapter 2 and Chapter 3, AVL-FIRE uses constant average grid size during the closed cycle simulation. However, CONVERGE includes several tools for controlling the grid size before and during the simulation. For example, grid scaling coarsens or refines the base grid size, fixed embedding refines the grid at specified locations and times and, adaptive mesh refinement (AMR) automatically changes the grid based on fluctuating and moving conditions. These tools enabled us to predict the spray behavior and flame propagation of dual-fuel combustion when using CONVERGE software. In the following section, CONVERGE's grid control techniques are explained in detail and then the predicted results of both CONVERGE and AVL-FIRE are compared with that of experiments at low to high load conditions.

A.1. Grid control in CONVERGE

A.1.1. Grid scaling

Grid scaling refers to changing the base grid size at specified times during simulation. Grid scaling can greatly reduce runtime by coarsening the grid during non-critical simulation times and can help

capture critical flow phenomena by refining the grid at other times. For example, for an in-cylinder diesel engine simulation that includes spray and combustion modeling, the grid needs a higher resolution to ensure accurate results during spray and combustion but lower grid resolution may be sufficient during compression [1].

A.1.2. Fixed embedding

Fixed embedding is used to refine the grid at specific locations in the domain where a finer resolution is critical for the accuracy of the solution. For example, when simulating sprays, an area of fixed embedding can be added by the nozzle to resolve the complex flow behavior as shown in Fig. A.1. Fixed embedding allows the rest of the grid to remain coarse to minimize the simulation time.

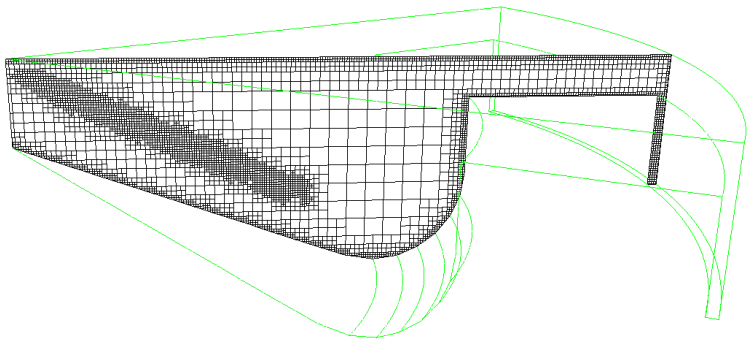

Fig. A.1: A grid generated using a nozzle embedding

A.1.2. Adaptive mesh refinement

Adaptive Mesh Refinement is used to automatically refine the grid based on fluctuating and moving conditions such as temperature or velocity. This option is useful for a highly refined grid to accurately simulate complex phenomena such as flame propagation or high velocity flow without unnecessarily slowing the simulation with a globally refined grid [1,2]. Ideally, a good AMR algorithm adds higher grid resolution (embedding) when the flow field is mostly under-resolved or when the sub-grid field is the largest (i.e., where the curvature gradient of a specified field variable is the highest). The AMR method in CONVERGE estimates the magnitude of the sub-grid field to determine when CONVERGE adds embedding.

A.2. Predicted results of AVL-FIRE and CONVERGE

Figures A.2 shows the predicted in-cylinder pressure and HRR of natural gas/diesel dual-fuel engine at BMEP=4.05 bar and engine speed of 910 rpm. As mentioned in Chapter 1, at low engine loads, there is no flame propagation of premixed natural gas/air mixture. At these conditions, the bulk of energy release comes from the ignition and subsequent rapid combustion of pilot diesel and a small part of entrained natural gas-air mixture. As shown in Fig. A.2a, AVL-FIRE can capture the experimental data of natural gas/diesel dual-fuel engine under low load conditions. However, it can be seen that HRR is slightly under-predicted during the last stage of combustion. As mentioned in Figure 1-2a of Chapter 1, this small energy comes from the bulk of the gaseous fuel-air charge farther away from the diesel spray plume (stage III) [3] where AVL-FIRE is unable to predict it. However, it can be observed in Fig. A.2b that CONVERGE is able to predict the last stage of combustion. This is mainly due to a better grid refinement in the spray and ignition kernel regions (owing to fixed embedding and AMR).

Under medium to high engine load conditions, after premixed combustion of the pilot diesel and entrained natural gas and diffusion combustion of diesel, turbulent flame starts to propagate from the ignition kernels (Figure 1-2b, Stage III) [3]. Figures A.3 shows the predicted in-cylinder pressure and HRR of natural gas/diesel dual-fuel engine at BMEP=11.24 bar and engine speed of 1750 rpm. It can be seen, from A.3a, that AVL-FIRE is not able to capture the flame propagation. However, the use of AMR and fixed embedding with small enough cell sizes (0.25 mm to 0.5 mm) in the flame region adequately resolves the turbulent flame front and the species gradients without the need of any sub-grid model [4,5]. In this study, AMR based on the third derivative of shear and normal components of velocity and temperature was used to resolve flow and propagating flames in the engine.

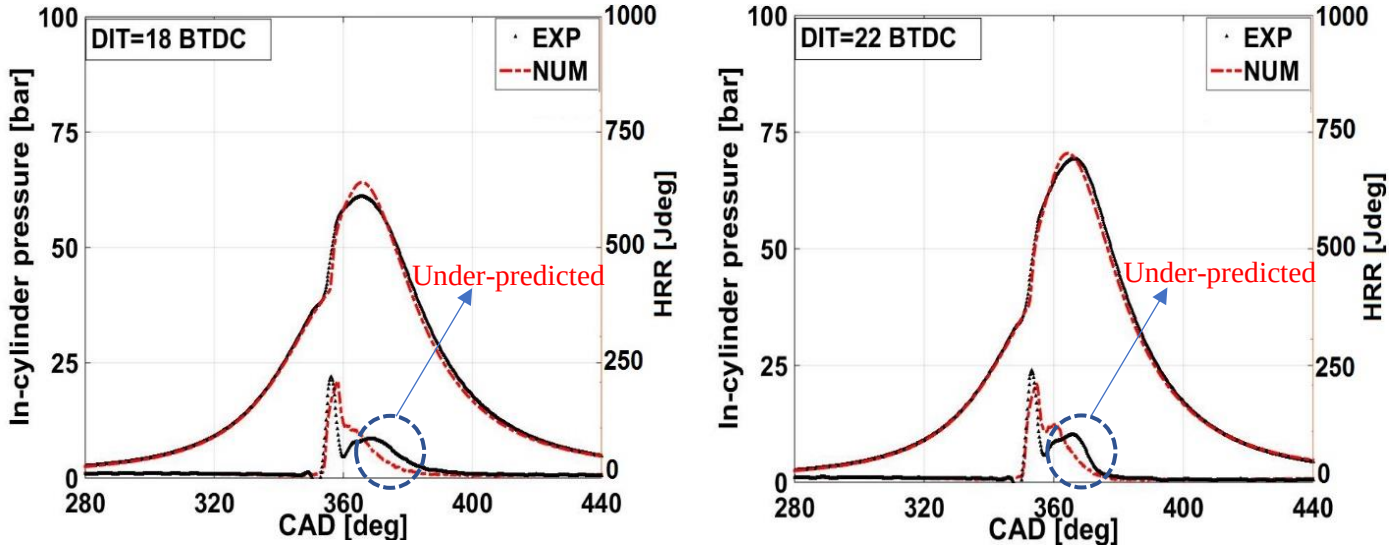

a) AVL-FIRE, CFD model 1

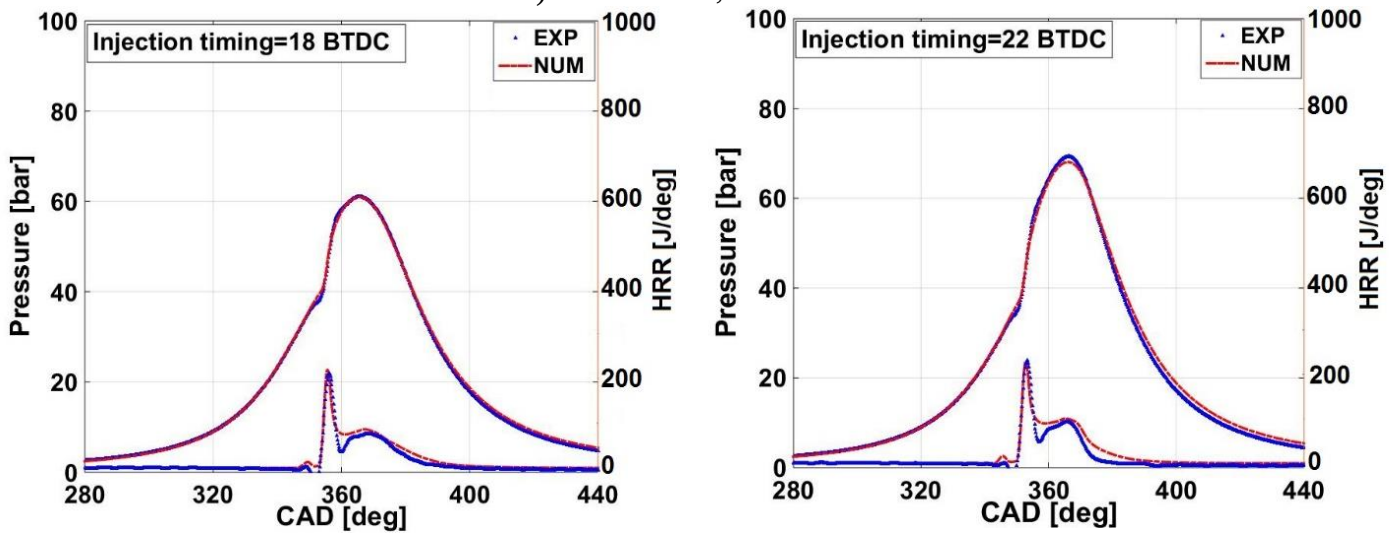

b) CONVERGE, CFD model 2

Fig. A.2: Predicted cylinder pressure and HRR at a low load condition using AVL-FIRE or CONVERGE

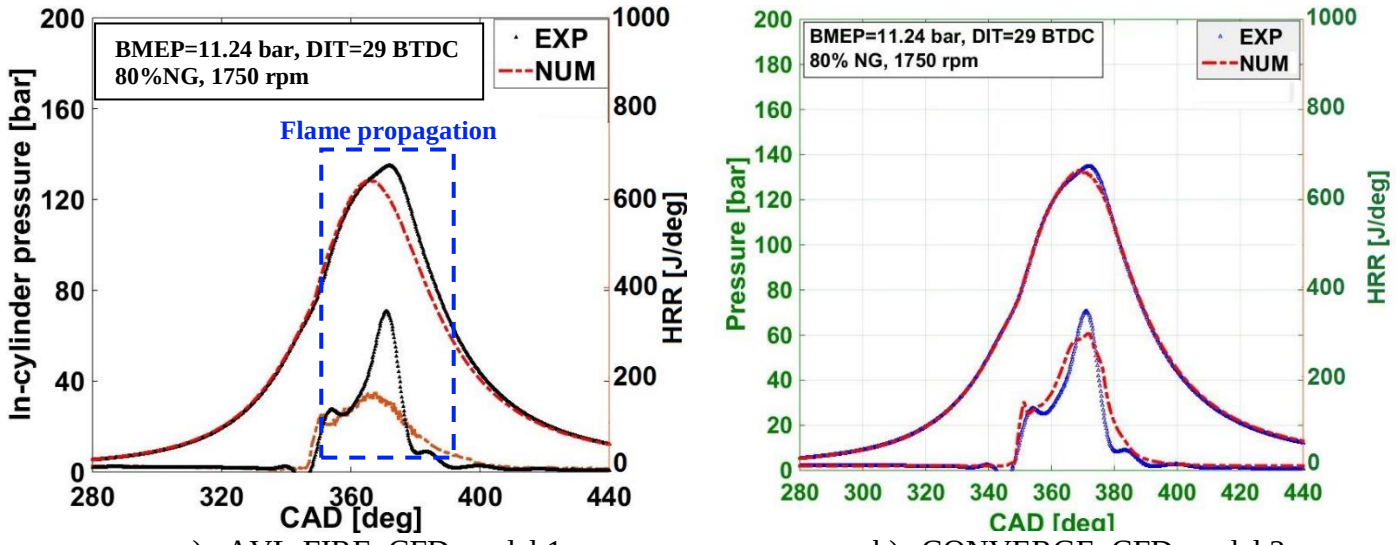

a) AVL-FIRE, CFD model 1

b) CONVERGE, CFD model 2

Fig. A.3: Predicted cylinder pressure and HRR at a medium load condition using AVL-FIRE or CONVERGE

A.3. References

[1] Richards K.J. SPK and PE. Converge Manual. Converg (Version 24) Manual," Converg Sci Inc, Madison, Wisconsin, USA 2017.

[2] Wijeyakulasuriya S. Multidimensional Modeling and Validation of Dual-Fuel Combustion in a Large Bore Medium Speed Diesel Engine. Proc ASME 2015 Intern Combust Engine Div Fall Tech Conf ICEF2015 Novemb 8-11, 2015, Houston, TX, USA 2015:1–14.

[3] Karim GA. Combustion in Gas Fueled Compression: Ignition Engines of the Dual Fuel Type. J Eng Gas Turbines Power 2003;125:827. doi:10.1115/1.1581894.

[4] Senecal PK, Richards KJ, Pomraning E, Yang T, Dai MZ, McDavid RM, et al. A New Parallel Cut-Cell Cartesian CFD Code for Rapid Grid Generation Applied to In-Cylinder Diesel Engine Simulations 2007;2007:776–90. doi:10.4271/2007-01-0159.

[5] Jupudi RS, Finney CEA, Primus R, Wijeyakulasuriya S, Klingbeil AE, Tamma B, et al. Application of High Performance Computing for Simulating Cycle-to-Cycle Variation in Dual-Fuel Combustion Engines 2016. doi:10.4271/2016-01-0798.